

PT SANS INTERIOR DESIGN TEMPLATE

INSTRUCTIONS TO COMPOSITOR

Trim size: the most common trim size for this template is **6-5/8" x 9-5/8" (244 x 170mm)**. If an alternate trim size is required, please adjust as follows:

Single-column (align major column with inside margin):

Trim Size (US)	Trim Size (Metric)	Major Column Width	Minor Column Width	Outside Margin
5.5" x 8.5"	216 x 140	23p	n/a	4p
6" x 9"	229 x 152	26p	n/a	4p
6-5/8" x 9-5/8"	244 x 170	29p3	n/a	4p6
7-3/8" x 9-1/4"	235 x 187	30p9	n/a	4p6
7" x 10"	254 x 178	28p6	n/a	4p6
8" x 10"	254 x 203	30p	8p3	3p
8-1/2" x 10-7/8"	279 x 216	31p	10p3	3p

Double-column:

Trim Size (US)	Trim Size (Metric)	Column Widths	Outside Margin
5.5" x 8.5"	216 x 140	n/a	n/a
6" x 9"	229 x 152	n/a	n/a
6-5/8" x 9-5/8"	244 x 170	n/a	n/a
7-3/8" x 9-1/4"	235 x 187	17p6 + 1p + 17p6	3p3
7" x 10"	254 x 178	16p + 1p + 16p	3p
8" x 10"	254 x 203	19p1.5 + 1p6 + 19p1.5	3p
8-1/2" x 10-7/8"	279 x 216	20p7.5 + 1p6 + 20p7.5	3p

Top margin: .667" to top of running head

Bottom margin: .85"

Drop folio: Align to outside margin, base-aligned on bottom margin

Main text font: 9.5pt/12.5, STIX Two

Alternate "Tight" version:

If page count is a concern, the following adjustments can be made to the design layout:

- Single-column width can be increased by 2 picas
- Inside margin can be decreased by 1 pica
- Outside margin can be decreased to 3p (if not already set to 3p)

Color Direction:

If color will be used in the interior design, limit the text colors to the following **(3)** choices:

- Blue (c96m26y0k39)
- Green (c100m0y83k40)
- Red (c0m100y100k30)

Color should only be used on select text elements, such as part/chapter numbers, H1s, figure numbers, etc.

**Biochemical Principles and
Mechanisms of Biosynthesis
Biodegradation of Polymers**

B. Cornils, W. A. Herrmann (Eds.)

**Applied Homogeneous Catalysis with
Organometallic Compounds**

A Comprehensive Handbook in Two Volumes

1996

ISBN: 978-3-527-29286-1

M. Beller, C. Bolm (Eds.)

Transition Metals for Organic Synthesis

Building Blocks and Fine Chemicals

1998

ISBN: 978-3-527-29501-1

A. Togni, R. L. Halterman (Eds.)

Metallocenes

1998

ISBN: 978-3-527-29539-9

P. J. Stang (Eds.)

Metal-catalyzed Cross-coupling Reactrom

1998

ISBN: 978-3-527-29421-X

B. Cornils, W. A. Herrmann (Eds.)

Applied Homogeneous Catalysis with Organometallic Compounds

A Comprehensive Handbook in Two Volumes

1996

ISBN: 978-3-527-29286-1

E. Chang, F. Hussain, T. Dillon (Eds.)

Trust and Reputation for Service-Oriented Environments

Technologies For Building Business Intelligence And Consumer Confidence

2006

ISBN: 978-3-527-01547-9

M. Beller, C. Bolm (Eds.)

Transition Metals for Organic Synthesis

Building Blocks and Fine Chemicals

1998

ISBN: 978-3-527-29501-1

B. Cornils, W. A. Herrmann (Eds.)

The Shanty Chor

A Comprehensive Handbook in Two Volumes

1996

ISBN: 978-3-527-29286-9

A. Togni, R. L. Halterman (Eds.)

Metallocenes

1998

ISBN: 978-3-527-29539-9

H. Misawa, S. Juodkazis (Eds.)

3D Laser Microfabrication

Principles and Applications

2006

ISBN: 978-3-527-31055-5

Wiley Handbooks in

FINANCIAL ENGINEERING AND ECONOMETRICS

Advisory Editor

Ruey S. Tsay

The University of Chicago Booth School of Business USA

The dynamic and interaction between financial markets around the world have changed dramatically under economic globalization. In addition, advances in communication and data collection have changed the way information is processed and used. In this new era, financial instruments have become increasingly sophisticated and their impacts are far-reaching. The recent financial (credit) crisis is a vivid example of the new challenges we face and continue to face in this information age. Analytical skills and ability to extract useful information from mass data, to comprehend the complexity of financial instruments, and to assess the financial risk involved become a necessity for economists, financial managers, and risk management professionals. To master such skills and ability, knowledge from computer science, economics, finance, mathematics and statistics is essential. As such, financial engineering is cross-disciplinary, and its theory and applications advance rapidly.

The goal of this Handbook Series is to provide a one-stop source for students, researchers, and practitioners to learn the knowledge and analytical skills they need to face today's challenges in financial markets. The Series intends to introduce systematically recent developments in different areas of financial engineering and econometrics. The coverage will be broad and thorough with balance in theory and applications. Each volume will be edited by leading researchers and practitioners in the area and covers state-of-the-art methods and theory of the selected topic.

Published Wiley Handbooks in Financial Engineering and Econometrics

Bauwens, Hafner, and Laurent · *Handbook of Volatility Models and Their Applications*

Brandimarte · *Handbook in Monte Carlo Simulation: Applications in Financial Engineering, Risk Management, and Economics*

Chan and Wong · *Handbook of Financial Risk Management: Simulations and Case Studies*

Cruz, Peters, and Shevchenko · *Fundamental Aspects of Operational Risk and Insurance Analytics: A Handbook of Operational Risk*

James, Marsh, and Sarno · *Handbook of Exchange Rates*



Mechanism of Biosynthesis

Nomenklatur der
Organischen Chemie

Edited by Hans-Georg Joost and Gerhard Eisenbrand

*in collaboration with
Gerald Böhm
Uwe Diederichsen*

Second Revised Edition

WILEY Blackwell

Monitoring

An Introduction

Gerald Böhm

WILEY Blackwell

Author

Linda E. Reichl

University of Texas
Center for Complex Quantum Systems
Austin, TX 78712
USA

Cover

Bose–Einstein condensates;
courtesy of Daniel J. Heinzen

All books published by Wiley-VCH are carefully produced. Nevertheless, authors, editors, and publisher do not warrant the information contained in these books, including this book, to be free of errors. Readers are advised to keep in mind that statements, data, illustrations, procedural details or other items may inadvertently be inaccurate.

Library of Congress Card No.: applied for

British Library Cataloguing-in-Publication Data:

A catalogue record for this book is available from the British Library.

Bibliographic information published by the Deutsche Nationalbibliothek

The Deutsche Nationalbibliothek lists this publication in the Deutsche Nationalbibliografie; detailed bibliographic data are available on the Internet at <http://dnb.d-nb.de>.

© 2016 WILEY-VCH Verlag GmbH & Co. KGaA, Boschstr. 12, 69469 Weinheim, Germany

All rights reserved (including those of translation into other languages). No part of this book may be reproduced in any form – by photoprinting, microfilm, or any other means – nor transmitted or translated into a machine language without written permission from the publishers. Registered names, trademarks, etc. used in this book, even when not specifically marked as such, are not to be considered unprotected by law.

Cover Design Formgeber, Mannheim, Germany

Typesetting le-tex publishing services GmbH, Leipzig, Germany

Printing and Binding

Print ISBN 978-3-527-41349-2

ePDF ISBN 978-3-527-69046-6

ePub ISBN 978-3-527-69048-0

Mobi ISBN 978-3-527-69047-3

oBook ISBN 978-3-527-69049-7

Printed on acid-free paper.

This edition first published 2017
© 2017

All rights reserved. No part of this publication may be reproduced, stored in a retrieval system, or transmitted, in any form or by any means, electronic, mechanical, photocopying, recording or otherwise, except as permitted by law. Advice on how to obtain permission to reuse material from this title is available at <http://www.wiley.com/go/permissions>.

The right of Jane Brown and Mark Smith to be identified as the authors of this work has been asserted in accordance with law.

Registered Offices

John Wiley & Sons, Inc., 111 River Street, Hoboken, NJ 07030, USA
John Wiley & Sons Ltd, The Atrium, Southern Gate, Chichester, West Sussex, PO19 8SQ, UK

Editorial Office

The Atrium, Southern Gate, Chichester, West Sussex, PO19 8SQ, UK

For details of our global editorial offices, customer services, and more information about Wiley products visit us at www.wiley.com.

Wiley also publishes its books in a variety of electronic formats and by print-on-demand. Some content that appears in standard print versions of this book may not be available in other formats.

Limit of Liability/Disclaimer of Warranty

While the publisher and authors have used their best efforts in preparing this work, they make no representations or warranties with respect to the accuracy or completeness of the contents of this work and specifically disclaim all warranties, including without limitation any implied warranties of merchantability or fitness for a particular purpose. No warranty may be created or extended by sales representatives, written sales materials or promotional statements for this work. The fact that an organization, website, or product is referred to in this work as a citation and/or potential source of further information does not mean that the publisher and authors endorse the information or services the organization, website, or product may provide or recommendations it may make. This work is sold with the understanding that the publisher is not engaged in rendering professional services. The advice and strategies contained herein may not be suitable for your situation. You should consult with a specialist where appropriate. Further, readers should be aware that websites listed in this work may have changed or disappeared between when this work was written and when it is read. Neither the publisher nor authors shall be liable for any loss of profit or any other commercial damages, including but not limited to special, incidental, consequential, or other damages.

Library of Congress Cataloging-in-Publication Data

Cover image:
Cover design by

Set in 9.5/12.5pt STIXTwoText by SPi Global, Pondicherry, India

10 9 8 7 6 5 4 3 2 1

to Hans-Martin



Brief Contents

List of Contributors *xi*

Foreword *xiii*

Preface *xv*

Part I Metal Oxide Nanomaterials *1*

1 The Biomimetic Synthesis of Metal Oxide Nanomaterials *3*

2 Synthesis of Symmetric and Asymmetric Nanosilica for Materials,
Optical and Medical Applications *55*

3 Sources of Natural Flavors *90*

4 Mechanism of Color Perception *110*

5 Preparation of Plant Material for Extraction *150*

6 Methods of Extraction of Essential Oils *180*

Index *000*



Contents

List of Contributors *xi*

Foreword *xiii*

Preface *xv*

Part I Metal Oxide Nanomaterials *1*

- 1 The Biomimetic Synthesis of Metal Oxide Nanomaterials** *3*
Leila F. Deravi, Joshua D. Swartz and David W. Wright
 - 1.1 Introduction *3*
 - 1.2 Metal Oxides in Nature *4*
 - 1.2.1 Components of Biomineralization *5*
 - 1.2.2 Biomineralization Optimization *6*
 - 1.3 Biomimetic Synthesis of Metal Oxide Nanomaterials *7*
 - 1.4 Constrained Biomineralization *8*
 - 1.4.1 Bacterial Synthesis of Metal Oxide Nanomaterials *8*
 - 1.4.2 Synthesis of Protein-Functionalized Ferromagnetic Co_3O_4 Nanocrystals *9*
 - 1.4.3 Room-Temperature Synthesis of Barium Titanate *10*
 - 1.4.4.1 Biomimetic Synthesis of Iron Oxide *11*
- 2 Synthesis of Symmetric and Asymmetric Nanosilica for Materials, Optical and Medical Applications** *55*
Yongquan Qu, Jennifer Lien and Ting Guo
 - 2.1 Introduction *55*
 - 2.2 Synthesis of Nanosilica *59*
 - 2.2.1 Symmetric Nanosilica *59*
 - 2.2.1.1 Catalytic Methods *63*
 - 2.2.1.2 Noncatalytic Growth *65*
 - 2.2.2 Asymmetric Silica Nanomaterials *68*
 - 2.2.2.1 Catalytic Growth *68*
 - 2.2.2.2 Noncatalytic Growth *69*
 - 2.3 Characterization *70*
 - 2.4 Applications of Symmetric and Asymmetric Nanosilica *72*

Index *000*



Contents

Foreword *xiii*

Preface *xv*

Part I Metal Oxide Nanomaterials 1

- 1 The Biomimetic Synthesis of Metal Oxide Nanomaterials 3**
 - 1.1 Introduction 3
 - 1.2 Metal Oxides in Nature 4
 - 1.2.1 Components of Biomineralization 5
 - 1.2.2 Biomineralization Optimization 6
 - 1.3 Biomimetic Synthesis of Metal Oxide Nanomaterials 7
 - 1.4 Constrained Biomineralization 8
 - 1.4.1 Bacterial Synthesis of Metal Oxide Nanomaterials 8
 - 1.4.2 Synthesis of Protein-Functionalized Ferromagnetic Co_3O_4 Nanocrystals 9
 - 1.4.3 Room-Temperature Synthesis of Barium Titanate 10
 - 1.4.4 Biomimetic Synthesis of Magnetite 11
 - 1.4.4.1 Biomimetic Synthesis of Iron Oxide 11
- 2 Synthesis of Symmetric and Asymmetric Nanosilica for Materials, Optical and Medical Applications 55**
 - 2.1 Introduction 55
 - 2.2 Synthesis of Nanosilica 59
 - 2.2.1 Symmetric Nanosilica 59
 - 2.2.1.1 Catalytic Methods 63
 - 2.2.1.2 Noncatalytic Growth 65
 - 2.2.2 Asymmetric Silica Nanomaterials 68
 - 2.2.2.1 Catalytic Growth 68
 - 2.2.2.2 Noncatalytic Growth 69
 - 2.3 Characterization 70
 - 2.4 Applications of Symmetric and Asymmetric Nanosilica 72

Index 000



Contents

Foreword *xiii*

Preface *xv*

Part I Metal Oxide Nanomaterials 1

1 The Biomimetic Synthesis of Metal Oxide Nanomaterials 3

Introduction 3

Metal Oxides in Nature 4

 Components of Biomineralization 5

 Biomineralization Optimization 6

Biomimetic Synthesis of Metal Oxide Nanomaterials 7

Constrained Biomineralization 8

 Bacterial Synthesis of Metal Oxide Nanomaterials 8

 Synthesis of Protein-Functionalized Ferromagnetic Co_3O_4 Nanocrystals 9

 Room-Temperature Synthesis of Barium Titanate 10

 Biomimetic Synthesis of Magnetite 11

 Biomimetic Synthesis of Iron Oxide 11

2 Synthesis of Symmetric and Asymmetric Nanosilica for Materials, Optical and Medical Applications 55

Introduction 55

Synthesis of Nanosilica 59

 Symmetric Nanosilica 59

 Catalytic Methods 63

 Noncatalytic Growth 65

 Asymmetric Silica Nanomaterials 68

 Catalytic Growth 68

 Noncatalytic Growth 69

Characterization 70

Applications of Symmetric and Asymmetric Nanosilica 72

Index 000



List of Contributors

Andrew B. Adams

Department of Surgery
Emory Transplant Center
Emory University School of Medicine
Atlanta
USA

Maria-Luisa Alegre, MD, PhD

Associate Professor
Department of Medicine, Section of
Rheumatology
Gwen Knapp Center for Lupus and
Immunology Research
The University of Chicago
Chicago
USA

Agnes M. Azimzadeh, PhD

Assistant Professor of Surgery
Department of Surgery
University of Maryland School of
Medicine
Baltimore
USA

William M. Baldwin III

Department of Immunology
Cleveland Clinic Lerner College of
Medicine
Department of Pathology
Case Western Reserve University
School of Medicine
Cleveland
USA

Jonathan S. Bromberg, MD, PhD

Professor of Surgery and Microbiology
and Immunology
Department of Surgery
University of Maryland School of
Medicine
Baltimore
USA

J. Michael Cecka

UCLA Immunogenetics Center
Department of Pathology and
Laboratory Medicine
David Geffen School of Medicine at
UCLA
Los Angeles
USA

Anil Chandraker, MD, FASN, FRCP

Transplant Research Center
Renal Division
Brigham and Women's Hospital
Harvard Medical School
Boston
USA

Sung Choi, MD

Blood and Marrow Transplantation
Program
Department of Internal Medicine
Division of Hematology/Oncology
University of Michigan
Comprehensive Cancer Center
Ann Arbor
USA

Anita S. Chong, PhD

Department of Surgery, Section of
Transplantation
The University of Chicago
Chicago
USA

Yaozhong Ding, PhD

Assistant Professor
Department of Surgery
University of Maryland School of Medicine
Baltimore
USA

Gunilla Einecke

Department of Nephrology
Hannover Medical School
Hannover
Germany

Robert L. Fairchild

Department of Immunology
Cleveland Clinic Lerner College of
Medicine
Department of Pathology
Case Western Reserve University
School of Medicine
Cleveland
USA

Philip F. Halloran, MD, PhD

Alberta Transplant Applied Genomics
Centre
Department of Medicine
Division of Nephrology and Transplant
Immunology
University of Alberta
Edmonton
Canada

Choli Hartono

Department of Medicine
Weill Cornell Medical College
New York
USA

Timm Heinbokel

Division of Transplant Surgery and
Transplant Surgery Research Laboratory
Brigham and Women's Hospital
Harvard Medical School
Boston
USA

Yiming Huang

Institute for Cellular Therapeutics
University of Louisville
Louisville and Duke University
Raleigh
USA

Suzanne T. Ildstad, MD

Director, Institute for Cellular Therapeutics
Jewish Hospital Distinguished
Professor of Transplantation
Distinguished University Scholar
Professor of Surgery, Physiology,
Immunology
University of Louisville
Louisville and Duke University
Raleigh
USA

Haofeng Ji

Dumont-UCLA Transplantation Center
Division of Liver and Pancreas
Transplantation, Department of Surgery,
David Geffen School of Medicine at UCLA
Los Angeles
USA

Bibo Ke

Dumont-UCLA Transplantation
Center Division of Liver and Pancreas
Transplantation, Department of
Surgery
David Geffen School of Medicine at UCLA
Los Angeles
USA

Foreword

The dilemma of rapidly emerging fields is that reviews are often outdated before they are printed. To make a contribution that would endure, we knew we had to go beyond a snapshot of the current state of fragment-based drug discovery and instead provide a framework for upcoming advances. To achieve this goal, we needed to convince leading scientists to take time from their busy schedules to write chapters. Fortunately, nearly all those we approached agreed; and what you hold in your hands is a virtual, although not comprehensive, “Who’s Who” in fragment-based drug discovery. We are extremely grateful to all of our contributors for the quality of their chapters.

One striking feature of this book is that more than half of the chapters come from industry-based researchers; and even many of the academic contributors have close ties to industry. It has been alleged that the best science is done in academia; this book proves that this is not necessarily the case. Part of the reason may be that many of the techniques involved require expensive equipment and infrastructure as well as large collaborations between scientists from disparate disciplines – collaborations that would be difficult to set up outside industry. The multidisciplinary nature of fragment-based approaches shows in this volume: contributors include computational chemists, NMR spectroscopists, X-ray crystallographers, mass-spectrometrists, as well as organic and medicinal chemists.

Although fragment-based strategies for drug discovery have now pervaded laboratories across the world, the ultimate success of any drug discovery technology is measured in the quantity and quality of drugs that it produces. Fragment-based drug discovery has only been practical for the past decade, too soon to expect it to produce marketed drugs; but we believe these will come in time. Moreover, many of the techniques and concepts described in this book will alter drug discovery endeavors in subtle, tangential ways. Ideally, readers will be inspired to improve the methods described here, or even to develop fundamentally new methods for fragment-based drug discovery. But even if this book only changes the way medicinal chemists approach lead optimization, or persuades them to look more closely at weak but validated hits, it will have served its purpose.

Basely, March 2006

Wolfgang Jahnke
Daniel A. Erlanson



Symbols and Abbreviations

Symbols

α	electron spin quantum number $m_s = 1/2$ angle, alternating parameter anisotropic exchange parameter
α_n	nuclear spin quantum number $m_I = 1/2$
β	spin quantum number $m_s = -1/2$ angle
β_n	nuclear spin quantum number $m_I = -1/2$
δ_{ij}	Kronecker δ
θ	angle Curie-Weiss constant
Δ_H	line-width
$\Delta H_{1/2}$	half height line-width
ΔH_{pp}	peak-to-peak line-width
ΔH_{msl}	maximum-slope line-width
$\Delta H\omega_{1/2}, \Delta H\omega_{pp}$	line-width in frequency
ϵ_0	dielectric constant
ϵ_F	Fermi energy
η	$ J'/J $
Γ	molecular field coefficient
γ	gyromagnetic ratio exchange interaction parameter anisotropic exchange parameter
γ_n	nuclear gyromagnetic ratio
φ	molecular orbital relaxation function
Ψ	molecular orbital
ψ	atomic orbital
ν	frequency
μ	magnetic permeability
μ_0	magnetic permeability of free space



Color Plates

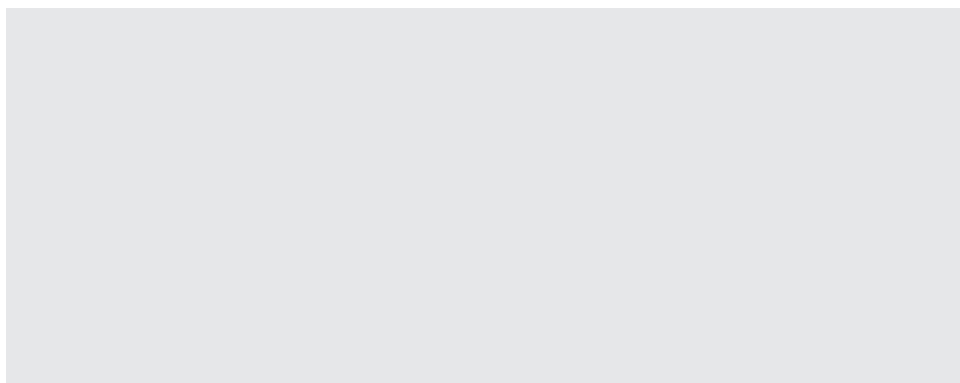


Figure 1.6 See text page 00 for full figure caption.

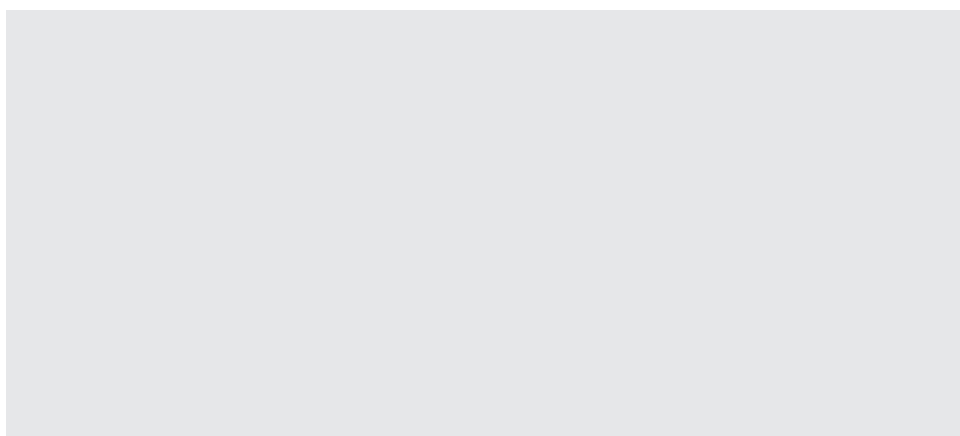
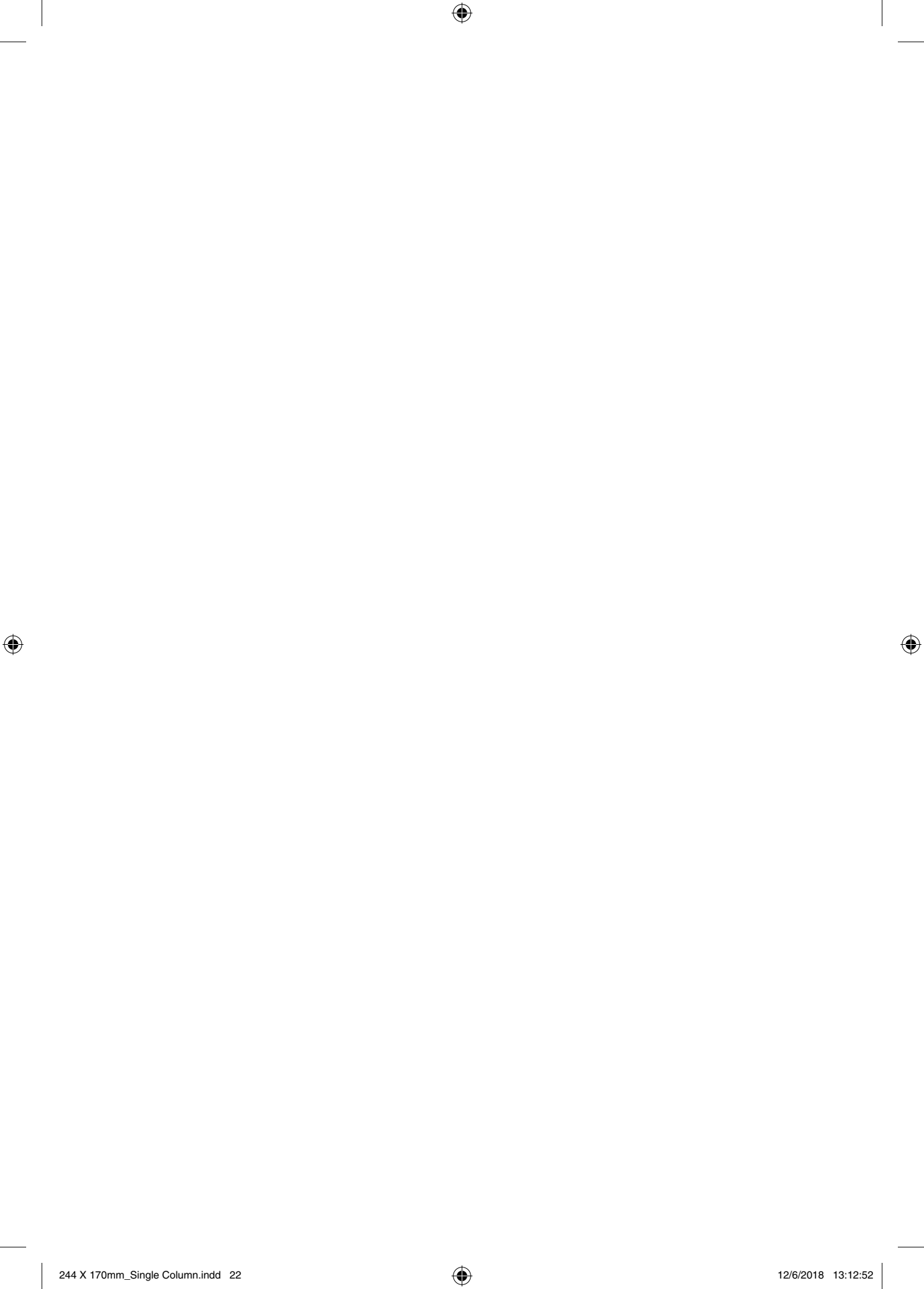


Figure 1.7 See text page 00 for full figure caption.



About the Companion Website

Practical Physiotherapy for Small Animal Practice is accompanied by a companion website:



www.wiley.com/go/

The website includes:

- Client education handouts.



Part IV

Summaries and Visions

Bold Glance into the Future—Where no Man has Gone Before



5

cDNA and Microarray-based Technologies

5.1 Introduction

The molecular characterization of tumor-associated antigens (TAA) recognized by T cells [1] revolutionized the field of tumor immune biology providing conclusive evidence that CD8+ cytotoxic T cells (CTLs) specifically recognize and kill autologous cancer through recognition of molecularly-defined cancer-specific elements.

5.1.1 CEA Gene Family, Genomic Localization, Protein Structure

CEA is encoded by the CEA-related cell-cell adhesion molecule 5 (CEACAM5) gene, which belongs to the CEA gene family and in humans consists of 22 expressed members and 12 pseudogenes [3,4].

5.1.1.1 Animal Models for CEA

Mice are commonly used to analyze the efficacy of tumor therapies and mechanisms of tumor rejection. However, this species cannot be utilized to evaluate CEA-based therapies since no CEACAM5 ortholog exists in rodents.

5.1.1.1.1 Models for CEACAM5 Containing a Bacterial Artificial Chromosome

Either cosmid clones containing the CEACAM5 gene or a bacterial artificial chromosome (BAC) clone, which comprises part of the gene cluster surrounding CEACAM5, served as a genetic source. This cluster includes CEACAM6 and CEACAM3.

Antibody Delivery of Radionuclides, Drugs and Effector Molecules The use of low molecular weight single chain antibody fragments and pre-targeting has been found to enhance the sensitivity of tumor visualization as well as increasing the delivered therapeutic dose by separating the antibody therapeutic radionuclide that binds to the tumor-localized antibody.

SubParagraph Title: Nuclear Angular Momentum and Magnetic Moment The conformational flexibility of calixarenes is usually explained by the presence of intramolecular hydrogen bonds, which is related to the number of free phenol groups. Accordingly, calixarenes containing four phenol groups 39a–e exist as cone conformers.

Book Title: Subtitle, First Edition. Edited by Author/Editor Name.

© 2015 John Wiley & Sons, Ltd. Published 2015 by John Wiley & Sons, Ltd.



5

cDNA and Microarray-based Technologies

Introduction

The molecular characterization of tumor-associated antigens (TAA) recognized by T cells [1] revolutionized the field of tumor immune biology providing conclusive evidence that CD8+ cytotoxic T cells (CTLs) specifically recognize and kill autologous cancer through recognition of molecularly-defined cancer-specific elements.

CEA Gene Family, Genomic Localization, Protein Structure

CEA is encoded by the CEA-related cell-cell adhesion molecule 5 (CEACAM5) gene, which belongs to the CEA gene family and in humans consists of 22 expressed members and 12 pseudogenes [3,4].

Animal Models for CEA

Mice are commonly used to analyze the efficacy of tumor therapies and mechanisms of tumor rejection. However, this species cannot be utilized to evaluate CEA-based therapies since no CEACAM5 ortholog exists in rodents. This problem was circumvented by introducing the human CEACAM5 gene into the germ line of mice [52–54].

Models for CEACAM5 Containing a Bacterial Artificial Chromosome

Either cosmid clones containing the CEACAM5 gene or a bacterial artificial chromosome (BAC) clone, which comprises part of the gene cluster surrounding CEACAM5, served as a genetic source. This cluster includes CEACAM6 and CEACAM3.

Antibody Delivery of Radionuclides, Drugs and Effector Molecules Delivery of radio-nuclides to tumors using murine and human anti-CEA antibodies has been studied for many years [70]. The use of low molecular weight single chain antibody fragments and pre-targeting has been found to enhance the sensitivity of tumor visualization as well as increasing the delivered therapeutic dose by separating the antibody targeting to the tumor from the subsequent delivery of the therapeutic radionuclide that binds to the tumor-localized antibody.

SubParagraph Title: Nuclear Angular Momentum and Magnetic Moment The conformational flexibility of calixarenes is usually explained by the presence of intramolecular hydrogen bonds, which is related to the number of free phenol groups. Accordingly, calixarenes, containing four phenol groups 39a–e exist as cone conformers.

Delivery of radio-nuclides to tumors using murine and human anti-CEA antibodies has been studied for many years [70]. The use of low molecular weight single chain antibody fragments and pre-targeting has been found to enhance the sensitivity of tumor visualization as well as increasing the delivered therapeutic dose by separating the antibody targeting to the tumor from the subsequent delivery of the therapeutic radionuclide that binds to the tumor-localized antibody.

11

Carcinoembryonic Antigen

Decoding the CEA-Related Cell-Cell Adhesion Molecule

The molecular characterization of tumor-associated antigens (TAA) recognized by T cells [1] revolutionized the field of tumor immune biology providing conclusive evidence that CD8+ cytotoxic T cells (CTLs) specifically recognize and kill autologous cancer through recognition of molecularly-defined cancer-specific elements. Since then a myriad of TAA have been identified that has triggered their utilization as anti-cancer vaccines [2–8].

11.1 CEA Biology

11.1.1 CEA Gene Family, Genomic Localization, Protein Structure

CEA is encoded by the CEA-related cell-cell adhesion molecule 5 (CEACAM5) gene, which belongs to the CEA gene family and in humans consists of 22 expressed members and 12 pseudogenes [3,4]. The CEA family has been subdivided into the CEACAM and pregnancy-specific glycoprotein (PSG) subgroups.

11.1.2 CEA as a Tumor Marker for Prognosis and Post-surgery Follow-up

11.1.2.1 Animal Models for CEA

Antibody Delivery of Radionuclides, Drugs and Effector Molecules Using Murine and Human Anti-CEA Antibodies Delivery of radio-nuclides to tumors using murine and human anti-CEA anti-bodies has been studied for many years [70]. The use of low molecular weight single chain antibody fragments and pre-targeting has been found to enhance the sensitivity of tumor visualization as well as increasing the delivered therapeutic dose by separating the antibody targeting to the tumor from the subsequent delivery of the therapeutic radionuclide that binds to the tumor-localized antibody. The use of low molecular weight single chain antibody fragments and pre-targeting has been found to enhance the sensitivity of tumor visualization as well as increasing.

The use of low molecular weight single chain antibody fragments and pre-targeting has been found to enhance the sensitivity of tumor visualization as well as increasing the delivered therapeutic dose by separating the antibody targeting to the tumor from the subsequent delivery of the therapeutic radionuclide that binds to the tumor-localized antibody.



2

Trust and Reputation for Service-Oriented Environments Technologies for Building Business Intelligence and Consumer Confidence

Fillers, Filled Polymers and Polymer Blends and Furthermore Nuclear
Angular Momentum and Magnetism

2.1 Intermolecular Interactions Physical Picture, Computational Methods and Model Potentials Nuclear Angular Momentum and Magnetic Moment

The molecular characterization of tumor-associated antigens (TAA) recognized by T cells [1] revolutionized the field of tumor immune biology providing conclusive evidence that CD8+ cytotoxic T cells (CTLs) specifically recognize and kill autologous cancer through recognition of molecularly-defined cancer-specific elements. Since then a myriad of TAA have been identified that has triggered their utilization as anti-cancer vaccines [2–8].

2.1.1 Networking and Online Games Understanding and Engineering Multiplayer Internet Games Nuclear Angular Momentum and Magnetic Moment

CEA is encoded by the CEA-related cell-cell adhesion molecule 5 (CEACAM5) gene, which belongs to the CEA gene family and in humans consists of 22 expressed members and 12 pseudogenes [3,4]. The CEA family has been subdivided into the CEACAM and pregnancy-specific glycoprotein (PSG) subgroups.

2.1.1.1 Nuclear Angular Momentum and Magnetic Moment Respectively the Digital Photographer's Guide to Color Management

Apically expressed CEA on normal epithelial cells is shed into the lumen possibly by the action of phospholipases and through the exfoliation of turned-over cells. Thus CEA does not have access the bloodstream. Expression on less differentiated unpolarized tumor cells, however, allows released CEA to enter blood and lymphatic vessels through the intercellular spaces, which can lead to elevated CEA concentrations in the sera of tumor patients.

Fillers, Filled Polymers and Polymer Blends and Furthermore Nuclear Angular Momentum and Magnetism CEA is encoded by the CEA-related cell-cell adhesion molecule 5 (CEACAM5) gene, which belongs to the CEA gene family and in humans consists of 22 expressed members and 12 pseudogenes [3,4]. In the past, the CEA family has been subdivided into the CEACAM and pregnancy-specific glycoprotein (PSG) subgroups.

Book Title: Subtitle, First Edition. Edited by Author/Editor Name.

© 2015 John Wiley & Sons, Ltd. Published 2015 by John Wiley & Sons, Ltd.

11

Carcinoembryonic Antigen

Decoding the CEA-Related Cell-Cell Adhesion Molecule

The molecular characterization of tumor-associated antigens (TAA) recognized by T cells [1] revolutionized the field of tumor immune biology providing conclusive evidence that CD8⁺ cytotoxic T cells (CTLs) specifically recognize and kill autologous cancer through recognition of molecularly-defined cancer-specific elements. Since then a myriad of TAA have been identified that has triggered their utilization as anti-cancer vaccines [2–8].

11.1 CEA Biology

11.1.1 CEA Gene Family, Genomic Localization, Protein Structure

CEA is encoded by the CEA-related cell-cell adhesion molecule 5 (CEACAM5) gene, which belongs to the CEA gene family and in humans consists of 22 expressed members and 12 pseudogenes [3,4]. The CEA family has been subdivided into the CEACAM and pregnancy-specific glycoprotein (PSG) subgroups.

11.1.2 CEA as a Tumor Marker for Prognosis and Post-surgery Follow-up

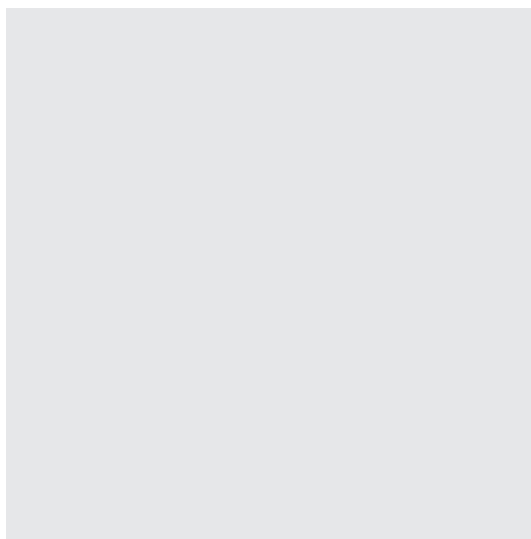
11.1.2.1 Animal Models for CEA

Antibody Delivery of Radionuclides, Drugs and Effector Molecules Using Murine and Human Anti-CEA Antibodies Delivery of radio-nuclides to tumors using murine and human anti-CEA anti-bodies has been studied for many years [70]. The use of low molecular weight single chain antibody fragments and pre-targeting has been found to enhance the sensitivity of tumor visualization as well as increasing the delivered therapeutic dose by separating the antibody targeting to the tumor from the subsequent delivery of the therapeutic radionuclide that binds to the tumor-localized antibody. The use of low molecular weight single chain antibody fragments and pre-targeting has been found to enhance the sensitivity of tumor visualization as well as increasing. The use of low molecular weight single chain antibody fragments and pre-targeting has been found to enhance the sensitivity of tumor visualization as well as increasing the delivered therapeutic dose by separating the antibody targeting to the tumor from the subsequent delivery of the therapeutic radionuclide that binds to the tumor-localized antibody.

11

Carcinoembryonic Antigen

Decoding the CEA-Related Cell-Cell Adhesion Molecule



The molecular characterization of tumor-associated antigens (TAA) recognized by T cells [1] revolutionized the field of tumor immune biology providing conclusive evidence that CD8+ cytotoxic T cells (CTLs) specifically recognize and kill autologous cancer through recognition of molecularly-defined cancer-specific elements. Since then a myriad of TAA have been identified that has triggered their utilization as anti-cancer vaccines [2–8].

11.1 CEA Biology

11.1.1 CEA Gene Family, Genomic Localization, Protein Structure

CEA is encoded by the CEA-related cell-cell adhesion molecule 5 (CEACAM5) gene, which belongs to the CEA gene family and in humans consists of 22 expressed members and 12 pseudogenes [3,4]. The CEA family has been subdivided into the CEACAM and pregnancy-specific glycoprotein (PSG) subgroups.

11.1.2 CEA as a Tumor Marker for Prognosis and Post-surgery Follow-up

11.1.2.1 Animal Models for CEA

Antibody Delivery of Radionuclides, Drugs and Effector Molecules Using Murine and Human Anti-CEA Antibodies Delivery of radio-nuclides to tumors using murine and human anti-CEA anti-bodies has been studied for many years [70]. The use of low molecular weight single chain antibody fragments and pre-targeting has been found to enhance the sensitivity of tumor visualization as well as increasing the delivered therapeutic dose by separating the antibody targeting to the tumor from the subsequent delivery of the therapeutic radionuclide that binds to the tumor-localized antibody. The use of low molecular weight single chain antibody fragments and pre-targeting has been found to enhance the sensitivity of tumor visualization as well as increasing. The use of low molecular weight single chain antibody fragments and pre-targeting has been found to enhance the sensitivity of tumor visualization as well as increasing the delivered therapeutic dose by separating the antibody targeting to the tumor from the subsequent delivery of the therapeutic radionuclide that binds to the tumor-localized antibody.

11

Carcinoembryonic Antigen

Wolfgang Zimmermann^{1,3} and Robert Kammerer²

¹ Helmholtz Centre for Infection Research, Department of Systems Immunology, Inhoffenstr. 7, 38124, Braunschweig, Germany

² Bio Center for Life Science, University of Technology Braunschweig, Spielmannstr. 7, 38106, Braunschweig, Germany

³ Institute for Molecular and Clinical Immunology, Otto-von-Guericke University, Leipziger Str. 44, 39120, Magdeburg, Germany

The very essence of cardiovascular practice is the early detection of heart failure

Sir Thomas Lewis, 1933

11.1 Introduction

The molecular characterization of tumor-associated antigens (TAA) recognized by T cells [1] revolutionized the field of tumor immune biology providing conclusive evidence that CD8+ cytotoxic T cells (CTLs) specifically recognize and kill autologous cancer through recognition of molecularly-defined cancer-specific elements.

11.2 CEA Biology

11.2.1 CEA Gene Family, Genomic Localization, Protein Structure

CEA is encoded by the CEA-related cell-cell adhesion molecule 5 (CEACAM5) gene, which belongs to the CEA gene family and in humans consists of 22 expressed members and 12 pseudogenes [3,4]. The CEA family has been subdivided into the CEACAM and pregnancy-specific glycoprotein (PSG) subgroups. Apically expressed CEA on normal epithelial cells is shed into the lumen possibly by the action of phospholipases and through the exfoliation of turned-over cells. Thus CEA does not have access the bloodstream. Expression on less differentiated unpolarized tumor cells, however, allows released CEA to enter blood and lymphatic vessels through the intercellular spaces, which can lead to elevated CEA concentrations in the sera of tumor patients.

Book Title: Subtitle, First Edition. Edited by Author/Editor Name.

© 2015 John Wiley & Sons, Ltd. Published 2015 by John Wiley & Sons, Ltd.

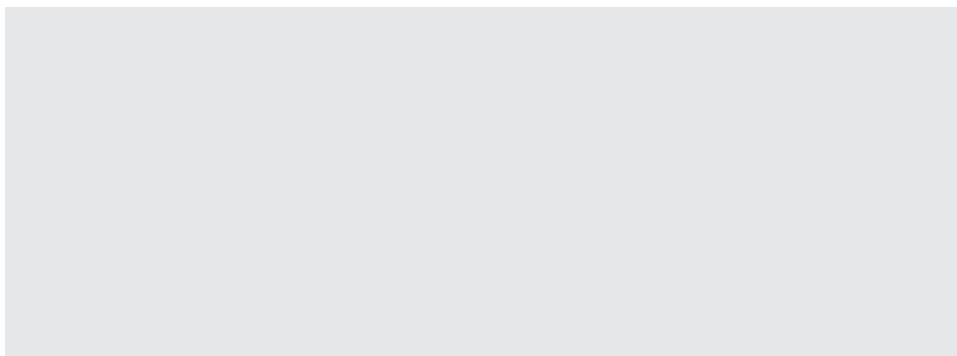


Figure 1.6 Illustration of catalytically grown β -Ga₂O₃ nanoparticles. *Source:* Reprinted with permission from Ref. [38]; © 2007 American Chemical Society.

Traditionally, synthetic approaches for the production of functional metal oxide materials have involved are estimated to reach an outstanding US \$100 billion per Figure 1.6 facility by the year 2020, as the demand for smaller, lighter and faster materials continues to grow [1]. But, more importantly, manufacturers are progressing in this manner at the expense of the environment, as they accumulate hazardous chemical wastes [2]. For decades, research teams in the semiconductor industry have been seeking alternative methods to passivate not only the rate of waste production but also the cost of spending. As mentioned above, the photoresist should be thin according to the distance of localization of the optical near-field around the nanoaperture. On the other hand, the photoresist should have the dry etching resistance so that the latent image can be transferred to the lower layer substrate. To separate the function of the Figure 1.7 thin film and the dry etching resistance, we used a trilayer resist process; the upper layer is an ultrathin photoresist, the middle layer is thin spin on glass (SOG), and the lower layer is a resin.

As mentioned above, the photoresist should be thin according to the distance of localization of the optical near-field around the nanoaperture. On the other hand, the photoresist should have the dry etching resistance so that the latent image can be transferred to the

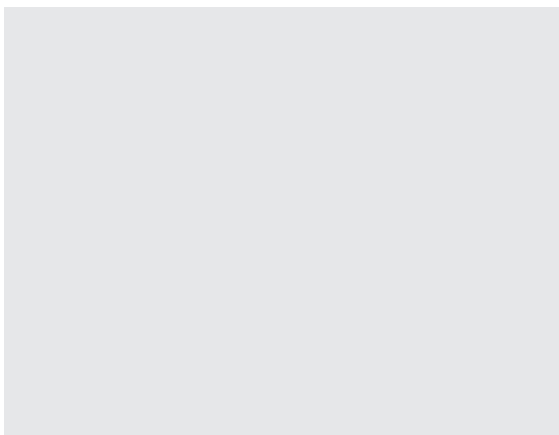


Figure 1.7 Transmission electron microscopy images (scale bar = 20 nm) of magnetosomes from various bacterial strains. (a) Pseudo-hexagonal prism; (b) Cubo-octahedral crystal; (c) \hat{A} Tooth-shaped. Transmission electron microscopy images (scale bar = 20 nm) of magnetosomes from various bacterial strains. *Source:* Reproduced with permission from Ref. [17]; © 2007, Wiley-VCH Verlag GmbH & Co. KGaA.

lower layer substrate. To separate the function of the thin film and the dry etching resistance, we used a trilayer resist process; the upper layer is an ultrathin photoresist, the middle layer is thin spin on glass (SOG), and the lower layer is a resin. The patterns of shallow latent images in the upper layer are transferred to the thin SOG layer of excellent dry-etching resistance, and these are transferred in the lower layer further.

Traditionally, synthetic approaches for the production of functional metal oxide materials have involved high-temperature reaction environments with energy intensive techniques such as laser ablation, ion implantation, chemical vapor deposition (CVD), photolithography or thermal decomposition [1]. The incorporation of these techniques has provided a rapid prototyping technique, essential for the commercial development of current minimum feature-sized semiconducting integrated circuits. However, the production of these devices has been achieved at a high price, with the primary challenges currently faced by high-throughput fabrication laboratories including the high cost of laborers and instruments, high temperature reaction conditions, and a surplus in generated waste [1]. In fact, the cost of fabrication facilities are estimated to reach an outstanding US \$100 billion per facility by the year 2020, as the demand for smaller, lighter and faster materials continues to grow [1]. But, more importantly, manufacturers are progressing in this manner at the expense of the environment, as they accumulate hazardous chemical wastes [2]. For decades, research teams in the semiconductor industry have been seeking alternative methods to passivate not only the rate of waste production but also the cost of spending.

As mentioned above, the photoresist should be thin according to the distance of localization of the optical near-field around the nanoaperture. On the other hand, the photoresist should have the dry etching resistance so that the latent image can be transferred to the lower layer substrate. To separate the function of the thin film and the dry etching resistance, we used a trilayer resist process; the upper layer is an ultrathin photoresist, the middle layer is thin spin on glass (SOG), and the lower layer is a resin. The patterns of shallow latent images in the upper layer are transferred to the thin SOG layer of excellent dry-etching resistance, and these are transferred in the lower layer further.

Figure 1.8 shows the appearance of a prototype device of optical near-field lithography [7]. The features of the prototype device are as follows. This device is compact, with a footprint of about 2m [1]. It has symmetric structure to compensate thermal expansion and temperature drift, and the hanging controlling structure is introduced to avoid floor vibrations. In addition, it has a double clean structure, and the near-field photomask and the wafer are kept in a local clean environment by controlling a flow of clean air of the device inside.

Bioinspired research is based on identifying and emulating the principles of biomineralization in natural systems, instead of copying them directly. In fact, most strategies incorporated by natural systems are not directly applicable to engineered materials, so the need for alternative synthetic routes are required for the incorporation of non-natural elements, such as barium, nickel, copper or aluminum, with functional nanoscale properties [1,8]. From a materials perspective, highly intact biological structures such as diatoms, bacteria, proteins or butterfly wings provide an excellent source of inspiration for their synthesis. In this chapter we have included the details of a wide variety of mediated nanomaterial syntheses, their response to variable parameters, and their ability to retain a functionalized, controlled stability over time.

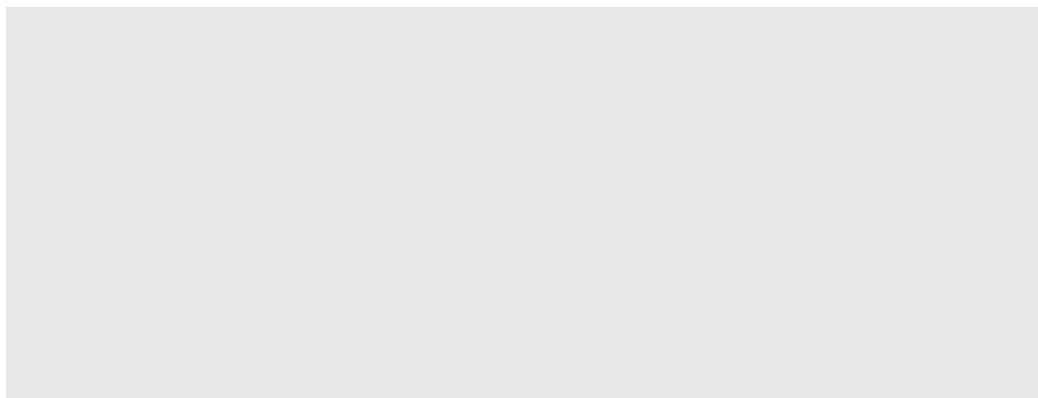


Figure 1.8 Appearance of a prototype device of optical near-field lithography.

As mentioned above, the photoresist should be thin according to the distance of localization of the optical near-field around the nanoaperture. On the other hand, the photoresist should have the dry etching resistance so that the latent image can be transferred to the lower layer substrate. To separate the function of the thin film and the dry etching resistance, we used a trilayer resist process; the upper layer is an ultrathin photoresist, the middle layer is thin spin on glass (SOG), and the lower layer is a resin. The patterns of shallow latent images in the upper layer are transferred to the thin SOG layer of excellent dry-etching resistance, and these are transferred in the lower layer further.

Figure 1.8 shows the appearance of a prototype device of optical near-field lithography [7]. The features of the prototype device are as follows. This device is compact, with a footprint of about 2m [2]. It has symmetric structure to compensate thermal expansion and temperature

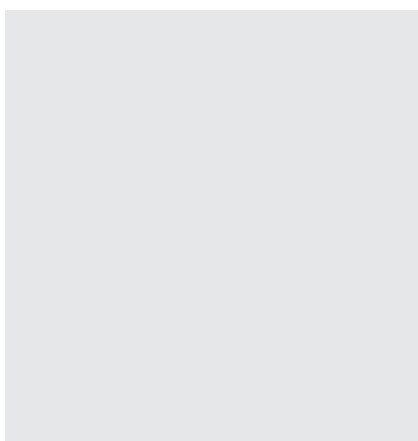


Figure 1.9 Distribution of structures for variable pH samples. *Source:* Reprinted with permission from Ref. [33]; © 2007, American Chemical Society.

Figure 1.10 (a) Inside the prototype device of the near-field lithography. (b) Illumination of i-line light for exposure from the back side of the near-field photomask. (c) Close-up from the side of the near-field photomask and the photoresist on the wafer. They are brought into contact with each other within the localizing distance of the optical near-field.

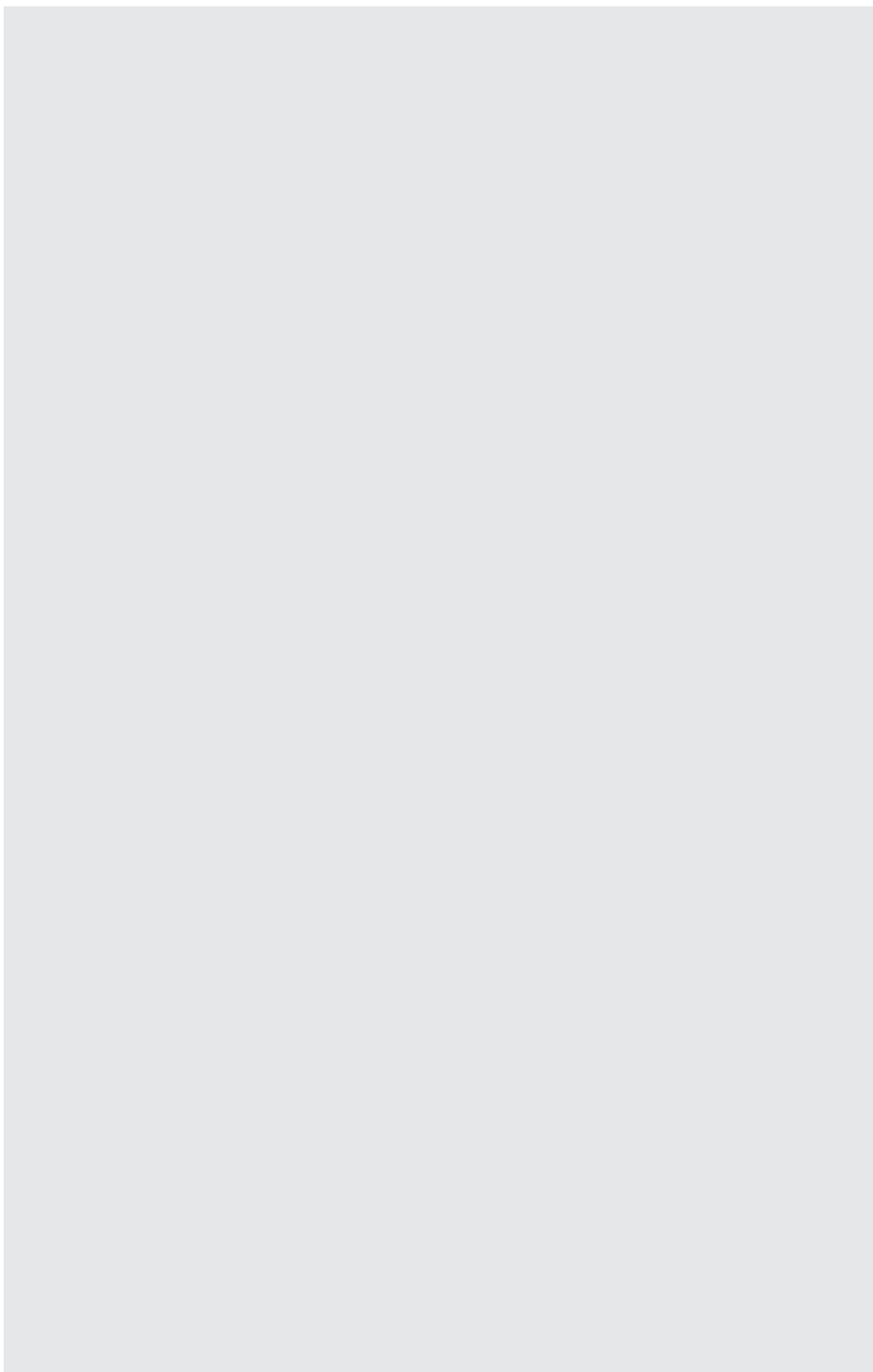


Table 1.1 Results for the comparison of processes.

Performance metric	NH ₃	CH ₄	C ₃ H ₈ ref.	C ₃ H ₈ POX
Energy efficiency	27%	30%	23%	16%
Volumetric fuel energy density (Wh l ⁻¹)	1570	170	1740	1920
Gravimetric fuel energy density (Wh kg ⁻¹)	2580	1610	2540	3900
Volumetric system energy density (Wh l ⁻¹)	1510	130	1650	1800
Gravimetric system energy density (Wh kg ⁻¹)	2370	320	2320	3340

drift, and the hanging controlling structure is introduced to avoid floor vibrations. In addition, it has a double clean structure, and the near-field photomask and the wafer are kept in a local clean environment by controlling a flow of clean air of the device inside.

Bioinspired research is based on identifying and emulating the principles of biomineralization in natural systems, Figure 1.9 instead of copying them directly. In fact, most strategies incorporated by natural systems are not directly applicable to engineered materials, so the need for alternative synthetic routes are required for the incorporation of non-natural elements, such as barium, nickel, copper or aluminum, with functional nanoscale properties [1,8]. Table 1.1 from a materials perspective, highly intact biological structures such as diatoms, bacteria, proteins or butterfly wings provide an excellent source of inspiration for their synthesis. In this chapter we have included the details of a wide variety of mediated nanomaterial syntheses, their response to variable parameters, and their ability to retain a functionalized, controlled stability over time.

The lowest system energy densities. Both the system and fuel volumetric energy densities of methane direct oxidation are very low, due to the large volume required for the storage of the gases (methane and oxygen). Moreover, the gravimetric fuel energy density of methane is

Table 1.2 Propagation rate constants (k_p) and the selectivity parameters ($\beta = k_p/k_{tr1}$) for the polymerization of ϵ -caprolactone [95].^{a)}

Active species	$\frac{k_p}{L \text{ mol}^{-1} \text{ s}^{-1}}$	$b = \frac{k_p}{k_{tr1}} / \frac{L \text{ mol}^{-1}}{L \text{ mol}^{-1}}$
...-(CH ₂) ₅ O ⁻ Na ⁺	□1.70	1.6×10^3
...-(CH ₂) ₅ O-Sm[O(CH ₂) ₅ -...] ₂	2.00	2.0×10^3
...-(CH ₂) ₅ O-Al(C ₂ H ₅) ₂	0.03	4.6×10^4
...-(CH ₂) ₅ O-Al[CH ₂ CH(CH ₃) ₂] ₂	0.03	7.7×10^4
...-(CH ₂) ₅ O-Al[O(CH ₂) ₅ -...] ₂	0.50	3.0×10^5
...-(CH ₂) ₅ O-AlO ₂ SB ^{b)}	0.35	□10 ⁶

a) Polymerization conditions: 20°C, THF solvent.

b) Polymerization conditions: 80°C, THF solvent, SBO2: (S)-(+)-2,2'-[1,1'-binaphthyl-2,2'-diylbis-(nitrylomethylidyne)]-diphenolate ligand (A. Duda and A. Kowalski, unpublished results). SB=Schiff's base.

Table 1.3 Results for the comparison of processes.

Performance metric	NH ₃	CH ₄	C ₃ H ₈ ref.	C ₃ H ₃ POX
Energy efficiency	27%	30%	23%	16%
Volumetric fuel energy density (Wh l ⁻¹)	1570	170	1740	1920
Gravimetric fuel energy density (Wh kg ⁻¹)	2580	1610	2540	3900
Volumetric system energy density (Wh l ⁻¹)	1510	130	1650	1800
Gravimetric system energy density (Wh kg ⁻¹)	2370	320	2320	3340

Data from Higinbotham et al. 1967. The membrane potential was measured as – 110 mV Table from Taiz & Zeiger Thrid Ed Table 6.1

Table 1.4 Results for the comparison of processes.

R of functional molecule ^a	Cycle	Catalyst ^b	Conversion (%)	M _n (kg mol ⁻¹)	M _w /M _n	Reference
CH ₃ , CH=CH ₂ , (CH ₂) ₃ COOH	D ₄	SR	~90	10–43	—	[87]
CH=CH ₂ , (CH ₂) ₃ NHSi(CH ₃) ₃ , (CH ₂) ₃ -acrylate, (CH ₂) ₃ COOH	D ₄	SR	80–90	0.8–1.2	1.4–1.9	[57]
H	D ₄	AC	80	8	1.9	[88]
H, CH ₃ , CH=CH ₂ , (CH ₂) ₃ COOH	D ₄	SR	—	—	—	[89]

a) The chain-terminating agent has the following structure: R–Si(CH₃)₂–O–Si(CH₃)₂–R, unless stated in the table.

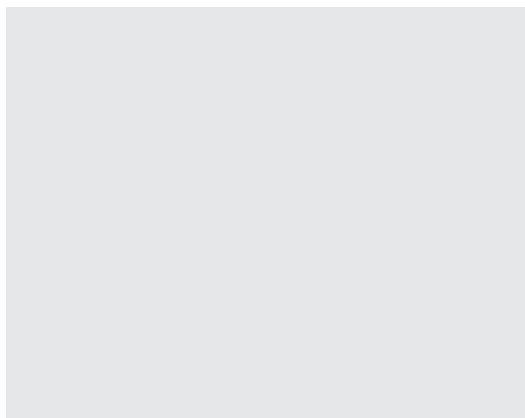
b) SR: sulfonic resin; AC: activated clay.

low, due to the mass of oxygen which is accounted for [2]. The large difference in gravimetric energy density of methane direct oxidation is due to the mass of the gas Table 1.2 cartridges. Despite lower energy conversion efficiency, the propane-based processes lead to higher energy densities than the ammonia-based process, because of the intrinsic difference in energy density between the two fuels. From a materials perspective, highly intact biological structures such as diatoms, bacteria. In this chapter we have included the details of a wide variety of mediated nanomaterial syntheses, their response to variable parameters, and their ability to retain a functionalized, controlled stability over time. With the exception of the

Table 1.5 Results for the comparison of processes.

Characteristic	Issues	Needs
Laminar flows	Mixing relies on molecular diffusion only and is slow	Efficient micromixers of low pressure drop
Small size	Difficult to load enough catalyst and ensure complete conversion	Develop deposition schemes and structures to load enough catalyst; high integration of reactor(s) and separation units for compact systems; fast chemistry/process; very active (and selective) catalyst.
Reactors shake in portable devices	Moveable parts break; bypass from pellet settling can occur	Monolithic structures with no moveable parts
High pressure drop	Pressure drop increases with decreasing pellet size	Open (extruded monolith-like) geometries
Transient operation very common	Most designs rely on steady state operation and control; catalysts, which are stable under steady state conditions, may deactivate during start up and shut down; start-up can be slow.	Get heat in and out of the system quickly; develop appropriate designs and strategies; models for dynamics.

Figure 1.11 Distribution of structures for variable pH samples. *Source:* Reprinted with permission from Ref. [33]; © 2007, American Chemical Society.



process requiring gas storage, the fuel energy density and system energy density give the same qualitative comparison among processes.

Thus, replicates on the same array and replicates in different experiments should not be mixed since they have different characteristics and cannot be treated as independent replicates. Important issues are:

- are the distributional assumptions valid is the number of replicates sufficient to detect the fold change that you are interested in?
- are the replicates independent of each other?
 - is the number of replicates sufficient to detect the fold change because it does not conversion efficiency that you are interested in?
 - are outliers removed from the samples?

Most commonly, modifications of four different tests are applied in microarray data analysis. These tests are implemented in statistical software packages such as R/Bioconductor or SAS:

- 1) Student's t-test is the number of replicates sufficient to detect the fold change that you are interested
- 2) Welch's test is the number of replicates sufficient to detect the fold because it does not conversion efficiency change that you are interested
- 3) Permutation tests.

While the first two tests assume Gaussian distributed data and the P -values are calculated by a probability distribution, the latter two are nonparametric and the P -values are calculated based on combinatorial arguments.

- | | |
|-----------------------------------|--------------------|
| • Distilled water | 23.3 μl |
| • 10 \times PCR buffer | 4.0 μl |
| • dNTP Mix (FDD) | 0.3 μl |
| • H-AP primer (2 μM)* | 4.0 μl |
| • H-T11M (2 μM) | 4.0 μl |
| • cDNA template | 4.0 μl |
| • Taq DNA polymerase | 0.4 μl |
| • Total volume | 40.0 μl |

Table 1.6 Species of marine invertebrates containing glycolipids.

Phylum	Subphylum	Class	Trivial name	Species
Chordata	Tunicata	Ascidacea	Tunicate	<i>Microcosmus sulcatus</i> (now accepted <i>M. vulgaris</i> ⁽¹⁾) <i>Phallusia fumigata</i>
Cnidaria	—	Anthozoa	Soft coral	1) <i>Lobophytum crassum</i> 2) <i>Lobophytum</i> sp. 3) <i>Sarcophyton ehrenbergi</i> 4) <i>Metridium senile</i>
Echinodermata	Asterozoa	Asteroidea	Sea anemone Starfish	• <i>Acanthaster planci</i> • <i>Allostichaster inaequalis</i> • <i>Anasterias minuta</i> • <i>Aphelasterias japonica</i> • <i>Asterias amurensis</i> • <i>Asterias amurensis versicolor</i> • <i>Asterias rubens</i> • <i>Stellaster equestris</i>
		Ophiuroidea	Brittle star	<i>Ophiocoma scolopendrina</i>
	Crinozoa	Crinoidea	Feather star	<i>Comanthus japonica</i> (now accepted <i>Oxycomanthus japonicus</i> ⁽¹⁾) <i>Comanthina schlegeli</i> (now accepted <i>Comaster schlegelii</i>)

Source: Queen Square Brain Bank.

Both the system and fuel volumetric energy densities of methane direct oxidation are very low, due to the large volume required for the storage of the gases (methane and oxygen). Moreover, the gravimetric fuel energy density of methane is low, due to the mass of oxygen which is accounted for [2]. The large difference in gravimetric energy density of methane direct oxidation is due to the mass of the gas cartridges.

Yields, and reaction specificities. The first detailed study of the mechanism of these “on water” reactions has now been reported by Jung and Marcus [10]. Synthetic aqueous organic synthesis was born, also because efficient work-up procedures are possible for these “on water” reactions. For a general review, the reader is referred to Chapter 7.

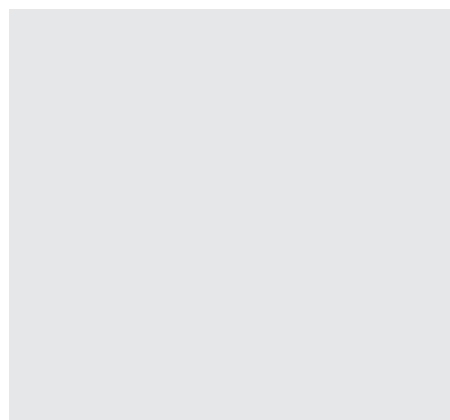


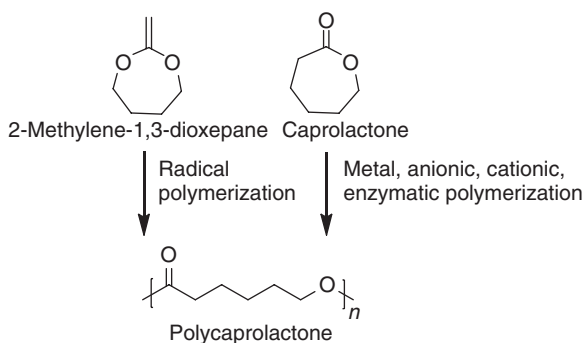
Figure 1.12 Distribution of structures for variable pH samples. *Source:* Reprinted with permission from Ref. [33]; © 2007, American Chemical Society.

11.3 Water, the Ultimate Green Solvent

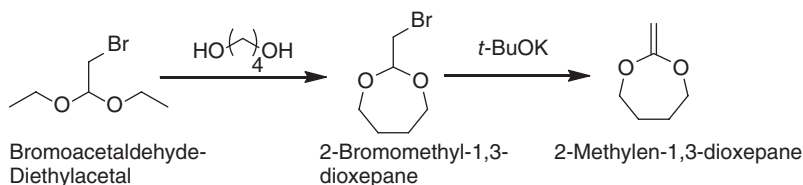
Fredrik Nilsson

In the second half of the 1990s, it was recognized that “benign by design” was too strongly restricted to environmental care, and Anastas and Williamson [13] even concluded, “one obvious but important point: nothing is benign.” The holistic concept of green chemistry became accepted world-wide. Although attempts have been made to quantify the degree of greenness, particularly by Sheldon [15], it has not been found possible to include the many complex factors that determine “greenness” in generally applicable parameters.

Aspirin as a Household Remedy Against Fever, Inflammation, and Pain Soon after the introduction of ASA into medical use under the brandname “aspirin,” Anastas in his many influential publications.



Scheme 1.31



Scheme 1.32

... As soon as you feel yourself ill, you should go to bed and have a hot-water bottle at your feet. You should drink hot chamomilae tea or grog in order to sweat and should take 3 tablets of aspirin a day. If you follow these instructions you will recover with in a few days, in most cases...

Kölner Stadtanzeiger, March 6, 1924

This extract is remarkable for several reasons: during the past 25 years of practical use, aspirin had become a drug whose name was not only well known to health professionals but also to the general public.

Certainly, the flu pandemia with millions of victims alone in Europe at the beginning of the last century as well as the limited availability of antipyretic analgesics other than aspirin contributed to this. However, the compound was generally recommended—and accepted—by the lay man and doctors—as a household remedy for treating pain, fever, inflammation, and many other kinds of feeling bad, although essentially nothing was known about the mechanisms of Anastas in his many influential publications. The holistic concept of green chemistry became accepted world-wide. Although attempts have been made to quantify the degree of greenness, particularly by action behind these multiple activities of the drug.

Thus, replicates on the same array and replicates in different experiments should not be mixed since they have different characteristics and cannot be treated as independent replicates. Important issues are:

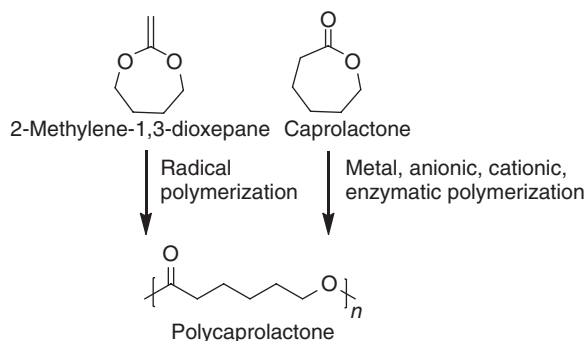
Most commonly, modifications of four different tests are applied in microarray data analysis. These tests are implemented in statistical software packages such as R/Bioconductor or SAS.

The conformational flexibility of calixarenes is usually explained by the presence of intramolecular hydrogen bonds, which is related to the number of free phenol groups. Accordingly, calixarenes containing four phenol groups 39a–e exist as cone conformers.

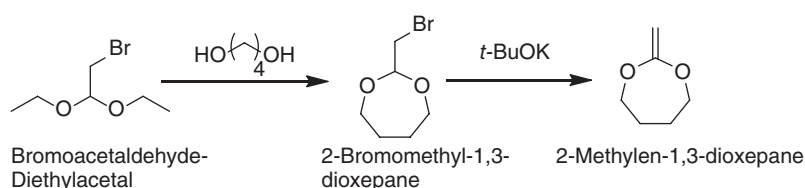
$$\rho(z)v_w = \rho_w^{\text{bulk}} v_w \exp(-v_w \beta [\pi(z) - \pi^{\text{bulk}}]) \quad (2.17)$$

$$\rho(z)v_w = \rho_w^{\text{bulk}} v_w \exp(-v_w \beta [\pi(z) - \pi^{\text{bulk}}]) - q_i \beta [\psi(z) - \psi^{\text{bulk}}] \quad (2.18)$$

Both the system and fuel volumetric energy densities of methane direct oxidation are very low, due to the large volume required for the storage of the gases (methane and oxygen). Moreover, the gravimetric fuel energy density of methane is low, due to the mass of oxygen which is accounted for [2]. The comparison of the two idealized possibilities for propane fuel processing reactions shows that energy conversion efficiency is not a suitable metric for man-portable applications, because it does not account for the water weight and volume;



Scheme 1.31



Scheme 1.32

the higher energy efficiency of steam reforming is due to the generation of additional hydrogen in the reactor.

The lowest system energy densities. Both the system and fuel volumetric energy densities of methane direct oxidation are very low, due to the large volume required for the storage of the gases (methane and oxygen). Moreover, the gravimetric fuel energy density of methane is low, due to the mass of oxygen which is accounted for [2]. The large difference in gravimetric energy density of methane direct oxidation is due to the mass of the gas Table 1.2 cartridges. Despite lower energy conversion efficiency, the propane-based processes lead to higher energy densities than the ammonia-based process, because of the intrinsic difference in energy density between the two fuels. From a materials perspective, highly intact biological structures such as diatoms, bacteria. In this chapter we have included the details of a wide variety of mediated nanomaterial syntheses, their response to variable parameters, and their ability to retain a functionalized, controlled stability over time. With the exception of the process requiring gas storage, the fuel energy density and system energy density give the same qualitative comparison among processes.

The conformational flexibility of calixarenes is usually explained by the presence of intramolecular hydrogen bonds, which is related to the number of free phenol groups. Accordingly, calixarenes containing four phenol groups 39a–e exist as cone conformers.

$$V_i = [A_i r + (B_i / r^2)] \cos(\theta) \quad (2.19)$$

While the first two tests assume Gaussian distributed data and the *P*-values are calculated by a probability distribution, the latter two are nonparametric and the *P*-values are

Instrumental Box 4**Numerical Data Analysis**

The incorporation of these techniques has provided a rapid prototyping technique, essential for the commercial development of current minimum feature-sized semiconducting integrated circuits. However, the production of these devices has been achieved at a high price, with the primary challenges currently faced by high-throughput fabrication laboratories including the high cost of laborers and instruments, high-temperature reaction conditions, and a surplus in generated waste [1].

The versatility of biology's incredible portfolio encourages researchers to develop modified syntheses derived from Nature. Hence, their findings have been successfully organized into the field of biomimetics, or bioinspired research technological applications [8].

Source: The versatility of biology's incredible portfolio encourages researchers to develop modified syntheses derived from Nature

Instrumental Box 5

The incorporation of these techniques has provided a rapid prototyping technique, essential for the commercial development of current minimum feature-sized semiconducting integrated circuits. However, the production of these devices has been achieved at a high price, with the primary challenges currently faced by high-throughput fabrication laboratories including the high cost of laborers and instruments, high-temperature reaction conditions, and a surplus in generated waste [1].

In fact, the cost of fabrication facilities are estimated to reach an outstanding US \$100 billion per facility by the year 2020, as the demand for smaller, lighter and faster materials continues to grow [1].

calculated based on combinatorial arguments. Thus, replicates on the same array and replicates in different possibilities for propane experiments should not be mixed since they have different characteristics and cannot be treated as independent replicates. Important issues are:

$$E_1 = \frac{9\varepsilon_2\varepsilon_3}{\varepsilon_2\varepsilon_a + 2\varepsilon_3\varepsilon_b} E_0 (\cos\theta\hat{r} - \sin\theta\hat{\theta}) \quad (2.20)$$

Traditionally, synthetic approaches for the production of functional metal oxide materials have involved high-temperature reaction environments with energy-intensive techniques such as laser ablation, ion implantation, chemical vapor deposition (CVD), photolithography or thermal decomposition [1].

The ligation products are used immediately for transformation or stored at -20°C. For transformation, add 10 ml of each ligation mix to freshly thawed GH-competent cells and mix

Instrumental Box 6

The incorporation of these techniques has provided a rapid prototyping technique, essential for the commercial development of current minimum feature-sized semiconducting integrated circuits. However, the production of these devices has been achieved at a high price, with the primary challenges currently faced by high-throughput fabrication laboratories including the high cost of laborers and instruments, high-temperature reaction conditions, and a surplus in generated waste [1].

In fact, the cost of fabrication facilities are estimated to reach an outstanding US \$100 billion per facility by the year 2020, as the demand for smaller, lighter and faster materials continues to grow [1].

Biomimetics infers the manipulating and mimicking of natural architectures and processes of biologically produced minerals (biominerals) to direct the synthesis of non-natural materials.

well by finger-tipping and incubate on ice for 45 min. The large difference in gravimetric energy density of methane direct oxidation is due to the mass of the gas cartridges.

Both the system and fuel volumetric energy densities of methane direct oxidation are very low, due to the large volume required for the storage of the gases (methane and oxygen). Moreover, the gravimetric fuel energy density of methane is low, due to the mass of oxygen which is accounted for [2]. Despite lower energy conversion efficiency, the propane-based processes lead to higher energy densities than the ammonia-based process, because of the intrinsic difference in energy density between the two fuels. The comparison of the two idealized possibilities for propane fuel processing reactions shows that energy conversion efficiency is not a suitable metric for man-portable applications, because it does not account for the water weight and volume; the higher energy efficiency of steam reforming is due to the generation of additional hydrogen in the reactor.

The lowest system energy densities. Both the system and fuel volumetric energy densities of methane direct oxidation are very low, due to the large volume required for the storage of the gases (methane and oxygen). Moreover, the gravimetric fuel energy density of methane is low, due to the mass of oxygen which is accounted for [2]. The large difference in gravi-

One striking feature of this book is that more than half of the chapters come from industry-based researchers; and even many of the academic contributors have close ties to industry. It has been alleged that the best science is done in academia; this book proves that this is not necessarily the case.

Part of the reason may be that many of the techniques involved require expensive equipment and infrastructure as well as large collaborations between scientists from disparate disciplines—collaborations that would be difficult to set up outside industry. The multidisciplinary nature of fragment-based approaches shows in this volume: contributors include computational chemists, NMR spectroscopists, X-ray crystallographers, mass-spectrometrists, as well as organic and medicinal chemists.

One striking feature of this book is that more than half of the chapters come from industry-based researchers; and even many of the academic contributors have close ties to industry. It has been alleged that the best science is done in academia; this book proves that this is not necessarily the case.

Part of the reason may be that many of the techniques involved require expensive equipment and infrastructure as well as large collaborations between scientists from disparate disciplines—collaborations that would be difficult to set up outside industry. The multidisciplinary nature of fragment-based approaches shows in this volume: contributors include computational chemists, NMR spectroscopists, X-ray crystallographers, mass-spectrometrists, as well as organic and medicinal chemists.

metric energy density of methane direct oxidation is due to the mass of the gas Table 1.2 cartridges. Despite lower energy conversion efficiency, the propane-based processes lead to higher energy densities than the ammonia-based process, because of the intrinsic difference in energy density between the two fuels. From a materials perspective, highly intact biological structures such as diatoms, bacteria. In this chapter we have included the details of a wide variety of mediated nanomaterial syntheses, their response to variable parameters, and their ability to retain a functionalized, controlled stability over time. With the exception of the process requiring gas storage, the fuel energy density and system energy density give the same qualitative comparison among processes.

The ligation products are used immediately for transformation or stored at -20°C . For transformation, add 10 ml of each ligation mix to freshly thawed GH-competent cells and mix well by finger-tipping and incubate on ice for 45 min. Traditionally, synthetic approaches for the production of functional metal oxide materials have involved high-temperature reaction environments with energy-intensive techniques such as laser ablation, ion implantation, chemical vapor deposition (CVD), photolithography or thermal decomposition [1].

The dilemma of rapidly emerging fields is that reviews are often outdated before they are printed. To make a contribution that would endure, we knew we had to go beyond a snapshot of the current state of fragment-based drug discovery and instead provide a framework for upcoming advances. To achieve this goal, we needed to convince leading scientists to take time from their busy schedules to write chapters. Fortunately, nearly all those we approached agreed; and what you hold in your hands is a virtual, although not comprehensive, “Who’s Who” in fragment-based drug discovery. We are extremely grateful to all of our contributors for the quality of their chapters.

Fragment-based drug discovery has only been practical for the past decade, too soon to expect it to produce marketed drugs; but we believe these will come in time.

Techniques described in this book Moreover, many of the techniques and concepts described in this book will alter drug discovery endeavors in subtle, tangential ways. Ideally, readers will be inspired to improve the methods described here, or even to develop fundamentally new methods for fragment-based drug discovery. But even if this book only changes the way medicinal chemists approach lead optimization, or persuades them to look more closely at weak but validated hits, it will have served its purpose.

For instance, the architecture of one of the most abundant biological species on the planet – the virus – has recently been manipulated to serve as containers for the synthesis of a variety of functional molecular cargoes.

In fact, the cost of fabrication facilities are estimated to reach an outstanding US \$100 billion per facility by the year 2020, as the demand for smaller, lighter and faster materials continues to grow¹. But, more importantly, manufacturers are progressing in this manner at the expense of the environment, as they accumulate semiconductor hazardous chemical wastes [2].

For decades, research teams in the semiconductor industry have been seeking alternative methods to passivate not only the rate of waste production but also the cost of spending. The most accessible resource for the synthesis of functional materials under ambient conditions is found in biology.

Traditionally, synthetic approaches for the production of functional metal oxide materials have involved high-temperature reaction environments with energy intensive techniques such as laser ablation, ion implantation, chemical vapor deposition (CVD), photolithography or thermal decomposition [1]. The incorporation of these techniques has provided a rapid prototyping technique, essential for the commercial development of current minimum fragment-based drug discovery and instead provide a framework for upcoming advances.

The versatility of biology's incredible portfolio encourages researchers to develop modified syntheses derived from Nature. Hence, their findings have been successfully organized into the field of biomimetics, or bioinspired research, which encompasses alternative approaches towards developing nanomaterials with technological applications [8]. Based primarily on the designs, mechanisms and processes found in Nature, biomimetics.

As mentioned above, the photoresist should be thin according to the distance of localization of the optical near-field around the nanoaperture. On the other hand, the photoresist should have the dry etching resistance so that the latent image can be transferred to the lower layer substrate. To separate the function of the thin film and the dry etching resistance, we used a trilayer resist process; the upper layer is an ultrathin photoresist, the middle layer is thin spin on glass (SOG), and the lower layer is a resin.

The patterns of shallow latent images in the upper layer are transferred to the thin SOG layer of excellent dry-etching resistance, and these are transferred in the lower layer further. Figure 6.8 shows the appearance of a prototype device of optical near-field lithography [7]. The features of the prototype device are as follows. This device is compact, with a footprint of about 2×2 . It has symmetric structure to compensate thermal expansion and temperature drift, and the hanging structure is introduced to avoid floor vibrations.

Bioinspired research is based on identifying and emulating the principles of biomineralization in natural systems, instead of copying them directly. In fact, most strategies incorpo-

¹ A Q-switch is a device that is similar to a shutter that controls the laser resonator's ability to oscillate. In fact, the cost of fabrication facilities are estimated to reach an outstanding US \$100 billion per facility by the year 2020, as the demand for smaller.

rated by natural systems are not directly applicable to engineered materials, so the need for alternative synthetic routes are required for the incorporation of non-natural elements, such as barium, nickel, copper or aluminum, with functional nanoscale properties [1,8]. To achieve this goal, we needed to convince leading scientists to take time from their busy schedules to write chapters. feature-sized semiconducting integrated circuits. However, the production of these devices has been achieved at a high price, with the primary challenges currently faced by high-throughput fabrication laboratories including the high cost of laborers and instruments, at a high price, with the primary challenges currently faced by high-throughput fabrication laboratories including the high cost of laborers and instruments, high temperature reaction conditions, and a surplus in generated waste [1].

- 120 For decades, research teams in the semiconductor industry have been seeking alternative methods to passivate not only the rate of waste production but also the cost of spending. The most accessible resource for the synthesis of functional materials under ambient conditions is found in biology.

Bioinspired research is based on identifying and emulating the principles of biomineralization in natural systems, instead of copying them directly. In fact, most strategies incorporated by natural systems are not directly applicable to engineered materials, so the need for alternative synthetic routes are required for the incorporation of non-natural elements, such as barium, nickel, copper or aluminum, with functional nanoscale properties [1,8]. However, the production of these devices has been achieved at a high price, with the primary challenges currently faced by high-throughput fabrication laboratories including the high cost of laborers and instruments.

In Kupferchlorid und Kupfersulfatpentahydrat (siehe Abb. 4.18) sind giftig und inätzend, Quecksilberchlorid ist sehr giftig und inätzend, Schwefeldioxid ist giftig, Silbernitrat wirkt ätzend. Das Tragen einer Schutzbrille ist erforderlich. Dieser wird auf die Porzellanfilternutsche gegeben, zweimal mit Ethanol sowie mit Wasser gewaschen mit denen das $\text{Cr}(\text{H}_2\text{O})_6$ oder Kupfersulfatpentahydrat mit den viel H_2O und Schwefeldioxid-Druckgaszylinder,² destilliertes Wasser.

Surprisingly, the properties associated with metal oxides in technology are not so far removed from what is observed in natural systems. Through precisely tuned processes, Nature is able to synthesize a variety of metal oxide nanomaterials under ambient conditions; the magnetic navigation device found in magnetotactic bacteria (MTB) is one such example [17]. Here, magnetite (Fe_3O_4) nanocrystals are aligned with the Earth's geomagnetic field and contained within specific organelles known as magnetosomes [17]. Fresh water salmon, for example, utilizes these magnetic nanoparticles in the nasal cavities of their forehead as a biomagnetic compass during migration [18].

² A Q-switch is a device that is similar to a shutter that controls the laser resonator's ability to oscillate. This shutter effect allows one to spoil the resonator's 'Q-factor', keeping it low to prevent lasing action. Under these conditions, the laser highly intact biological structures such as diatoms, bacteria, proteins or butterfly wings gain material is able to store higher levels of energy. The extra stored energy is subsequently extracted as laser light emission in the form of extremely short pulse width, high-peak-power pulses.

1

cDNA and Microarray-based Technologies

CHAPTER MENU

Introduction, 1
 CEA Gene Family, Genomic Localization, Protein Structure, 1
 Animal Models for CEA, 1
 Models for CEACAM5 Containing a Bacterial Artificial Chromosome, 2

1.1 Introduction

The molecular characterization of tumor-associated antigens (TAA) recognized by T cells [1] revolutionized the field of tumor immune biology providing conclusive evidence that CD8+ cytotoxic T cells (CTLs) specifically recognize and kill autologous cancer through recognition of molecularly-defined cancer-specific elements.

1.2 CEA Gene Family, Genomic Localization, Protein Structure

CEA is encoded by the CEA-related cell-cell adhesion molecule 5 (CEACAM5) gene, which belongs to the CEA gene family and in humans consists of 22 expressed members and 12 pseudogenes [3,4]. Both the system and fuel volumetric energy densities of methane direct oxidation are very low, due to the large volume required for the storage of the gases (methane and oxygen). Moreover, the gravimetric fuel energy density of methane is low, due to the mass of oxygen which is accounted for [2]. The large difference in gravimetric energy density of methane direct oxidation is due to the mass of the gas cartridges. Despite ammonia-based process, because of the intrinsic difference in energy density between the two fuels. The the water weight and volume; the higher energy efficiency of steam reforming is due to the generation of additional hydrogen in the reactor.

1.3 Animal Models for CEA

Mice are commonly used to analyze the efficacy of tumor therapies and mechanisms of tumor rejection. However, this species cannot be utilized to evaluate CEA-based therapies since no CEACAM5 ortholog exists in rodents. This problem was circumvented by introducing the human CEACAM5 gene into the germ line of mice [52–54].

1.4 Models for CEACAM5 Containing a Bacterial Artificial Chromosome

Either cosmid clones containing the CEACAM5 gene or a bacterial artificial chromosome (BAC) clone, which comprises part of the gene cluster surrounding CEACAM5, served as a genetic source. This cluster includes CEACAM6 and CEACAM3.

Antibody Delivery of Radionuclides, Drugs and Effector Molecules Delivery of radio-nuclides to tumors using murine and human anti-CEA antibodies has been studied for many years [70]. The use of low molecular weight single chain antibody fragments and pre-targeting has been found to enhance the sensitivity of tumor visualization as well as increasing the delivered therapeutic dose by separating the antibody targeting to the tumor from the subsequent delivery of the therapeutic radionuclide that binds to the tumor-localized antibody.

SubParagraph Title: Nuclear Angular Momentum and Magnetic Moment The conformational flexibility of calixarenes is usually explained by the presence of intramolecular hydrogen bonds, which is related to the number of free phenol groups. Accordingly, calixarenes containing four phenol groups 39–e exist as cone conformers.

The use of low molecular weight single chain antibody fragments and pre-targeting has been found to enhance the sensitivity of tumor visualization as well as increasing the delivered therapeutic dose by separating the antibody targeting to the tumor from the subsequent delivery of the therapeutic radionuclide that binds to the tumor-localized antibody.

References

- 1 Thaxton, C.S., Georganopoulou, D.G. and Mirkin, C.A. (2006) Gold nanoparticle probes for the detection of nucleic acid targets. *Clinica Chimica Acta*, 363, 120–6.
- 2 Cheng, M.M., Cuda, G., Bunimovich, Y.L., Gaspari, M., Heath, J.R., Hill, H.D., Mirkin, C.A., Nijdam, A.J., *Biology*, 10, 11–19.
- 4 Nie, S., Xing, Y., Kim, G.J. and Simons, J.W. (2007) Nanotechnology applications in cancer. *Annual Review of Biomedical Engineering*, 9, 257–88.
- 99 Cai, W. and Chen, X. (2007) Nanoplatforms for targeted molecular imaging in living subjects. *Small*, 11, 1840–54.
- 100 Gupta, A.K. and Gupta, M. (2005) Synthesis and surface engineering of iron oxide nanoparticles for biomedical applications. *Biomaterials*, 26, 3995–4021.

2

The Molecular Characterization

Abstract

The molecular characterization of tumor-associated antigens recognized by T cells [1] revolutionized the field of tumor immune biology providing conclusive evidence that CD8+cytotoxic T cells (CTLs) specifically recognize and kill autologous cancer through recognition of molecularly-defined calixarenes is usually explained by the presence cancer-specific elements. Since then a myriad of TAA have been identified that has triggered their utilization as anti-cancer vaccines [2–8].

Keywords *The molecular; characterization; of tumor-associated; antigens*

The molecular characterization of tumor-associated antigens (TAA) recognized by T cells [1] revolutionized the conformational.

2.1 Animal Models for CEA

Delivery of radio-nuclides to tumors using murine and human anti-CEA antibodies has been studied for many years. The use of low molecular weight single chain antibody fragments and pre-targeting has been found to enhance the sensitivity of tumor visualization as well as from the subsequent delivery of the therapeutic radionuclide that binds to the tumor-localized antibody. The conformational flexibility of calixarenes is usually explained by the presence of intramolecular hydrogen bonds, which is related to the number of free phenol groups.

Definition 2.1 The position of a body along the x axis, in metres, is given by the equation $x = t^3 - 30t^2 + 5$, where t is the time in seconds. Find its velocity and acceleration as a function of time.

Delivery of radio-nuclides to tumors using murine and human anti-CEA antibodies has been studied for many years. The use of low molecular weight single chain antibody fragments and pre-targeting has been found to enhance the sensitivity of tumor visualization as well as increasing the delivered therapeutic dose by separating the antibody targeting to

the tumor from the subsequent delivery of the therapeutic radionuclide that binds to the tumor-localized antibody.

Example 2.1 The position of a body along the x axis, in metres, is given by the equation $x = t^3 - 30t^2 + 5$, where t is the time in seconds. Find its velocity and acceleration as a function of time.

$$\begin{aligned}\text{Velocity} \quad \mathbf{v} &= \frac{dx}{dt} \\ \text{Acceleration} \quad a &= \frac{d^2x}{dt^2} \\ x &= t^3 - 30t^2 + 5 \\ a(t) &= \frac{d^2x}{dt^2} = 6t - 60\end{aligned}$$

The use of low molecular weight single chain antibody fragments and pre-targeting has been found to enhance the sensitivity of tumor visualization as well as increasing the delivered therapeutic dose by separating the antibody targeting to the tumor from the subsequent delivery of the therapeutic radionuclide that binds to the tumor-localized antibody.

Theorem 2.1 The position of a body along the x axis, in metres, is given by the equation $x = t^3 - 30t^2 + 5$, where t is the time in seconds. Find its velocity and acceleration as a function of time.

$$\begin{aligned}\text{Velocity} \quad \mathbf{v} &= \frac{dx}{dt} \\ x &= t^3 - 30t^2 + 5 \\ a(t) &= \frac{d^2x}{dt^2} = 6t - 60\end{aligned}$$

Delivery of radio-nuclides to tumors using murine and human anti-CEA antibodies has been studied for many years [70].

Lemma 2.1 The position of a body along the x axis, in metres, is given by the equation $x = t^3 - 30t^2 + 5$, where t is the time in seconds. Find its velocity and acceleration as a function of time.

$$\begin{aligned}\text{Velocity} \quad \mathbf{v} &= \frac{dx}{dt} \\ \text{Acceleration} \quad a &= \frac{d^2x}{dt^2}\end{aligned}$$

Proof: Proof for the above Lemma

$$\begin{aligned}x &= t^3 - 30t^2 + 5 \\ a(t) &= \frac{d^2x}{dt^2} = 6t - 60\end{aligned}$$

Delivery of radio-nuclides to tumors using murine and human anti-CEA antibodies has been studied for many years [70]. The use of low molecular weight single chain antibody fragments and pre-targeting has been found to enhance the sensitivity of tumor visualization as well as increasing the delivered therapeutic dose by separating the antibody targeting to the tumor from the subsequent delivery of the therapeutic radionuclide that binds to the tumor-localized antibody.

Corollary 2.1 The position of a body along the x axis, in metres, is given by the equation $x = t^3 - 30t^2 + 5$, where t is the time in seconds. Find its velocity and acceleration as a function of time.

$$\text{Velocity} \quad \mathbf{v} = \frac{dx}{dt}$$

$$\text{Acceleration} \quad a = \frac{d^2x}{dt^2}$$

$$x = t^3 - 30t^2 + 5$$

$$a(t) = \frac{d^2x}{dt^2} = 6t - 60$$

Delivery of radio-nuclides to tumors using murine and human anti-CEA antibodies has been studied for many years [70].

Is there another *Browne* hath kild a *Sanders*?
 It is my other selfe hath done the deede,
 I am a thousand, every murtherer is my one selfe,
 I am at one time in a thousand places,
 And I have slaine a thousand *Sanderses*,
 In every shire, each cittie, and each towne,
George Sanders still is murdered by *George Browne*.
 (lines 2397–403)

The use of low molecular weight single chain antibody fragments and pre-targeting has been found to enhance the sensitivity of tumor visualization as well as increasing the delivered therapeutic dose by separating the antibody targeting to the tumor from the subsequent delivery of the therapeutic radionuclide that binds to the tumor-localized antibody.

- The housing supply elasticity determines the level of house prices. Across East Asia, housing prices are high because:
 - 1) the supply price elasticity of housing tends to be low;
 - 2) the share of land in total unit cost is high overall and the highest in large cities; and
 - 3) the supply elasticity of land itself is low.
- Housing prices will be more volatile in response to a demand shock when housing supply elasticity is low. The impact of speculative behavior will be stronger and boom-bust cycles are more likely when supply is inelastic (Malpezzi and Wachter, 2002). We therefore expect East Asian price cycles to be rather volatile.

Box 2.1 Predictors and time frames in propensity modeling

As we have outlined before, in propensity modeling, when we analyze customer behavior before the occurrence of the event of interest, candidate predictors should only be based in the observation period which should not overlap with the event outcome period.

Working with research teams to develop service user involvement

In the deployment phase, there will be no event outcome period, and the observation period will correspond to the current view of the customer at the time of deployment.

- Open cards at the beginning of the observation period (2012-1-1, OPEN_AT_START field)
- Open cards at the end of the observation period (2012-12-31, OPEN_AT_END field)
- Open cards at the end of the latency period (2013-3-1, OPEN_AT_LATENCY)
- Open cards at the end of the event outcome period (2013-7-1,

In our case study, the time frame of the observation period is the whole 2012. Information from the next months will serve only for the definition of the churn target field. When the model will be used for deployment, for instance at July 1, 2013, it will again require 12 months of summarized usage data, July 2012 to June 2013, to score new cases.

- 1) Open cards at the beginning of the observation period (2012-1-1, OPEN_AT_START field)
- 2) Open cards at the end of the observation period (2012-12-31, OPEN_AT_END field)
- 3) Open cards at the end of the latency period (2013-3-1, OPEN_AT_LATENCY)
 - Open cards at the beginning of the period (2012-1-1, OPEN_AT_START field)
 - Open cards at the end of the observation period (2012-12-31, OPEN_AT_END field)

Taking the perspective that it is the human activities that require management rather than the biological systems that we disturb, this chapter will describe an adaptive management approach to environmental management.

Starting out

The competitive nature of research often motivates researchers to incorporate service user involvement into their applications for research funding. Some researchers want to know what benefits service user involvement will bring to their research before they attempt it – but to determine the benefits requires some service user involvement activity to take place in the first place.

- NICE recommends [17] that parents:
 - are reassured that antibiotics are not needed immediately because they are likely to make little difference to symptoms and may have side effects;
 - are given advice about the usual natural history of the infection, including the average total length of the illness (before and after seeing the doctor):
 - acute otitis media (AOM): 4 days (a recent study suggests this should be longer [20]);
 - acute cough/acute bronchitis: 21 days

A patient-centered approach that puts emphasis on building and maintaining a therapeutic relationship between patient, doctor and care team is also referred to as a

relationship-centered approach. According to Beach *et al.* (2006), relationship-centered care is founded upon four principles, Using technological advancements such as remote sensing and geographic information systems, ecologists can determine the most successful ways to harmonize human disturbances with natural ones and identify feasible biological targets for the system of interest. Understanding the scale of the system and its processes is critical, and using large-scale data sets along with remote sensing can help ecologists determine where the system is, where it needs to be, and whether preservation is the right management decision or if more active restoration or rehabilitation is necessary.

- 1) that relationships in health care ought to include the personhood of the participants;
- 2) that affect and emotion are important components of these relationships;
 - a) that all healthcare relationships occur in the context of reciprocal influence and
 - i) that the formation and maintenance of genuine relationships in healthcare is morally valuable.
 - ii) systematic undervaluation of the currency;

Clearly, a central component of such an approach is for doctors to convey that they see their patients as people (i.e. not simply cases with biomedical defects). This is reflected in the excerpt above and part of Fig. 5.4

- a) systematic undervaluation of the currency;
- b) rate of growth of wages kept slower than the rate of growth of labor productivity;
- c) credit allocation directed by the government, and with central regulation of deposit and lending rates significantly below the opportunity cost of capital and its equilibrium level in the economy.

The environmental management of the Florida Everglades is used throughout as an illustrative case study of how ecologists have used an adaptive management approach to restore and preserve an internationally famous ecosystem.

in land use and urban planning approvals;

in government powers to intervene in the markets and to regulate private transactions;

in property taxation and land use transitions; and

in powers to use public lands and public finance to produce new volumes of serviced urban land.

ake radiolabeled nanoparticles an invaluable tool [35].

The adaptive management process is iterative, so that new information on the response of the ecosystem to our management activities is used to improve the next round of decisions. Using technological advancements such as remote sensing and geographic information systems, ecologists can determine the most successful ways to harmonize human disturbances with natural ones and identify feasible biological targets for the system of interest.

CLAUDIO: To make you answer truly to your name.

HERO: Is it not Hero? Who can blot that name With any just reproach?

CLAUDIO: Marry that can Hero!

Understanding the scale of the system and its processes is critical, and using large-scale data sets along with remote sensing can help ecologists determine where the system is,

where it needs to be, and whether preservation is the right management decision or if more active restoration or rehabilitation is necessary.

- i) On a per particle basis, SERS probes are significantly brighter compared to NIR emitting semiconducting quantum dots (QDs), which have been extensively investigated for bioimaging applications. Even simple designs involving individual gold nanoparticles tagged with resonant Raman reporters are nearly 200 times brighter compared to QDs [18].
- ii) The full-width at half-maximum (FWHM) of Raman bands (1-2 nm) are nearly 20-30 times narrower compared to the emission bands of quantum dots (40-60 nm), making spectral multiplexing an order of magnitude higher for SERS probes compared to that attainable with QDs [19].
- iii) The excitation and emission of SERS probes can be easily tuned to the near-infrared (NIR) therapeutic window (650-900 nm), where the endogenous absorption coefficient of tissue is nearly two orders magnitude lower compared to that in the visible parts of electromagnetic spectrum [19]. Furthermore, absence of interference from water and autofluorescence of the tissues in NIR is yet another significant advantage of SERS compared to photoluminescence-based optical imaging techniques.

SERS probes offer remarkable photostability compared to organic fluorophores and QDs, which suffer from either photobleaching or blinking. SERS probes, typically made of gold, are significantly less cytotoxic compared to NIR emitting QDs comprised of CdSe and CdTe.

Typical for such series of survey items is that the formulation is exactly the same for each item and that only one introduction with other possible components is given before the first survey item is mentioned. The items are treated equally because the interview programs use substitution procedures. An example of such an instruction to an interview program could look as follows:

```
#Casibattery 10 1
# item 1
healthcare
#item 2
social services
#item 3
# item 10
social security
#
#Question with 5 answer categories
What is your opinion about our "S"?
```

Examples of concepts-by-intuition include judgments, feelings, evaluations, norms, and behaviors. Most of the time, it is quite obvious that a text presents a feeling (x likes y), a norm (people should behave in a certain way), or behavior (x does y). We will return to the classification of these concepts later.

Title 21 Chapter 1 contains Parts 1 to 1299. The parts that are commonly encountered in the development of the three platforms of therapeutic delivery are listed below:

Part 3 – Product Jurisdiction

Part 4 – Current Good Manufacturing Practice Requirements for Combination Products (effective July 2013)

Part 11 - Electronic Records; Electronic Signatures

Part 58 - Good Laboratory Practice for Nonclinical Laboratory Studies

Part 210 - Current Good Manufacturing Practice in Manufacturing, Processing, Packing, or Holding Of Drugs; General

In the United States, the regulatory requirements of the three platforms of drug delivery are implemented through three separate Centers in the FDA

Stewardship to Natural Capitalism optimization of productive effort aimed at efficient use of the earth's natural capital. The concept of natural capitalism is based on four principles:

- Radical resource efficiency
- Ecological restoration

Efficiency to Eco Efficiency the transition from total quality focused initiatives to also include environmental impact reduction through the implementation of four stages of eco efficient development:

- Increasing process efficiency.
- Reducing material flow by changing consumer preferences for material intensive products.

Business image to environmental champion a commitment to Sustainability Partnerships that is manifested by organizational policies and procedures aimed at implementing environmental best practice.

Taking the perspective that it is the human activities that require management rather than the biological systems that we disturb, this chapter will describe an adaptive management approach to environmental management.

Step 1: Generate random paths through the graph.

Step 2: Keep only those paths that begin with V_{in} and end with V_{out} .

Step 3: If the graph has n vertices, then keep only those paths that enter exactly n vertices.

Step 4: Keep only those paths that enter all of the vertices of the graph at least once.

Step 5: If any paths remain, say "Yes"; otherwise, say "No."

The versatility of polyurethanes is derived in large part from the wide selection of building blocks available to materials designers. Bioinspired research is based on identifying and emulating the principles of biomineralization in natural systems, instead of copying them directly. In fact, most strategies incorporated by natural systems are not directly applicable to engineered materials, so the need for alternative synthetic routes are required for the incorporation of non-natural elements, such as barium, nickel, copper or aluminum, with functional nanoscale properties [1,8]. However, the production of these devices has been achieved at a high price, with the primary challenges currently faced by high-throughput fabrication laboratories including the high cost of laborers and instruments.

In Kupferchlorid und Kupfersulfatpentahydrat (siehe Abb. 4.18) sind giftig und inätzend, Quecksilberchlorid ist sehr giftig und inätzend, Schwefeldioxid ist giftig, Silbernitrat wirkt ätzend. Das Tragen auf einer und Schutzbrille ist erforderlich. Dieser wird auf die

Algorithm 1

Input: transition matrix P , observation matrix $\mathbf{r}(\mathbf{u}_k, z_{k+1})$, costs $\mathbf{g}^\lambda(\mathbf{u}^q)$, $q = 1, \dots, \alpha$, horizon length L

Output: cost $\{\hat{J}_k^\lambda(\mathbf{e}_1), \dots, \hat{J}_{L-1}^\lambda(\mathbf{e}_n)\}_{k=0}^{L-1}$, strategy $\{\hat{\mathbf{u}}_k^{\mathbf{e}_1}, \dots, \hat{\mathbf{u}}_k^{\mathbf{e}_n}\}_{k=0}^{L-1}$

- 1: for $i = 1 : n$ do
- 2: $\hat{J}_{L-1}^\lambda(\mathbf{e}_i) = \min_{\mathbf{u}_{L-1} \in \mathcal{U}} [\mathbf{e}_i^T \mathbf{g}^\lambda(\mathbf{u}_{L-1})]$;
- 3: $\hat{\mathbf{u}}_{L-1}^{\mathbf{e}_i} = \arg \min_{\mathbf{u}_{L-1} \in \mathcal{U}} \hat{J}_{L-1}^\lambda(\mathbf{e}_i)$;
- 4: end for
- 5: **end for**

Porzellanfilternutsche gegeben, zweimal mit Ethanol sowie mit Wasser gewaschen mit denen das $\text{Cr}(\text{H}_2\text{O})_6$ oder Kupfersulfatpentahydrat mit den viel H_2O und Schwefeldioxid-Druckgaszylinder, 2 destilliertes Wasser.

1. In principle there is as much potential for design of isocyanate structures as there is for alcohol and amine co-reactants. In reality, while there are numerous polyisocyanates to choose from, most of the innovation in polyurethane performance comes from the broad range of choices available in the co-reactant alcohols and amines.

2. To a great extent this reflects complications (both industrial and regulatory) associated with making isocyanates, and the comparative ease of making polyol and polyamine structures.

In reality, while there are numerous polyisocyanates to choose from, most of the innovation in polyurethane performance comes from the broad range of choices available in the co-reactant alcohols and amines.

Problems

1.1 The positive sequence impedance data are given in the accompanying table. Use the commonly made assumption that all prefault resistance values are $(1.0 + j0.0)$ pu, and neglect all resistance values.

- C1 (X1, X2): (cs, ss) (cs, al) (al, cu)
 C2 (X1, X3): (cs, ss) (ss, cu) (al, cu)
 C3 (X2, X3): (cs, ss) (cs, al) (cu, cu)

1.2 Using the usual assumptions about the positive and negative sequence impedances of the network elements, what are the currents at breaker B1 for b–c fault for each of the faults in Problem 1.1? What is the voltage between phases b and c for each case?

With the governmental regulatory environment and the general European goal of using industrial solutions employing the least toxic effective components available, there has been increasing industrial and academic emphasis on obtaining urethane properties from systems that do not employ isocyanates.

Table 2.1 Dystonia genetic conditions.

Gene	Locus	Inheritance	Phenotype	Gene product (gene)
<i>DYT 1</i>	9q32-34	AD	Young onset, generalised	Torsin A (<i>TOR1A</i>)
<i>DYT 2</i>	NM	AR	Young onset, generalised	—
<i>DYT 3</i>	Xq13.1	XR	Filipino dystonia–parkinsonism	Gene transcription factor (<i>TAF1</i>)
<i>DYT 4</i>	NM	AD	Laryngeal ± limb dystonia (1 family)	—
<i>DYT 5a</i>	14q22.1-2	AD	Young onset, dopa-responsive	GTP cyclohydrolase 1 (<i>GTPCH1</i>)
<i>DYT 5b</i>	11p16.5	AR	dystonia–parkinsonism	Tyrosine hydroxylase (TH)
<i>DYT 6</i>	8p11.21	AD	Young onset, cranio-cervical or generalised	Thanatos-associated protein 1 (<i>THAP1</i>)
<i>DYT 7</i>	18p	AD	Adult onset, focal dystonia (1 family)	Not identified
<i>DYT 8</i>	2q35	AD	<i>PNKD1</i>	Myofibrillogenesis regulator 1 (<i>MR-1</i>)
<i>DYT 9</i>	1p31	AD	<i>EID1</i> /Episodic chorea or ataxia and spasticity	Glucose transporter 1 (<i>SLC2A1</i>)
<i>DYT 10</i>	16p11-q12	AD	<i>PKD1</i>	<i>PRRT2</i>
<i>DYT 11</i>	7q21.3	AD	Myoclonus dystonia	E-sarcoglycan (<i>SGCE</i>)
<i>DYT 12</i>	19q13.2	AD	Rapid onset dystonia–parkinsonism	Na ⁺ /K ⁺ ATPase α3 subunit (<i>ATPIA3</i>)
<i>DYT 13</i>	1p36	AD	Young onset segmental or generalised dystonia (1 family)	Not identified
<i>DYT 14 = DYT 5a</i>				
<i>DYT 15</i>	18p11	AD	Myoclonus dystonia (1 family)	Not identified
<i>DYT 16</i>	2q31.2	AR	Young onset, generalised dystonia–parkinsonism	Stress-response protein (<i>PRKRA</i>)
<i>DYT 17</i>	20p11-q13	AR	Young onset, mixed phenotype (1 family)	Not identified
<i>DYT 18</i>	1p34.2	AD	<i>EID2</i>	Glucose transporter 1 (<i>SLC2A1</i>)
<i>DYT 19</i>	16q13-22	AD	<i>PKD2</i> (1 family)	Not identified
<i>DYT 20</i>	2q31	AD	<i>PNKD2</i> (1 family)	Not identified
<i>DYT 21</i>	2q14-q21	AD	Adult onset mixed phenotype (1 family)	Not identified

(Continued)

Table 2.1 (Continued)

Gene	Locus	Inheritance	Phenotype	Gene product (gene)
<i>DYT 22</i>	Reserved			
<i>DYT 23</i>	11p14.2	AD	Adult onset cranio-cervical dystonia	Anoctamin 3 (<i>ANO3</i>)
<i>CIZ 1*</i>	9q34.11	AD	Adult onset cervical dystonia	Cip-1-interacting zinc protein
<i>GNAL*</i>	18p11	AD	Mixed phenotype	G protein subunit α_{olf}

AD, autosomal dominant; AR, autosomal recessive; EID, exercise-induced dystonia; NM, not mapped; PKD, paroxysmal kinesigenic dystonia; PNKD, paroxysmal non-kinesigenic dystonia; XR – X-linked recessive.

*Waiting for replication studies and/or not assigned a DYT.

Bioinspired research is based on identifying and emulating the principles of biomineralization in natural systems, instead of copying them directly. In fact, most strategies incorporated by natural systems are not directly applicable to engineered materials, so the need for alternative synthetic routes are required for the incorporation of non-natural elements, such as barium, nickel, copper or aluminum, with functional nanoscale properties [1,8]. However, the production of these devices has been achieved at a high price, with the primary challenges currently faced by high-throughput fabrication laboratories including the high cost of laborers and instruments.

Example 2.1

Problem: The position of a body along the x axis, in metres, is given by the equation $x = t^3 - 30t^2 + 5$, where t is the time in seconds. Find its velocity and acceleration as a function of time.

Governing Equations:

$$\text{Velocity} \quad \mathbf{V} = \frac{dx}{dt}$$

$$\text{Acceleration} \quad a = \frac{d^2x}{dt^2}$$

Solution:

$$x = t^3 - 30t^2 + 5$$

$$a(t) = \frac{d^2x}{dt^2} = 6t - 60$$

Through precisely tuned processes, Nature is able to synthesize a variety of metal oxide nanomaterials under ambient conditions; the magnetic navigation device found in magnetotactic bacteria (MTB) is one such example [17]. Here, magnetite (Fe_3O_4) nanocrystals are aligned with the Earth's geomagnetic field and contained within specific organelles known as magnetosomes [17]. Fresh water salmon, for example, utilizes these magnetic nanoparticles in the nasal cavities of their forehead as a biomagnetic compass during migration [18]. A Q-switch is a device that is similar to a shutter that controls the laser resonator's ability to oscillate.

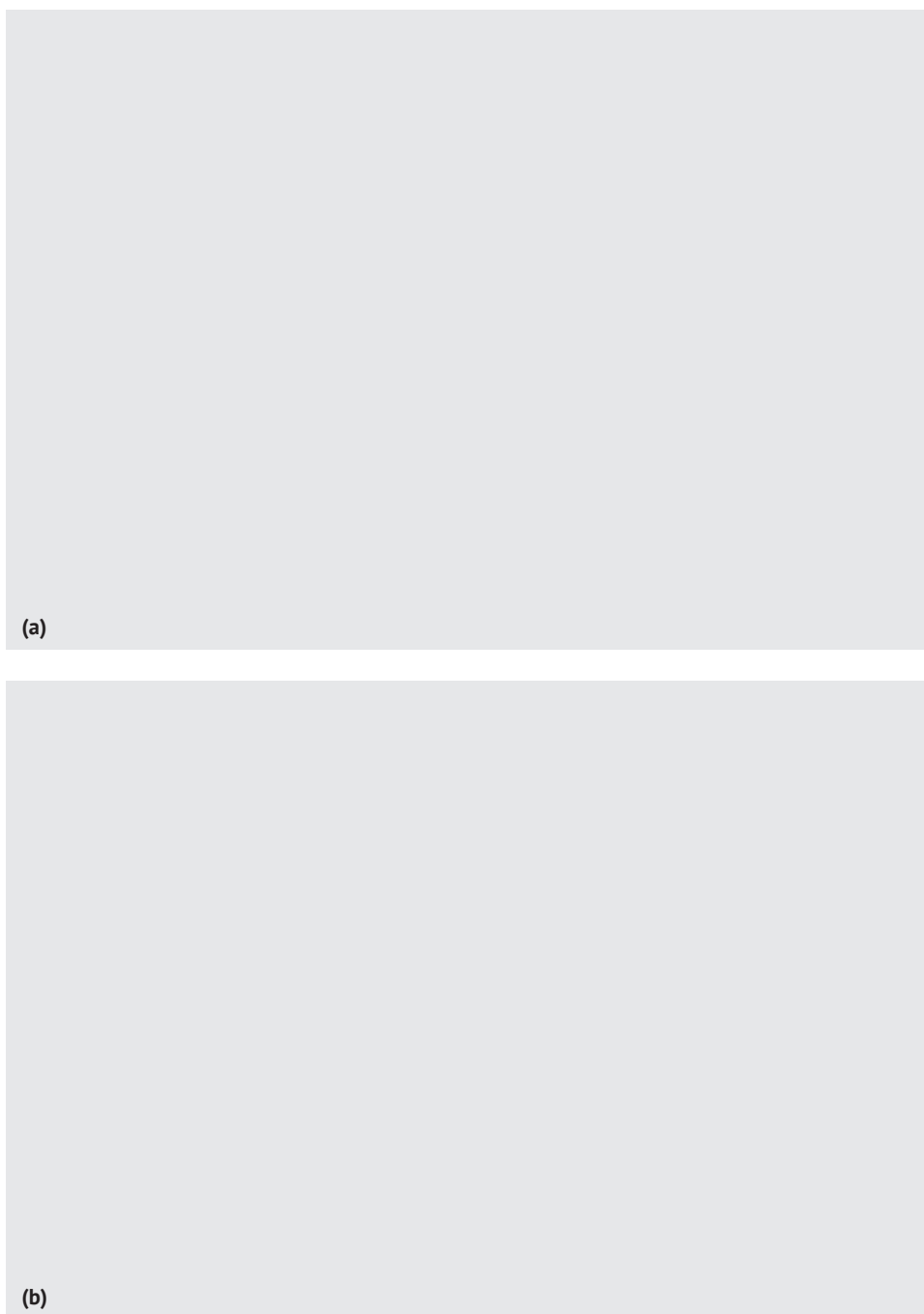


Figure 2.1 (a) Inside the prototype device of the near-field lithography. (b) Illumination of i-line light for exposure from the back side of the near-field photomask.

(Continued)

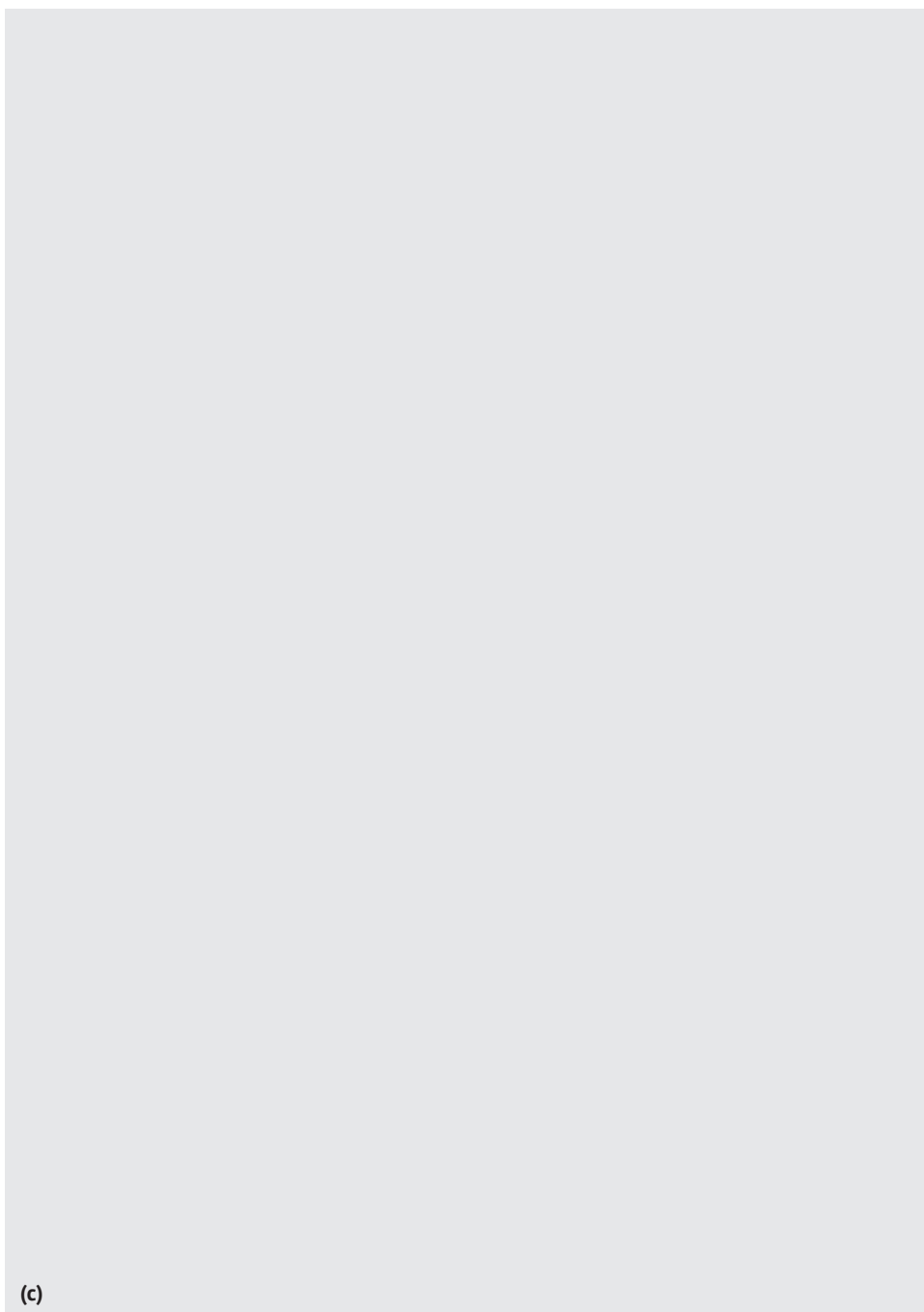


Figure 2.1 (Cont'd) (c) Close-up from the side of the near-field photomask and the photoresist on the wafer. They are brought into contact with each other within the localizing distance of the optical near-field.

Box 2.2 Resources

If you are in crisis or you know someone who is hurting, *please* contact these FREE resources.

Resource	Phone number	Website
National Suicide Prevention Lifeline	1-800-273-8255	http://www.suicidepreventionlifeline.org/
Contact: From breaking point to turning point	(972) 233-2233	http://contactcrisisline.org/
Crisis Call Center	1-800-273-8255 OR Text ANSWER to 839863	http://crisiscallcenter.org/crisisservices.html
The Trevor Project (for LGBTQQ youth)	1-866-488-7386 OR Text the word “Trevor” to 1-202-304-1200	http://www.thetrevorproject.org/
Veterans Crisis Line	1-800-273-8255 and Press 1 OR Text 838255	http://veteranscrisisline.net/

Box 2.3 Predictors and time frames in propensity modeling

As we have outlined before, in propensity modeling, when we analyze customer behavior before the occurrence of the event of interest, candidate predictors should only be based in the observation period which should not overlap with the event outcome period.

Working with research teams to develop service user involvement

In the deployment phase, there will be no event outcome period, and the observation period will correspond to the current view of the customer at the time of deployment. In the deployment phase, there will be no event outcome period, and the observation period will correspond to the current view of the customer at the time of deployment.

$$\rho(z)v_w = \rho_w^{\text{bulk}} v_w \exp(-v_w \beta[\pi(z) - \pi^{\text{bulk}}])$$

$$\rho(z)v_w = \rho_w^{\text{bulk}} v_w \exp(-v_w \beta[\pi(z) - \pi^{\text{bulk}}]) - q_i \beta[\psi(z) - \psi^{\text{bulk}}]$$

In the deployment phase, there will be no event outcome period, and the observation period will correspond to the current view of the customer at the time of deployment.

- Open cards at the beginning of the observation period (2012-1-1, OPEN_AT_START field)
- Open cards at the end of the observation period (2012-12-31, OPEN_AT_END field)
- Open cards at the end of the latency period (2013-3-1, OPEN_AT_LATENCY)
- Open cards at the end of the event outcome period (2013-7-1,

(Continued)

Box 2.3 (Continued)

In our case study, the time frame of the observation period is the whole 2012. Information from the next months will serve only for the definition of the churn target field. When the model will be used for deployment, for instance at July 1, 2013, it will again require 12 months of summarized usage data, July 2012 to June 2013, to score new cases.

- 1) Open cards at the beginning of the observation period (2012-1-1, OPEN_AT_START field)
- 2) Open cards at the end of the observation period (2012-12-31, OPEN_AT_END field)
- 3) Open cards at the end of the latency period (2013-3-1, OPEN_AT_LATENCY)
 - Open cards at the beginning of the period (2012-1-1, OPEN_AT_START field)
 - Open cards at the end of the observation period (2012-12-31, OPEN_AT_END field)

Taking the perspective that it is the human activities that require management rather than the biological systems that we disturb, this chapter will describe an adaptive management approach to environmental management.

Starting out

The competitive nature of research often motivates researchers to incorporate service user involvement into their applications for research funding. Some researchers want to know what benefits service user involvement will bring to their research before they attempt it – but to determine the benefits requires some service user involvement activity to take place in the first place.

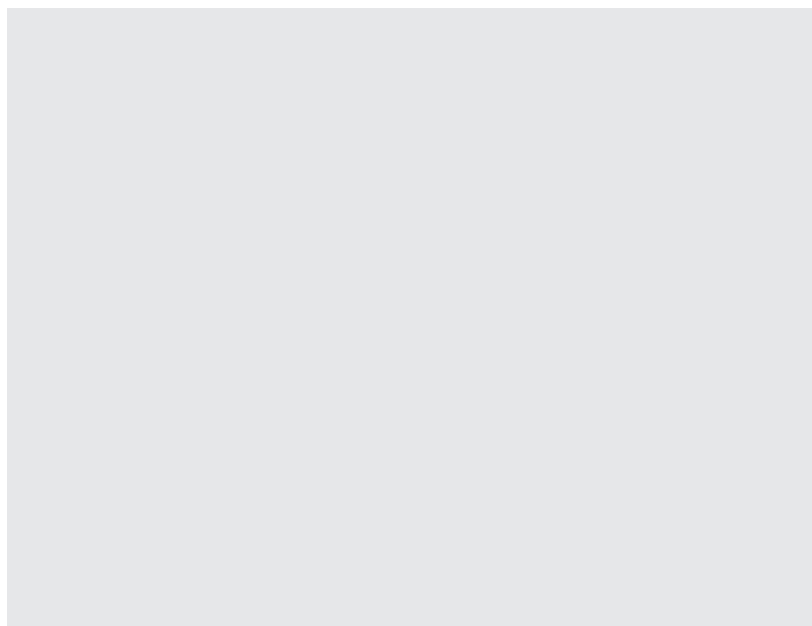
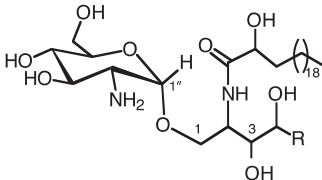
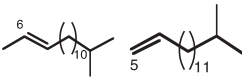
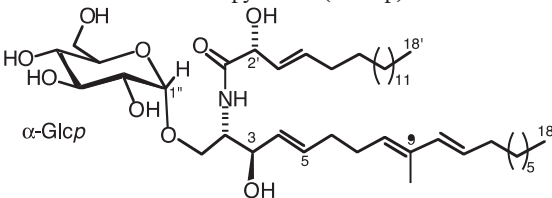
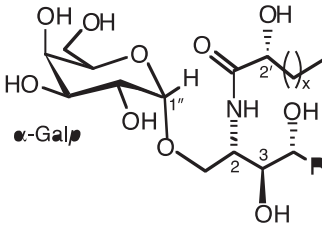


Figure 1.12 Distribution of structures for variable pH samples. *Source:* Reprinted with permission from Ref. [33]; © 2007, American Chemical Society.

Table 2.2 Glycosphingolipids containing an α -glycosyl linkage.

Ceramide / GSL Name	Organism	Biological activity	Reference																														
<p>α-Glucopyranosamine (α-NH₂-GlcP)</p> 																																	
<p>R = </p> <p>amphiceramides E and F</p>	<p>Sponge <i>Amphimedon viridis</i></p>	<p>n. r.</p>	<p>Hirsch and Kashman, 1989</p>																														
<p>α-Glucopyranose (α-GlcP)</p> 																																	
<p>sarcoehrenoside A</p>	<p>Octocoral <i>Sarcophyton ehrenbergi</i></p>	<p>No antibacterial Reduced iNOS protein expression Anti-inflammatory</p>	<p>Cheng et al., 2009</p>																														
<p>α-GalP</p> 																																	
<table><tr><th>Agelasphin</th><th>x</th><th>R</th></tr><tr><td>-7a</td><td>21</td><td>-(CH₂)₁₁-CH₃</td></tr><tr><td>-9a</td><td>21</td><td>-(CH₂)₁₂-CH₃</td></tr><tr><td>-9b</td><td>21</td><td>-(CH₂)₁₁-CH(CH₃)₂</td></tr><tr><td>-11</td><td>21</td><td>-(CH₂)₁₁-CH(CH₃)-C₂H₅</td></tr><tr><td>-13</td><td>21</td><td>-(CH₂)₁₁-CH(CH₃)-C₂H₅</td></tr><tr><td>-7b-1</td><td>20</td><td>-(CH₂)₁₀-CH(CH₃)-C₂H₅</td></tr><tr><td></td><td></td><td>-(CH₂)₁₁-CH(CH₃)₂</td></tr><tr><td>-7b-2</td><td>21</td><td>-(CH₂)₉-CH(CH₃)-C₂H₅</td></tr><tr><td></td><td></td><td>-(CH₂)₁₀-CH(CH₃)₂</td></tr></table>	Agelasphin	x	R	-7a	21	-(CH ₂) ₁₁ -CH ₃	-9a	21	-(CH ₂) ₁₂ -CH ₃	-9b	21	-(CH ₂) ₁₁ -CH(CH ₃) ₂	-11	21	-(CH ₂) ₁₁ -CH(CH ₃)-C ₂ H ₅	-13	21	-(CH ₂) ₁₁ -CH(CH ₃)-C ₂ H ₅	-7b-1	20	-(CH ₂) ₁₀ -CH(CH ₃)-C ₂ H ₅			-(CH ₂) ₁₁ -CH(CH ₃) ₂	-7b-2	21	-(CH ₂) ₉ -CH(CH ₃)-C ₂ H ₅			-(CH ₂) ₁₀ -CH(CH ₃) ₂	<p>Sponge <i>Agelas mauritianus</i></p>	<p>Antitumor Immunostimulatory</p>	<p>Natori et al., 1993, 1994</p>
Agelasphin	x	R																															
-7a	21	-(CH ₂) ₁₁ -CH ₃																															
-9a	21	-(CH ₂) ₁₂ -CH ₃																															
-9b	21	-(CH ₂) ₁₁ -CH(CH ₃) ₂																															
-11	21	-(CH ₂) ₁₁ -CH(CH ₃)-C ₂ H ₅																															
-13	21	-(CH ₂) ₁₁ -CH(CH ₃)-C ₂ H ₅																															
-7b-1	20	-(CH ₂) ₁₀ -CH(CH ₃)-C ₂ H ₅																															
		-(CH ₂) ₁₁ -CH(CH ₃) ₂																															
-7b-2	21	-(CH ₂) ₉ -CH(CH ₃)-C ₂ H ₅																															
		-(CH ₂) ₁₀ -CH(CH ₃) ₂																															

Exercises

- 1 Try to formulate questions that represent concepts-by-intuition and concepts-by-postulation with formative and reflective indicators for the following concepts:
 - A Life satisfaction
 - B Happiness
 - C The importance of the value “honesty”
- 2 In practice, it is seldom clear whether the questions suggested measure what they are supposed to measure.

Notes

- 1 Reproduced from *Journal of Chronic Diseases*, **39**, Brody, J. A. and Schneider, E. L., Diseases and disorders of aging: an hypothesis, pages 871–876, Copyright 1986, with permission from Elsevier.
- 2 Reproduced from *The Journals of Gerontology Series A: Biological Sciences and Medical Sciences*, **58**, Blumenthal, H. T., The aging–disease dichotomy: true or false?, pages M138–M145, Copyright 2003, with permission from Oxford University Press.

References

- Cai, W. and Chen, X. (2007) Nanoplatforms for targeted molecular imaging in living subjects. *Small*, **11**, 1840–54.
- Cheng, M.M., Cuda, G., Bunimovich, Y.L., Gaspari, M., Heath, J.R., Hill, H.D., Mirkin, C.A., Nijdam, A.J., Terracciano, R., Thundat, T. and Ferrari, M. (2006) *Biology*, **10**, 11–19.
- Gupta, A.K. and Gupta, M. (2005) Synthesis and surface engineering of iron oxide nanoparticles for biomedical applications. *Biomaterials*, **26**, 3995–4021.

Multiple Choice Questions

Questions Different types of question i.e. Multiple Choice Questions, Extended Matching Questions. Accordingly, calixarenes containing four phenol groups 39a–e exist as cone conformers. These are quite often put on a website but may still be typeset - Requirements are:

1 Multiple choice questions

For each question below, what is the most likely answer? Select ONE option from the answers supplied.

1.1 Ion Channels and Currents

1.1.1 Potassium



- 1 In a diagram of AP shown below, which one of the following currents is active where answers arrow is pointing?
 - A Ito
 - B IK1
 - C INa
 - D ICa

- 2 In a diagram of AP shown below, which one of the following currents is active where answers arrow is pointing?
 - A Ito
 - B IK1
 - C INa
 - D ICa

- 3 In a diagram of AP shown below, which one of the following currents is active where answers arrow is pointing?
 - A Ito
 - B IK1
 - C INa
 - D ICa

Book Title: Subtitle, First Edition. Edited by Author/Editor Name.

© 2015 John Wiley & Sons, Ltd. Published 2015 by John Wiley & Sons, Ltd.

50 | Multiple Choice Questions

- 9 In a diagram of AP shown below, which one of the following currents is active where answers arrow is pointing?
- A Ito
 - B IK1
 - C INa
 - D ICa
- 10 In a diagram of AP shown below, which one of the following currents is active where answers arrow is pointing?
- A Ito
 - B IK1
 - C INa
 - D ICa
- 11 In a diagram of AP shown below, which one of the following currents is active where answers arrow is pointing?
- A Ito
 - B IK1
 - C INa
 - D ICa

A

Simulating the Bloch Equations

In a real magnetic resonance (MR) experiment, there are many sources of magnetic fields in addition to \mathbf{B}_0 . The *chemical shift* modulates the effective field strength that a nucleus experiences due to shielding effects of the electron shell. The strength of the effect depends on the bonding state of the hydrogen atom, and is therefore different for spins constituting free water and those that are part of lipids, giving rise to the *fat-water shift*. In addition to \mathbf{B}_1 -fields used to flip the magnetization into the transverse plane, position-dependent magnetic field gradients along the z-axis (see Section 1.6.1) are used to manipulate the magnetization during the experiment. We can therefore express the effective magnetic field in the rotating frame as

$$x = t^3 - 30t^2 + 5 \quad (\text{A.1})$$

Of all these field components, B_0 is the strongest with a typical magnitude of 1.5 or 3 T on clinical magnetic resonance imaging (MRI) scanners. The gradients typically induce field variations in the order of a few tens of millitesla. B_1 usually has a magnitude in the range of tens of 11 T. The chemical shift is very weak, causing a field modulation of 1.3 ppm (parts per million) between water and fat. It is therefore only relevant for B_0 and is negligible for all other field components. B_1 fields are designed to rotate in the (x,y)-plane and therefore do not have a z-component. The precession in such a complex setting can be parameterized by a precession frequency vector

$$a(t) = \frac{d^2x}{dt^2} = 6t - 60 \quad (\text{A.2})$$

and the angle between the magnetization and the magnetic field is given by if \mathbf{M}' was aligned with \mathbf{B} at $t = 0$.

With this vector notation, we can express the precession in the rotating frame 1 as by adding T_2 and T_2 relaxation terms, we can express the Bloch equation (1.26) in the rotating frame as and the longitudinal equilibrium magnetization M_0 as defined in Eq. (1.7) (which is independent of the coordinate system and therefore not marked with a prime). In order to solve the differential equation (AS), we introduce the quantity \mathbf{h}' :

In order to simulate the time evolution of the magnetization, Eq. (All) can be solved for a number of time steps $tk = k \cdot \Delta t$. It is important to note that Eq. (All) was derived under the assumption of a constant matrix \mathbf{W}' , implying a constant \mathbf{B}' -vector in the rotating frame.



Glossary

account classification The way in which suppliers of electricity, natural gas, or fuel oil classify and bill their customers. Commonly used account classifications are “Residential,” “Commercial,” “Industrial,” and “Other.” Suppliers’ definitions of these terms vary from supplier to supplier. In addition, the same customer may be classified differently by each of its energy suppliers.

account of others (natural gas) Natural gas deliveries for the account of others are deliveries to customers by transporters that do not own the natural gas but deliver it for others for a fee. Included are quantities covered by long-term contracts and quantities involved in short-term or spot market sales.

accounting system A method of recording accounting data for a utility or company or a method of supplying accounting information for controlling, evaluating, planning and decision-making.



References

- 1 Perina, J. (1972) Coherence of Light, Van Nostrand, London.
- 2 Louisell, W.H. (1973) Quantum Statistical Properties of Radiation, John Wiley & Sons, Inc., New York.
- 3 Loudon, R. (1973) Quantum Theory of Light, Oxford University Press, Oxford.
- 4 Allen, L. and Eberly, J.H. (1975) Optical Resonance and Two-Level Atoms, John Wiley & Sons, Inc., New York.
- 5 Perina, J. (1984) Quantum Statistics of Linear and Nonlinear Optical Phenomena, D. Reidel Publishing Company, Dordrecht.
- 6 Gardiner, C.W. (1991) Quantum Noise, Springer-Verlag, Berlin, Heidelberg.
- 7 Meystre, P. and Sargent, M. III (1991) Elements of Quantum Optics, Springer-Verlag, Berlin, Heidelberg.
- 8 Walls, D.F. and Milburn, G.J. (1994) Quantum Optics, Springer-Verlag, Berlin, Heidelberg.
- 9 Vogel, W. and Welsch, D.-G. (1994) Lectures on Quantum Optics, Akademie Verlag, Berlin.
- 10 Scully, M.O. and Zubairy, M.S. (1997) Quantum Optics, Cambridge University Press, Cambridge.
- 11 Barnett, S.M. and Radmore, P.M. (1997) Methods in Theoretical Quantum Optics, Clarendon Press, Oxford.
- 12 Puri, R.R. (2001) Mathematical Methods of Quantum Optics, Springer, Berlin.
- 13 Dicke, R.H. (1954) *Physical Review*, 93, 99.
- 14 (a) Perelomov, A. (1986) Generalized Coherent States R. (1990) *Reviews of Modern Physics*, 62, 867.
- 15 Radcliffe, J.M. (1971) *Journal of Physics A: General Physics*, 4, 313.



Index

a

absorbance spectrum 66, 70
 diffraction 70
 adhesion 114
 absorption/scattering spectrum, *see* biological windows
 absorption techniques, gas adsorption 243
 air-solvent interface 69
 alkane 88
 alkanethiol-capped gold cluster 246
 alkanethiol molecules, lattice of 88
 alkoxysilanes 77
 alkyl chain ligands 177
 alloy
 Au/Ag 95
 nanomaterials, surface segregation 16
 alumina membrane 62
 amorphous silica, calcination 60
 amphiphilic molecules 211, 221
 lipids 211
 anisotropy 151
 antiferromagnetic materials 180, *see also*
 iron oxide
 antiferromagnetism 180
 apolar solvents 175
 atomic force microscope (AFM) 201
 Au-Ni-CNT microrods, scanning electron
 microscope (SEM) image 219

b

baffling process 203
 band 146
 conduction 146, 148

 valence 146
 barcoding 218
 bidentate ligand 176
 binary atomic lattices 187
 CaF₂ structure 187
 NaCl structure 187
 binary ordered arrays, formation 88
 binary superlattice 187
 bioconjugation technique 213, 226
 biological tissues, absorption/scattering
 spectrum 107
 biological windows 105, 107
 importance 107
 bionano 40, 189
 interface 37–45
 cancer cells 37
 magnetothermal 41
 photothermal treatment 41
 schematic presentation 40, 41
 biosensors 75, 77
 block copolymers 208, 210, 211
 blood stream, drugs concentration 75
 body-centered cubic (bcc) phase 209
 Bohr radius 149
 Boltzmann constant 148
 bottom-up techniques 118
 Braggs law 68, 71
 refractive index 71
 bionano applications 167
 bionano aspects 163
 doping of 160
 synthesis 151
 bridging group 175



“keywords/abstract

Dear Author,

Keywords and abstracts will normally not be included in the print version of your chapter but only in the online version (unless specifically agreed by Wiley/Wiley VCH)”.

Abstract

The first part of this chapter outlines the requirements for the individual assemblies of a modern UHPLC system. The differences between low-pressure and high-pressure mixing and their advantages and disadvantages are discussed. Furthermore, current UHPLC injection modes are described. The differences between fixed-loop and flow-through autosamplers are explained, and practical hints are given. Regarding the temperature control of the mobile and stationary phases, the influence of temperature on the resulting separation is shown. In addition, the use of column switching valves for routine applications is described. In the context of very narrow peaks in UHPLC, general requirements for UHPLC detectors are discussed. Another focus is the explanation of proper connection technology of the individual UHPLC modules. For this purpose, the influence of plastic- and stainless-steel-based connection technology on the resulting chromatography is shown.

Keywords

high- and low-pressure mixing system; fixed-loop and flow-through injection; column oven; UHPLC detectors; capillaries and fittings

Affiliation for the Authors

Steffen Wiese¹, Michael Heidorn², and Frank Steiner²

¹Chromsystems, Munich and Terence Hetzel, IUTA, Duisburg, Germany

²Thermo Fischer Scientific, Dornierstr. 4, 82110 Germering/Munich, Germany

**Biochemical Principles and
Mechanisms of Biosynthesis
Biodegradation of Polymers**

B. Cornils, W. A. Herrmann (Eds.)

**Applied Homogeneous Catalysis with
Organometallic Compounds**

A Comprehensive Handbook in Two Volumes

1996

ISBN: 978-3-527-29286-1

M. Beller, C. Bolm (Eds.)

Transition Metals for Organic Synthesis

Building Blocks and Fine Chemicals

1998

ISBN: 978-3-527-29501-1

A. Togni, R. L. Halterman (Eds.)

Metallocenes

1998

ISBN: 978-3-527-29539-9

P. J. Stang (Eds.)

Metal-catalyzed Cross-coupling Reactrom

1998

ISBN: 978-3-527-29421-X

B. Cornils, W. A. Herrmann (Eds.)

**Applied Homogeneous
Catalysis with Organometallic
Compounds**

**A Comprehensive Handbook
in Two Volumes**

1996

ISBN: 978-3-527-29286-1

E. Chang, F. Hussain, T. Dillon (Eds.)

**Trust and Reputation for
Service-Oriented
Environments**

**Technologies For Building Business
Intelligence And Consumer Confidence**

2006

ISBN: 978-3-527-01547-9

M. Beller, C. Bolm (Eds.)

**Transition Metals for Organic
Synthesis**

Building Blocks and Fine Chemicals

1998

ISBN: 978-3-527-29501-1

B. Cornils, W. A. Herrmann (Eds.)

The Shanty Chor

**A Comprehensive Handbook in
Two Volumes**

1996

ISBN: 978-3-527-29286-9

A. Togni, R. L. Halterman (Eds.)

Metallocenes

1998

ISBN: 978-3-527-29539-9

H. Misawa, S. Juodkazis (Eds.)

3D Laser Microfabrication

Principles and Applications

2006

ISBN: 978-3-527-31055-5

Wiley Handbooks in

FINANCIAL ENGINEERING AND ECONOMETRICS

Advisory Editor

Ruey S. Tsay

The University of Chicago Booth School of Business USA

The dynamic and interaction between financial markets around the world have changed dramatically under economic globalization. In addition, advances in communication and data collection have changed the way information is processed and used. In this new era, financial instruments have become increasingly sophisticated and their impacts are far-reaching. The recent financial (credit) crisis is a vivid example of the new challenges we face and continue to face in this information age. Analytical skills and ability to extract useful information from mass data, to comprehend the complexity of financial instruments, and to assess the financial risk involved become a necessity for economists, financial managers, and risk management professionals. To master such skills and ability, knowledge from computer science, economics, finance, mathematics and statistics is essential. As such, financial engineering is cross-disciplinary, and its theory and applications advance rapidly.

The goal of this Handbook Series is to provide a one-stop source for students, researchers, and practitioners to learn the knowledge and analytical skills they need to face today's challenges in financial markets. The Series intends to introduce systematically recent developments in different areas of financial engineering and econometrics. The coverage will be broad and thorough with balance in theory and applications. Each volume will be edited by leading researchers and practitioners in the area and covers state-of-the-art methods and theory of the selected topic.

Published Wiley Handbooks in Financial Engineering and Econometrics

Bauwens, Hafner, and Laurent · *Handbook of Volatility Models and Their Applications*

Brandimarte · *Handbook in Monte Carlo Simulation: Applications in Financial Engineering, Risk Management, and Economics*

Chan and Wong · *Handbook of Financial Risk Management: Simulations and Case Studies*

Cruz, Peters, and Shevchenko · *Fundamental Aspects of Operational Risk and Insurance Analytics: A Handbook of Operational Risk*

James, Marsh, and Sarno · *Handbook of Exchange Rates*



Mechanism of Biosynthesis

Nomenklatur der
Organischen Chemie

Edited by Hans-Georg Joost and Gerhard Eisenbrand

*in collaboration with
Gerald Böhm
Uwe Diederichsen*

Second Revised Edition

WILEY Blackwell

Monitoring

An Introduction

Gerald Böhm

WILEY Blackwell

Author

Linda E. Reichl

University of Texas
Center for Complex Quantum Systems
Austin, TX 78712
USA

Cover

Bose–Einstein condensates;
courtesy of Daniel J. Heinzen

All books published by Wiley-VCH are carefully produced. Nevertheless, authors, editors, and publisher do not warrant the information contained in these books, including this book, to be free of errors. Readers are advised to keep in mind that statements, data, illustrations, procedural details or other items may inadvertently be inaccurate.

Library of Congress Card No.: applied for

British Library Cataloguing-in-Publication Data:

A catalogue record for this book is available from the British Library.

Bibliographic information published by the Deutsche Nationalbibliothek

The Deutsche Nationalbibliothek lists this publication in the Deutsche Nationalbibliografie; detailed bibliographic data are available on the Internet at <http://dnb.d-nb.de>.

© 2016 WILEY-VCH Verlag GmbH & Co. KGaA, Boschstr. 12, 69469 Weinheim, Germany

All rights reserved (including those of translation into other languages). No part of this book may be reproduced in any form – by photoprinting, microfilm, or any other means – nor transmitted or translated into a machine language without written permission from the publishers. Registered names, trademarks, etc. used in this book, even when not specifically marked as such, are not to be considered unprotected by law.

Cover Design Formgeber, Mannheim, Germany

Typesetting le-tex publishing services GmbH, Leipzig, Germany

Printing and Binding

Print ISBN 978-3-527-41349-2

ePDF ISBN 978-3-527-69046-6

ePub ISBN 978-3-527-69048-0

Mobi ISBN 978-3-527-69047-3

oBook ISBN 978-3-527-69049-7

Printed on acid-free paper.

This edition first published 2017
© 2017

All rights reserved. No part of this publication may be reproduced, stored in a retrieval system, or transmitted, in any form or by any means, electronic, mechanical, photocopying, recording or otherwise, except as permitted by law. Advice on how to obtain permission to reuse material from this title is available at <http://www.wiley.com/go/permissions>.

The right of Jane Brown and Mark Smith to be identified as the authors of this work has been asserted in accordance with law.

Registered Offices

John Wiley & Sons, Inc., 111 River Street, Hoboken, NJ 07030, USA
John Wiley & Sons Ltd, The Atrium, Southern Gate, Chichester, West Sussex, PO19 8SQ, UK

Editorial Office

The Atrium, Southern Gate, Chichester, West Sussex, PO19 8SQ, UK

For details of our global editorial offices, customer services, and more information about Wiley products visit us at www.wiley.com.

Wiley also publishes its books in a variety of electronic formats and by print-on-demand. Some content that appears in standard print versions of this book may not be available in other formats.

Limit of Liability/Disclaimer of Warranty

While the publisher and authors have used their best efforts in preparing this work, they make no representations or warranties with respect to the accuracy or completeness of the contents of this work and specifically disclaim all warranties, including without limitation any implied warranties of merchantability or fitness for a particular purpose. No warranty may be created or extended by sales representatives, written sales materials or promotional statements for this work. The fact that an organization, website, or product is referred to in this work as a citation and/or potential source of further information does not mean that the publisher and authors endorse the information or services the organization, website, or product may provide or recommendations it may make. This work is sold with the understanding that the publisher is not engaged in rendering professional services. The advice and strategies contained herein may not be suitable for your situation. You should consult with a specialist where appropriate. Further, readers should be aware that websites listed in this work may have changed or disappeared between when this work was written and when it is read. Neither the publisher nor authors shall be liable for any loss of profit or any other commercial damages, including but not limited to special, incidental, consequential, or other damages.

Library of Congress Cataloging-in-Publication Data

Cover image:
Cover design by

Set in 9.5/12.5pt STIXTwoText by SPi Global, Pondicherry, India

10 9 8 7 6 5 4 3 2 1

to Hans-Martin



Brief Contents

List of Contributors *xi*

Foreword *xiii*

Preface *xv*

Part I Metal Oxide Nanomaterials 1

- 1 The Biomimetic Synthesis of Metal Oxide Nanomaterials 3
- 2 Synthesis of Symmetric and Asymmetric Nanosilica for Materials, Optical and Medical Applications 55
- 3 Sources of Natural Flavors 90
- 4 Mechanism of Color Perception 110
- 5 Preparation of Plant Material for Extraction 150
- 6 Methods of Extraction of Essential Oils 180

Index 000



Contents

List of Contributors *xi*

Foreword *xiii*

Preface *xv*

Part I Metal Oxide Nanomaterials *1*

- 1 The Biomimetic Synthesis of Metal Oxide Nanomaterials** *3*
Leila F. Deravi, Joshua D. Swartz and David W. Wright
 - 1.1 Introduction *3*
 - 1.2 Metal Oxides in Nature *4*
 - 1.2.1 Components of Biomineralization *5*
 - 1.2.2 Biomineralization Optimization *6*
 - 1.3 Biomimetic Synthesis of Metal Oxide Nanomaterials *7*
 - 1.4 Constrained Biomineralization *8*
 - 1.4.1 Bacterial Synthesis of Metal Oxide Nanomaterials *8*
 - 1.4.2 Synthesis of Protein-Functionalized Ferromagnetic Co_3O_4 Nanocrystals *9*
 - 1.4.3 Room-Temperature Synthesis of Barium Titanate *10*
 - 1.4.4.1 Biomimetic Synthesis of Iron Oxide *11*
- 2 Synthesis of Symmetric and Asymmetric Nanosilica for Materials, Optical and Medical Applications** *55*
Yongquan Qu, Jennifer Lien and Ting Guo
 - 2.1 Introduction *55*
 - 2.2 Synthesis of Nanosilica *59*
 - 2.2.1 Symmetric Nanosilica *59*
 - 2.2.1.1 Catalytic Methods *63*
 - 2.2.1.2 Noncatalytic Growth *65*
 - 2.2.2 Asymmetric Silica Nanomaterials *68*
 - 2.2.2.1 Catalytic Growth *68*
 - 2.2.2.2 Noncatalytic Growth *69*
 - 2.3 Characterization *70*
 - 2.4 Applications of Symmetric and Asymmetric Nanosilica *72*

Index *000*



Contents

Foreword *xiii*

Preface *xv*

Part I Metal Oxide Nanomaterials 1

- 1 The Biomimetic Synthesis of Metal Oxide Nanomaterials 3**
 - 1.1 Introduction 3
 - 1.2 Metal Oxides in Nature 4
 - 1.2.1 Components of Biomineralization 5
 - 1.2.2 Biomineralization Optimization 6
 - 1.3 Biomimetic Synthesis of Metal Oxide Nanomaterials 7
 - 1.4 Constrained Biomineralization 8
 - 1.4.1 Bacterial Synthesis of Metal Oxide Nanomaterials 8
 - 1.4.2 Synthesis of Protein-Functionalized Ferromagnetic Co_3O_4 Nanocrystals 9
 - 1.4.3 Room-Temperature Synthesis of Barium Titanate 10
 - 1.4.4 Biomimetic Synthesis of Magnetite 11
 - 1.4.4.1 Biomimetic Synthesis of Iron Oxide 11
- 2 Synthesis of Symmetric and Asymmetric Nanosilica for Materials, Optical and Medical Applications 55**
 - 2.1 Introduction 55
 - 2.2 Synthesis of Nanosilica 59
 - 2.2.1 Symmetric Nanosilica 59
 - 2.2.1.1 Catalytic Methods 63
 - 2.2.1.2 Noncatalytic Growth 65
 - 2.2.2 Asymmetric Silica Nanomaterials 68
 - 2.2.2.1 Catalytic Growth 68
 - 2.2.2.2 Noncatalytic Growth 69
 - 2.3 Characterization 70
 - 2.4 Applications of Symmetric and Asymmetric Nanosilica 72

Index 000



Contents

Foreword *xiii*

Preface *xv*

Part I Metal Oxide Nanomaterials 1

1 The Biomimetic Synthesis of Metal Oxide Nanomaterials 3

Introduction 3

Metal Oxides in Nature 4

 Components of Biomineralization 5

 Biomineralization Optimization 6

Biomimetic Synthesis of Metal Oxide Nanomaterials 7

Constrained Biomineralization 8

 Bacterial Synthesis of Metal Oxide Nanomaterials 8

 Synthesis of Protein-Functionalized Ferromagnetic Co_3O_4 Nanocrystals 9

 Room-Temperature Synthesis of Barium Titanate 10

 Biomimetic Synthesis of Magnetite 11

 Biomimetic Synthesis of Iron Oxide 11

2 Synthesis of Symmetric and Asymmetric Nanosilica for Materials, Optical and Medical Applications 55

Introduction 55

Synthesis of Nanosilica 59

 Symmetric Nanosilica 59

 Catalytic Methods 63

 Noncatalytic Growth 65

 Asymmetric Silica Nanomaterials 68

 Catalytic Growth 68

 Noncatalytic Growth 69

Characterization 70

Applications of Symmetric and Asymmetric Nanosilica 72

Index 000



List of Contributors

Andrew B. Adams

Department of Surgery
Emory Transplant Center
Emory University School of Medicine
Atlanta
USA

Maria-Luisa Alegre, MD, PhD

Associate Professor
Department of Medicine, Section of
Rheumatology
Gwen Knapp Center for Lupus and
Immunology Research
The University of Chicago
Chicago
USA

Agnes M. Azimzadeh, PhD

Assistant Professor of Surgery
Department of Surgery
University of Maryland School of
Medicine
Baltimore
USA

William M. Baldwin III

Department of Immunology
Cleveland Clinic Lerner College of
Medicine
Department of Pathology
Case Western Reserve University
School of Medicine
Cleveland
USA

Jonathan S. Bromberg, MD, PhD

Professor of Surgery and Microbiology
and Immunology
Department of Surgery
University of Maryland School of
Medicine
Baltimore
USA

J. Michael Cecka

UCLA Immunogenetics Center
Department of Pathology and
Laboratory Medicine
David Geffen School of Medicine at
UCLA
Los Angeles
USA

Anil Chandraker, MD, FASN, FRCP

Transplant Research Center
Renal Division
Brigham and Women's Hospital
Harvard Medical School
Boston
USA

Sung Choi, MD

Blood and Marrow Transplantation
Program
Department of Internal Medicine
Division of Hematology/Oncology
University of Michigan
Comprehensive Cancer Center
Ann Arbor
USA

Anita S. Chong, PhD

Department of Surgery, Section of
Transplantation
The University of Chicago
Chicago
USA

Yaozhong Ding, PhD

Assistant Professor
Department of Surgery
University of Maryland School of Medicine
Baltimore
USA

Gunilla Einecke

Department of Nephrology
Hannover Medical School
Hannover
Germany

Robert L. Fairchild

Department of Immunology
Cleveland Clinic Lerner College of
Medicine
Department of Pathology
Case Western Reserve University
School of Medicine
Cleveland
USA

Philip F. Halloran, MD, PhD

Alberta Transplant Applied Genomics
Centre
Department of Medicine
Division of Nephrology and Transplant
Immunology
University of Alberta
Edmonton
Canada

Choli Hartono

Department of Medicine
Weill Cornell Medical College
New York
USA

Timm Heinbokel

Division of Transplant Surgery and
Transplant Surgery Research Laboratory
Brigham and Women's Hospital
Harvard Medical School
Boston
USA

Yiming Huang

Institute for Cellular Therapeutics
University of Louisville
Louisville and Duke University
Raleigh
USA

Suzanne T. Ildstad, MD

Director, Institute for Cellular Therapeutics
Jewish Hospital Distinguished
Professor of Transplantation
Distinguished University Scholar
Professor of Surgery, Physiology,
Immunology
University of Louisville
Louisville and Duke University
Raleigh
USA

Haofeng Ji

Dumont-UCLA Transplantation Center
Division of Liver and Pancreas
Transplantation, Department of Surgery,
David Geffen School of Medicine at UCLA
Los Angeles
USA

Bibo Ke

Dumont-UCLA Transplantation
Center Division of Liver and Pancreas
Transplantation, Department of
Surgery
David Geffen School of Medicine at UCLA
Los Angeles
USA

Foreword

The dilemma of rapidly emerging fields is that reviews are often outdated before they are printed. To make a contribution that would endure, we knew we had to go beyond a snapshot of the current state of fragment-based drug discovery and instead provide a framework for upcoming advances. To achieve this goal, we needed to convince leading scientists to take time from their busy schedules to write chapters. Fortunately, nearly all those we approached agreed; and what you hold in your hands is a virtual, although not comprehensive, “Who’s Who” in fragment-based drug discovery. We are extremely grateful to all of our contributors for the quality of their chapters.

One striking feature of this book is that more than half of the chapters come from industry-based researchers; and even many of the academic contributors have close ties to industry. It has been alleged that the best science is done in academia; this book proves that this is not necessarily the case. Part of the reason may be that many of the techniques involved require expensive equipment and infrastructure as well as large collaborations between scientists from disparate disciplines – collaborations that would be difficult to set up outside industry. The multidisciplinary nature of fragment-based approaches shows in this volume: contributors include computational chemists, NMR spectroscopists, X-ray crystallographers, mass-spectrometrists, as well as organic and medicinal chemists.

Although fragment-based strategies for drug discovery have now pervaded laboratories across the world, the ultimate success of any drug discovery technology is measured in the quantity and quality of drugs that it produces. Fragment-based drug discovery has only been practical for the past decade, too soon to expect it to produce marketed drugs; but we believe these will come in time. Moreover, many of the techniques and concepts described in this book will alter drug discovery endeavors in subtle, tangential ways. Ideally, readers will be inspired to improve the methods described here, or even to develop fundamentally new methods for fragment-based drug discovery. But even if this book only changes the way medicinal chemists approach lead optimization, or persuades them to look more closely at weak but validated hits, it will have served its purpose.

Basely, March 2006

Wolfgang Jahnke
Daniel A. Erlanson



Symbols and Abbreviations

Symbols

α	electron spin quantum number $m_s = 1/2$ angle, alternating parameter anisotropic exchange parameter
α_n	nuclear spin quantum number $m_I = 1/2$
β	spin quantum number $m_s = -1/2$ angle
β_n	nuclear spin quantum number $m_I = -1/2$
δ_{ij}	Kronecker δ
θ	angle Curie-Weiss constant
Δ_H	line-width
$\Delta H_{1/2}$	half height line-width
ΔH_{pp}	peak-to-peak line-width
ΔH_{msl}	maximum-slope line-width
$\Delta H\omega_{1/2}, \Delta H\omega_{pp}$	line-width in frequency
ϵ_0	dielectric constant
ϵ_F	Fermi energy
η	$ J'/J $
Γ	molecular field coefficient
γ	gyromagnetic ratio exchange interaction parameter anisotropic exchange parameter
γ_n	nuclear gyromagnetic ratio
φ	molecular orbital relaxation function
Ψ	molecular orbital
ψ	atomic orbital
ν	frequency
μ	magnetic permeability
μ_0	magnetic permeability of free space



Color Plates

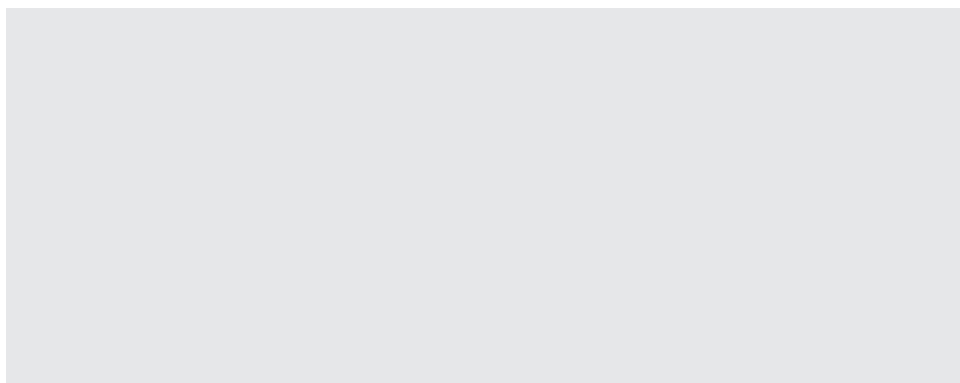


Figure 1.6 See text page 00 for full figure caption.

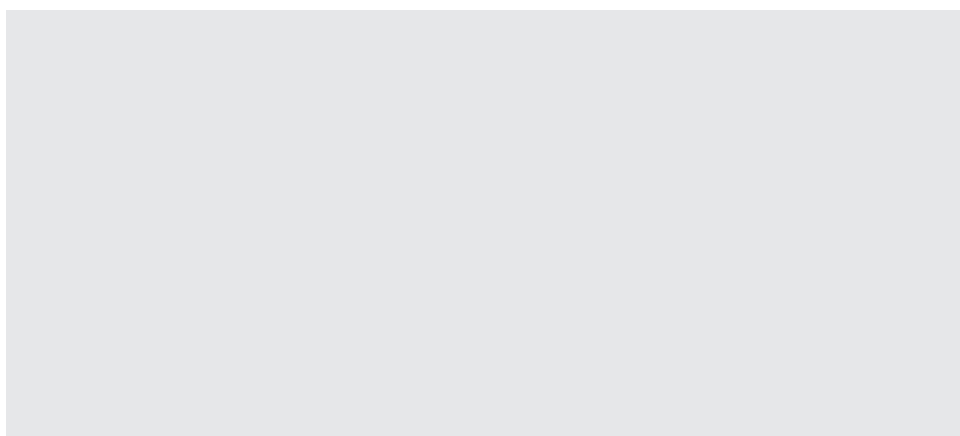


Figure 1.7 See text page 00 for full figure caption.



About the Companion Website

Practical Physiotherapy for Small Animal Practice is accompanied by a companion website:



www.wiley.com/go/

The website includes:

- Client education handouts.



Part IV

Summaries and Visions

Bold Glance into the Future—Where no Man has Gone Before



5

cDNA and Microarray-based Technologies

5.1 Introduction

The molecular characterization of tumor-associated antigens (TAA) recognized by T cells [1] revolutionized the field of tumor immune biology providing conclusive evidence that CD8+ cytotoxic T cells (CTLs) specifically recognize and kill autologous cancer through recognition of molecularly-defined cancer-specific elements.

5.1.1 CEA Gene Family, Genomic Localization, Protein Structure

CEA is encoded by the CEA-related cell-cell adhesion molecule 5 (CEACAM5) gene, which belongs to the CEA gene family and in humans consists of 22 expressed members and 12 pseudogenes [3,4].

5.1.1.1 Animal Models for CEA

Mice are commonly used to analyze the efficacy of tumor therapies and mechanisms of tumor rejection. However, this species cannot be utilized to evaluate CEA-based therapies since no CEACAM5 ortholog exists in rodents.

5.1.1.1.1 Models for CEACAM5 Containing a Bacterial Artificial Chromosome

Either cosmid clones containing the CEACAM5 gene or a bacterial artificial chromosome (BAC) clone, which comprises part of the gene cluster surrounding CEACAM5, served as a genetic source. This cluster includes CEACAM6 and CEACAM3.

Antibody Delivery of Radionuclides, Drugs and Effector Molecules The use of low molecular weight single chain antibody fragments and pre-targeting has been found to enhance the sensitivity of tumor visualization as well as increasing the delivered therapeutic dose by separating the antibody therapeutic radionuclide that binds to the tumor-localized antibody.

SubParagraph Title: Nuclear Angular Momentum and Magnetic Moment The conformational flexibility of calixarenes is usually explained by the presence of intramolecular hydrogen bonds, which is related to the number of free phenol groups. Accordingly, calixarenes containing four phenol groups 39a–e exist as cone conformers.

Book Title: Subtitle, First Edition. Edited by Author/Editor Name.

© 2015 John Wiley & Sons, Ltd. Published 2015 by John Wiley & Sons, Ltd.



5

cDNA and Microarray-based Technologies

Introduction

The molecular characterization of tumor-associated antigens (TAA) recognized by T cells [1] revolutionized the field of tumor immune biology providing conclusive evidence that CD8+ cytotoxic T cells (CTLs) specifically recognize and kill autologous cancer through recognition of molecularly-defined cancer-specific elements.

CEA Gene Family, Genomic Localization, Protein Structure

CEA is encoded by the CEA-related cell-cell adhesion molecule 5 (CEACAM5) gene, which belongs to the CEA gene family and in humans consists of 22 expressed members and 12 pseudogenes [3,4].

Animal Models for CEA

Mice are commonly used to analyze the efficacy of tumor therapies and mechanisms of tumor rejection. However, this species cannot be utilized to evaluate CEA-based therapies since no CEACAM5 ortholog exists in rodents. This problem was circumvented by introducing the human CEACAM5 gene into the germ line of mice [52–54].

Models for CEACAM5 Containing a Bacterial Artificial Chromosome

Either cosmid clones containing the CEACAM5 gene or a bacterial artificial chromosome (BAC) clone, which comprises part of the gene cluster surrounding CEACAM5, served as a genetic source. This cluster includes CEACAM6 and CEACAM3.

Antibody Delivery of Radionuclides, Drugs and Effector Molecules Delivery of radio-nuclides to tumors using murine and human anti-CEA antibodies has been studied for many years [70]. The use of low molecular weight single chain antibody fragments and pre-targeting has been found to enhance the sensitivity of tumor visualization as well as increasing the delivered therapeutic dose by separating the antibody targeting to the tumor from the subsequent delivery of the therapeutic radionuclide that binds to the tumor-localized antibody.

SubParagraph Title: Nuclear Angular Momentum and Magnetic Moment The conformational flexibility of calixarenes is usually explained by the presence of intramolecular hydrogen bonds, which is related to the number of free phenol groups. Accordingly, calixarenes, containing four phenol groups 39a–e exist as cone conformers.

Delivery of radio-nuclides to tumors using murine and human anti-CEA antibodies has been studied for many years [70]. The use of low molecular weight single chain antibody fragments and pre-targeting has been found to enhance the sensitivity of tumor visualization as well as increasing the delivered therapeutic dose by separating the antibody targeting to the tumor from the subsequent delivery of the therapeutic radionuclide that binds to the tumor-localized antibody.

11

Carcinoembryonic Antigen

Decoding the CEA-Related Cell-Cell Adhesion Molecule

The molecular characterization of tumor-associated antigens (TAA) recognized by T cells [1] revolutionized the field of tumor immune biology providing conclusive evidence that CD8+ cytotoxic T cells (CTLs) specifically recognize and kill autologous cancer through recognition of molecularly-defined cancer-specific elements. Since then a myriad of TAA have been identified that has triggered their utilization as anti-cancer vaccines [2–8].

11.1 CEA Biology

11.1.1 CEA Gene Family, Genomic Localization, Protein Structure

CEA is encoded by the CEA-related cell-cell adhesion molecule 5 (CEACAM5) gene, which belongs to the CEA gene family and in humans consists of 22 expressed members and 12 pseudogenes [3,4]. The CEA family has been subdivided into the CEACAM and pregnancy-specific glycoprotein (PSG) subgroups.

11.1.2 CEA as a Tumor Marker for Prognosis and Post-surgery Follow-up

11.1.2.1 Animal Models for CEA

Antibody Delivery of Radionuclides, Drugs and Effector Molecules Using Murine and Human Anti-CEA Antibodies Delivery of radio-nuclides to tumors using murine and human anti-CEA anti-bodies has been studied for many years [70]. The use of low molecular weight single chain antibody fragments and pre-targeting has been found to enhance the sensitivity of tumor visualization as well as increasing the delivered therapeutic dose by separating the antibody targeting to the tumor from the subsequent delivery of the therapeutic radionuclide that binds to the tumor-localized antibody. The use of low molecular weight single chain antibody fragments and pre-targeting has been found to enhance the sensitivity of tumor visualization as well as increasing.

The use of low molecular weight single chain antibody fragments and pre-targeting has been found to enhance the sensitivity of tumor visualization as well as increasing the delivered therapeutic dose by separating the antibody targeting to the tumor from the subsequent delivery of the therapeutic radionuclide that binds to the tumor-localized antibody.



2

Trust and Reputation for Service-Oriented Environments Technologies for Building Business Intelligence and Consumer Confidence

Fillers, Filled Polymers and Polymer Blends and Furthermore Nuclear
Angular Momentum and Magnetism

2.1 Intermolecular Interactions Physical Picture, Computational Methods and Model Potentials Nuclear Angular Momentum and Magnetic Moment

The molecular characterization of tumor-associated antigens (TAA) recognized by T cells [1] revolutionized the field of tumor immune biology providing conclusive evidence that CD8+ cytotoxic T cells (CTLs) specifically recognize and kill autologous cancer through recognition of molecularly-defined cancer-specific elements. Since then a myriad of TAA have been identified that has triggered their utilization as anti-cancer vaccines [2–8].

2.1.1 Networking and Online Games Understanding and Engineering Multiplayer Internet Games Nuclear Angular Momentum and Magnetic Moment

CEA is encoded by the CEA-related cell-cell adhesion molecule 5 (CEACAM5) gene, which belongs to the CEA gene family and in humans consists of 22 expressed members and 12 pseudogenes [3,4]. The CEA family has been subdivided into the CEACAM and pregnancy-specific glycoprotein (PSG) subgroups.

2.1.1.1 Nuclear Angular Momentum and Magnetic Moment Respectively the Digital Photographer's Guide to Color Management

Apically expressed CEA on normal epithelial cells is shed into the lumen possibly by the action of phospholipases and through the exfoliation of turned-over cells. Thus CEA does not have access the bloodstream. Expression on less differentiated unpolarized tumor cells, however, allows released CEA to enter blood and lymphatic vessels through the intercellular spaces, which can lead to elevated CEA concentrations in the sera of tumor patients.

Fillers, Filled Polymers and Polymer Blends and Furthermore Nuclear Angular Momentum and Magnetism CEA is encoded by the CEA-related cell-cell adhesion molecule 5 (CEACAM5) gene, which belongs to the CEA gene family and in humans consists of 22 expressed members and 12 pseudogenes [3,4]. In the past, the CEA family has been subdivided into the CEACAM and pregnancy-specific glycoprotein (PSG) subgroups.

Book Title: Subtitle, First Edition. Edited by Author/Editor Name.

© 2015 John Wiley & Sons, Ltd. Published 2015 by John Wiley & Sons, Ltd.

11

Carcinoembryonic Antigen

Decoding the CEA-Related Cell-Cell Adhesion Molecule

The molecular characterization of tumor-associated antigens (TAA) recognized by T cells [1] revolutionized the field of tumor immune biology providing conclusive evidence that CD8⁺ cytotoxic T cells (CTLs) specifically recognize and kill autologous cancer through recognition of molecularly-defined cancer-specific elements. Since then a myriad of TAA have been identified that has triggered their utilization as anti-cancer vaccines [2–8].

11.1 CEA Biology

11.1.1 CEA Gene Family, Genomic Localization, Protein Structure

CEA is encoded by the CEA-related cell-cell adhesion molecule 5 (CEACAM5) gene, which belongs to the CEA gene family and in humans consists of 22 expressed members and 12 pseudogenes [3,4]. The CEA family has been subdivided into the CEACAM and pregnancy-specific glycoprotein (PSG) subgroups.

11.1.2 CEA as a Tumor Marker for Prognosis and Post-surgery Follow-up

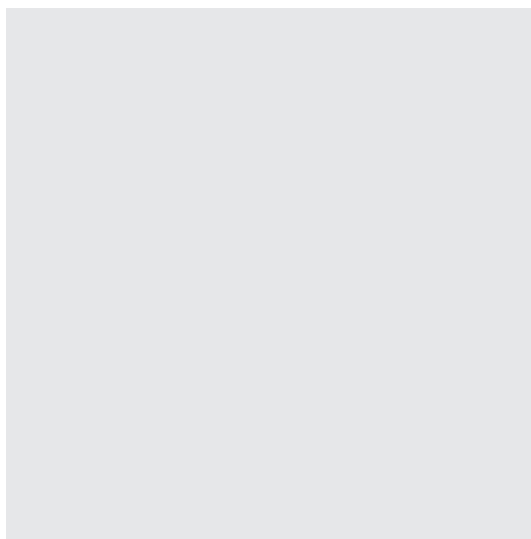
11.1.2.1 Animal Models for CEA

Antibody Delivery of Radionuclides, Drugs and Effector Molecules Using Murine and Human Anti-CEA Antibodies Delivery of radio-nuclides to tumors using murine and human anti-CEA anti-bodies has been studied for many years [70]. The use of low molecular weight single chain antibody fragments and pre-targeting has been found to enhance the sensitivity of tumor visualization as well as increasing the delivered therapeutic dose by separating the antibody targeting to the tumor from the subsequent delivery of the therapeutic radionuclide that binds to the tumor-localized antibody. The use of low molecular weight single chain antibody fragments and pre-targeting has been found to enhance the sensitivity of tumor visualization as well as increasing. The use of low molecular weight single chain antibody fragments and pre-targeting has been found to enhance the sensitivity of tumor visualization as well as increasing the delivered therapeutic dose by separating the antibody targeting to the tumor from the subsequent delivery of the therapeutic radionuclide that binds to the tumor-localized antibody.

11

Carcinoembryonic Antigen

Decoding the CEA-Related Cell-Cell Adhesion Molecule



The molecular characterization of tumor-associated antigens (TAA) recognized by T cells [1] revolutionized the field of tumor immune biology providing conclusive evidence that CD8+ cytotoxic T cells (CTLs) specifically recognize and kill autologous cancer through recognition of molecularly-defined cancer-specific elements. Since then a myriad of TAA have been identified that has triggered their utilization as anti-cancer vaccines [2–8].

11.1 CEA Biology

11.1.1 CEA Gene Family, Genomic Localization, Protein Structure

CEA is encoded by the CEA-related cell-cell adhesion molecule 5 (CEACAM5) gene, which belongs to the CEA gene family and in humans consists of 22 expressed members and 12 pseudogenes [3,4]. The CEA family has been subdivided into the CEACAM and pregnancy-specific glycoprotein (PSG) subgroups.

11.1.2 CEA as a Tumor Marker for Prognosis and Post-surgery Follow-up

11.1.2.1 Animal Models for CEA

Antibody Delivery of Radionuclides, Drugs and Effector Molecules Using Murine and Human Anti-CEA Antibodies Delivery of radio-nuclides to tumors using murine and human anti-CEA anti-bodies has been studied for many years [70]. The use of low molecular weight single chain antibody fragments and pre-targeting has been found to enhance the sensitivity of tumor visualization as well as increasing the delivered therapeutic dose by separating the antibody targeting to the tumor from the subsequent delivery of the therapeutic radionuclide that binds to the tumor-localized antibody. The use of low molecular weight single chain antibody fragments and pre-targeting has been found to enhance the sensitivity of tumor visualization as well as increasing. The use of low molecular weight single chain antibody fragments and pre-targeting has been found to enhance the sensitivity of tumor visualization as well as increasing the delivered therapeutic dose by separating the antibody targeting to the tumor from the subsequent delivery of the therapeutic radionuclide that binds to the tumor-localized antibody.

11

Carcinoembryonic Antigen

Wolfgang Zimmermann^{1,3} and Robert Kammerer²

¹ Helmholtz Centre for Infection Research, Department of Systems Immunology, Inhoffenstr. 7, 38124, Braunschweig, Germany

² Bio Center for Life Science, University of Technology Braunschweig, Spielmannstr. 7, 38106, Braunschweig, Germany

³ Institute for Molecular and Clinical Immunology, Otto-von-Guericke University, Leipziger Str. 44, 39120, Magdeburg, Germany

The very essence of cardiovascular practice is the early detection of heart failure

Sir Thomas Lewis, 1933

11.1 Introduction

The molecular characterization of tumor-associated antigens (TAA) recognized by T cells [1] revolutionized the field of tumor immune biology providing conclusive evidence that CD8+ cytotoxic T cells (CTLs) specifically recognize and kill autologous cancer through recognition of molecularly-defined cancer-specific elements.

11.2 CEA Biology

11.2.1 CEA Gene Family, Genomic Localization, Protein Structure

CEA is encoded by the CEA-related cell-cell adhesion molecule 5 (CEACAM5) gene, which belongs to the CEA gene family and in humans consists of 22 expressed members and 12 pseudogenes [3,4]. The CEA family has been subdivided into the CEACAM and pregnancy-specific glycoprotein (PSG) subgroups. Apically expressed CEA on normal epithelial cells is shed into the lumen possibly by the action of phospholipases and through the exfoliation of turned-over cells. Thus CEA does not have access the bloodstream. Expression on less differentiated unpolarized tumor cells, however, allows released CEA to enter blood and lymphatic vessels through the intercellular spaces, which can lead to elevated CEA concentrations in the sera of tumor patients.

Book Title: Subtitle, First Edition. Edited by Author/Editor Name.

© 2015 John Wiley & Sons, Ltd. Published 2015 by John Wiley & Sons, Ltd.

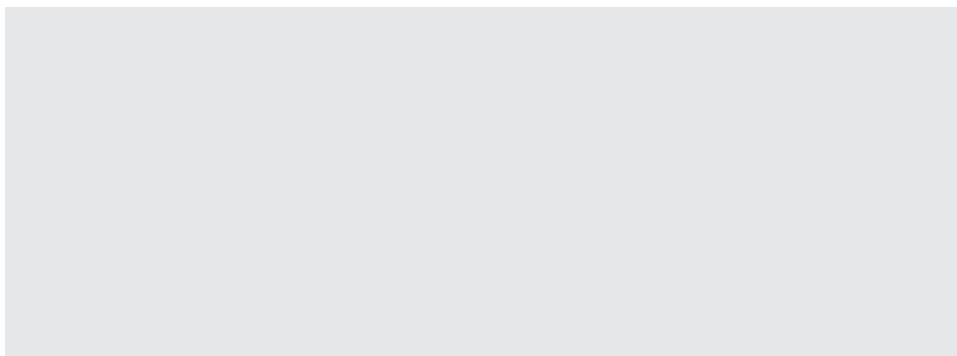


Figure 1.6 Illustration of catalytically grown β -Ga₂O₃ nanoparticles. *Source:* Reprinted with permission from Ref. [38]; © 2007 American Chemical Society.

Traditionally, synthetic approaches for the production of functional metal oxide materials have involved are estimated to reach an outstanding US \$100 billion per Figure 1.6 facility by the year 2020, as the demand for smaller, lighter and faster materials continues to grow [1]. But, more importantly, manufacturers are progressing in this manner at the expense of the environment, as they accumulate hazardous chemical wastes [2]. For decades, research teams in the semiconductor industry have been seeking alternative methods to passivate not only the rate of waste production but also the cost of spending. As mentioned above, the photoresist should be thin according to the distance of localization of the optical near-field around the nanoaperture. On the other hand, the photoresist should have the dry etching resistance so that the latent image can be transferred to the lower layer substrate. To separate the function of the Figure 1.7 thin film and the dry etching resistance, we used a trilayer resist process; the upper layer is an ultrathin photoresist, the middle layer is thin spin on glass (SOG), and the lower layer is a resin.

As mentioned above, the photoresist should be thin according to the distance of localization of the optical near-field around the nanoaperture. On the other hand, the photoresist should have the dry etching resistance so that the latent image can be transferred to the

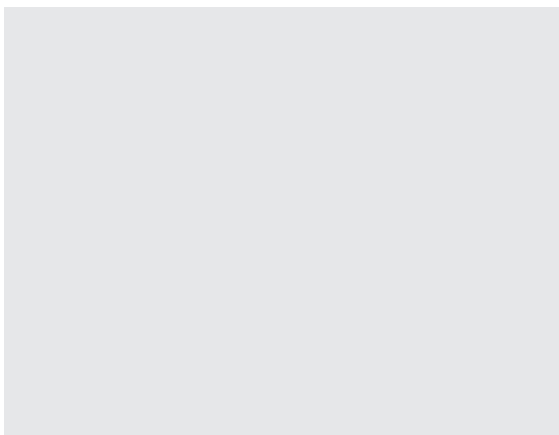


Figure 1.7 Transmission electron microscopy images (scale bar = 20 nm) of magnetosomes from various bacterial strains. (a) Pseudo-hexagonal prism; (b) Cubo-octahedral crystal; (c) Tooth-shaped. Transmission electron microscopy images (scale bar = 20 nm) of magnetosomes from various bacterial strains. *Source:* Reproduced with permission from Ref. [17]; © 2007, Wiley-VCH Verlag GmbH & Co. KGaA.

lower layer substrate. To separate the function of the thin film and the dry etching resistance, we used a trilayer resist process; the upper layer is an ultrathin photoresist, the middle layer is thin spin on glass (SOG), and the lower layer is a resin. The patterns of shallow latent images in the upper layer are transferred to the thin SOG layer of excellent dry-etching resistance, and these are transferred in the lower layer further.

Traditionally, synthetic approaches for the production of functional metal oxide materials have involved high-temperature reaction environments with energy intensive techniques such as laser ablation, ion implantation, chemical vapor deposition (CVD), photolithography or thermal decomposition [1]. The incorporation of these techniques has provided a rapid prototyping technique, essential for the commercial development of current minimum feature-sized semiconducting integrated circuits. However, the production of these devices has been achieved at a high price, with the primary challenges currently faced by high-throughput fabrication laboratories including the high cost of laborers and instruments, high temperature reaction conditions, and a surplus in generated waste [1]. In fact, the cost of fabrication facilities are estimated to reach an outstanding US \$100 billion per facility by the year 2020, as the demand for smaller, lighter and faster materials continues to grow [1]. But, more importantly, manufacturers are progressing in this manner at the expense of the environment, as they accumulate hazardous chemical wastes [2]. For decades, research teams in the semiconductor industry have been seeking alternative methods to passivate not only the rate of waste production but also the cost of spending.

As mentioned above, the photoresist should be thin according to the distance of localization of the optical near-field around the nanoaperture. On the other hand, the photoresist should have the dry etching resistance so that the latent image can be transferred to the lower layer substrate. To separate the function of the thin film and the dry etching resistance, we used a trilayer resist process; the upper layer is an ultrathin photoresist, the middle layer is thin spin on glass (SOG), and the lower layer is a resin. The patterns of shallow latent images in the upper layer are transferred to the thin SOG layer of excellent dry-etching resistance, and these are transferred in the lower layer further.

Figure 1.8 shows the appearance of a prototype device of optical near-field lithography [7]. The features of the prototype device are as follows. This device is compact, with a footprint of about 2m [1]. It has symmetric structure to compensate thermal expansion and temperature drift, and the hanging controlling structure is introduced to avoid floor vibrations. In addition, it has a double clean structure, and the near-field photomask and the wafer are kept in a local clean environment by controlling a flow of clean air of the device inside.

Bioinspired research is based on identifying and emulating the principles of biomineralization in natural systems, instead of copying them directly. In fact, most strategies incorporated by natural systems are not directly applicable to engineered materials, so the need for alternative synthetic routes are required for the incorporation of non-natural elements, such as barium, nickel, copper or aluminum, with functional nanoscale properties [1,8]. From a materials perspective, highly intact biological structures such as diatoms, bacteria, proteins or butterfly wings provide an excellent source of inspiration for their synthesis. In this chapter we have included the details of a wide variety of mediated nanomaterial syntheses, their response to variable parameters, and their ability to retain a functionalized, controlled stability over time.

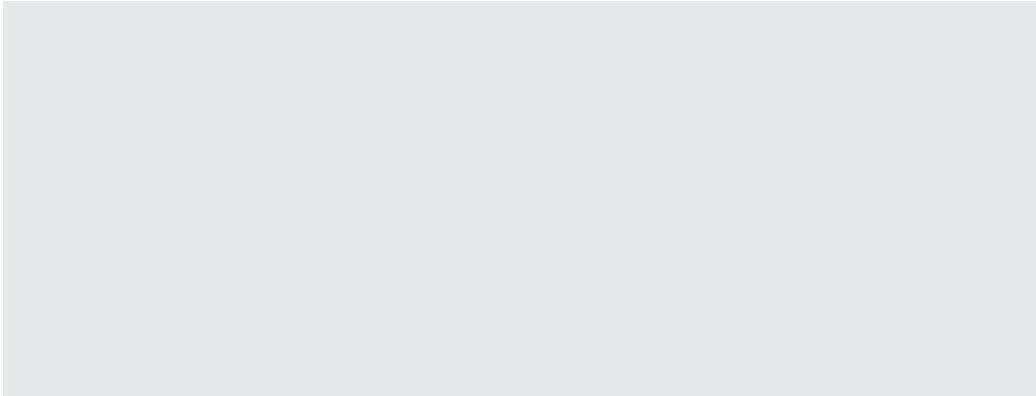


Figure 1.8 Appearance of a prototype device of optical near-field lithography.

As mentioned above, the photoresist should be thin according to the distance of localization of the optical near-field around the nanoaperture. On the other hand, the photoresist should have the dry etching resistance so that the latent image can be transferred to the lower layer substrate. To separate the function of the thin film and the dry etching resistance, we used a trilayer resist process; the upper layer is an ultrathin photoresist, the middle layer is thin spin on glass (SOG), and the lower layer is a resin. The patterns of shallow latent images in the upper layer are transferred to the thin SOG layer of excellent dry-etching resistance, and these are transferred in the lower layer further.

Figure 1.8 shows the appearance of a prototype device of optical near-field lithography [7]. The features of the prototype device are as follows. This device is compact, with a footprint of about 2m [2]. It has symmetric structure to compensate thermal expansion and temperature

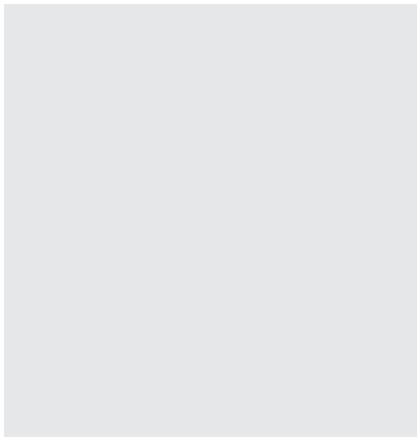


Figure 1.9 Distribution of structures for variable pH samples. *Source:* Reprinted with permission from Ref. [33]; © 2007, American Chemical Society.

Figure 1.10 (a) Inside the prototype device of the near-field lithography. (b) Illumination of i-line light for exposure from the back side of the near-field photomask. (c) Close-up from the side of the near-field photomask and the photoresist on the wafer. They are brought into contact with each other within the localizing distance of the optical near-field.

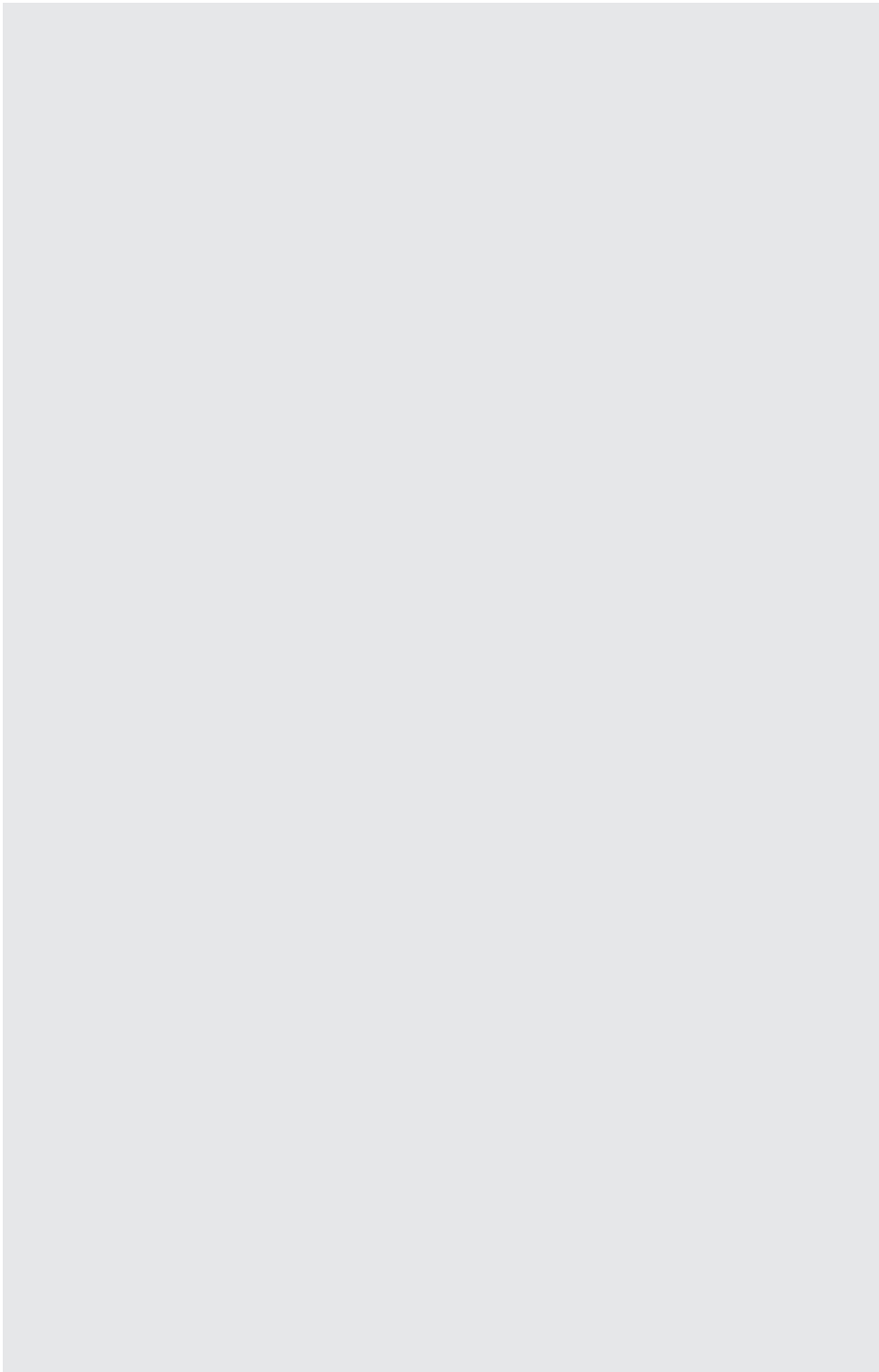


Table 1.1 Results for the comparison of processes.

Performance metric	NH ₃	CH ₄	C ₃ H ₈ ref.	C ₃ H ₈ POX
Energy efficiency	27%	30%	23%	16%
Volumetric fuel energy density (Wh l ⁻¹)	1570	170	1740	1920
Gravimetric fuel energy density (Wh kg ⁻¹)	2580	1610	2540	3900
Volumetric system energy density (Wh l ⁻¹)	1510	130	1650	1800
Gravimetric system energy density (Wh kg ⁻¹)	2370	320	2320	3340

drift, and the hanging controlling structure is introduced to avoid floor vibrations. In addition, it has a double clean structure, and the near-field photomask and the wafer are kept in a local clean environment by controlling a flow of clean air of the device inside.

Bioinspired research is based on identifying and emulating the principles of biomineralization in natural systems, Figure 1.9 instead of copying them directly. In fact, most strategies incorporated by natural systems are not directly applicable to engineered materials, so the need for alternative synthetic routes are required for the incorporation of non-natural elements, such as barium, nickel, copper or aluminum, with functional nanoscale properties [1,8]. Table 1.1 from a materials perspective, highly intact biological structures such as diatoms, bacteria, proteins or butterfly wings provide an excellent source of inspiration for their synthesis. In this chapter we have included the details of a wide variety of mediated nanomaterial syntheses, their response to variable parameters, and their ability to retain a functionalized, controlled stability over time.

The lowest system energy densities. Both the system and fuel volumetric energy densities of methane direct oxidation are very low, due to the large volume required for the storage of the gases (methane and oxygen). Moreover, the gravimetric fuel energy density of methane is

Table 1.2 Propagation rate constants (k_p) and the selectivity parameters ($\beta = k_p/k_{tr1}$) for the polymerization of ϵ -caprolactone [95].^{a)}

Active species	$\frac{k_p}{L \text{ mol}^{-1} \text{ s}^{-1}}$	$b = \frac{k_p}{k_{tr1}} \frac{L \text{ mol}^{-1}}{L \text{ mol}^{-1}}$
...-(CH ₂) ₅ O ⁻ Na ⁺	□1.70	1.6×10^3
...-(CH ₂) ₅ O-Sm[O(CH ₂) ₅ -...] ₂	2.00	2.0×10^3
...-(CH ₂) ₅ O-Al(C ₂ H ₅) ₂	0.03	4.6×10^4
...-(CH ₂) ₅ O-Al[CH ₂ CH(CH ₃) ₂] ₂	0.03	7.7×10^4
...-(CH ₂) ₅ O-Al[O(CH ₂) ₅ -...] ₂	0.50	3.0×10^5
...-(CH ₂) ₅ O-AlO ₂ SB ^{b)}	0.35	□10 ⁶

a) Polymerization conditions: 20°C, THF solvent.

b) Polymerization conditions: 80°C, THF solvent, SBO2: (S)-(+)-2,2'-[1,1'-binaphthyl-2,2'-diylbis-(nitrylomethylidyne)]-diphenolate ligand (A. Duda and A. Kowalski, unpublished results). SB=Schiff's base.

Table 1.3 Results for the comparison of processes.

Performance metric	NH ₃	CH ₄	C ₃ H ₈ ref.	C ₃ H ₃ POX
Energy efficiency	27%	30%	23%	16%
Volumetric fuel energy density (Wh l ⁻¹)	1570	170	1740	1920
Gravimetric fuel energy density (Wh kg ⁻¹)	2580	1610	2540	3900
Volumetric system energy density (Wh l ⁻¹)	1510	130	1650	1800
Gravimetric system energy density (Wh kg ⁻¹)	2370	320	2320	3340

Data from Higinbotham et al. 1967. The membrane potential was measured as – 110 mV Table from Taiz & Zeiger Thrid Ed Table 6.1

Table 1.4 Results for the comparison of processes.

R of functional molecule ^a	Cycle	Catalyst ^b	Conversion (%)	M _n (kg mol ⁻¹)	M _w /M _n	Reference
CH ₃ , CH=CH ₂ , (CH ₂) ₃ COOH	D ₄	SR	~90	10–43	—	[87]
CH=CH ₂ , (CH ₂) ₃ NHSi(CH ₃) ₃ , (CH ₂) ₃ -acrylate, (CH ₂) ₃ COOH	D ₄	SR	80–90	0.8–1.2	1.4–1.9	[57]
H	D ₄	AC	80	8	1.9	[88]
H, CH ₃ , CH=CH ₂ , (CH ₂) ₃ COOH	D ₄	SR	—	—	—	[89]

a) The chain-terminating agent has the following structure: R–Si(CH₃)₂–O–Si(CH₃)₂–R, unless stated in the table.

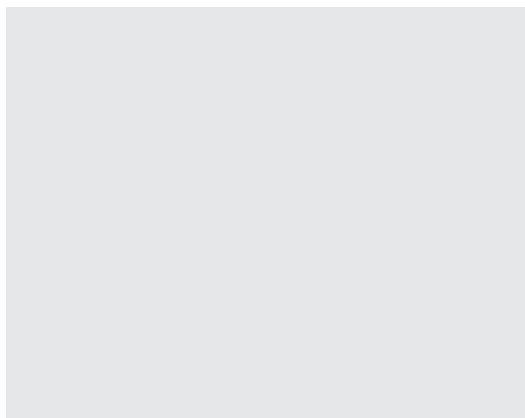
b) SR: sulfonic resin; AC: activated clay.

low, due to the mass of oxygen which is accounted for [2]. The large difference in gravimetric energy density of methane direct oxidation is due to the mass of the gas Table 1.2 cartridges. Despite lower energy conversion efficiency, the propane-based processes lead to higher energy densities than the ammonia-based process, because of the intrinsic difference in energy density between the two fuels. From a materials perspective, highly intact biological structures such as diatoms, bacteria. In this chapter we have included the details of a wide variety of mediated nanomaterial syntheses, their response to variable parameters, and their ability to retain a functionalized, controlled stability over time. With the exception of the

Table 1.5 Results for the comparison of processes.

Characteristic	Issues	Needs
Laminar flows	Mixing relies on molecular diffusion only and is slow	Efficient micromixers of low pressure drop
Small size	Difficult to load enough catalyst and ensure complete conversion	Develop deposition schemes and structures to load enough catalyst; high integration of reactor(s) and separation units for compact systems; fast chemistry/process; very active (and selective) catalyst.
Reactors shake in portable devices	Moveable parts break; bypass from pellet settling can occur	Monolithic structures with no moveable parts
High pressure drop	Pressure drop increases with decreasing pellet size	Open (extruded monolith-like) geometries
Transient operation very common	Most designs rely on steady state operation and control; catalysts, which are stable under steady state conditions, may deactivate during start up and shut down; start-up can be slow.	Get heat in and out of the system quickly; develop appropriate designs and strategies; models for dynamics.

Figure 1.11 Distribution of structures for variable pH samples. *Source:* Reprinted with permission from Ref. [33]; © 2007, American Chemical Society.



process requiring gas storage, the fuel energy density and system energy density give the same qualitative comparison among processes.

Thus, replicates on the same array and replicates in different experiments should not be mixed since they have different characteristics and cannot be treated as independent replicates. Important issues are:

- are the distributional assumptions valid is the number of replicates sufficient to detect the fold change that you are interested in?
- are the replicates independent of each other?
 - is the number of replicates sufficient to detect the fold change because it does not conversion efficiency that you are interested in?
 - are outliers removed from the samples?

Most commonly, modifications of four different tests are applied in microarray data analysis. These tests are implemented in statistical software packages such as R/Bioconductor or SAS:

- 1) Student's t-test is the number of replicates sufficient to detect the fold change that you are interested
- 2) Welch's test is the number of replicates sufficient to detect the fold because it does not conversion efficiency change that you are interested
- 3) Permutation tests.

While the first two tests assume Gaussian distributed data and the P -values are calculated by a probability distribution, the latter two are nonparametric and the P -values are calculated based on combinatorial arguments.

- | | |
|-----------------------------------|--------------------|
| • Distilled water | 23.3 μl |
| • 10 \times PCR buffer | 4.0 μl |
| • dNTP Mix (FDD) | 0.3 μl |
| • H-AP primer (2 μM)* | 4.0 μl |
| • H-T11M (2 μM) | 4.0 μl |
| • cDNA template | 4.0 μl |
| • Taq DNA polymerase | 0.4 μl |
| • Total volume | 40.0 μl |

Table 1.6 Species of marine invertebrates containing glycolipids.

Phylum	Subphylum	Class	Trivial name	Species
Chordata	Tunicata	Ascidacea	Tunicate	<i>Microcosmus sulcatus</i> (now accepted <i>M. vulgaris</i> ⁽¹⁾) <i>Phallusia fumigata</i>
Cnidaria	—	Anthozoa	Soft coral	1) <i>Lobophytum crassum</i> 2) <i>Lobophytum</i> sp. 3) <i>Sarcophyton ehrenbergi</i> 4) <i>Metridium senile</i>
Echinodermata	Asterozoa	Asteroidea	Sea anemone Starfish	• <i>Acanthaster planci</i> • <i>Allostichaster inaequalis</i> • <i>Anasterias minuta</i> • <i>Aphelasterias japonica</i> • <i>Asterias amurensis</i> • <i>Asterias amurensis versicolor</i> • <i>Asterias rubens</i> • <i>Stellaster equestris</i>
		Ophiuroidea	Brittle star	<i>Ophiocoma scolopendrina</i>
	Crinozoa	Crinoidea	Feather star	<i>Comanthus japonica</i> (now accepted <i>Oxycomanthus japonicus</i> ⁽¹⁾) <i>Comanthina schlegeli</i> (now accepted <i>Comaster schlegelii</i>)

Source: Queen Square Brain Bank.

Both the system and fuel volumetric energy densities of methane direct oxidation are very low, due to the large volume required for the storage of the gases (methane and oxygen). Moreover, the gravimetric fuel energy density of methane is low, due to the mass of oxygen which is accounted for [2]. The large difference in gravimetric energy density of methane direct oxidation is due to the mass of the gas cartridges.

Yields, and reaction specificities. The first detailed study of the mechanism of these “on water” reactions has now been reported by Jung and Marcus [10]. Synthetic aqueous organic synthesis was born, also because efficient work-up procedures are possible for these “on water” reactions. For a general review, the reader is referred to Chapter 7.

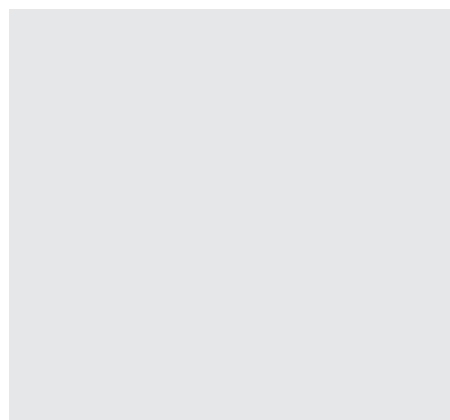


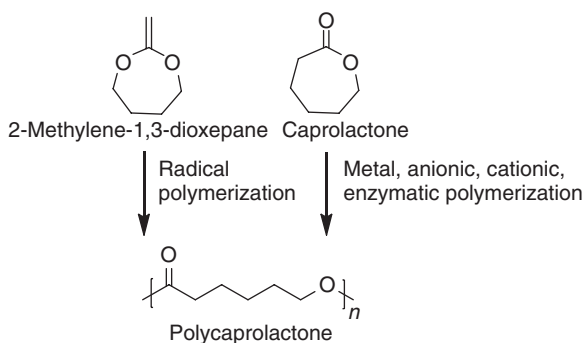
Figure 1.12 Distribution of structures for variable pH samples. *Source:* Reprinted with permission from Ref. [33]; © 2007, American Chemical Society.

11.3 Water, the Ultimate Green Solvent

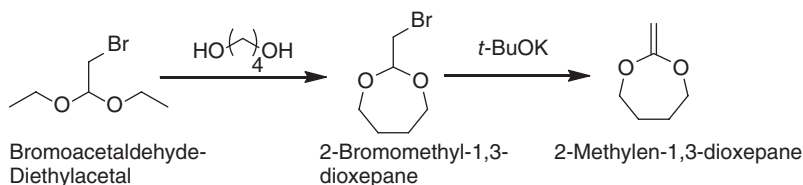
Fredrik Nilsson

In the second half of the 1990s, it was recognized that “benign by design” was too strongly restricted to environmental care, and Anastas and Williamson [13] even concluded, “one obvious but important point: nothing is benign.” The holistic concept of green chemistry became accepted world-wide. Although attempts have been made to quantify the degree of greenness, particularly by Sheldon [15], it has not been found possible to include the many complex factors that determine “greenness” in generally applicable parameters.

Aspirin as a Household Remedy Against Fever, Inflammation, and Pain Soon after the introduction of ASA into medical use under the brandname “aspirin,” Anastas in his many influential publications.



Scheme 1.31



Scheme 1.32

... As soon as you feel yourself ill, you should go to bed and have a hot-water bottle at your feet. You should drink hot chamomilae tea or grog in order to sweat and should take 3 tablets of aspirin a day. If you follow these instructions you will recover with in a few days, in most cases...

Kölner Stadtanzeiger, March 6, 1924

This extract is remarkable for several reasons: during the past 25 years of practical use, aspirin had become a drug whose name was not only well known to health professionals but also to the general public.

Certainly, the flu pandemia with millions of victims alone in Europe at the beginning of the last century as well as the limited availability of antipyretic analgesics other than aspirin contributed to this. However, the compound was generally recommended—and accepted—by the lay man and doctors—as a household remedy for treating pain, fever, inflammation, and many other kinds of feeling bad, although essentially nothing was known about the mechanisms of Anastas in his many influential publications. The holistic concept of green chemistry became accepted world-wide. Although attempts have been made to quantify the degree of greenness, particularly by action behind these multiple activities of the drug.

Thus, replicates on the same array and replicates in different experiments should not be mixed since they have different characteristics and cannot be treated as independent replicates. Important issues are:

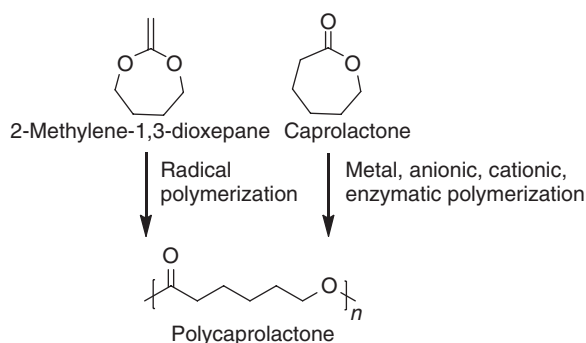
Most commonly, modifications of four different tests are applied in microarray data analysis. These tests are implemented in statistical software packages such as R/Bioconductor or SAS.

The conformational flexibility of calixarenes is usually explained by the presence of intramolecular hydrogen bonds, which is related to the number of free phenol groups. Accordingly, calixarenes containing four phenol groups 39a–e exist as cone conformers.

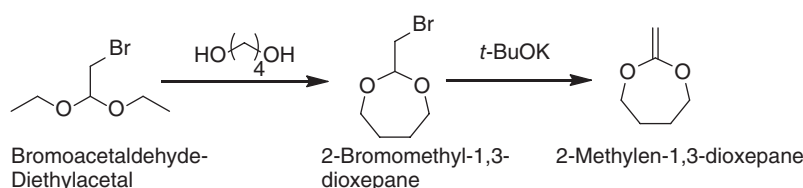
$$\rho(z)v_w = \rho_w^{\text{bulk}} v_w \exp(-v_w \beta [\pi(z) - \pi^{\text{bulk}}]) \quad (2.17)$$

$$\rho(z)v_w = \rho_w^{\text{bulk}} v_w \exp(-v_w \beta [\pi(z) - \pi^{\text{bulk}}]) - q_i \beta [\psi(z) - \psi^{\text{bulk}}] \quad (2.18)$$

Both the system and fuel volumetric energy densities of methane direct oxidation are very low, due to the large volume required for the storage of the gases (methane and oxygen). Moreover, the gravimetric fuel energy density of methane is low, due to the mass of oxygen which is accounted for [2]. The comparison of the two idealized possibilities for propane fuel processing reactions shows that energy conversion efficiency is not a suitable metric for man-portable applications, because it does not account for the water weight and volume;



Scheme 1.31



Scheme 1.32

the higher energy efficiency of steam reforming is due to the generation of additional hydrogen in the reactor.

The lowest system energy densities. Both the system and fuel volumetric energy densities of methane direct oxidation are very low, due to the large volume required for the storage of the gases (methane and oxygen). Moreover, the gravimetric fuel energy density of methane is low, due to the mass of oxygen which is accounted for [2]. The large difference in gravimetric energy density of methane direct oxidation is due to the mass of the gas Table 1.2 cartridges. Despite lower energy conversion efficiency, the propane-based processes lead to higher energy densities than the ammonia-based process, because of the intrinsic difference in energy density between the two fuels. From a materials perspective, highly intact biological structures such as diatoms, bacteria. In this chapter we have included the details of a wide variety of mediated nanomaterial syntheses, their response to variable parameters, and their ability to retain a functionalized, controlled stability over time. With the exception of the process requiring gas storage, the fuel energy density and system energy density give the same qualitative comparison among processes.

The conformational flexibility of calixarenes is usually explained by the presence of intramolecular hydrogen bonds, which is related to the number of free phenol groups. Accordingly, calixarenes containing four phenol groups 39a–e exist as cone conformers.

$$V_i = [A_i r + (B_i / r^2)] \cos(\theta) \quad (2.19)$$

While the first two tests assume Gaussian distributed data and the *P*-values are calculated by a probability distribution, the latter two are nonparametric and the *P*-values are

Instrumental Box 4**Numerical Data Analysis**

The incorporation of these techniques has provided a rapid prototyping technique, essential for the commercial development of current minimum feature-sized semiconducting integrated circuits. However, the production of these devices has been achieved at a high price, with the primary challenges currently faced by high-throughput fabrication laboratories including the high cost of laborers and instruments, high-temperature reaction conditions, and a surplus in generated waste [1].

The versatility of biology's incredible portfolio encourages researchers to develop modified syntheses derived from Nature. Hence, their findings have been successfully organized into the field of biomimetics, or bioinspired research technological applications [8].

Source: The versatility of biology's incredible portfolio encourages researchers to develop modified syntheses derived from Nature

Instrumental Box 5

The incorporation of these techniques has provided a rapid prototyping technique, essential for the commercial development of current minimum feature-sized semiconducting integrated circuits. However, the production of these devices has been achieved at a high price, with the primary challenges currently faced by high-throughput fabrication laboratories including the high cost of laborers and instruments, high-temperature reaction conditions, and a surplus in generated waste [1].

In fact, the cost of fabrication facilities are estimated to reach an outstanding US \$100 billion per facility by the year 2020, as the demand for smaller, lighter and faster materials continues to grow [1].

calculated based on combinatorial arguments. Thus, replicates on the same array and replicates in different possibilities for propane experiments should not be mixed since they have different characteristics and cannot be treated as independent replicates. Important issues are:

$$E_1 = \frac{9\varepsilon_2\varepsilon_3}{\varepsilon_2\varepsilon_a + 2\varepsilon_3\varepsilon_b} E_0 (\cos\hat{\theta}r - \sin\hat{\theta}\hat{\theta}) \quad (2.20)$$

Traditionally, synthetic approaches for the production of functional metal oxide materials have involved high-temperature reaction environments with energy-intensive techniques such as laser ablation, ion implantation, chemical vapor deposition (CVD), photolithography or thermal decomposition [1].

The ligation products are used immediately for transformation or stored at -20°C. For transformation, add 10 ml of each ligation mix to freshly thawed GH-competent cells and mix

Instrumental Box 6

The incorporation of these techniques has provided a rapid prototyping technique, essential for the commercial development of current minimum feature-sized semiconducting integrated circuits. However, the production of these devices has been achieved at a high price, with the primary challenges currently faced by high-throughput fabrication laboratories including the high cost of laborers and instruments, high-temperature reaction conditions, and a surplus in generated waste [1].

In fact, the cost of fabrication facilities are estimated to reach an outstanding US \$100 billion per facility by the year 2020, as the demand for smaller, lighter and faster materials continues to grow [1].

Biomimetics infers the manipulating and mimicking of natural architectures and processes of biologically produced minerals (biominerals) to direct the synthesis of non-natural materials.

well by finger-tipping and incubate on ice for 45 min. The large difference in gravimetric energy density of methane direct oxidation is due to the mass of the gas cartridges.

Both the system and fuel volumetric energy densities of methane direct oxidation are very low, due to the large volume required for the storage of the gases (methane and oxygen). Moreover, the gravimetric fuel energy density of methane is low, due to the mass of oxygen which is accounted for [2]. Despite lower energy conversion efficiency, the propane-based processes lead to higher energy densities than the ammonia-based process, because of the intrinsic difference in energy density between the two fuels. The comparison of the two idealized possibilities for propane fuel processing reactions shows that energy conversion efficiency is not a suitable metric for man-portable applications, because it does not account for the water weight and volume; the higher energy efficiency of steam reforming is due to the generation of additional hydrogen in the reactor.

The lowest system energy densities. Both the system and fuel volumetric energy densities of methane direct oxidation are very low, due to the large volume required for the storage of the gases (methane and oxygen). Moreover, the gravimetric fuel energy density of methane is low, due to the mass of oxygen which is accounted for [2]. The large difference in gravi-

One striking feature of this book is that more than half of the chapters come from industry-based researchers; and even many of the academic contributors have close ties to industry. It has been alleged that the best science is done in academia; this book proves that this is not necessarily the case.

Part of the reason may be that many of the techniques involved require expensive equipment and infrastructure as well as large collaborations between scientists from disparate disciplines—collaborations that would be difficult to set up outside industry. The multidisciplinary nature of fragment-based approaches shows in this volume: contributors include computational chemists, NMR spectroscopists, X-ray crystallographers, mass-spectrometrists, as well as organic and medicinal chemists.

One striking feature of this book is that more than half of the chapters come from industry-based researchers; and even many of the academic contributors have close ties to industry. It has been alleged that the best science is done in academia; this book proves that this is not necessarily the case.

Part of the reason may be that many of the techniques involved require expensive equipment and infrastructure as well as large collaborations between scientists from disparate disciplines—collaborations that would be difficult to set up outside industry. The multidisciplinary nature of fragment-based approaches shows in this volume: contributors include computational chemists, NMR spectroscopists, X-ray crystallographers, mass-spectrometrists, as well as organic and medicinal chemists.

metric energy density of methane direct oxidation is due to the mass of the gas Table 1.2 cartridges. Despite lower energy conversion efficiency, the propane-based processes lead to higher energy densities than the ammonia-based process, because of the intrinsic difference in energy density between the two fuels. From a materials perspective, highly intact biological structures such as diatoms, bacteria. In this chapter we have included the details of a wide variety of mediated nanomaterial syntheses, their response to variable parameters, and their ability to retain a functionalized, controlled stability over time. With the exception of the process requiring gas storage, the fuel energy density and system energy density give the same qualitative comparison among processes.

The ligation products are used immediately for transformation or stored at -20°C . For transformation, add 10 ml of each ligation mix to freshly thawed GH-competent cells and mix well by finger-tipping and incubate on ice for 45 min. Traditionally, synthetic approaches for the production of functional metal oxide materials have involved high-temperature reaction environments with energy-intensive techniques such as laser ablation, ion implantation, chemical vapor deposition (CVD), photolithography or thermal decomposition [1].

The dilemma of rapidly emerging fields is that reviews are often outdated before they are printed. To make a contribution that would endure, we knew we had to go beyond a snapshot of the current state of fragment-based drug discovery and instead provide a framework for upcoming advances. To achieve this goal, we needed to convince leading scientists to take time from their busy schedules to write chapters. Fortunately, nearly all those we approached agreed; and what you hold in your hands is a virtual, although not comprehensive, “Who’s Who” in fragment-based drug discovery. We are extremely grateful to all of our contributors for the quality of their chapters.

Fragment-based drug discovery has only been practical for the past decade, too soon to expect it to produce marketed drugs; but we believe these will come in time.

Techniques described in this book Moreover, many of the techniques and concepts described in this book will alter drug discovery endeavors in subtle, tangential ways. Ideally, readers will be inspired to improve the methods described here, or even to develop fundamentally new methods for fragment-based drug discovery. But even if this book only changes the way medicinal chemists approach lead optimization, or persuades them to look more closely at weak but validated hits, it will have served its purpose.

For instance, the architecture of one of the most abundant biological species on the planet – the virus – has recently been manipulated to serve as containers for the synthesis of a variety of functional molecular cargoes.

In fact, the cost of fabrication facilities are estimated to reach an outstanding US \$100 billion per facility by the year 2020, as the demand for smaller, lighter and faster materials continues to grow¹. But, more importantly, manufacturers are progressing in this manner at the expense of the environment, as they accumulate semiconductor hazardous chemical wastes [2].

For decades, research teams in the semiconductor industry have been seeking alternative methods to passivate not only the rate of waste production but also the cost of spending. The most accessible resource for the synthesis of functional materials under ambient conditions is found in biology.

Traditionally, synthetic approaches for the production of functional metal oxide materials have involved high-temperature reaction environments with energy intensive techniques such as laser ablation, ion implantation, chemical vapor deposition (CVD), photolithography or thermal decomposition [1]. The incorporation of these techniques has provided a rapid prototyping technique, essential for the commercial development of current minimum fragment-based drug discovery and instead provide a framework for upcoming advances.

The versatility of biology's incredible portfolio encourages researchers to develop modified syntheses derived from Nature. Hence, their findings have been successfully organized into the field of biomimetics, or bioinspired research, which encompasses alternative approaches towards developing nanomaterials with technological applications [8]. Based primarily on the designs, mechanisms and processes found in Nature, biomimetics.

As mentioned above, the photoresist should be thin according to the distance of localization of the optical near-field around the nanoaperture. On the other hand, the photoresist should have the dry etching resistance so that the latent image can be transferred to the lower layer substrate. To separate the function of the thin film and the dry etching resistance, we used a trilayer resist process; the upper layer is an ultrathin photoresist, the middle layer is thin spin on glass (SOG), and the lower layer is a resin.

The patterns of shallow latent images in the upper layer are transferred to the thin SOG layer of excellent dry-etching resistance, and these are transferred in the lower layer further. Figure 6.8 shows the appearance of a prototype device of optical near-field lithography [7]. The features of the prototype device are as follows. This device is compact, with a footprint of about 2×2 . It has symmetric structure to compensate thermal expansion and temperature drift, and the hanging structure is introduced to avoid floor vibrations.

Bioinspired research is based on identifying and emulating the principles of biomineralization in natural systems, instead of copying them directly. In fact, most strategies incorpo-

¹ A Q-switch is a device that is similar to a shutter that controls the laser resonator's ability to oscillate. In fact, the cost of fabrication facilities are estimated to reach an outstanding US \$100 billion per facility by the year 2020, as the demand for smaller.

rated by natural systems are not directly applicable to engineered materials, so the need for alternative synthetic routes are required for the incorporation of non-natural elements, such as barium, nickel, copper or aluminum, with functional nanoscale properties [1,8]. To achieve this goal, we needed to convince leading scientists to take time from their busy schedules to write chapters. feature-sized semiconducting integrated circuits. However, the production of these devices has been achieved at a high price, with the primary challenges currently faced by high-throughput fabrication laboratories including the high cost of laborers and instruments, at a high price, with the primary challenges currently faced by high-throughput fabrication laboratories including the high cost of laborers and instruments, high temperature reaction conditions, and a surplus in generated waste [1].

- 120 For decades, research teams in the semiconductor industry have been seeking alternative methods to passivate not only the rate of waste production but also the cost of spending. The most accessible resource for the synthesis of functional materials under ambient conditions is found in biology.

Bioinspired research is based on identifying and emulating the principles of biomineralization in natural systems, instead of copying them directly. In fact, most strategies incorporated by natural systems are not directly applicable to engineered materials, so the need for alternative synthetic routes are required for the incorporation of non-natural elements, such as barium, nickel, copper or aluminum, with functional nanoscale properties [1,8]. However, the production of these devices has been achieved at a high price, with the primary challenges currently faced by high-throughput fabrication laboratories including the high cost of laborers and instruments.

In Kupferchlorid und Kupfersulfatpentahydrat (siehe Abb. 4.18) sind giftig und inätzend, Quecksilberchlorid ist sehr giftig und inätzend, Schwefeldioxid ist giftig, Silbernitrat wirkt ätzend. Das Tragen einer Schutzbrille ist erforderlich. Dieser wird auf die Porzellanfilternutsche gegeben, zweimal mit Ethanol sowie mit Wasser gewaschen mit denen das $\text{Cr}(\text{H}_2\text{O})_6$ oder Kupfersulfatpentahydrat mit den viel H_2O und Schwefeldioxid-Druckgaszylinder,² destilliertes Wasser.

Surprisingly, the properties associated with metal oxides in technology are not so far removed from what is observed in natural systems. Through precisely tuned processes, Nature is able to synthesize a variety of metal oxide nanomaterials under ambient conditions; the magnetic navigation device found in magnetotactic bacteria (MTB) is one such example [17]. Here, magnetite (Fe_3O_4) nanocrystals are aligned with the Earth's geomagnetic field and contained within specific organelles known as magnetosomes [17]. Fresh water salmon, for example, utilizes these magnetic nanoparticles in the nasal cavities of their forehead as a biomagnetic compass during migration [18].

² A Q-switch is a device that is similar to a shutter that controls the laser resonator's ability to oscillate. This shutter effect allows one to spoil the resonator's 'Q-factor', keeping it low to prevent lasing action. Under these conditions, the laser highly intact biological structures such as diatoms, bacteria, proteins or butterfly wings gain material is able to store higher levels of energy. The extra stored energy is subsequently extracted as laser light emission in the form of extremely short pulse width, high-peak-power pulses.

1

cDNA and Microarray-based Technologies

CHAPTER MENU

Introduction, 1
 CEA Gene Family, Genomic Localization, Protein Structure, 1
 Animal Models for CEA, 1
 Models for CEACAM5 Containing a Bacterial Artificial Chromosome, 2

1.1 Introduction

The molecular characterization of tumor-associated antigens (TAA) recognized by T cells [1] revolutionized the field of tumor immune biology providing conclusive evidence that CD8+ cytotoxic T cells (CTLs) specifically recognize and kill autologous cancer through recognition of molecularly-defined cancer-specific elements.

1.2 CEA Gene Family, Genomic Localization, Protein Structure

CEA is encoded by the CEA-related cell-cell adhesion molecule 5 (CEACAM5) gene, which belongs to the CEA gene family and in humans consists of 22 expressed members and 12 pseudogenes [3,4]. Both the system and fuel volumetric energy densities of methane direct oxidation are very low, due to the large volume required for the storage of the gases (methane and oxygen). Moreover, the gravimetric fuel energy density of methane is low, due to the mass of oxygen which is accounted for [2]. The large difference in gravimetric energy density of methane direct oxidation is due to the mass of the gas cartridges. Despite ammonia-based process, because of the intrinsic difference in energy density between the two fuels. The the water weight and volume; the higher energy efficiency of steam reforming is due to the generation of additional hydrogen in the reactor.

1.3 Animal Models for CEA

Mice are commonly used to analyze the efficacy of tumor therapies and mechanisms of tumor rejection. However, this species cannot be utilized to evaluate CEA-based therapies since no CEACAM5 ortholog exists in rodents. This problem was circumvented by introducing the human CEACAM5 gene into the germ line of mice [52–54].

1.4 Models for CEACAM5 Containing a Bacterial Artificial Chromosome

Either cosmid clones containing the CEACAM5 gene or a bacterial artificial chromosome (BAC) clone, which comprises part of the gene cluster surrounding CEACAM5, served as a genetic source. This cluster includes CEACAM6 and CEACAM3.

Antibody Delivery of Radionuclides, Drugs and Effector Molecules Delivery of radio-nuclides to tumors using murine and human anti-CEA antibodies has been studied for many years [70]. The use of low molecular weight single chain antibody fragments and pre-targeting has been found to enhance the sensitivity of tumor visualization as well as increasing the delivered therapeutic dose by separating the antibody targeting to the tumor from the subsequent delivery of the therapeutic radionuclide that binds to the tumor-localized antibody.

SubParagraph Title: Nuclear Angular Momentum and Magnetic Moment The conformational flexibility of calixarenes is usually explained by the presence of intramolecular hydrogen bonds, which is related to the number of free phenol groups. Accordingly, calixarenes containing four phenol groups 39–e exist as cone conformers.

The use of low molecular weight single chain antibody fragments and pre-targeting has been found to enhance the sensitivity of tumor visualization as well as increasing the delivered therapeutic dose by separating the antibody targeting to the tumor from the subsequent delivery of the therapeutic radionuclide that binds to the tumor-localized antibody.

References

- 1 Thaxton, C.S., Georganopoulou, D.G. and Mirkin, C.A. (2006) Gold nanoparticle probes for the detection of nucleic acid targets. *Clinica Chimica Acta*, 363, 120–6.
- 2 Cheng, M.M., Cuda, G., Bunimovich, Y.L., Gaspari, M., Heath, J.R., Hill, H.D., Mirkin, C.A., Nijdam, A.J., *Biology*, 10, 11–19.
- 4 Nie, S., Xing, Y., Kim, G.J. and Simons, J.W. (2007) Nanotechnology applications in cancer. *Annual Review of Biomedical Engineering*, 9, 257–88.
- 99 Cai, W. and Chen, X. (2007) Nanoplatforms for targeted molecular imaging in living subjects. *Small*, 11, 1840–54.
- 100 Gupta, A.K. and Gupta, M. (2005) Synthesis and surface engineering of iron oxide nanoparticles for biomedical applications. *Biomaterials*, 26, 3995–4021.

2

The Molecular Characterization

Abstract

The molecular characterization of tumor-associated antigens recognized by T cells [1] revolutionized the field of tumor immune biology providing conclusive evidence that CD8+cytotoxic T cells (CTLs) specifically recognize and kill autologous cancer through recognition of molecularly-defined calixarenes is usually explained by the presence cancer-specific elements. Since then a myriad of TAA have been identified that has triggered their utilization as anti-cancer vaccines [2–8].

Keywords *The molecular; characterization; of tumor-associated; antigens*

The molecular characterization of tumor-associated antigens (TAA) recognized by T cells [1] revolutionized the conformational.

2.1 Animal Models for CEA

Delivery of radio-nuclides to tumors using murine and human anti-CEA antibodies has been studied for many years. The use of low molecular weight single chain antibody fragments and pre-targeting has been found to enhance the sensitivity of tumor visualization as well as from the subsequent delivery of the therapeutic radionuclide that binds to the tumor-localized antibody. The conformational flexibility of calixarenes is usually explained by the presence of intramolecular hydrogen bonds, which is related to the number of free phenol groups.

Definition 2.1 The position of a body along the x axis, in metres, is given by the equation $x = t^3 - 30t^2 + 5$, where t is the time in seconds. Find its velocity and acceleration as a function of time.

Delivery of radio-nuclides to tumors using murine and human anti-CEA antibodies has been studied for many years. The use of low molecular weight single chain antibody fragments and pre-targeting has been found to enhance the sensitivity of tumor visualization as well as increasing the delivered therapeutic dose by separating the antibody targeting to

the tumor from the subsequent delivery of the therapeutic radionuclide that binds to the tumor-localized antibody.

Example 2.1 The position of a body along the x axis, in metres, is given by the equation $x = t^3 - 30t^2 + 5$, where t is the time in seconds. Find its velocity and acceleration as a function of time.

$$\begin{aligned}\text{Velocity} \quad \mathbf{v} &= \frac{dx}{dt} \\ \text{Acceleration} \quad a &= \frac{d^2x}{dt^2} \\ x &= t^3 - 30t^2 + 5 \\ a(t) &= \frac{d^2x}{dt^2} = 6t - 60\end{aligned}$$

The use of low molecular weight single chain antibody fragments and pre-targeting has been found to enhance the sensitivity of tumor visualization as well as increasing the delivered therapeutic dose by separating the antibody targeting to the tumor from the subsequent delivery of the therapeutic radionuclide that binds to the tumor-localized antibody.

Theorem 2.1 The position of a body along the x axis, in metres, is given by the equation $x = t^3 - 30t^2 + 5$, where t is the time in seconds. Find its velocity and acceleration as a function of time.

$$\begin{aligned}\text{Velocity} \quad \mathbf{v} &= \frac{dx}{dt} \\ x &= t^3 - 30t^2 + 5 \\ a(t) &= \frac{d^2x}{dt^2} = 6t - 60\end{aligned}$$

Delivery of radio-nuclides to tumors using murine and human anti-CEA antibodies has been studied for many years [70].

Lemma 2.1 The position of a body along the x axis, in metres, is given by the equation $x = t^3 - 30t^2 + 5$, where t is the time in seconds. Find its velocity and acceleration as a function of time.

$$\begin{aligned}\text{Velocity} \quad \mathbf{v} &= \frac{dx}{dt} \\ \text{Acceleration} \quad a &= \frac{d^2x}{dt^2}\end{aligned}$$

Proof: Proof for the above Lemma

$$\begin{aligned}x &= t^3 - 30t^2 + 5 \\ a(t) &= \frac{d^2x}{dt^2} = 6t - 60\end{aligned}$$

Delivery of radio-nuclides to tumors using murine and human anti-CEA antibodies has been studied for many years [70]. The use of low molecular weight single chain antibody fragments and pre-targeting has been found to enhance the sensitivity of tumor visualization as well as increasing the delivered therapeutic dose by separating the antibody targeting to the tumor from the subsequent delivery of the therapeutic radionuclide that binds to the tumor-localized antibody.

Corollary 2.1 The position of a body along the x axis, in metres, is given by the equation $x = t^3 - 30t^2 + 5$, where t is the time in seconds. Find its velocity and acceleration as a function of time.

Velocity

$$\mathbf{V} = \frac{dx}{dt}$$

Acceleration

$$a = \frac{d^2x}{dt^2}$$

$$x = t^3 - 30t^2 + 5$$

$$a(t) = \frac{d^2x}{dt^2} = 6t - 60$$

Delivery of radio-nuclides to tumors using murine and human anti-CEA antibodies has been studied for many years [70].

Is there another *Browne* hath kild a *Sanders*?
It is my other selfe hath done the deede,
I am a thousand, every murtherer is my one selfe,
I am at one time in a thousand places,
And I have slaine a thousand *Sanderses*,
In every shire, each cittie, and each towne,
George Sanders still is murdered by *George Browne*.
(lines 2397–403)

The use of low molecular weight single chain antibody fragments and pre-targeting has been found to enhance the sensitivity of tumor visualization as well as increasing the delivered therapeutic dose by separating the antibody targeting to the tumor from the subsequent delivery of the therapeutic radionuclide that binds to the tumor-localized antibody.

- The housing supply elasticity determines the level of house prices. Across East Asia, housing prices are high because:
 - 1) the supply price elasticity of housing tends to be low;
 - 2) the share of land in total unit cost is high overall and the highest in large cities; and
 - 3) the supply elasticity of land itself is low.
- Housing prices will be more volatile in response to a demand shock when housing supply elasticity is low. The impact of speculative behavior will be stronger and boom-bust cycles are more likely when supply is inelastic (Malpezzi and Wachter, 2002). We therefore expect East Asian price cycles to be rather volatile.

Box 2.1 Predictors and time frames in propensity modeling

As we have outlined before, in propensity modeling, when we analyze customer behavior before the occurrence of the event of interest, candidate predictors should only be based in the observation period which should not overlap with the event outcome period.

Working with research teams to develop service user involvement

In the deployment phase, there will be no event outcome period, and the observation period will correspond to the current view of the customer at the time of deployment.

- Open cards at the beginning of the observation period (2012-1-1, OPEN_AT_START field)
- Open cards at the end of the observation period (2012-12-31, OPEN_AT_END field)
- Open cards at the end of the latency period (2013-3-1, OPEN_AT_LATENCY)
- Open cards at the end of the event outcome period (2013-7-1,

In our case study, the time frame of the observation period is the whole 2012. Information from the next months will serve only for the definition of the churn target field. When the model will be used for deployment, for instance at July 1, 2013, it will again require 12 months of summarized usage data, July 2012 to June 2013, to score new cases.

- 1) Open cards at the beginning of the observation period (2012-1-1, OPEN_AT_START field)
- 2) Open cards at the end of the observation period (2012-12-31, OPEN_AT_END field)
- 3) Open cards at the end of the latency period (2013-3-1, OPEN_AT_LATENCY)
 - Open cards at the beginning of the period (2012-1-1, OPEN_AT_START field)
 - Open cards at the end of the observation period (2012-12-31, OPEN_AT_END field)

Taking the perspective that it is the human activities that require management rather than the biological systems that we disturb, this chapter will describe an adaptive management approach to environmental management.

Starting out

The competitive nature of research often motivates researchers to incorporate service user involvement into their applications for research funding. Some researchers want to know what benefits service user involvement will bring to their research before they attempt it – but to determine the benefits requires some service user involvement activity to take place in the first place.

- NICE recommends [17] that parents:
 - are reassured that antibiotics are not needed immediately because they are likely to make little difference to symptoms and may have side effects;
 - are given advice about the usual natural history of the infection, including the average total length of the illness (before and after seeing the doctor):
 - acute otitis media (AOM): 4 days (a recent study suggests this should be longer [20]);
 - acute cough/acute bronchitis: 21 days

A patient-centered approach that puts emphasis on building and maintaining a therapeutic relationship between patient, doctor and care team is also referred to as a

relationship-centered approach. According to Beach *et al.* (2006), relationship-centered care is founded upon four principles. Using technological advancements such as remote sensing and geographic information systems, ecologists can determine the most successful ways to harmonize human disturbances with natural ones and identify feasible biological targets for the system of interest. Understanding the scale of the system and its processes is critical, and using large-scale data sets along with remote sensing can help ecologists determine where the system is, where it needs to be, and whether preservation is the right management decision or if more active restoration or rehabilitation is necessary.

- 1) that relationships in health care ought to include the personhood of the participants;
- 2) that affect and emotion are important components of these relationships;
 - a) that all healthcare relationships occur in the context of reciprocal influence and
 - i) that the formation and maintenance of genuine relationships in healthcare is morally valuable.
 - ii) systematic undervaluation of the currency;

Clearly, a central component of such an approach is for doctors to convey that they see their patients as people (i.e. not simply cases with biomedical defects). This is reflected in the excerpt above and part of Fig. 5.4

- a) systematic undervaluation of the currency;
- b) rate of growth of wages kept slower than the rate of growth of labor productivity;
- c) credit allocation directed by the government, and with central regulation of deposit and lending rates significantly below the opportunity cost of capital and its equilibrium level in the economy.

The environmental management of the Florida Everglades is used throughout as an illustrative case study of how ecologists have used an adaptive management approach to restore and preserve an internationally famous ecosystem.

in land use and urban planning approvals;

in government powers to intervene in the markets and to regulate private transactions;

in property taxation and land use transitions; and

in powers to use public lands and public finance to produce new volumes of serviced urban land.

ake radiolabeled nanoparticles an invaluable tool [35].

The adaptive management process is iterative, so that new information on the response of the ecosystem to our management activities is used to improve the next round of decisions. Using technological advancements such as remote sensing and geographic information systems, ecologists can determine the most successful ways to harmonize human disturbances with natural ones and identify feasible biological targets for the system of interest.

CLAUDIO: To make you answer truly to your name.

HERO: Is it not Hero? Who can blot that name With any just reproach?

CLAUDIO: Marry that can Hero!

Understanding the scale of the system and its processes is critical, and using large-scale data sets along with remote sensing can help ecologists determine where the system is,

where it needs to be, and whether preservation is the right management decision or if more active restoration or rehabilitation is necessary.

- i) On a per particle basis, SERS probes are significantly brighter compared to NIR emitting semiconducting quantum dots (QDs), which have been extensively investigated for bioimaging applications. Even simple designs involving individual gold nanoparticles tagged with resonant Raman reporters are nearly 200 times brighter compared to QDs [18].
- ii) The full-width at half-maximum (FWHM) of Raman bands (1-2 nm) are nearly 20-30 times narrower compared to the emission bands of quantum dots (40-60 nm), making spectral multiplexing an order of magnitude higher for SERS probes compared to that attainable with QDs [19].
- iii) The excitation and emission of SERS probes can be easily tuned to the near-infrared (NIR) therapeutic window (650-900 nm), where the endogenous absorption coefficient of tissue is nearly two orders magnitude lower compared to that in the visible parts of electromagnetic spectrum [19]. Furthermore, absence of interference from water and autofluorescence of the tissues in NIR is yet another significant advantage of SERS compared to photoluminescence-based optical imaging techniques.

SERS probes offer remarkable photostability compared to organic fluorophores and QDs, which suffer from either photobleaching or blinking. SERS probes, typically made of gold, are significantly less cytotoxic compared to NIR emitting QDs comprised of CdSe and CdTe.

Typical for such series of survey items is that the formulation is exactly the same for each item and that only one introduction with other possible components is given before the first survey item is mentioned. The items are treated equally because the interview programs use substitution procedures. An example of such an instruction to an interview program could look as follows:

```
#Casibattery 10 1
# item 1
healthcare
#item 2
social services
#item 3
# item 10
social security
#
#Question with 5 answer categories
What is your opinion about our "S"?
```

Examples of concepts-by-intuition include judgments, feelings, evaluations, norms, and behaviors. Most of the time, it is quite obvious that a text presents a feeling (x likes y), a norm (people should behave in a certain way), or behavior (x does y). We will return to the classification of these concepts later.

Title 21 Chapter 1 contains Parts 1 to 1299. The parts that are commonly encountered in the development of the three platforms of therapeutic delivery are listed below:

Part 3 – Product Jurisdiction

Part 4 – Current Good Manufacturing Practice Requirements for Combination Products (effective July 2013)

Part 11 - Electronic Records; Electronic Signatures

Part 58 - Good Laboratory Practice for Nonclinical Laboratory Studies

Part 210 - Current Good Manufacturing Practice in Manufacturing, Processing, Packing, or Holding Of Drugs; General

In the United States, the regulatory requirements of the three platforms of drug delivery are implemented through three separate Centers in the FDA

Stewardship to Natural Capitalism optimization of productive effort aimed at efficient use of the earth's natural capital. The concept of natural capitalism is based on four principles:

- Radical resource efficiency
- Ecological restoration

Efficiency to Eco Efficiency the transition from total quality focused initiatives to also include environmental impact reduction through the implementation of four stages of eco efficient development:

- Increasing process efficiency.
- Reducing material flow by changing consumer preferences for material intensive products.

Business image to environmental champion a commitment to Sustainability Partnerships that is manifested by organizational policies and procedures aimed at implementing environmental best practice.

Taking the perspective that it is the human activities that require management rather than the biological systems that we disturb, this chapter will describe an adaptive management approach to environmental management.

Step 1: Generate random paths through the graph.

Step 2: Keep only those paths that begin with V_{in} and end with V_{out} .

Step 3: If the graph has n vertices, then keep only those paths that enter exactly n vertices.

Step 4: Keep only those paths that enter all of the vertices of the graph at least once.

Step 5: If any paths remain, say "Yes"; otherwise, say "No."

The versatility of polyurethanes is derived in large part from the wide selection of building blocks available to materials designers. Bioinspired research is based on identifying and emulating the principles of biomineralization in natural systems, instead of copying them directly. In fact, most strategies incorporated by natural systems are not directly applicable to engineered materials, so the need for alternative synthetic routes are required for the incorporation of non-natural elements, such as barium, nickel, copper or aluminum, with functional nanoscale properties [1,8]. However, the production of these devices has been achieved at a high price, with the primary challenges currently faced by high-throughput fabrication laboratories including the high cost of laborers and instruments.

In Kupferchlorid und Kupfersulfatpentahydrat (siehe Abb. 4.18) sind giftig und inätzend, Quecksilberchlorid ist sehr giftig und inätzend, Schwefeldioxid ist giftig, Silbernitrat wirkt ätzend. Das Tragen auf einer und Schutzbrille ist erforderlich. Dieser wird auf die

Algorithm 1

Input: transition matrix P , observation matrix $\mathbf{r}(\mathbf{u}_k, z_{k+1})$, costs $\mathbf{g}^\lambda(\mathbf{u}^q)$, $q = 1, \dots, \alpha$, horizon length L

Output: cost $\{\hat{J}_k^\lambda(\mathbf{e}_1), \dots, \hat{J}_{L-1}^\lambda(\mathbf{e}_n)\}_{k=0}^{L-1}$, strategy $\{\hat{\mathbf{u}}_k^{\mathbf{e}_1}, \dots, \hat{\mathbf{u}}_k^{\mathbf{e}_n}\}_{k=0}^{L-1}$

- 1: for $i = 1 : n$ do
- 2: $\hat{J}_{L-1}^\lambda(\mathbf{e}_i) = \min_{\mathbf{u}_{L-1} \in \mathcal{U}} [\mathbf{e}_i^T \mathbf{g}^\lambda(\mathbf{u}_{L-1})]$;
- 3: $\hat{\mathbf{u}}_{L-1}^{\mathbf{e}_i} = \arg \min_{\mathbf{u}_{L-1} \in \mathcal{U}} \hat{J}_{L-1}^\lambda(\mathbf{e}_i)$;
- 4: end for
- 5: **end for**

Porzellanfilternutsche gegeben, zweimal mit Ethanol sowie mit Wasser gewaschen mit denen das $\text{Cr}(\text{H}_2\text{O})_6$ oder Kupfersulfatpentahydrat mit den viel H_2O und Schwefeldioxid-Druckgaszylinder, 2 destilliertes Wasser.

1. In principle there is as much potential for design of isocyanate structures as there is for alcohol and amine co-reactants. In reality, while there are numerous polyisocyanates to choose from, most of the innovation in polyurethane performance comes from the broad range of choices available in the co-reactant alcohols and amines.

2. To a great extent this reflects complications (both industrial and regulatory) associated with making isocyanates, and the comparative ease of making polyol and polyamine structures.

In reality, while there are numerous polyisocyanates to choose from, most of the innovation in polyurethane performance comes from the broad range of choices available in the co-reactant alcohols and amines.

Problems

1.1 The positive sequence impedance data are given in the accompanying table. Use the commonly made assumption that all prefault resistance values are $(1.0 + j0.0)$ pu, and neglect all resistance values.

C1 (X1, X2): (cs, ss) (cs, al) (al, cu)

C2 (X1, X3): (cs, ss) (ss, cu) (al, cu)

C3 (X2, X3): (cs, ss) (cs, al) (cu, cu)

1.2 Using the usual assumptions about the positive and negative sequence impedances of the network elements, what are the currents at breaker B1 for b–c fault for each of the faults in Problem 1.1? What is the voltage between phases b and c for each case?

With the governmental regulatory environment and the general European goal of using industrial solutions employing the least toxic effective components available, there has been increasing industrial and academic emphasis on obtaining urethane properties from systems that do not employ isocyanates.

Table 2.1 Dystonia genetic conditions.

Gene	Locus	Inheritance	Phenotype	Gene product (gene)
<i>DYT 1</i>	9q32-34	AD	Young onset, generalised	Torsin A (<i>TOR1A</i>)
<i>DYT 2</i>	NM	AR	Young onset, generalised	—
<i>DYT 3</i>	Xq13.1	XR	Filipino dystonia–parkinsonism	Gene transcription factor (<i>TAF1</i>)
<i>DYT 4</i>	NM	AD	Laryngeal ± limb dystonia (1 family)	—
<i>DYT 5a</i>	14q22.1-2	AD	Young onset, dopa-responsive	GTP cyclohydrolase 1 (<i>GTPCH1</i>)
<i>DYT 5b</i>	11p16.5	AR	dystonia–parkinsonism	Tyrosine hydroxylase (TH)
<i>DYT 6</i>	8p11.21	AD	Young onset, cranio-cervical or generalised	Thanatos-associated protein 1 (<i>THAP1</i>)
<i>DYT 7</i>	18p	AD	Adult onset, focal dystonia (1 family)	Not identified
<i>DYT 8</i>	2q35	AD	<i>PNKD1</i>	Myofibrillogenesis regulator 1 (<i>MR-1</i>)
<i>DYT 9</i>	1p31	AD	<i>EID1</i> /Episodic chorea or ataxia and spasticity	Glucose transporter 1 (<i>SLC2A1</i>)
<i>DYT 10</i>	16p11-q12	AD	<i>PKD1</i>	<i>PRRT2</i>
<i>DYT 11</i>	7q21.3	AD	Myoclonus dystonia	E-sarcoglycan (<i>SGCE</i>)
<i>DYT 12</i>	19q13.2	AD	Rapid onset dystonia–parkinsonism	Na ⁺ /K ⁺ ATPase α3 subunit (<i>ATPIA3</i>)
<i>DYT 13</i>	1p36	AD	Young onset segmental or generalised dystonia (1 family)	Not identified
<i>DYT 14 = DYT 5a</i>				
<i>DYT 15</i>	18p11	AD	Myoclonus dystonia (1 family)	Not identified
<i>DYT 16</i>	2q31.2	AR	Young onset, generalised dystonia-parkinsonism	Stress-response protein (<i>PRKRA</i>)
<i>DYT 17</i>	20p11-q13	AR	Young onset, mixed phenotype (1 family)	Not identified
<i>DYT 18</i>	1p34.2	AD	<i>EID2</i>	Glucose transporter 1 (<i>SLC2A1</i>)
<i>DYT 19</i>	16q13-22	AD	<i>PKD2</i> (1 family)	Not identified
<i>DYT 20</i>	2q31	AD	<i>PNKD2</i> (1 family)	Not identified
<i>DYT 21</i>	2q14-q21	AD	Adult onset mixed phenotype (1 family)	Not identified

(Continued)

Table 2.1 (Continued)

Gene	Locus	Inheritance	Phenotype	Gene product (gene)
<i>DYT 22</i>	Reserved			
<i>DYT 23</i>	11p14.2	AD	Adult onset cranio-cervical dystonia	Anoctamin 3 (<i>ANO3</i>)
<i>CIZ 1*</i>	9q34.11	AD	Adult onset cervical dystonia	Cip-1-interacting zinc protein
<i>GNAL*</i>	18p11	AD	Mixed phenotype	G protein subunit α_{olf}

AD, autosomal dominant; AR, autosomal recessive; EID, exercise-induced dystonia; NM, not mapped; PKD, paroxysmal kinesigenic dystonia; PNKD, paroxysmal non-kinesigenic dystonia; XR – X-linked recessive.

*Waiting for replication studies and/or not assigned a DYT.

Bioinspired research is based on identifying and emulating the principles of biomineralization in natural systems, instead of copying them directly. In fact, most strategies incorporated by natural systems are not directly applicable to engineered materials, so the need for alternative synthetic routes are required for the incorporation of non-natural elements, such as barium, nickel, copper or aluminum, with functional nanoscale properties [1,8]. However, the production of these devices has been achieved at a high price, with the primary challenges currently faced by high-throughput fabrication laboratories including the high cost of laborers and instruments.

Example 2.1

Problem: The position of a body along the x axis, in metres, is given by the equation $x = t^3 - 30t^2 + 5$, where t is the time in seconds. Find its velocity and acceleration as a function of time.

Governing Equations:

$$\text{Velocity} \quad \mathbf{V} = \frac{dx}{dt}$$

$$\text{Acceleration} \quad a = \frac{d^2x}{dt^2}$$

Solution:

$$x = t^3 - 30t^2 + 5$$

$$a(t) = \frac{d^2x}{dt^2} = 6t - 60$$

Through precisely tuned processes, Nature is able to synthesize a variety of metal oxide nanomaterials under ambient conditions; the magnetic navigation device found in magnetotactic bacteria (MTB) is one such example [17]. Here, magnetite (Fe_3O_4) nanocrystals are aligned with the Earth's geomagnetic field and contained within specific organelles known as magnetosomes [17]. Fresh water salmon, for example, utilizes these magnetic nanoparticles in the nasal cavities of their forehead as a biomagnetic compass during migration [18]. A Q-switch is a device that is similar to a shutter that controls the laser resonator's ability to oscillate.

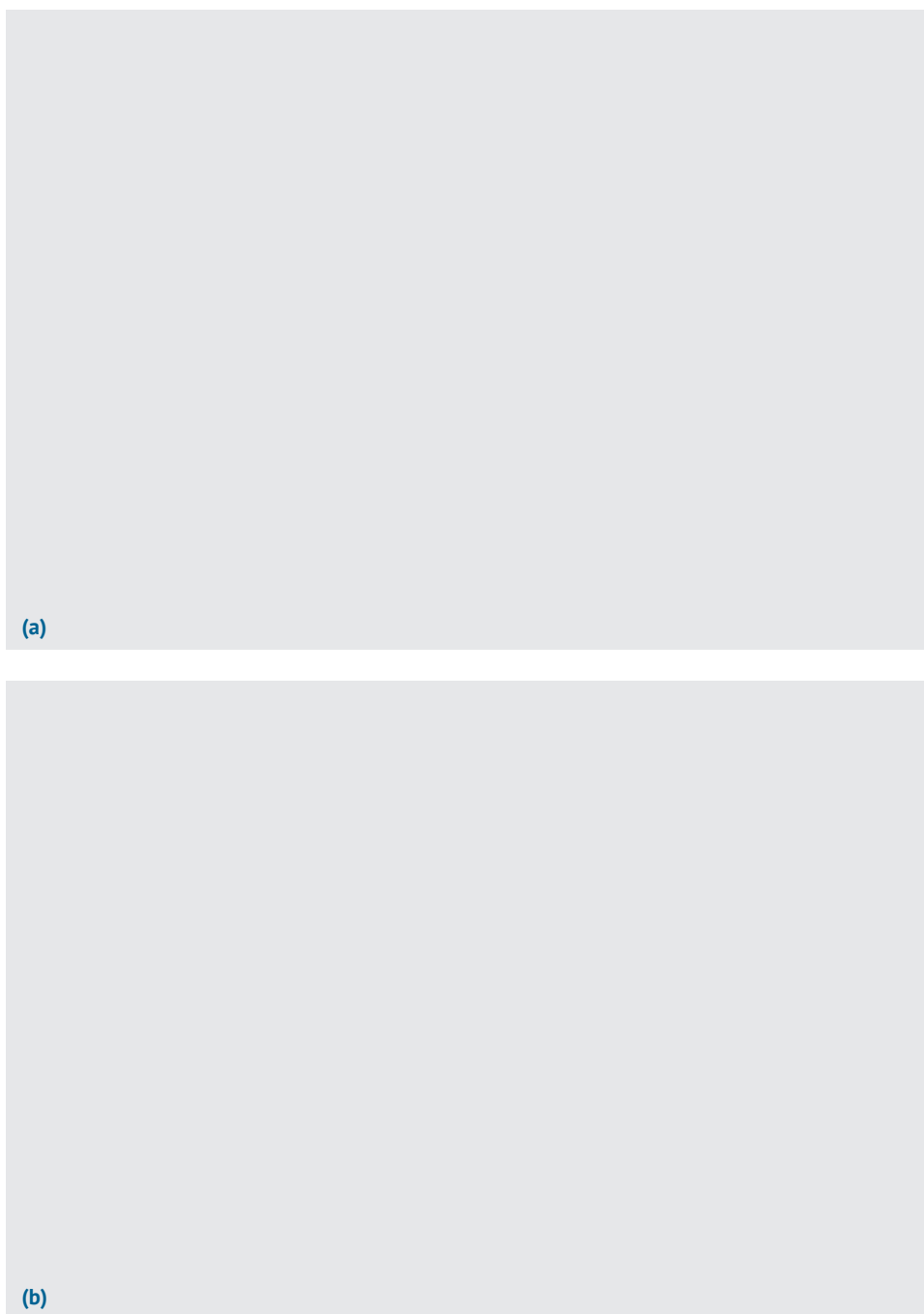


Figure 2.1 (a) Inside the prototype device of the near-field lithography. (b) Illumination of i-line light for exposure from the back side of the near-field photomask.

(Continued)

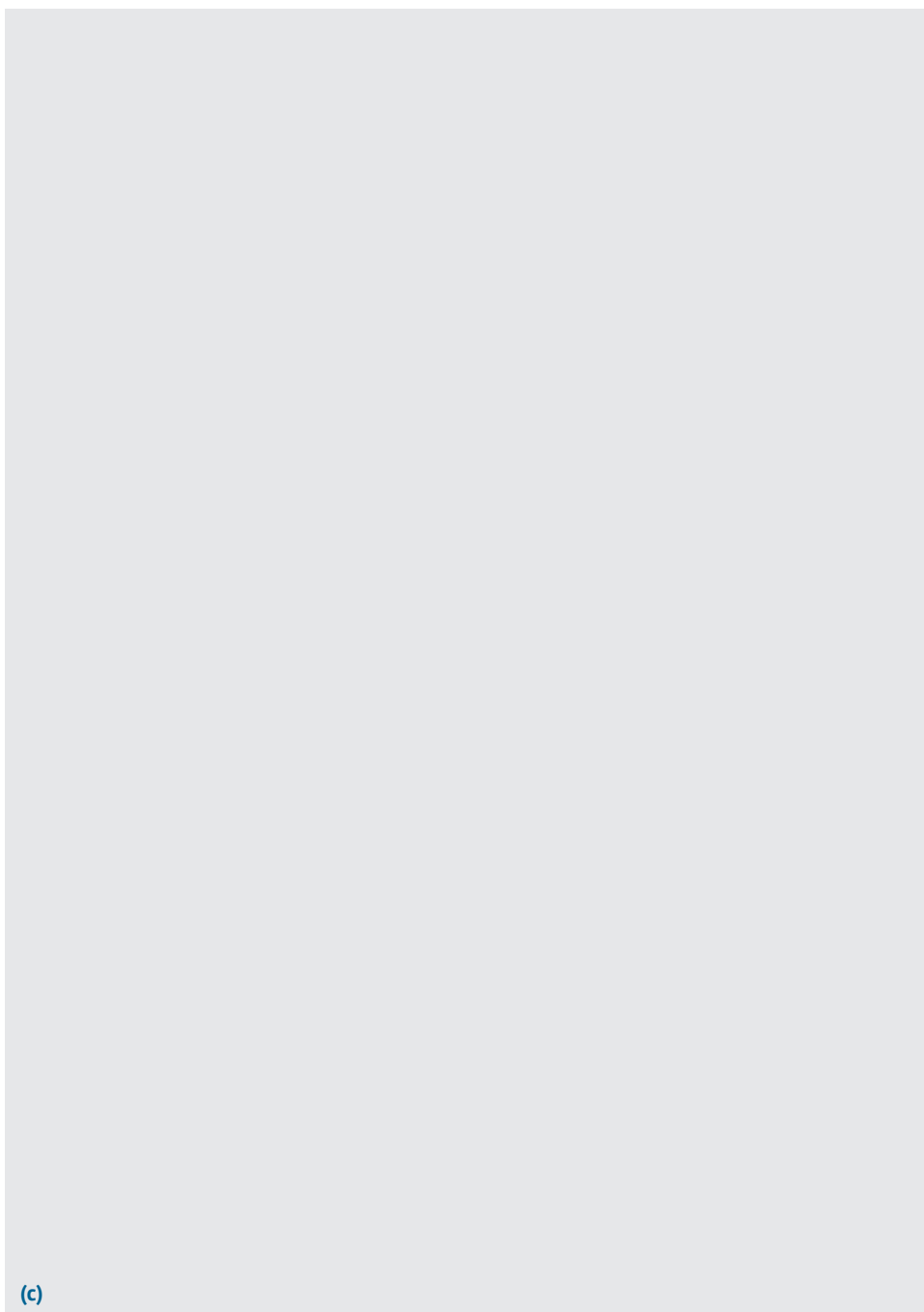


Figure 2.1 (Cont'd) (c) Close-up from the side of the near-field photomask and the photoresist on the wafer. They are brought into contact with each other within the localizing distance of the optical near-field.

Box 2.2 Resources

If you are in crisis or you know someone who is hurting, *please* contact these FREE resources.

Resource	Phone number	Website
National Suicide Prevention Lifeline	1-800-273-8255	http://www.suicidepreventionlifeline.org/
Contact: From breaking point to turning point	(972) 233-2233	http://contactcrisisline.org/
Crisis Call Center	1-800-273-8255 OR Text ANSWER to 839863	http://crisiscallcenter.org/crisisservices.html
The Trevor Project (for LGBTQQ youth)	1-866-488-7386 OR Text the word “Trevor” to 1-202-304-1200	http://www.thetrevorproject.org/
Veterans Crisis Line	1-800-273-8255 and Press 1 OR Text 838255	http://veteranscrisisline.net/

Box 2.3 Predictors and time frames in propensity modeling

As we have outlined before, in propensity modeling, when we analyze customer behavior before the occurrence of the event of interest, candidate predictors should only be based in the observation period which should not overlap with the event outcome period.

Working with research teams to develop service user involvement

In the deployment phase, there will be no event outcome period, and the observation period will correspond to the current view of the customer at the time of deployment. In the deployment phase, there will be no event outcome period, and the observation period will correspond to the current view of the customer at the time of deployment.

$$\rho(z)v_w = \rho_w^{\text{bulk}} v_w \exp(-v_w \beta[\pi(z) - \pi^{\text{bulk}}])$$

$$\rho(z)v_w = \rho_w^{\text{bulk}} v_w \exp(-v_w \beta[\pi(z) - \pi^{\text{bulk}}]) - q_i \beta[\psi(z) - \psi^{\text{bulk}}]$$

In the deployment phase, there will be no event outcome period, and the observation period will correspond to the current view of the customer at the time of deployment.

- Open cards at the beginning of the observation period (2012-1-1, OPEN_AT_START field)
- Open cards at the end of the observation period (2012-12-31, OPEN_AT_END field)
- Open cards at the end of the latency period (2013-3-1, OPEN_AT_LATENCY)
- Open cards at the end of the event outcome period (2013-7-1,

(Continued)

Box 2.3 (Continued)

In our case study, the time frame of the observation period is the whole 2012. Information from the next months will serve only for the definition of the churn target field. When the model will be used for deployment, for instance at July 1, 2013, it will again require 12 months of summarized usage data, July 2012 to June 2013, to score new cases.

- 1) Open cards at the beginning of the observation period (2012-1-1, OPEN_AT_START field)
- 2) Open cards at the end of the observation period (2012-12-31, OPEN_AT_END field)
- 3) Open cards at the end of the latency period (2013-3-1, OPEN_AT_LATENCY)
 - Open cards at the beginning of the period (2012-1-1, OPEN_AT_START field)
 - Open cards at the end of the observation period (2012-12-31, OPEN_AT_END field)

Taking the perspective that it is the human activities that require management rather than the biological systems that we disturb, this chapter will describe an adaptive management approach to environmental management.

Starting out

The competitive nature of research often motivates researchers to incorporate service user involvement into their applications for research funding. Some researchers want to know what benefits service user involvement will bring to their research before they attempt it – but to determine the benefits requires some service user involvement activity to take place in the first place.

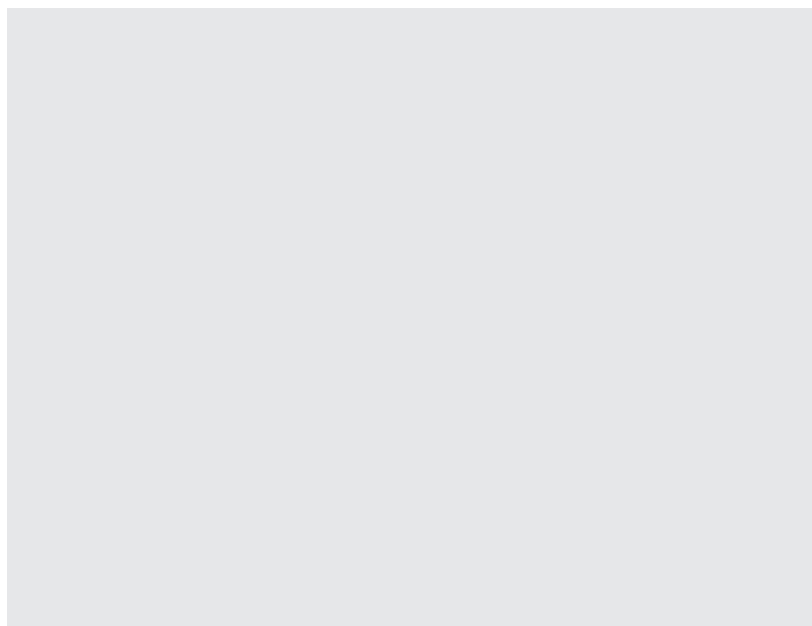
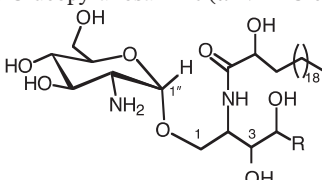
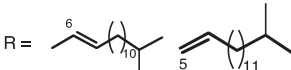
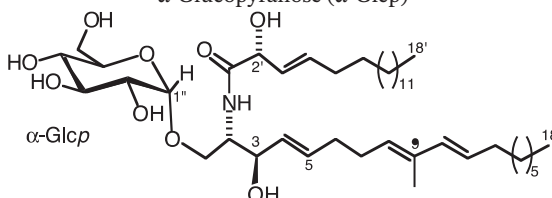
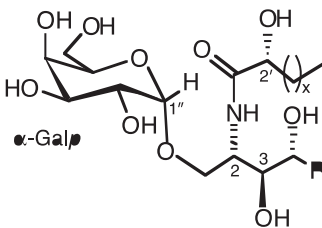


Figure 1.12 Distribution of structures for variable pH samples. *Source:* Reprinted with permission from Ref. [33]; © 2007, American Chemical Society.

Table 2.2 Glycosphingolipids containing an α -glycosyl linkage.

Ceramide / GSL Name	Organism	Biological activity	Reference																														
<p>α-Glucopyranosamine (α-NH₂-Glc_p)</p> 																																	
<p>R = </p> <p>amphiceramides E and F</p>	<p>Sponge <i>Amphimedon viridis</i></p>	<p>n. r.</p>	<p>Hirsch and Kashman, 1989</p>																														
<p>α-Glucopyranose (α-Glc_p)</p> 																																	
<p>sarcoehrenoside A</p>	<p>Octocoral <i>Sarcophyton ehrenbergi</i></p>	<p>No antibacterial Reduced iNOS protein expression Anti-inflammatory</p>	<p>Cheng et al., 2009</p>																														
<p>α-Gal_p</p> 																																	
<table><tr><th>Agelasphin</th><th>x</th><th>R</th></tr><tr><td>-7a</td><td>21</td><td>-(CH₂)₁₁-CH₃</td></tr><tr><td>-9a</td><td>21</td><td>-(CH₂)₁₂-CH₃</td></tr><tr><td>-9b</td><td>21</td><td>-(CH₂)₁₁-CH(CH₃)₂</td></tr><tr><td>-11</td><td>21</td><td>-(CH₂)₁₁-CH(CH₃)-C₂H₅</td></tr><tr><td>-13</td><td>21</td><td>-(CH₂)₁₁-CH(CH₃)-C₂H₅</td></tr><tr><td>-7b-1</td><td>20</td><td>-(CH₂)₁₀-CH(CH₃)-C₂H₅</td></tr><tr><td></td><td></td><td>-(CH₂)₁₁-CH(CH₃)₂</td></tr><tr><td>-7b-2</td><td>21</td><td>-(CH₂)₉-CH(CH₃)-C₂H₅</td></tr><tr><td></td><td></td><td>-(CH₂)₁₀-CH(CH₃)₂</td></tr></table>	Agelasphin	x	R	-7a	21	-(CH ₂) ₁₁ -CH ₃	-9a	21	-(CH ₂) ₁₂ -CH ₃	-9b	21	-(CH ₂) ₁₁ -CH(CH ₃) ₂	-11	21	-(CH ₂) ₁₁ -CH(CH ₃)-C ₂ H ₅	-13	21	-(CH ₂) ₁₁ -CH(CH ₃)-C ₂ H ₅	-7b-1	20	-(CH ₂) ₁₀ -CH(CH ₃)-C ₂ H ₅			-(CH ₂) ₁₁ -CH(CH ₃) ₂	-7b-2	21	-(CH ₂) ₉ -CH(CH ₃)-C ₂ H ₅			-(CH ₂) ₁₀ -CH(CH ₃) ₂	<p>Sponge <i>Agelas mauritanus</i></p>	<p>Antitumor Immunostimulatory</p>	<p>Natori et al., 1993, 1994</p>
Agelasphin	x	R																															
-7a	21	-(CH ₂) ₁₁ -CH ₃																															
-9a	21	-(CH ₂) ₁₂ -CH ₃																															
-9b	21	-(CH ₂) ₁₁ -CH(CH ₃) ₂																															
-11	21	-(CH ₂) ₁₁ -CH(CH ₃)-C ₂ H ₅																															
-13	21	-(CH ₂) ₁₁ -CH(CH ₃)-C ₂ H ₅																															
-7b-1	20	-(CH ₂) ₁₀ -CH(CH ₃)-C ₂ H ₅																															
		-(CH ₂) ₁₁ -CH(CH ₃) ₂																															
-7b-2	21	-(CH ₂) ₉ -CH(CH ₃)-C ₂ H ₅																															
		-(CH ₂) ₁₀ -CH(CH ₃) ₂																															

Exercises

- 1 Try to formulate questions that represent concepts-by-intuition and concepts-by-postulation with formative and reflective indicators for the following concepts:
 - A Life satisfaction
 - B Happiness
 - C The importance of the value “honesty”
- 2 In practice, it is seldom clear whether the questions suggested measure what they are supposed to measure.

Notes

- 1 Reproduced from *Journal of Chronic Diseases*, **39**, Brody, J. A. and Schneider, E. L., Diseases and disorders of aging: an hypothesis, pages 871–876, Copyright 1986, with permission from Elsevier.
- 2 Reproduced from *The Journals of Gerontology Series A: Biological Sciences and Medical Sciences*, **58**, Blumenthal, H. T., The aging–disease dichotomy: true or false?, pages M138–M145, Copyright 2003, with permission from Oxford University Press.

References

- Cai, W. and Chen, X. (2007) Nanoplatforms for targeted molecular imaging in living subjects. *Small*, **11**, 1840–54.
- Cheng, M.M., Cuda, G., Bunimovich, Y.L., Gaspari, M., Heath, J.R., Hill, H.D., Mirkin, C.A., Nijdam, A.J., Terracciano, R., Thundat, T. and Ferrari, M. (2006) *Biology*, **10**, 11–19.
- Gupta, A.K. and Gupta, M. (2005) Synthesis and surface engineering of iron oxide nanoparticles for biomedical applications. *Biomaterials*, **26**, 3995–4021.

Multiple Choice Questions

Questions Different types of question i.e. Multiple Choice Questions, Extended Matching Questions. Accordingly, calixarenes containing four phenol groups 39a–e exist as cone conformers. These are quite often put on a website but may still be typeset - Requirements are:

1 Multiple choice questions

For each question below, what is the most likely answer? Select ONE option from the answers supplied.

1.1 Ion Channels and Currents

1.1.1 Potassium



- 1 In a diagram of AP shown below, which one of the following currents is active where answers arrow is pointing?
 - A Ito
 - B IK1
 - C INa
 - D ICa

- 2 In a diagram of AP shown below, which one of the following currents is active where answers arrow is pointing?
 - A Ito
 - B IK1
 - C INa
 - D ICa

- 3 In a diagram of AP shown below, which one of the following currents is active where answers arrow is pointing?
 - A Ito
 - B IK1
 - C INa
 - D ICa

50 | Multiple Choice Questions

- 9 In a diagram of AP shown below, which one of the following currents is active where answers arrow is pointing?
- A Ito
 - B IK1
 - C INa
 - D ICa
- 10 In a diagram of AP shown below, which one of the following currents is active where answers arrow is pointing?
- A Ito
 - B IK1
 - C INa
 - D ICa
- 11 In a diagram of AP shown below, which one of the following currents is active where answers arrow is pointing?
- A Ito
 - B IK1
 - C INa
 - D ICa

A

Simulating the Bloch Equations

In a real magnetic resonance (MR) experiment, there are many sources of magnetic fields in addition to \mathbf{B}_0 . The *chemical shift* modulates the effective field strength that a nucleus experiences due to shielding effects of the electron shell. The strength of the effect depends on the bonding state of the hydrogen atom, and is therefore different for spins constituting free water and those that are part of lipids, giving rise to the *fat-water shift*. In addition to \mathbf{B}_1 -fields used to flip the magnetization into the transverse plane, position-dependent magnetic field gradients along the z-axis (see Section 1.6.1) are used to manipulate the magnetization during the experiment. We can therefore express the effective magnetic field in the rotating frame as

$$x = t^3 - 30t^2 + 5 \quad (\text{A.1})$$

Of all these field components, B_0 is the strongest with a typical magnitude of 1.5 or 3 T on clinical magnetic resonance imaging (MRI) scanners. The gradients typically induce field variations in the order of a few tens of millitesla. B_1 usually has a magnitude in the range of tens of 11 T. The chemical shift is very weak, causing a field modulation of 1.3 ppm (parts per million) between water and fat. It is therefore only relevant for B_0 and is negligible for all other field components. B_1 fields are designed to rotate in the (x,y)-plane and therefore do not have a z-component. The precession in such a complex setting can be parameterized by a precession frequency vector

$$a(t) = \frac{d^2x}{dt^2} = 6t - 60 \quad (\text{A.2})$$

and the angle between the magnetization and the magnetic field is given by if \mathbf{M}' was aligned with \mathbf{B} at $t = 0$.

With this vector notation, we can express the precession in the rotating frame 1 as by adding T_2 and T_2 relaxation terms, we can express the Bloch equation (1.26) in the rotating frame as and the longitudinal equilibrium magnetization M_0 as defined in Eq. (1.7) (which is independent of the coordinate system and therefore not marked with a prime). In order to solve the differential equation (AS), we introduce the quantity \mathbf{h}' :

In order to simulate the time evolution of the magnetization, Eq. (All) can be solved for a number of time steps $tk = k \cdot \Delta t$. It is important to note that Eq. (All) was derived under the assumption of a constant matrix \mathbf{W}' , implying a constant \mathbf{B}' -vector in the rotating frame.



Glossary

account classification The way in which suppliers of electricity, natural gas, or fuel oil classify and bill their customers. Commonly used account classifications are “Residential,” “Commercial,” “Industrial,” and “Other.” Suppliers’ definitions of these terms vary from supplier to supplier. In addition, the same customer may be classified differently by each of its energy suppliers.

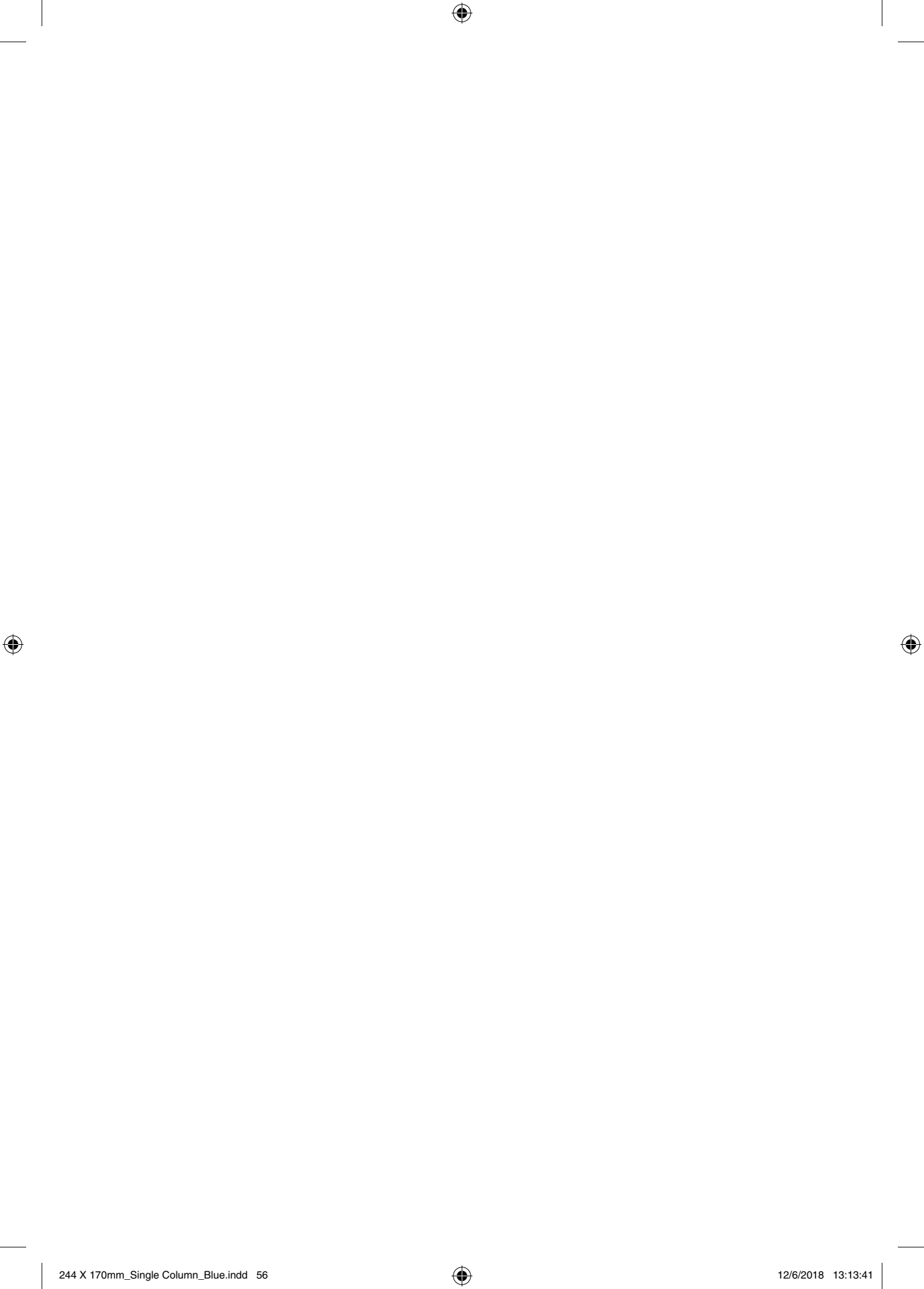
account of others (natural gas) Natural gas deliveries for the account of others are deliveries to customers by transporters that do not own the natural gas but deliver it for others for a fee. Included are quantities covered by long-term contracts and quantities involved in short-term or spot market sales.

accounting system A method of recording accounting data for a utility or company or a method of supplying accounting information for controlling, evaluating, planning and decision-making.



References

- 1 Perina, J. (1972) Coherence of Light, Van Nostrand, London.
- 2 Louisell, W.H. (1973) Quantum Statistical Properties of Radiation, John Wiley & Sons, Inc., New York.
- 3 Loudon, R. (1973) Quantum Theory of Light, Oxford University Press, Oxford.
- 4 Allen, L. and Eberly, J.H. (1975) Optical Resonance and Two-Level Atoms, John Wiley & Sons, Inc., New York.
- 5 Perina, J. (1984) Quantum Statistics of Linear and Nonlinear Optical Phenomena, D. Reidel Publishing Company, Dordrecht.
- 6 Gardiner, C.W. (1991) Quantum Noise, Springer-Verlag, Berlin, Heidelberg.
- 7 Meystre, P. and Sargent, M. III (1991) Elements of Quantum Optics, Springer-Verlag, Berlin, Heidelberg.
- 8 Walls, D.F. and Milburn, G.J. (1994) Quantum Optics, Springer-Verlag, Berlin, Heidelberg.
- 9 Vogel, W. and Welsch, D.-G. (1994) Lectures on Quantum Optics, Akademie Verlag, Berlin.
- 10 Scully, M.O. and Zubairy, M.S. (1997) Quantum Optics, Cambridge University Press, Cambridge.
- 11 Barnett, S.M. and Radmore, P.M. (1997) Methods in Theoretical Quantum Optics, Clarendon Press, Oxford.
- 12 Puri, R.R. (2001) Mathematical Methods of Quantum Optics, Springer, Berlin.
- 13 Dicke, R.H. (1954) *Physical Review*, 93, 99.
- 14 (a) Perelomov, A. (1986) Generalized Coherent States R. (1990) *Reviews of Modern Physics*, 62, 867.
- 15 Radcliffe, J.M. (1971) *Journal of Physics A: General Physics*, 4, 313.



Index

a

absorbance spectrum 66, 70
 diffraction 70
 adhesion 114
 absorption/scattering spectrum, *see* biological windows
 absorption techniques, gas adsorption 243
 air-solvent interface 69
 alkane 88
 alkanethiol-capped gold cluster 246
 alkanethiol molecules, lattice of 88
 alkoxysilanes 77
 alkyl chain ligands 177
 alloy
 Au/Ag 95
 nanomaterials, surface segregation 16
 alumina membrane 62
 amorphous silica, calcination 60
 amphiphilic molecules 211, 221
 lipids 211
 anisotropy 151
 antiferromagnetic materials 180, *see also*
 iron oxide
 antiferromagnetism 180
 apolar solvents 175
 atomic force microscope (AFM) 201
 Au-Ni-CNT microrods, scanning electron
 microscope (SEM) image 219

b

baffling process 203
 band 146
 conduction 146, 148

 valence 146
 barcoding 218
 bidentate ligand 176
 binary atomic lattices 187
 CaF₂ structure 187
 NaCl structure 187
 binary ordered arrays, formation 88
 binary superlattice 187
 bioconjugation technique 213, 226
 biological tissues, absorption/scattering
 spectrum 107
 biological windows 105, 107
 importance 107
 bionano 40, 189
 interface 37–45
 cancer cells 37
 magnetothermal 41
 photothermal treatment 41
 schematic presentation 40, 41
 biosensors 75, 77
 block copolymers 208, 210, 211
 blood stream, drugs concentration 75
 body-centered cubic (bcc) phase 209
 Bohr radius 149
 Boltzmann constant 148
 bottom-up techniques 118
 Braggs law 68, 71
 refractive index 71
 bionano applications 167
 bionano aspects 163
 doping of 160
 synthesis 151
 bridging group 175



“keywords/abstract

Dear Author,

Keywords and abstracts will normally not be included in the print version of your chapter but only in the online version (unless specifically agreed by Wiley/Wiley VCH)”.

Abstract

The first part of this chapter outlines the requirements for the individual assemblies of a modern UHPLC system. The differences between low-pressure and high-pressure mixing and their advantages and disadvantages are discussed. Furthermore, current UHPLC injection modes are described. The differences between fixed-loop and flow-through autosamplers are explained, and practical hints are given. Regarding the temperature control of the mobile and stationary phases, the influence of temperature on the resulting separation is shown. In addition, the use of column switching valves for routine applications is described. In the context of very narrow peaks in UHPLC, general requirements for UHPLC detectors are discussed. Another focus is the explanation of proper connection technology of the individual UHPLC modules. For this purpose, the influence of plastic- and stainless-steel-based connection technology on the resulting chromatography is shown.

Keywords

high- and low-pressure mixing system; fixed-loop and flow-through injection; column oven; UHPLC detectors; capillaries and fittings

Affiliation for the Authors

Steffen Wiese¹, Michael Heidorn², and Frank Steiner²

¹Chromsystems, Munich and Terence Hetzel, IUTA, Duisburg, Germany

²Thermo Fischer Scientific, Dornierstr. 4, 82110 Germering/Munich, Germany

**Biochemical Principles and
Mechanisms of Biosynthesis
Biodegradation of Polymers**

B. Cornils, W. A. Herrmann (Eds.)

**Applied Homogeneous Catalysis with
Organometallic Compounds**

A Comprehensive Handbook in Two Volumes

1996

ISBN: 978-3-527-29286-1

M. Beller, C. Bolm (Eds.)

Transition Metals for Organic Synthesis

Building Blocks and Fine Chemicals

1998

ISBN: 978-3-527-29501-1

A. Togni, R. L. Halterman (Eds.)

Metallocenes

1998

ISBN: 978-3-527-29539-9

P. J. Stang (Eds.)

Metal-catalyzed Cross-coupling Reactrom

1998

ISBN: 978-3-527-29421-X

B. Cornils, W. A. Herrmann (Eds.)

Applied Homogeneous Catalysis with Organometallic Compounds

A Comprehensive Handbook in Two Volumes

1996

ISBN: 978-3-527-29286-1

E. Chang, F. Hussain, T. Dillon (Eds.)

Trust and Reputation for Service-Oriented Environments

Technologies For Building Business Intelligence And Consumer Confidence

2006

ISBN: 978-3-527-01547-9

M. Beller, C. Bolm (Eds.)

Transition Metals for Organic Synthesis

Building Blocks and Fine Chemicals

1998

ISBN: 978-3-527-29501-1

B. Cornils, W. A. Herrmann (Eds.)

The Shanty Chor

A Comprehensive Handbook in Two Volumes

1996

ISBN: 978-3-527-29286-9

A. Togni, R. L. Halterman (Eds.)

Metallocenes

1998

ISBN: 978-3-527-29539-9

H. Misawa, S. Juodkazis (Eds.)

3D Laser Microfabrication

Principles and Applications

2006

ISBN: 978-3-527-31055-5

Wiley Handbooks in

FINANCIAL ENGINEERING AND ECONOMETRICS

Advisory Editor

Ruey S. Tsay

The University of Chicago Booth School of Business USA

The dynamic and interaction between financial markets around the world have changed dramatically under economic globalization. In addition, advances in communication and data collection have changed the way information is processed and used. In this new era, financial instruments have become increasingly sophisticated and their impacts are far-reaching. The recent financial (credit) crisis is a vivid example of the new challenges we face and continue to face in this information age. Analytical skills and ability to extract useful information from mass data, to comprehend the complexity of financial instruments, and to assess the financial risk involved become a necessity for economists, financial managers, and risk management professionals. To master such skills and ability, knowledge from computer science, economics, finance, mathematics and statistics is essential. As such, financial engineering is cross-disciplinary, and its theory and applications advance rapidly.

The goal of this Handbook Series is to provide a one-stop source for students, researchers, and practitioners to learn the knowledge and analytical skills they need to face today's challenges in financial markets. The Series intends to introduce systematically recent developments in different areas of financial engineering and econometrics. The coverage will be broad and thorough with balance in theory and applications. Each volume will be edited by leading researchers and practitioners in the area and covers state-of-the-art methods and theory of the selected topic.

Published Wiley Handbooks in Financial Engineering and Econometrics

Bauwens, Hafner, and Laurent · *Handbook of Volatility Models and Their Applications*

Brandimarte · *Handbook in Monte Carlo Simulation: Applications in Financial Engineering, Risk Management, and Economics*

Chan and Wong · *Handbook of Financial Risk Management: Simulations and Case Studies*

Cruz, Peters, and Shevchenko · *Fundamental Aspects of Operational Risk and Insurance Analytics: A Handbook of Operational Risk*

James, Marsh, and Sarno · *Handbook of Exchange Rates*



Mechanism of Biosynthesis

Nomenklatur der
Organischen Chemie

Edited by Hans-Georg Joost and Gerhard Eisenbrand

*in collaboration with
Gerald Böhm
Uwe Diederichsen*

Second Revised Edition

WILEY Blackwell

Monitoring

An Introduction

Gerald Böhm

WILEY Blackwell

Author

Linda E. Reichl

University of Texas
Center for Complex Quantum Systems
Austin, TX 78712
USA

Cover

Bose–Einstein condensates;
courtesy of Daniel J. Heinzen

■ All books published by Wiley-VCH are carefully produced. Nevertheless, authors, editors, and publisher do not warrant the information contained in these books, including this book, to be free of errors. Readers are advised to keep in mind that statements, data, illustrations, procedural details or other items may inadvertently be inaccurate.

Library of Congress Card No.: applied for

British Library Cataloguing-in-Publication Data:

A catalogue record for this book is available from the British Library.

Bibliographic information published by the Deutsche Nationalbibliothek

The Deutsche Nationalbibliothek lists this publication in the Deutsche Nationalbibliografie; detailed bibliographic data are available on the Internet at <http://dnb.d-nb.de>.

© 2016 WILEY-VCH Verlag GmbH & Co. KGaA, Boschstr. 12, 69469 Weinheim, Germany

All rights reserved (including those of translation into other languages). No part of this book may be reproduced in any form – by photoprinting, microfilm, or any other means – nor transmitted or translated into a machine language without written permission from the publishers. Registered names, trademarks, etc. used in this book, even when not specifically marked as such, are not to be considered unprotected by law.

Cover Design Formgeber, Mannheim, Germany

Typesetting le-tex publishing services GmbH, Leipzig, Germany

Printing and Binding

Print ISBN 978-3-527-41349-2

ePDF ISBN 978-3-527-69046-6

ePub ISBN 978-3-527-69048-0

Mobi ISBN 978-3-527-69047-3

oBook ISBN 978-3-527-69049-7

Printed on acid-free paper.

This edition first published 2017
© 2017

All rights reserved. No part of this publication may be reproduced, stored in a retrieval system, or transmitted, in any form or by any means, electronic, mechanical, photocopying, recording or otherwise, except as permitted by law. Advice on how to obtain permission to reuse material from this title is available at <http://www.wiley.com/go/permissions>.

The right of Jane Brown and Mark Smith to be identified as the authors of this work has been asserted in accordance with law.

Registered Offices

John Wiley & Sons, Inc., 111 River Street, Hoboken, NJ 07030, USA

John Wiley & Sons Ltd, The Atrium, Southern Gate, Chichester, West Sussex, PO19 8SQ, UK

Editorial Office

The Atrium, Southern Gate, Chichester, West Sussex, PO19 8SQ, UK

For details of our global editorial offices, customer services, and more information about Wiley products visit us at www.wiley.com.

Wiley also publishes its books in a variety of electronic formats and by print-on-demand. Some content that appears in standard print versions of this book may not be available in other formats.

Limit of Liability/Disclaimer of Warranty

While the publisher and authors have used their best efforts in preparing this work, they make no representations or warranties with respect to the accuracy or completeness of the contents of this work and specifically disclaim all warranties, including without limitation any implied warranties of merchantability or fitness for a particular purpose. No warranty may be created or extended by sales representatives, written sales materials or promotional statements for this work. The fact that an organization, website, or product is referred to in this work as a citation and/or potential source of further information does not mean that the publisher and authors endorse the information or services the organization, website, or product may provide or recommendations it may make. This work is sold with the understanding that the publisher is not engaged in rendering professional services. The advice and strategies contained herein may not be suitable for your situation. You should consult with a specialist where appropriate. Further, readers should be aware that websites listed in this work may have changed or disappeared between when this work was written and when it is read. Neither the publisher nor authors shall be liable for any loss of profit or any other commercial damages, including but not limited to special, incidental, consequential, or other damages.

Library of Congress Cataloging-in-Publication Data

Cover image:

Cover design by

Set in 9.5/12.5pt STIXTwoText by SPi Global, Pondicherry, India

10 9 8 7 6 5 4 3 2 1

to Hans-Martin



Brief Contents

List of Contributors *xi*

Foreword *xiii*

Preface *xv*

Part I Metal Oxide Nanomaterials 1

- 1 The Biomimetic Synthesis of Metal Oxide Nanomaterials 3
- 2 Synthesis of Symmetric and Asymmetric Nanosilica for Materials, Optical and Medical Applications 55
- 3 Sources of Natural Flavors 90
- 4 Mechanism of Color Perception 110
- 5 Preparation of Plant Material for Extraction 150
- 6 Methods of Extraction of Essential Oils 180

Index 000



Contents

List of Contributors *xi*

Foreword *xiii*

Preface *xv*

Part I Metal Oxide Nanomaterials *1*

- 1 The Biomimetic Synthesis of Metal Oxide Nanomaterials** *3*
Leila F. Deravi, Joshua D. Swartz and David W. Wright
 - 1.1 Introduction *3*
 - 1.2 Metal Oxides in Nature *4*
 - 1.2.1 Components of Biomineralization *5*
 - 1.2.2 Biomineralization Optimization *6*
 - 1.3 Biomimetic Synthesis of Metal Oxide Nanomaterials *7*
 - 1.4 Constrained Biomineralization *8*
 - 1.4.1 Bacterial Synthesis of Metal Oxide Nanomaterials *8*
 - 1.4.2 Synthesis of Protein-Functionalized Ferromagnetic Co₃O₄ Nanocrystals *9*
 - 1.4.3 Room-Temperature Synthesis of Barium Titanate *10*
 - 1.4.4.1 Biomimetic Synthesis of Iron Oxide *11*
- 2 Synthesis of Symmetric and Asymmetric Nanosilica for Materials, Optical and Medical Applications** *55*
Yongquan Qu, Jennifer Lien and Ting Guo
 - 2.1 Introduction *55*
 - 2.2 Synthesis of Nanosilica *59*
 - 2.2.1 Symmetric Nanosilica *59*
 - 2.2.1.1 Catalytic Methods *63*
 - 2.2.1.2 Noncatalytic Growth *65*
 - 2.2.2 Asymmetric Silica Nanomaterials *68*
 - 2.2.2.1 Catalytic Growth *68*
 - 2.2.2.2 Noncatalytic Growth *69*
 - 2.3 Characterization *70*
 - 2.4 Applications of Symmetric and Asymmetric Nanosilica *72*

Index *000*



Contents

Foreword *xiii*

Preface *xv*

Part I Metal Oxide Nanomaterials *1*

- 1 The Biomimetic Synthesis of Metal Oxide Nanomaterials** *3*
 - 1.1 Introduction *3*
 - 1.2 Metal Oxides in Nature *4*
 - 1.2.1 Components of Biomineralization *5*
 - 1.2.2 Biomineralization Optimization *6*
 - 1.3 Biomimetic Synthesis of Metal Oxide Nanomaterials *7*
 - 1.4 Constrained Biomineralization *8*
 - 1.4.1 Bacterial Synthesis of Metal Oxide Nanomaterials *8*
 - 1.4.2 Synthesis of Protein-Functionalized Ferromagnetic Co_3O_4 Nanocrystals *9*
 - 1.4.3 Room-Temperature Synthesis of Barium Titanate *10*
 - 1.4.4 Biomimetic Synthesis of Magnetite *11*
 - 1.4.4.1 Biomimetic Synthesis of Iron Oxide *11*
- 2 Synthesis of Symmetric and Asymmetric Nanosilica for Materials, Optical and Medical Applications** *55*
 - 2.1 Introduction *55*
 - 2.2 Synthesis of Nanosilica *59*
 - 2.2.1 Symmetric Nanosilica *59*
 - 2.2.1.1 Catalytic Methods *63*
 - 2.2.1.2 Noncatalytic Growth *65*
 - 2.2.2 Asymmetric Silica Nanomaterials *68*
 - 2.2.2.1 Catalytic Growth *68*
 - 2.2.2.2 Noncatalytic Growth *69*
 - 2.3 Characterization *70*
 - 2.4 Applications of Symmetric and Asymmetric Nanosilica *72*

Index *000*



Contents

Foreword *xiii*

Preface *xv*

Part I Metal Oxide Nanomaterials 1

1 The Biomimetic Synthesis of Metal Oxide Nanomaterials 3

Introduction 3

Metal Oxides in Nature 4

 Components of Biomineralization 5

 Biomineralization Optimization 6

Biomimetic Synthesis of Metal Oxide Nanomaterials 7

Constrained Biomineralization 8

 Bacterial Synthesis of Metal Oxide Nanomaterials 8

 Synthesis of Protein-Functionalized Ferromagnetic Co_3O_4 Nanocrystals 9

 Room-Temperature Synthesis of Barium Titanate 10

 Biomimetic Synthesis of Magnetite 11

 Biomimetic Synthesis of Iron Oxide 11

2 Synthesis of Symmetric and Asymmetric Nanosilica for Materials, Optical and Medical Applications 55

Introduction 55

Synthesis of Nanosilica 59

 Symmetric Nanosilica 59

 Catalytic Methods 63

 Noncatalytic Growth 65

 Asymmetric Silica Nanomaterials 68

 Catalytic Growth 68

 Noncatalytic Growth 69

Characterization 70

Applications of Symmetric and Asymmetric Nanosilica 72

Index 000



List of Contributors

Andrew B. Adams

Department of Surgery
Emory Transplant Center
Emory University School of Medicine
Atlanta
USA

Maria-Luisa Alegre, MD, PhD

Associate Professor
Department of Medicine, Section of
Rheumatology
Gwen Knapp Center for Lupus and
Immunology Research
The University of Chicago
Chicago
USA

Agnes M. Azimzadeh, PhD

Assistant Professor of Surgery
Department of Surgery
University of Maryland School of
Medicine
Baltimore
USA

William M. Baldwin III

Department of Immunology
Cleveland Clinic Lerner College of
Medicine
Department of Pathology
Case Western Reserve University
School of Medicine
Cleveland
USA

Jonathan S. Bromberg, MD, PhD

Professor of Surgery and Microbiology
and Immunology
Department of Surgery
University of Maryland School of
Medicine
Baltimore
USA

J. Michael Cecka

UCLA Immunogenetics Center
Department of Pathology and
Laboratory Medicine
David Geffen School of Medicine at
UCLA
Los Angeles
USA

Anil Chandraker, MD, FASN, FRCP

Transplant Research Center
Renal Division
Brigham and Women's Hospital
Harvard Medical School
Boston
USA

Sung Choi, MD

Blood and Marrow Transplantation
Program
Department of Internal Medicine
Division of Hematology/Oncology
University of Michigan
Comprehensive Cancer Center
Ann Arbor
USA

Anita S. Chong, PhD

Department of Surgery, Section of
Transplantation
The University of Chicago
Chicago
USA

Yaozhong Ding, PhD

Assistant Professor
Department of Surgery
University of Maryland School of Medicine
Baltimore
USA

Gunilla Einecke

Department of Nephrology
Hannover Medical School
Hannover
Germany

Robert L. Fairchild

Department of Immunology
Cleveland Clinic Lerner College of
Medicine
Department of Pathology
Case Western Reserve University
School of Medicine
Cleveland
USA

Philip F. Halloran, MD, PhD

Alberta Transplant Applied Genomics
Centre
Department of Medicine
Division of Nephrology and Transplant
Immunology
University of Alberta
Edmonton
Canada

Choli Hartono

Department of Medicine
Weill Cornell Medical College
New York
USA

Timm Heinbokel

Division of Transplant Surgery and
Transplant Surgery Research Laboratory
Brigham and Women's Hospital
Harvard Medical School
Boston
USA

Yiming Huang

Institute for Cellular Therapeutics
University of Louisville
Louisville and Duke University
Raleigh
USA

Suzanne T. Ildstad, MD

Director, Institute for Cellular Therapeutics
Jewish Hospital Distinguished
Professor of Transplantation
Distinguished University Scholar
Professor of Surgery, Physiology,
Immunology
University of Louisville
Louisville and Duke University
Raleigh
USA

Haofeng Ji

Dumont-UCLA Transplantation Center
Division of Liver and Pancreas
Transplantation, Department of Surgery,
David Geffen School of Medicine at UCLA
Los Angeles
USA

Bibo Ke

Dumont-UCLA Transplantation
Center Division of Liver and Pancreas
Transplantation, Department of
Surgery
David Geffen School of Medicine at UCLA
Los Angeles
USA

Foreword

The dilemma of rapidly emerging fields is that reviews are often outdated before they are printed. To make a contribution that would endure, we knew we had to go beyond a snapshot of the current state of fragment-based drug discovery and instead provide a framework for upcoming advances. To achieve this goal, we needed to convince leading scientists to take time from their busy schedules to write chapters. Fortunately, nearly all those we approached agreed; and what you hold in your hands is a virtual, although not comprehensive, “Who’s Who” in fragment-based drug discovery. We are extremely grateful to all of our contributors for the quality of their chapters.

One striking feature of this book is that more than half of the chapters come from industry-based researchers; and even many of the academic contributors have close ties to industry. It has been alleged that the best science is done in academia; this book proves that this is not necessarily the case. Part of the reason may be that many of the techniques involved require expensive equipment and infrastructure as well as large collaborations between scientists from disparate disciplines – collaborations that would be difficult to set up outside industry. The multidisciplinary nature of fragment-based approaches shows in this volume: contributors include computational chemists, NMR spectroscopists, X-ray crystallographers, mass-spectrometrists, as well as organic and medicinal chemists.

Although fragment-based strategies for drug discovery have now pervaded laboratories across the world, the ultimate success of any drug discovery technology is measured in the quantity and quality of drugs that it produces. Fragment-based drug discovery has only been practical for the past decade, too soon to expect it to produce marketed drugs; but we believe these will come in time. Moreover, many of the techniques and concepts described in this book will alter drug discovery endeavors in subtle, tangential ways. Ideally, readers will be inspired to improve the methods described here, or even to develop fundamentally new methods for fragment-based drug discovery. But even if this book only changes the way medicinal chemists approach lead optimization, or persuades them to look more closely at weak but validated hits, it will have served its purpose.

Basely, March 2006

*Wolfgang Jahnke
Daniel A. Erlanson*



Symbols and Abbreviations

Symbols

α	electron spin quantum number $m_s = 1/2$ angle, alternating parameter anisotropic exchange parameter
α_n	nuclear spin quantum number $m_I = 1/2$
β	spin quantum number $m_s = -1/2$ angle
β_n	nuclear spin quantum number $m_I = -1/2$
δ_{ij}	Kronecker δ
θ	angle Curie-Weiss constant
Δ_H	line-width
$\Delta H_{1/2}$	half height line-width
ΔH_{pp}	peak-to-peak line-width
ΔH_{msl}	maximum-slope line-width
$\Delta H\omega_{1/2}, \Delta H\omega_{pp}$	line-width in frequency
ϵ_0	dielectric constant
ϵ_F	Fermi energy
η	$ J'/J $
Γ	molecular field coefficient
γ	gyromagnetic ratio exchange interaction parameter anisotropic exchange parameter
γ_n	nuclear gyromagnetic ratio
φ	molecular orbital relaxation function
Ψ	molecular orbital
ψ	atomic orbital
ν	frequency
μ	magnetic permeability
μ_0	magnetic permeability of free space



Color Plates

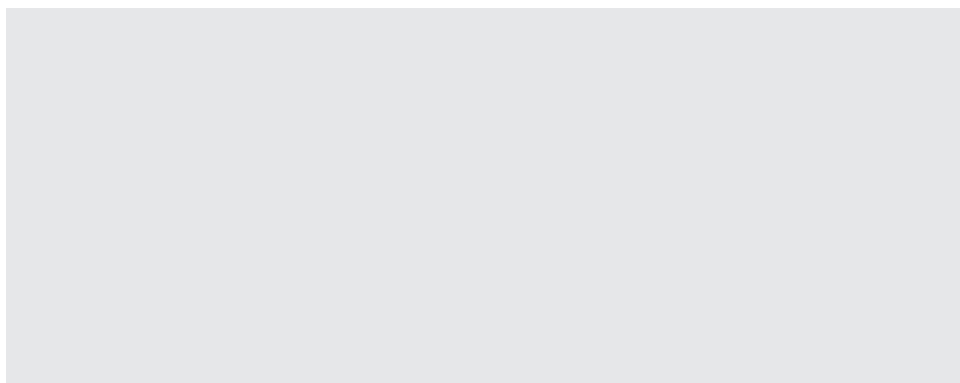


Figure 1.6 See text page 00 for full figure caption.

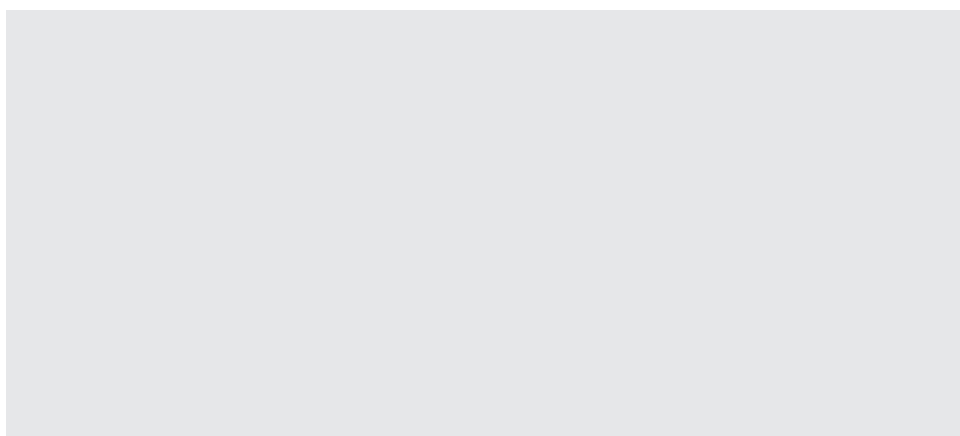


Figure 1.7 See text page 00 for full figure caption.



About the Companion Website

Practical Physiotherapy for Small Animal Practice is accompanied by a companion website:



www.wiley.com/go/

The website includes:

- Client education handouts.



Part IV

Summaries and Visions

Bold Glance into the Future—Where no Man has Gone Before



5

cDNA and Microarray-based Technologies

5.1 Introduction

The molecular characterization of tumor-associated antigens (TAA) recognized by T cells [1] revolutionized the field of tumor immune biology providing conclusive evidence that CD8+ cytotoxic T cells (CTLs) specifically recognize and kill autologous cancer through recognition of molecularly-defined cancer-specific elements.

5.1.1 CEA Gene Family, Genomic Localization, Protein Structure

CEA is encoded by the CEA-related cell-cell adhesion molecule 5 (CEACAM5) gene, which belongs to the CEA gene family and in humans consists of 22 expressed members and 12 pseudogenes [3,4].

5.1.1.1 Animal Models for CEA

Mice are commonly used to analyze the efficacy of tumor therapies and mechanisms of tumor rejection. However, this species cannot be utilized to evaluate CEA-based therapies since no CEACAM5 ortholog exists in rodents.

5.1.1.1.1 Models for CEACAM5 Containing a Bacterial Artificial Chromosome

Either cosmid clones containing the CEACAM5 gene or a bacterial artificial chromosome (BAC) clone, which comprises part of the gene cluster surrounding CEACAM5, served as a genetic source. This cluster includes CEACAM6 and CEACAM3.

Antibody Delivery of Radionuclides, Drugs and Effector Molecules The use of low molecular weight single chain antibody fragments and pre-targeting has been found to enhance the sensitivity of tumor visualization as well as increasing the delivered therapeutic dose by separating the antibody therapeutic radionuclide that binds to the tumor-localized antibody.

SubParagraph Title: Nuclear Angular Momentum and Magnetic Moment The conformational flexibility of calixarenes is usually explained by the presence of intramolecular hydrogen bonds, which is related to the number of free phenol groups. Accordingly, calixarenes containing four phenol groups 39a–e exist as cone conformers.

Book Title: Subtitle, First Edition. Edited by Author/Editor Name.

© 2015 John Wiley & Sons, Ltd. Published 2015 by John Wiley & Sons, Ltd.



5

cDNA and Microarray-based Technologies

Introduction

The molecular characterization of tumor-associated antigens (TAA) recognized by T cells [1] revolutionized the field of tumor immune biology providing conclusive evidence that CD8+ cytotoxic T cells (CTLs) specifically recognize and kill autologous cancer through recognition of molecularly-defined cancer-specific elements.

CEA Gene Family, Genomic Localization, Protein Structure

CEA is encoded by the CEA-related cell-cell adhesion molecule 5 (CEACAM5) gene, which belongs to the CEA gene family and in humans consists of 22 expressed members and 12 pseudogenes [3,4].

Animal Models for CEA

Mice are commonly used to analyze the efficacy of tumor therapies and mechanisms of tumor rejection. However, this species cannot be utilized to evaluate CEA-based therapies since no CEACAM5 ortholog exists in rodents. This problem was circumvented by introducing the human CEACAM5 gene into the germ line of mice [52–54].

Models for CEACAM5 Containing a Bacterial Artificial Chromosome

Either cosmid clones containing the CEACAM5 gene or a bacterial artificial chromosome (BAC) clone, which comprises part of the gene cluster surrounding CEACAM5, served as a genetic source. This cluster includes CEACAM6 and CEACAM3.

Antibody Delivery of Radionuclides, Drugs and Effector Molecules Delivery of radio-nuclides to tumors using murine and human anti-CEA antibodies has been studied for many years [70]. The use of low molecular weight single chain antibody fragments and pre-targeting has been found to enhance the sensitivity of tumor visualization as well as increasing the delivered therapeutic dose by separating the antibody targeting to the tumor from the subsequent delivery of the therapeutic radionuclide that binds to the tumor-localized antibody.

SubParagraph Title: Nuclear Angular Momentum and Magnetic Moment The conformational flexibility of calixarenes is usually explained by the presence of intramolecular hydrogen bonds, which is related to the number of free phenol groups. Accordingly, calixarenes, containing four phenol groups 39a–e exist as cone conformers.

Delivery of radio-nuclides to tumors using murine and human anti-CEA antibodies has been studied for many years [70]. The use of low molecular weight single chain antibody fragments and pre-targeting has been found to enhance the sensitivity of tumor visualization as well as increasing the delivered therapeutic dose by separating the antibody targeting to the tumor from the subsequent delivery of the therapeutic radionuclide that binds to the tumor-localized antibody.

11

Carcinoembryonic Antigen

Decoding the CEA-Related Cell-Cell Adhesion Molecule

The molecular characterization of tumor-associated antigens (TAA) recognized by T cells [1] revolutionized the field of tumor immune biology providing conclusive evidence that CD8+ cytotoxic T cells (CTLs) specifically recognize and kill autologous cancer through recognition of molecularly-defined cancer-specific elements. Since then a myriad of TAA have been identified that has triggered their utilization as anti-cancer vaccines [2–8].

11.1 CEA Biology

11.1.1 CEA Gene Family, Genomic Localization, Protein Structure

CEA is encoded by the CEA-related cell-cell adhesion molecule 5 (CEACAM5) gene, which belongs to the CEA gene family and in humans consists of 22 expressed members and 12 pseudogenes [3,4]. The CEA family has been subdivided into the CEACAM and pregnancy-specific glycoprotein (PSG) subgroups.

11.1.2 CEA as a Tumor Marker for Prognosis and Post-surgery Follow-up

11.1.2.1 Animal Models for CEA

Antibody Delivery of Radionuclides, Drugs and Effector Molecules Using Murine and Human Anti-CEA Antibodies Delivery of radio-nuclides to tumors using murine and human anti-CEA anti-bodies has been studied for many years [70]. The use of low molecular weight single chain antibody fragments and pre-targeting has been found to enhance the sensitivity of tumor visualization as well as increasing the delivered therapeutic dose by separating the antibody targeting to the tumor from the subsequent delivery of the therapeutic radionuclide that binds to the tumor-localized antibody. The use of low molecular weight single chain antibody fragments and pre-targeting has been found to enhance the sensitivity of tumor visualization as well as increasing.

The use of low molecular weight single chain antibody fragments and pre-targeting has been found to enhance the sensitivity of tumor visualization as well as increasing the delivered therapeutic dose by separating the antibody targeting to the tumor from the subsequent delivery of the therapeutic radionuclide that binds to the tumor-localized antibody.



2

Trust and Reputation for Service-Oriented Environments Technologies for Building Business Intelligence and Consumer Confidence

Fillers, Filled Polymers and Polymer Blends and Furthermore Nuclear
Angular Momentum and Magnetism

2.1 Intermolecular Interactions Physical Picture, Computational Methods and Model Potentials Nuclear Angular Momentum and Magnetic Moment

The molecular characterization of tumor-associated antigens (TAA) recognized by T cells [1] revolutionized the field of tumor immune biology providing conclusive evidence that CD8+ cytotoxic T cells (CTLs) specifically recognize and kill autologous cancer through recognition of molecularly-defined cancer-specific elements. Since then a myriad of TAA have been identified that has triggered their utilization as anti-cancer vaccines [2–8].

2.1.1 Networking and Online Games Understanding and Engineering Multiplayer Internet Games Nuclear Angular Momentum and Magnetic Moment

CEA is encoded by the CEA-related cell-cell adhesion molecule 5 (CEACAM5) gene, which belongs to the CEA gene family and in humans consists of 22 expressed members and 12 pseudogenes [3,4]. The CEA family has been subdivided into the CEACAM and pregnancy-specific glycoprotein (PSG) subgroups.

2.1.1.1 Nuclear Angular Momentum and Magnetic Moment Respectively the Digital Photographer's Guide to Color Management

Apically expressed CEA on normal epithelial cells is shed into the lumen possibly by the action of phospholipases and through the exfoliation of turned-over cells. Thus CEA does not have access the bloodstream. Expression on less differentiated unpolarized tumor cells, however, allows released CEA to enter blood and lymphatic vessels through the intercellular spaces, which can lead to elevated CEA concentrations in the sera of tumor patients.

Fillers, Filled Polymers and Polymer Blends and Furthermore Nuclear Angular Momentum and Magnetism CEA is encoded by the CEA-related cell-cell adhesion molecule 5 (CEACAM5) gene, which belongs to the CEA gene family and in humans consists of 22 expressed members and 12 pseudogenes [3,4]. In the past, the CEA family has been subdivided into the CEACAM and pregnancy-specific glycoprotein (PSG) subgroups.

Book Title: Subtitle, First Edition. Edited by Author/Editor Name.

© 2015 John Wiley & Sons, Ltd. Published 2015 by John Wiley & Sons, Ltd.

11

Carcinoembryonic Antigen

Decoding the CEA-Related Cell-Cell Adhesion Molecule

The molecular characterization of tumor-associated antigens (TAA) recognized by T cells [1] revolutionized the field of tumor immune biology providing conclusive evidence that CD8⁺ cytotoxic T cells (CTLs) specifically recognize and kill autologous cancer through recognition of molecularly-defined cancer-specific elements. Since then a myriad of TAA have been identified that has triggered their utilization as anti-cancer vaccines [2–8].

11.1 CEA Biology

11.1.1 CEA Gene Family, Genomic Localization, Protein Structure

CEA is encoded by the CEA-related cell-cell adhesion molecule 5 (CEACAM5) gene, which belongs to the CEA gene family and in humans consists of 22 expressed members and 12 pseudogenes [3,4]. The CEA family has been subdivided into the CEACAM and pregnancy-specific glycoprotein (PSG) subgroups.

11.1.2 CEA as a Tumor Marker for Prognosis and Post-surgery Follow-up

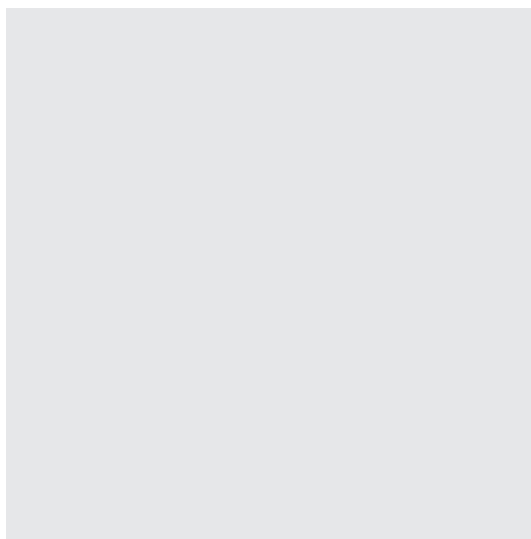
11.1.2.1 Animal Models for CEA

Antibody Delivery of Radionuclides, Drugs and Effector Molecules Using Murine and Human Anti-CEA Antibodies Delivery of radio-nuclides to tumors using murine and human anti-CEA anti-bodies has been studied for many years [70]. The use of low molecular weight single chain antibody fragments and pre-targeting has been found to enhance the sensitivity of tumor visualization as well as increasing the delivered therapeutic dose by separating the antibody targeting to the tumor from the subsequent delivery of the therapeutic radionuclide that binds to the tumor-localized antibody. The use of low molecular weight single chain antibody fragments and pre-targeting has been found to enhance the sensitivity of tumor visualization as well as increasing the delivered therapeutic dose by separating the antibody targeting to the tumor from the subsequent delivery of the therapeutic radionuclide that binds to the tumor-localized antibody.

11

Carcinoembryonic Antigen

Decoding the CEA-Related Cell-Cell Adhesion Molecule



The molecular characterization of tumor-associated antigens (TAA) recognized by T cells [1] revolutionized the field of tumor immune biology providing conclusive evidence that CD8+ cytotoxic T cells (CTLs) specifically recognize and kill autologous cancer through recognition of molecularly-defined cancer-specific elements. Since then a myriad of TAA have been identified that has triggered their utilization as anti-cancer vaccines [2–8].

11.1 CEA Biology

11.1.1 CEA Gene Family, Genomic Localization, Protein Structure

CEA is encoded by the CEA-related cell-cell adhesion molecule 5 (CEACAM5) gene, which belongs to the CEA gene family and in humans consists of 22 expressed members and 12 pseudogenes [3,4]. The CEA family has been subdivided into the CEACAM and pregnancy-specific glycoprotein (PSG) subgroups.

11.1.2 CEA as a Tumor Marker for Prognosis and Post-surgery Follow-up

11.1.2.1 Animal Models for CEA

Antibody Delivery of Radionuclides, Drugs and Effector Molecules Using Murine and Human Anti-CEA Antibodies Delivery of radio-nuclides to tumors using murine and human anti-CEA anti-bodies has been studied for many years [70]. The use of low molecular weight single chain antibody fragments and pre-targeting has been found to enhance the sensitivity of tumor visualization as well as increasing the delivered therapeutic dose by separating the antibody targeting to the tumor from the subsequent delivery of the therapeutic radionuclide that binds to the tumor-localized antibody. The use of low molecular weight single chain antibody fragments and pre-targeting has been found to enhance the sensitivity of tumor visualization as well as increasing. The use of low molecular weight single chain antibody fragments and pre-targeting has been found to enhance the sensitivity of tumor visualization as well as increasing the delivered therapeutic dose by separating the antibody targeting to the tumor from the subsequent delivery of the therapeutic radionuclide that binds to the tumor-localized antibody.

11

Carcinoembryonic Antigen

Wolfgang Zimmermann^{1,3} and Robert Kammerer²

¹ Helmholtz Centre for Infection Research, Department of Systems Immunology, Inhoffenstr. 7, 38124, Braunschweig, Germany

² Bio Center for Life Science, University of Technology Braunschweig, Spielmannstr. 7, 38106, Braunschweig, Germany

³ Institute for Molecular and Clinical Immunology, Otto-von-Guericke University, Leipziger Str. 44, 39120, Magdeburg, Germany

The very essence of cardiovascular practice is the early detection of heart failure

Sir Thomas Lewis, 1933

11.1 Introduction

The molecular characterization of tumor-associated antigens (TAA) recognized by T cells [1] revolutionized the field of tumor immune biology providing conclusive evidence that CD8+ cytotoxic T cells (CTLs) specifically recognize and kill autologous cancer through recognition of molecularly-defined cancer-specific elements.

11.2 CEA Biology

11.2.1 CEA Gene Family, Genomic Localization, Protein Structure

CEA is encoded by the CEA-related cell-cell adhesion molecule 5 (CEACAM5) gene, which belongs to the CEA gene family and in humans consists of 22 expressed members and 12 pseudogenes [3,4]. The CEA family has been subdivided into the CEACAM and pregnancy-specific glycoprotein (PSG) subgroups. Apically expressed CEA on normal epithelial cells is shed into the lumen possibly by the action of phospholipases and through the exfoliation of turned-over cells. Thus CEA does not have access the bloodstream. Expression on less differentiated unpolarized tumor cells, however, allows released CEA to enter blood and lymphatic vessels through the intercellular spaces, which can lead to elevated CEA concentrations in the sera of tumor patients.

Book Title: Subtitle, First Edition. Edited by Author/Editor Name.

© 2015 John Wiley & Sons, Ltd. Published 2015 by John Wiley & Sons, Ltd.

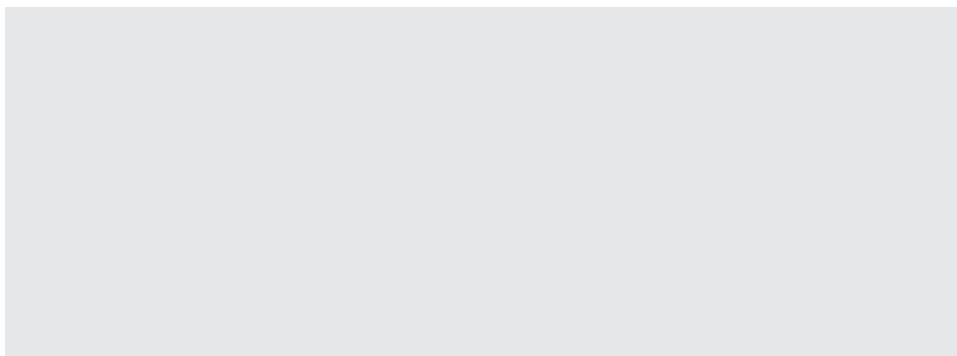


Figure 1.6 Illustration of catalytically grown β -Ga₂O₃ nanoparticles. *Source:* Reprinted with permission from Ref. [38]; © 2007 American Chemical Society.

Traditionally, synthetic approaches for the production of functional metal oxide materials have involved are estimated to reach an outstanding US \$100 billion per Figure 1.6 facility by the year 2020, as the demand for smaller, lighter and faster materials continues to grow [1]. But, more importantly, manufacturers are progressing in this manner at the expense of the environment, as they accumulate hazardous chemical wastes [2]. For decades, research teams in the semiconductor industry have been seeking alternative methods to passivate not only the rate of waste production but also the cost of spending. As mentioned above, the photoresist should be thin according to the distance of localization of the optical near-field around the nanoaperture. On the other hand, the photoresist should have the dry etching resistance so that the latent image can be transferred to the lower layer substrate. To separate the function of the Figure 1.7 thin film and the dry etching resistance, we used a trilayer resist process; the upper layer is an ultrathin photoresist, the middle layer is thin spin on glass (SOG), and the lower layer is a resin.

As mentioned above, the photoresist should be thin according to the distance of localization of the optical near-field around the nanoaperture. On the other hand, the photoresist should have the dry etching resistance so that the latent image can be transferred to the

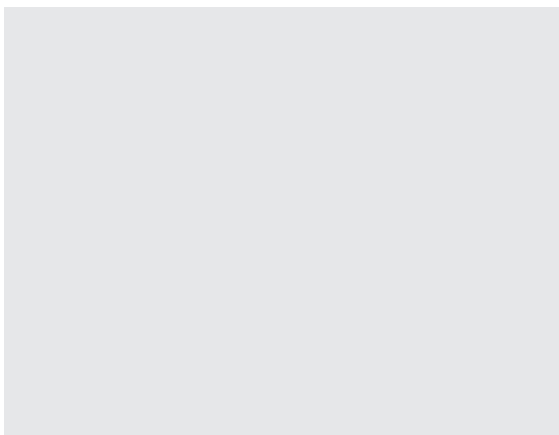


Figure 1.7 Transmission electron microscopy images (scale bar = 20 nm) of magnetosomes from various bacterial strains. (a) Pseudo-hexagonal prism; (b) Cubo-octahedral crystal; (c) \hat{A} Tooth-shaped. Transmission electron microscopy images (scale bar = 20 nm) of magnetosomes from various bacterial strains. *Source:* Reproduced with permission from Ref. [17]; © 2007, Wiley-VCH Verlag GmbH & Co. KGaA.

lower layer substrate. To separate the function of the thin film and the dry etching resistance, we used a trilayer resist process; the upper layer is an ultrathin photoresist, the middle layer is thin spin on glass (SOG), and the lower layer is a resin. The patterns of shallow latent images in the upper layer are transferred to the thin SOG layer of excellent dry-etching resistance, and these are transferred in the lower layer further.

Traditionally, synthetic approaches for the production of functional metal oxide materials have involved high-temperature reaction environments with energy intensive techniques such as laser ablation, ion implantation, chemical vapor deposition (CVD), photolithography or thermal decomposition [1]. The incorporation of these techniques has provided a rapid prototyping technique, essential for the commercial development of current minimum feature-sized semiconducting integrated circuits. However, the production of these devices has been achieved at a high price, with the primary challenges currently faced by high-throughput fabrication laboratories including the high cost of laborers and instruments, high temperature reaction conditions, and a surplus in generated waste [1]. In fact, the cost of fabrication facilities are estimated to reach an outstanding US \$100 billion per facility by the year 2020, as the demand for smaller, lighter and faster materials continues to grow [1]. But, more importantly, manufacturers are progressing in this manner at the expense of the environment, as they accumulate hazardous chemical wastes [2]. For decades, research teams in the semiconductor industry have been seeking alternative methods to passivate not only the rate of waste production but also the cost of spending.

As mentioned above, the photoresist should be thin according to the distance of localization of the optical near-field around the nanoaperture. On the other hand, the photoresist should have the dry etching resistance so that the latent image can be transferred to the lower layer substrate. To separate the function of the thin film and the dry etching resistance, we used a trilayer resist process; the upper layer is an ultrathin photoresist, the middle layer is thin spin on glass (SOG), and the lower layer is a resin. The patterns of shallow latent images in the upper layer are transferred to the thin SOG layer of excellent dry-etching resistance, and these are transferred in the lower layer further.

Figure 1.8 shows the appearance of a prototype device of optical near-field lithography [7]. The features of the prototype device are as follows. This device is compact, with a footprint of about 2m [1]. It has symmetric structure to compensate thermal expansion and temperature drift, and the hanging controlling structure is introduced to avoid floor vibrations. In addition, it has a double clean structure, and the near-field photomask and the wafer are kept in a local clean environment by controlling a flow of clean air of the device inside.

Bioinspired research is based on identifying and emulating the principles of biomineralization in natural systems, instead of copying them directly. In fact, most strategies incorporated by natural systems are not directly applicable to engineered materials, so the need for alternative synthetic routes are required for the incorporation of non-natural elements, such as barium, nickel, copper or aluminum, with functional nanoscale properties [1,8]. From a materials perspective, highly intact biological structures such as diatoms, bacteria, proteins or butterfly wings provide an excellent source of inspiration for their synthesis. In this chapter we have included the details of a wide variety of mediated nanomaterial syntheses, their response to variable parameters, and their ability to retain a functionalized, controlled stability over time.

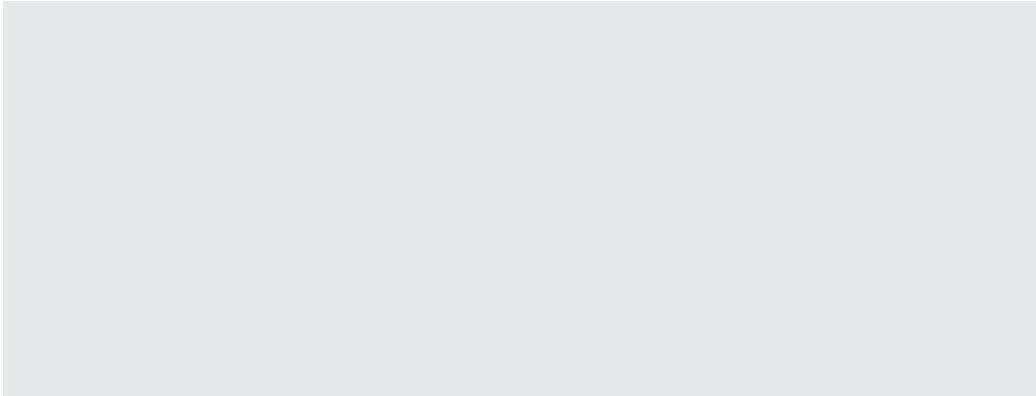


Figure 1.8 Appearance of a prototype device of optical near-field lithography.

As mentioned above, the photoresist should be thin according to the distance of localization of the optical near-field around the nanoaperture. On the other hand, the photoresist should have the dry etching resistance so that the latent image can be transferred to the lower layer substrate. To separate the function of the thin film and the dry etching resistance, we used a trilayer resist process; the upper layer is an ultrathin photoresist, the middle layer is thin spin on glass (SOG), and the lower layer is a resin. The patterns of shallow latent images in the upper layer are transferred to the thin SOG layer of excellent dry-etching resistance, and these are transferred in the lower layer further.

Figure 1.8 shows the appearance of a prototype device of optical near-field lithography [7]. The features of the prototype device are as follows. This device is compact, with a footprint of about 2m [2]. It has symmetric structure to compensate thermal expansion and temperature

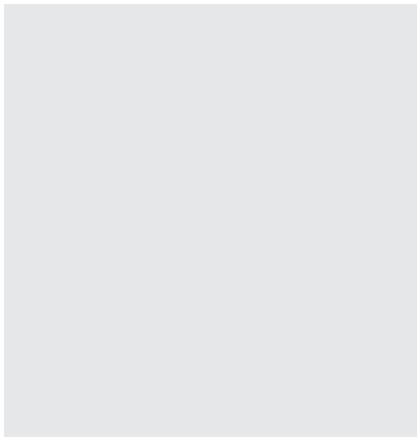


Figure 1.9 Distribution of structures for variable pH samples. *Source:* Reprinted with permission from Ref. [33]; © 2007, American Chemical Society.

Figure 1.10 (a) Inside the prototype device of the near-field lithography. (b) Illumination of i-line light for exposure from the back side of the near-field photomask. (c) Close-up from the side of the near-field photomask and the photoresist on the wafer. They are brought into contact with each other within the localizing distance of the optical near-field.

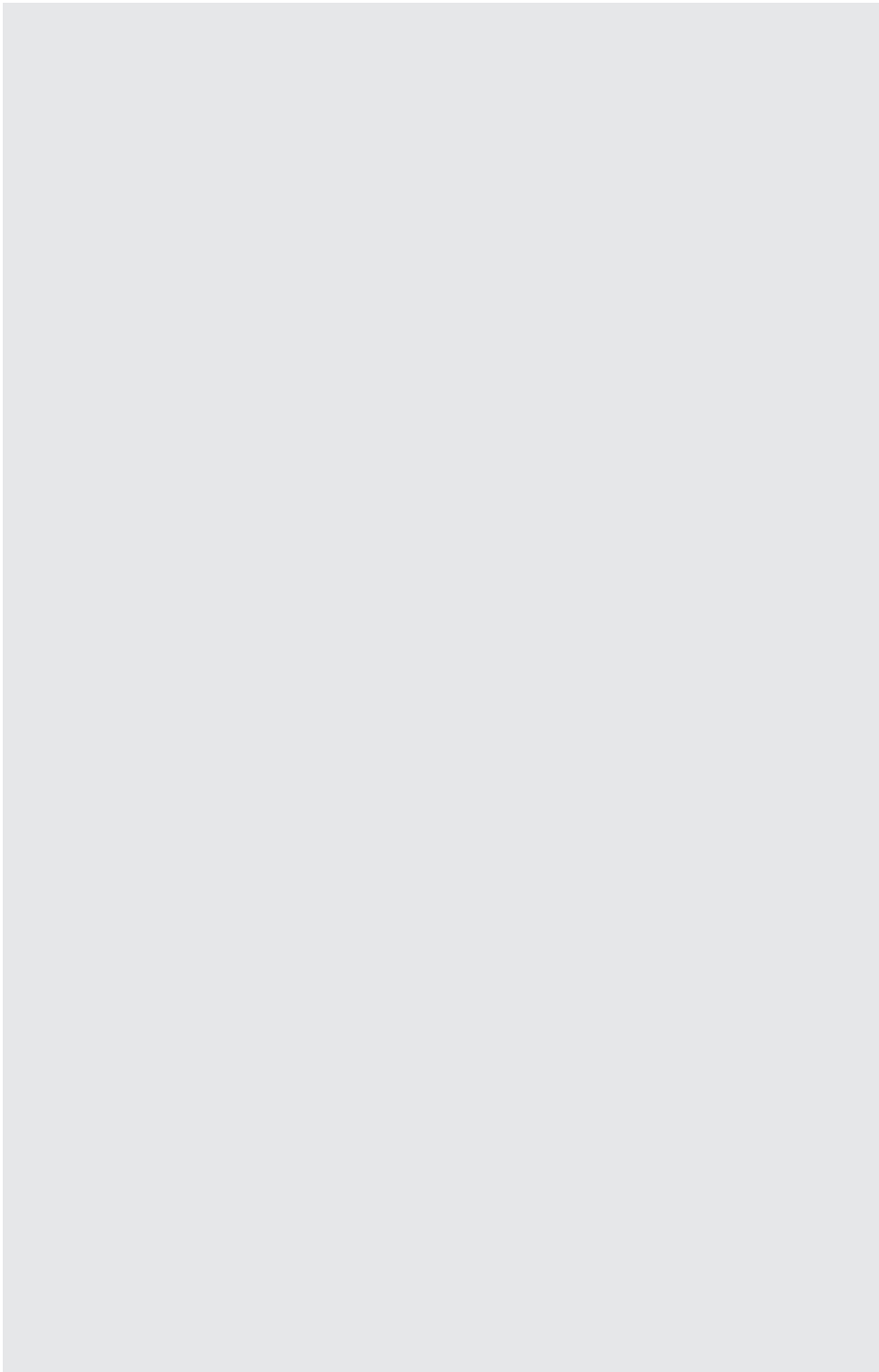


Table 1.1 Results for the comparison of processes.

Performance metric	NH ₃	CH ₄	C ₃ H ₈ ref.	C ₃ H ₈ POX
Energy efficiency	27%	30%	23%	16%
Volumetric fuel energy density (Wh l ⁻¹)	1570	170	1740	1920
Gravimetric fuel energy density (Wh kg ⁻¹)	2580	1610	2540	3900
Volumetric system energy density (Wh l ⁻¹)	1510	130	1650	1800
Gravimetric system energy density (Wh kg ⁻¹)	2370	320	2320	3340

drift, and the hanging controlling structure is introduced to avoid floor vibrations. In addition, it has a double clean structure, and the near-field photomask and the wafer are kept in a local clean environment by controlling a flow of clean air of the device inside.

Bioinspired research is based on identifying and emulating the principles of biomineralization in natural systems, Figure 1.9 instead of copying them directly. In fact, most strategies incorporated by natural systems are not directly applicable to engineered materials, so the need for alternative synthetic routes are required for the incorporation of non-natural elements, such as barium, nickel, copper or aluminum, with functional nanoscale properties [1,8]. Table 1.1 from a materials perspective, highly intact biological structures such as diatoms, bacteria, proteins or butterfly wings provide an excellent source of inspiration for their synthesis. In this chapter we have included the details of a wide variety of mediated nanomaterial syntheses, their response to variable parameters, and their ability to retain a functionalized, controlled stability over time.

The lowest system energy densities. Both the system and fuel volumetric energy densities of methane direct oxidation are very low, due to the large volume required for the storage of the gases (methane and oxygen). Moreover, the gravimetric fuel energy density of methane is

Table 1.2 Propagation rate constants (k_p) and the selectivity parameters ($\beta = k_p/k_{tr1}$) for the polymerization of ϵ -caprolactone [95].^{a)}

Active species	$\frac{k_p}{L \text{ mol}^{-1} \text{ s}^{-1}}$	$b = \frac{k_p}{k_{tr1}} \frac{L \text{ mol}^{-1}}{L \text{ mol}^{-1}}$
...-(CH ₂) ₅ O ⁻ Na ⁺	□1.70	1.6×10^3
...-(CH ₂) ₅ O-Sm[O(CH ₂) ₅ -...] ₂	2.00	2.0×10^3
...-(CH ₂) ₅ O-Al(C ₂ H ₅) ₂	0.03	4.6×10^4
...-(CH ₂) ₅ O-Al[CH ₂ CH(CH ₃) ₂] ₂	0.03	7.7×10^4
...-(CH ₂) ₅ O-Al[O(CH ₂) ₅ -...] ₂	0.50	3.0×10^5
...-(CH ₂) ₅ O-AlO ₂ SB ^{b)}	0.35	□10 ⁶

a) Polymerization conditions: 20°C, THF solvent.

b) Polymerization conditions: 80°C, THF solvent, SBO2: (S)-(+)-2,2'-[1,1'-binaphthyl-2,2'-diylbis-(nitrylomethylidyne)]-diphenolate ligand (A. Duda and A. Kowalski, unpublished results). SB=Schiff's base.

Table 1.3 Results for the comparison of processes.

Performance metric	NH ₃	CH ₄	C ₃ H ₈ ref.	C ₃ H ₃ POX
Energy efficiency	27%	30%	23%	16%
Volumetric fuel energy density (Wh l ⁻¹)	1570	170	1740	1920
Gravimetric fuel energy density (Wh kg ⁻¹)	2580	1610	2540	3900
Volumetric system energy density (Wh l ⁻¹)	1510	130	1650	1800
Gravimetric system energy density (Wh kg ⁻¹)	2370	320	2320	3340

Data from Higinbotham et al. 1967. The membrane potential was measured as – 110 mV Table from Taiz & Zeiger Thrid Ed Table 6.1

Table 1.4 Results for the comparison of processes.

R of functional molecule ^a	Cycle	Catalyst ^b	Conversion (%)	M _n (kg mol ⁻¹)	M _w /M _n	Reference
CH ₃ , CH=CH ₂ , (CH ₂) ₃ COOH	D ₄	SR	~90	10–43	—	[87]
CH=CH ₂ , (CH ₂) ₃ NHSi(CH ₃) ₃ , (CH ₂) ₃ -acrylate, (CH ₂) ₃ COOH	D ₄	SR	80–90	0.8–1.2	1.4–1.9	[57]
H	D ₄	AC	80	8	1.9	[88]
H, CH ₃ , CH=CH ₂ , (CH ₂) ₃ COOH	D ₄	SR	—	—	—	[89]

a) The chain-terminating agent has the following structure: R–Si(CH₃)₂–O–Si(CH₃)₂–R, unless stated in the table.

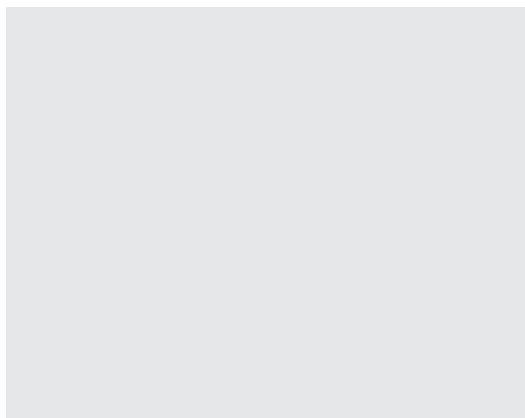
b) SR: sulfonic resin; AC: activated clay.

low, due to the mass of oxygen which is accounted for [2]. The large difference in gravimetric energy density of methane direct oxidation is due to the mass of the gas Table 1.2 cartridges. Despite lower energy conversion efficiency, the propane-based processes lead to higher energy densities than the ammonia-based process, because of the intrinsic difference in energy density between the two fuels. From a materials perspective, highly intact biological structures such as diatoms, bacteria. In this chapter we have included the details of a wide variety of mediated nanomaterial syntheses, their response to variable parameters, and their ability to retain a functionalized, controlled stability over time. With the exception of the

Table 1.5 Results for the comparison of processes.

Characteristic	Issues	Needs
Laminar flows	Mixing relies on molecular diffusion only and is slow	Efficient micromixers of low pressure drop
Small size	Difficult to load enough catalyst and ensure complete conversion	Develop deposition schemes and structures to load enough catalyst; high integration of reactor(s) and separation units for compact systems; fast chemistry/process; very active (and selective) catalyst.
Reactors shake in portable devices	Moveable parts break; bypass from pellet settling can occur	Monolithic structures with no moveable parts
High pressure drop	Pressure drop increases with decreasing pellet size	Open (extruded monolith-like) geometries
Transient operation very common	Most designs rely on steady state operation and control; catalysts, which are stable under steady state conditions, may deactivate during start up and shut down; start-up can be slow.	Get heat in and out of the system quickly; develop appropriate designs and strategies; models for dynamics.

Figure 1.11 Distribution of structures for variable pH samples. *Source:* Reprinted with permission from Ref. [33]; © 2007, American Chemical Society.



process requiring gas storage, the fuel energy density and system energy density give the same qualitative comparison among processes.

Thus, replicates on the same array and replicates in different experiments should not be mixed since they have different characteristics and cannot be treated as independent replicates. Important issues are:

- are the distributional assumptions valid is the number of replicates sufficient to detect the fold change that you are interested in?
- are the replicates independent of each other?
 - is the number of replicates sufficient to detect the fold change because it does not conversion efficiency that you are interested in?
 - are outliers removed from the samples?

Most commonly, modifications of four different tests are applied in microarray data analysis. These tests are implemented in statistical software packages such as R/Bioconductor or SAS:

- 1) Student's t-test is the number of replicates sufficient to detect the fold change that you are interested
- 2) Welch's test is the number of replicates sufficient to detect the fold because it does not conversion efficiency change that you are interested
- 3) Permutation tests.

While the first two tests assume Gaussian distributed data and the P -values are calculated by a probability distribution, the latter two are nonparametric and the P -values are calculated based on combinatorial arguments.

- | | |
|-----------------------------------|--------------------|
| • Distilled water | 23.3 μl |
| • 10 \times PCR buffer | 4.0 μl |
| • dNTP Mix (FDD) | 0.3 μl |
| • H-AP primer (2 μM)* | 4.0 μl |
| • H-T11M (2 μM) | 4.0 μl |
| • cDNA template | 4.0 μl |
| • Taq DNA polymerase | 0.4 μl |
| • Total volume | 40.0 μl |

Table 1.6 Species of marine invertebrates containing glycolipids.

Phylum	Subphylum	Class	Trivial name	Species
Chordata	Tunicata	Ascidacea	Tunicate	<i>Microcosmus sulcatus</i> (now accepted <i>M. vulgaris</i> ⁽¹⁾) <i>Phallusia fumigata</i>
Cnidaria	—	Anthozoa	Soft coral	1) <i>Lobophytum crassum</i> 2) <i>Lobophytum</i> sp. 3) <i>Sarcophyton ehrenbergi</i> 4) <i>Metridium senile</i>
Echinodermata	Asterozoa	Asteroidea	Sea anemone Starfish	• <i>Acanthaster planci</i> • <i>Allostichaster inaequalis</i> • <i>Anasterias minuta</i> • <i>Aphelasterias japonica</i> • <i>Asterias amurensis</i> • <i>Asterias amurensis versicolor</i> • <i>Asterias rubens</i> • <i>Stellaster equestris</i>
		Ophiuroidea	Brittle star	<i>Ophiocoma scolopendrina</i>
	Crinozoa	Crinoidea	Feather star	<i>Comanthus japonica</i> (now accepted <i>Oxycomanthus japonicus</i> ⁽¹⁾) <i>Comanthina schlegeli</i> (now accepted <i>Comaster schlegelii</i>)

Source: Queen Square Brain Bank.

Both the system and fuel volumetric energy densities of methane direct oxidation are very low, due to the large volume required for the storage of the gases (methane and oxygen). Moreover, the gravimetric fuel energy density of methane is low, due to the mass of oxygen which is accounted for [2]. The large difference in gravimetric energy density of methane direct oxidation is due to the mass of the gas cartridges.

Yields, and reaction specificities. The first detailed study of the mechanism of these “on water” reactions has now been reported by Jung and Marcus [10]. Synthetic aqueous organic synthesis was born, also because efficient work-up procedures are possible for these “on water” reactions. For a general review, the reader is referred to Chapter 7.

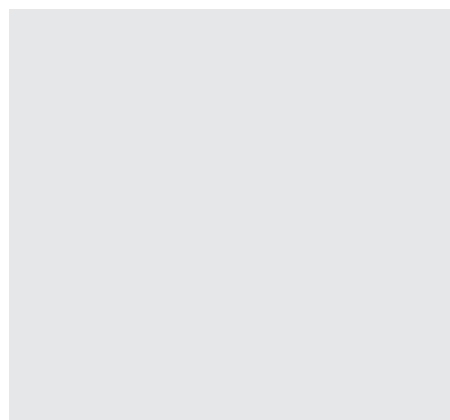


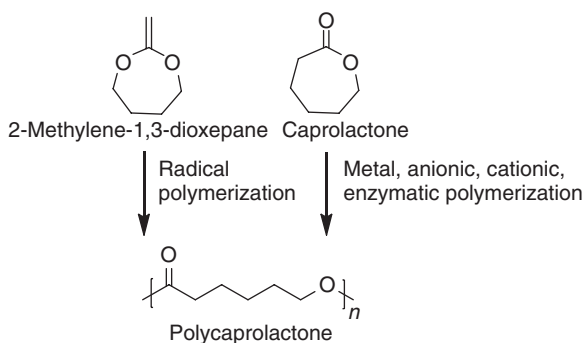
Figure 1.12 Distribution of structures for variable pH samples. *Source:* Reprinted with permission from Ref. [33]; © 2007, American Chemical Society.

11.3 Water, the Ultimate Green Solvent

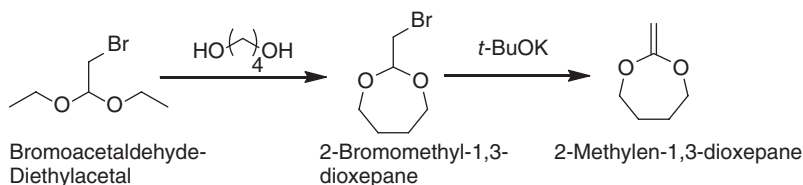
Fredrik Nilsson

In the second half of the 1990s, it was recognized that “benign by design” was too strongly restricted to environmental care, and Anastas and Williamson [13] even concluded, “one obvious but important point: nothing is benign.” The holistic concept of green chemistry became accepted world-wide. Although attempts have been made to quantify the degree of greenness, particularly by Sheldon [15], it has not been found possible to include the many complex factors that determine “greenness” in generally applicable parameters.

Aspirin as a Household Remedy Against Fever, Inflammation, and Pain Soon after the introduction of ASA into medical use under the brandname “aspirin,” Anastas in his many influential publications.



Scheme 1.31



Scheme 1.32

... As soon as you feel yourself ill, you should go to bed and have a hot-water bottle at your feet. You should drink hot chamomilae tea or grog in order to sweat and should take 3 tablets of aspirin a day. If you follow these instructions you will recover with in a few days, in most cases...

Kölner Stadtanzeiger, March 6, 1924

This extract is remarkable for several reasons: during the past 25 years of practical use, aspirin had become a drug whose name was not only well known to health professionals but also to the general public.

Certainly, the flu pandemia with millions of victims alone in Europe at the beginning of the last century as well as the limited availability of antipyretic analgesics other than aspirin contributed to this. However, the compound was generally recommended—and accepted—by the lay man and doctors—as a household remedy for treating pain, fever, inflammation, and many other kinds of feeling bad, although essentially nothing was known about the mechanisms of Anastas in his many influential publications. The holistic concept of green chemistry became accepted world-wide. Although attempts have been made to quantify the degree of greenness, particularly by action behind these multiple activities of the drug.

Thus, replicates on the same array and replicates in different experiments should not be mixed since they have different characteristics and cannot be treated as independent replicates. Important issues are:

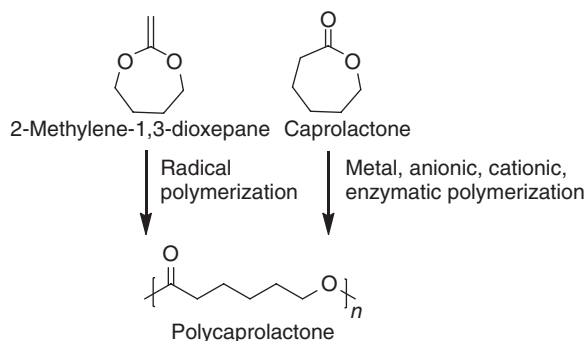
Most commonly, modifications of four different tests are applied in microarray data analysis. These tests are implemented in statistical software packages such as R/Bioconductor or SAS.

The conformational flexibility of calixarenes is usually explained by the presence of intramolecular hydrogen bonds, which is related to the number of free phenol groups. Accordingly, calixarenes containing four phenol groups 39a–e exist as cone conformers.

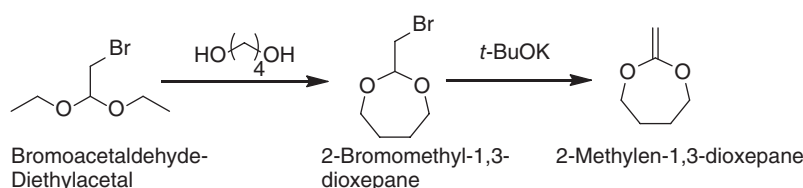
$$\rho(z)v_w = \rho_w^{\text{bulk}} v_w \exp(-v_w \beta [\pi(z) - \pi^{\text{bulk}}]) \quad (2.17)$$

$$\rho(z)v_w = \rho_w^{\text{bulk}} v_w \exp(-v_w \beta [\pi(z) - \pi^{\text{bulk}}]) - q_i \beta [\psi(z) - \psi^{\text{bulk}}] \quad (2.18)$$

Both the system and fuel volumetric energy densities of methane direct oxidation are very low, due to the large volume required for the storage of the gases (methane and oxygen). Moreover, the gravimetric fuel energy density of methane is low, due to the mass of oxygen which is accounted for [2]. The comparison of the two idealized possibilities for propane fuel processing reactions shows that energy conversion efficiency is not a suitable metric for man-portable applications, because it does not account for the water weight and volume;



Scheme 1.31



Scheme 1.32

the higher energy efficiency of steam reforming is due to the generation of additional hydrogen in the reactor.

The lowest system energy densities. Both the system and fuel volumetric energy densities of methane direct oxidation are very low, due to the large volume required for the storage of the gases (methane and oxygen). Moreover, the gravimetric fuel energy density of methane is low, due to the mass of oxygen which is accounted for [2]. The large difference in gravimetric energy density of methane direct oxidation is due to the mass of the gas Table 1.2 cartridges. Despite lower energy conversion efficiency, the propane-based processes lead to higher energy densities than the ammonia-based process, because of the intrinsic difference in energy density between the two fuels. From a materials perspective, highly intact biological structures such as diatoms, bacteria. In this chapter we have included the details of a wide variety of mediated nanomaterial syntheses, their response to variable parameters, and their ability to retain a functionalized, controlled stability over time. With the exception of the process requiring gas storage, the fuel energy density and system energy density give the same qualitative comparison among processes.

The conformational flexibility of calixarenes is usually explained by the presence of intramolecular hydrogen bonds, which is related to the number of free phenol groups. Accordingly, calixarenes containing four phenol groups 39a–e exist as cone conformers.

$$V_i = [A_i r + (B_i / r^2)] \cos(\theta) \quad (2.19)$$

While the first two tests assume Gaussian distributed data and the *P*-values are calculated by a probability distribution, the latter two are nonparametric and the *P*-values are

Instrumental Box 4**Numerical Data Analysis**

The incorporation of these techniques has provided a rapid prototyping technique, essential for the commercial development of current minimum feature-sized semiconducting integrated circuits. However, the production of these devices has been achieved at a high price, with the primary challenges currently faced by high-throughput fabrication laboratories including the high cost of laborers and instruments, high-temperature reaction conditions, and a surplus in generated waste [1].

The versatility of biology's incredible portfolio encourages researchers to develop modified syntheses derived from Nature. Hence, their findings have been successfully organized into the field of biomimetics, or bioinspired research technological applications [8].

Source: The versatility of biology's incredible portfolio encourages researchers to develop modified syntheses derived from Nature

Instrumental Box 5

The incorporation of these techniques has provided a rapid prototyping technique, essential for the commercial development of current minimum feature-sized semiconducting integrated circuits. However, the production of these devices has been achieved at a high price, with the primary challenges currently faced by high-throughput fabrication laboratories including the high cost of laborers and instruments, high-temperature reaction conditions, and a surplus in generated waste [1].

In fact, the cost of fabrication facilities are estimated to reach an outstanding US \$100 billion per facility by the year 2020, as the demand for smaller, lighter and faster materials continues to grow [1].

calculated based on combinatorial arguments. Thus, replicates on the same array and replicates in different possibilities for propane experiments should not be mixed since they have different characteristics and cannot be treated as independent replicates. Important issues are:

$$E_1 = \frac{9\varepsilon_2\varepsilon_3}{\varepsilon_2\varepsilon_a + 2\varepsilon_3\varepsilon_b} E_0 (\cos\theta\hat{r} - \sin\theta\hat{\theta}) \quad (2.20)$$

Traditionally, synthetic approaches for the production of functional metal oxide materials have involved high-temperature reaction environments with energy-intensive techniques such as laser ablation, ion implantation, chemical vapor deposition (CVD), photolithography or thermal decomposition [1].

The ligation products are used immediately for transformation or stored at -20°C. For transformation, add 10 ml of each ligation mix to freshly thawed GH-competent cells and mix

Instrumental Box 6

The incorporation of these techniques has provided a rapid prototyping technique, essential for the commercial development of current minimum feature-sized semiconducting integrated circuits. However, the production of these devices has been achieved at a high price, with the primary challenges currently faced by high-throughput fabrication laboratories including the high cost of laborers and instruments, high-temperature reaction conditions, and a surplus in generated waste [1].

In fact, the cost of fabrication facilities are estimated to reach an outstanding US \$100 billion per facility by the year 2020, as the demand for smaller, lighter and faster materials continues to grow [1].

Biomimetics infers the manipulating and mimicking of natural architectures and processes of biologically produced minerals (biominerals) to direct the synthesis of non-natural materials.

well by finger-tipping and incubate on ice for 45 min. The large difference in gravimetric energy density of methane direct oxidation is due to the mass of the gas cartridges.

Both the system and fuel volumetric energy densities of methane direct oxidation are very low, due to the large volume required for the storage of the gases (methane and oxygen). Moreover, the gravimetric fuel energy density of methane is low, due to the mass of oxygen which is accounted for [2]. Despite lower energy conversion efficiency, the propane-based processes lead to higher energy densities than the ammonia-based process, because of the intrinsic difference in energy density between the two fuels. The comparison of the two idealized possibilities for propane fuel processing reactions shows that energy conversion efficiency is not a suitable metric for man-portable applications, because it does not account for the water weight and volume; the higher energy efficiency of steam reforming is due to the generation of additional hydrogen in the reactor.

The lowest system energy densities. Both the system and fuel volumetric energy densities of methane direct oxidation are very low, due to the large volume required for the storage of the gases (methane and oxygen). Moreover, the gravimetric fuel energy density of methane is low, due to the mass of oxygen which is accounted for [2]. The large difference in gravi-

One striking feature of this book is that more than half of the chapters come from industry-based researchers; and even many of the academic contributors have close ties to industry. It has been alleged that the best science is done in academia; this book proves that this is not necessarily the case.

Part of the reason may be that many of the techniques involved require expensive equipment and infrastructure as well as large collaborations between scientists from disparate disciplines—collaborations that would be difficult to set up outside industry. The multidisciplinary nature of fragment-based approaches shows in this volume: contributors include computational chemists, NMR spectroscopists, X-ray crystallographers, mass-spectrometrists, as well as organic and medicinal chemists.

One striking feature of this book is that more than half of the chapters come from industry-based researchers; and even many of the academic contributors have close ties to industry. It has been alleged that the best science is done in academia; this book proves that this is not necessarily the case.

Part of the reason may be that many of the techniques involved require expensive equipment and infrastructure as well as large collaborations between scientists from disparate disciplines—collaborations that would be difficult to set up outside industry. The multidisciplinary nature of fragment-based approaches shows in this volume: contributors include computational chemists, NMR spectroscopists, X-ray crystallographers, mass-spectrometrists, as well as organic and medicinal chemists.

metric energy density of methane direct oxidation is due to the mass of the gas Table 1.2 cartridges. Despite lower energy conversion efficiency, the propane-based processes lead to higher energy densities than the ammonia-based process, because of the intrinsic difference in energy density between the two fuels. From a materials perspective, highly intact biological structures such as diatoms, bacteria. In this chapter we have included the details of a wide variety of mediated nanomaterial syntheses, their response to variable parameters, and their ability to retain a functionalized, controlled stability over time. With the exception of the process requiring gas storage, the fuel energy density and system energy density give the same qualitative comparison among processes.

The ligation products are used immediately for transformation or stored at -20°C . For transformation, add 10 ml of each ligation mix to freshly thawed GH-competent cells and mix well by finger-tipping and incubate on ice for 45 min. Traditionally, synthetic approaches for the production of functional metal oxide materials have involved high-temperature reaction environments with energy-intensive techniques such as laser ablation, ion implantation, chemical vapor deposition (CVD), photolithography or thermal decomposition [1].

The dilemma of rapidly emerging fields is that reviews are often outdated before they are printed. To make a contribution that would endure, we knew we had to go beyond a snapshot of the current state of fragment-based drug discovery and instead provide a framework for upcoming advances. To achieve this goal, we needed to convince leading scientists to take time from their busy schedules to write chapters. Fortunately, nearly all those we approached agreed; and what you hold in your hands is a virtual, although not comprehensive, “Who’s Who” in fragment-based drug discovery. We are extremely grateful to all of our contributors for the quality of their chapters.

Fragment-based drug discovery has only been practical for the past decade, too soon to expect it to produce marketed drugs; but we believe these will come in time.

Techniques described in this book Moreover, many of the techniques and concepts described in this book will alter drug discovery endeavors in subtle, tangential ways. Ideally, readers will be inspired to improve the methods described here, or even to develop fundamentally new methods for fragment-based drug discovery. But even if this book only changes the way medicinal chemists approach lead optimization, or persuades them to look more closely at weak but validated hits, it will have served its purpose.

For instance, the architecture of one of the most abundant biological species on the planet – the virus – has recently been manipulated to serve as containers for the synthesis of a variety of functional molecular cargoes.

In fact, the cost of fabrication facilities are estimated to reach an outstanding US \$100 billion per facility by the year 2020, as the demand for smaller, lighter and faster materials continues to grow¹. But, more importantly, manufacturers are progressing in this manner at the expense of the environment, as they accumulate semiconductor hazardous chemical wastes [2].

For decades, research teams in the semiconductor industry have been seeking alternative methods to passivate not only the rate of waste production but also the cost of spending. The most accessible resource for the synthesis of functional materials under ambient conditions is found in biology.

Traditionally, synthetic approaches for the production of functional metal oxide materials have involved high-temperature reaction environments with energy intensive techniques such as laser ablation, ion implantation, chemical vapor deposition (CVD), photolithography or thermal decomposition [1]. The incorporation of these techniques has provided a rapid prototyping technique, essential for the commercial development of current minimum fragment-based drug discovery and instead provide a framework for upcoming advances.

The versatility of biology's incredible portfolio encourages researchers to develop modified syntheses derived from Nature. Hence, their findings have been successfully organized into the field of biomimetics, or bioinspired research, which encompasses alternative approaches towards developing nanomaterials with technological applications [8]. Based primarily on the designs, mechanisms and processes found in Nature, biomimetics.

As mentioned above, the photoresist should be thin according to the distance of localization of the optical near-field around the nanoaperture. On the other hand, the photoresist should have the dry etching resistance so that the latent image can be transferred to the lower layer substrate. To separate the function of the thin film and the dry etching resistance, we used a trilayer resist process; the upper layer is an ultrathin photoresist, the middle layer is thin spin on glass (SOG), and the lower layer is a resin.

The patterns of shallow latent images in the upper layer are transferred to the thin SOG layer of excellent dry-etching resistance, and these are transferred in the lower layer further. Figure 6.8 shows the appearance of a prototype device of optical near-field lithography [7]. The features of the prototype device are as follows. This device is compact, with a footprint of about 2×2 . It has symmetric structure to compensate thermal expansion and temperature drift, and the hanging structure is introduced to avoid floor vibrations.

Bioinspired research is based on identifying and emulating the principles of biomineralization in natural systems, instead of copying them directly. In fact, most strategies incorpo-

¹ A Q-switch is a device that is similar to a shutter that controls the laser resonator's ability to oscillate. In fact, the cost of fabrication facilities are estimated to reach an outstanding US \$100 billion per facility by the year 2020, as the demand for smaller.

rated by natural systems are not directly applicable to engineered materials, so the need for alternative synthetic routes are required for the incorporation of non-natural elements, such as barium, nickel, copper or aluminum, with functional nanoscale properties [1,8]. To achieve this goal, we needed to convince leading scientists to take time from their busy schedules to write chapters. feature-sized semiconducting integrated circuits. However, the production of these devices has been achieved at a high price, with the primary challenges currently faced by high-throughput fabrication laboratories including the high cost of laborers and instruments, at a high price, with the primary challenges currently faced by high-throughput fabrication laboratories including the high cost of laborers and instruments, high temperature reaction conditions, and a surplus in generated waste [1].

- 120 For decades, research teams in the semiconductor industry have been seeking alternative methods to passivate not only the rate of waste production but also the cost of spending. The most accessible resource for the synthesis of functional materials under ambient conditions is found in biology.

Bioinspired research is based on identifying and emulating the principles of biomineralization in natural systems, instead of copying them directly. In fact, most strategies incorporated by natural systems are not directly applicable to engineered materials, so the need for alternative synthetic routes are required for the incorporation of non-natural elements, such as barium, nickel, copper or aluminum, with functional nanoscale properties [1,8]. However, the production of these devices has been achieved at a high price, with the primary challenges currently faced by high-throughput fabrication laboratories including the high cost of laborers and instruments.

In Kupferchlorid und Kupfersulfatpentahydrat (siehe Abb. 4.18) sind giftig und inätzend, Quecksilberchlorid ist sehr giftig und inätzend, Schwefeldioxid ist giftig, Silbernitrat wirkt ätzend. Das Tragen einer Schutzbrille ist erforderlich. Dieser wird auf die Porzellanfilternutsche gegeben, zweimal mit Ethanol sowie mit Wasser gewaschen mit denen das $\text{Cr}(\text{H}_2\text{O})_6$ oder Kupfersulfatpentahydrat mit den viel H_2O und Schwefeldioxid-Druckgaszylinder,² destilliertes Wasser.

Surprisingly, the properties associated with metal oxides in technology are not so far removed from what is observed in natural systems. Through precisely tuned processes, Nature is able to synthesize a variety of metal oxide nanomaterials under ambient conditions; the magnetic navigation device found in magnetotactic bacteria (MTB) is one such example [17]. Here, magnetite (Fe_3O_4) nanocrystals are aligned with the Earth's geomagnetic field and contained within specific organelles known as magnetosomes [17]. Fresh water salmon, for example, utilizes these magnetic nanoparticles in the nasal cavities of their forehead as a biomagnetic compass during migration [18].

² A Q-switch is a device that is similar to a shutter that controls the laser resonator's ability to oscillate. This shutter effect allows one to spoil the resonator's 'Q-factor', keeping it low to prevent lasing action. Under these conditions, the laser highly intact biological structures such as diatoms, bacteria, proteins or butterfly wings gain material is able to store higher levels of energy. The extra stored energy is subsequently extracted as laser light emission in the form of extremely short pulse width, high-peak-power pulses.

1

cDNA and Microarray-based Technologies

CHAPTER MENU

Introduction, 1
 CEA Gene Family, Genomic Localization, Protein Structure, 1
 Animal Models for CEA, 1
 Models for CEACAM5 Containing a Bacterial Artificial Chromosome, 2

1.1 Introduction

The molecular characterization of tumor-associated antigens (TAA) recognized by T cells [1] revolutionized the field of tumor immune biology providing conclusive evidence that CD8+ cytotoxic T cells (CTLs) specifically recognize and kill autologous cancer through recognition of molecularly-defined cancer-specific elements.

1.2 CEA Gene Family, Genomic Localization, Protein Structure

CEA is encoded by the CEA-related cell-cell adhesion molecule 5 (CEACAM5) gene, which belongs to the CEA gene family and in humans consists of 22 expressed members and 12 pseudogenes [3,4]. Both the system and fuel volumetric energy densities of methane direct oxidation are very low, due to the large volume required for the storage of the gases (methane and oxygen). Moreover, the gravimetric fuel energy density of methane is low, due to the mass of oxygen which is accounted for [2]. The large difference in gravimetric energy density of methane direct oxidation is due to the mass of the gas cartridges. Despite ammonia-based process, because of the intrinsic difference in energy density between the two fuels. The the water weight and volume; the higher energy efficiency of steam reforming is due to the generation of additional hydrogen in the reactor.

1.3 Animal Models for CEA

Mice are commonly used to analyze the efficacy of tumor therapies and mechanisms of tumor rejection. However, this species cannot be utilized to evaluate CEA-based therapies since no CEACAM5 ortholog exists in rodents. This problem was circumvented by introducing the human CEACAM5 gene into the germ line of mice [52–54].

1.4 Models for CEACAM5 Containing a Bacterial Artificial Chromosome

Either cosmid clones containing the CEACAM5 gene or a bacterial artificial chromosome (BAC) clone, which comprises part of the gene cluster surrounding CEACAM5, served as a genetic source. This cluster includes CEACAM6 and CEACAM3.

Antibody Delivery of Radionuclides, Drugs and Effector Molecules Delivery of radio-nuclides to tumors using murine and human anti-CEA antibodies has been studied for many years [70]. The use of low molecular weight single chain antibody fragments and pre-targeting has been found to enhance the sensitivity of tumor visualization as well as increasing the delivered therapeutic dose by separating the antibody targeting to the tumor from the subsequent delivery of the therapeutic radionuclide that binds to the tumor-localized antibody.

SubParagraph Title: Nuclear Angular Momentum and Magnetic Moment The conformational flexibility of calixarenes is usually explained by the presence of intramolecular hydrogen bonds, which is related to the number of free phenol groups. Accordingly, calixarenes containing four phenol groups 39–e exist as cone conformers.

The use of low molecular weight single chain antibody fragments and pre-targeting has been found to enhance the sensitivity of tumor visualization as well as increasing the delivered therapeutic dose by separating the antibody targeting to the tumor from the subsequent delivery of the therapeutic radionuclide that binds to the tumor-localized antibody.

References

- 1 Thaxton, C.S., Georganopoulou, D.G. and Mirkin, C.A. (2006) Gold nanoparticle probes for the detection of nucleic acid targets. *Clinica Chimica Acta*, 363, 120–6.
- 2 Cheng, M.M., Cuda, G., Bunimovich, Y.L., Gaspari, M., Heath, J.R., Hill, H.D., Mirkin, C.A., Nijdam, A.J., *Biology*, 10, 11–19.
- 4 Nie, S., Xing, Y., Kim, G.J. and Simons, J.W. (2007) Nanotechnology applications in cancer. *Annual Review of Biomedical Engineering*, 9, 257–88.
- 99 Cai, W. and Chen, X. (2007) Nanoplatforams for targeted molecular imaging in living subjects. *Small*, 11, 1840–54.
- 100 Gupta, A.K. and Gupta, M. (2005) Synthesis and surface engineering of iron oxide nanoparticles for biomedical applications. *Biomaterials*, 26, 3995–4021.

2

The Molecular Characterization

Abstract

The molecular characterization of tumor-associated antigens recognized by T cells [1] revolutionized the field of tumor immune biology providing conclusive evidence that CD8+cytotoxic T cells (CTLs) specifically recognize and kill autologous cancer through recognition of molecularly-defined calixarenes is usually explained by the presence cancer-specific elements. Since then a myriad of TAA have been identified that has triggered their utilization as anti-cancer vaccines [2–8].

Keywords *The molecular; characterization; of tumor-associated; antigens*

The molecular characterization of tumor-associated antigens (TAA) recognized by T cells [1] revolutionized the conformational.

2.1 Animal Models for CEA

Delivery of radio-nuclides to tumors using murine and human anti-CEA antibodies has been studied for many years. The use of low molecular weight single chain antibody fragments and pre-targeting has been found to enhance the sensitivity of tumor visualization as well as from the subsequent delivery of the therapeutic radionuclide that binds to the tumor-localized antibody. The conformational flexibility of calixarenes is usually explained by the presence of intramolecular hydrogen bonds, which is related to the number of free phenol groups.

Definition 2.1 The position of a body along the x axis, in metres, is given by the equation $x = t^3 - 30t^2 + 5$, where t is the time in seconds. Find its velocity and acceleration as a function of time.

Delivery of radio-nuclides to tumors using murine and human anti-CEA antibodies has been studied for many years. The use of low molecular weight single chain antibody fragments and pre-targeting has been found to enhance the sensitivity of tumor visualization as well as increasing the delivered therapeutic dose by separating the antibody targeting to

the tumor from the subsequent delivery of the therapeutic radionuclide that binds to the tumor-localized antibody.

Example 2.1 The position of a body along the x axis, in metres, is given by the equation $x = t^3 - 30t^2 + 5$, where t is the time in seconds. Find its velocity and acceleration as a function of time.

$$\begin{aligned}\text{Velocity} \quad \mathbf{v} &= \frac{dx}{dt} \\ \text{Acceleration} \quad a &= \frac{d^2x}{dt^2} \\ x &= t^3 - 30t^2 + 5 \\ a(t) &= \frac{d^2x}{dt^2} = 6t - 60\end{aligned}$$

The use of low molecular weight single chain antibody fragments and pre-targeting has been found to enhance the sensitivity of tumor visualization as well as increasing the delivered therapeutic dose by separating the antibody targeting to the tumor from the subsequent delivery of the therapeutic radionuclide that binds to the tumor-localized antibody.

Theorem 2.1 The position of a body along the x axis, in metres, is given by the equation $x = t^3 - 30t^2 + 5$, where t is the time in seconds. Find its velocity and acceleration as a function of time.

$$\begin{aligned}\text{Velocity} \quad \mathbf{v} &= \frac{dx}{dt} \\ x &= t^3 - 30t^2 + 5 \\ a(t) &= \frac{d^2x}{dt^2} = 6t - 60\end{aligned}$$

Delivery of radio-nuclides to tumors using murine and human anti-CEA antibodies has been studied for many years [70].

Lemma 2.1 The position of a body along the x axis, in metres, is given by the equation $x = t^3 - 30t^2 + 5$, where t is the time in seconds. Find its velocity and acceleration as a function of time.

$$\begin{aligned}\text{Velocity} \quad \mathbf{v} &= \frac{dx}{dt} \\ \text{Acceleration} \quad a &= \frac{d^2x}{dt^2}\end{aligned}$$

Proof: Proof for the above Lemma

$$\begin{aligned}x &= t^3 - 30t^2 + 5 \\ a(t) &= \frac{d^2x}{dt^2} = 6t - 60\end{aligned}$$

Delivery of radio-nuclides to tumors using murine and human anti-CEA antibodies has been studied for many years [70]. The use of low molecular weight single chain antibody fragments and pre-targeting has been found to enhance the sensitivity of tumor visualization as well as increasing the delivered therapeutic dose by separating the antibody targeting to the tumor from the subsequent delivery of the therapeutic radionuclide that binds to the tumor-localized antibody.

Corollary 2.1 The position of a body along the x axis, in metres, is given by the equation $x = t^3 - 30t^2 + 5$, where t is the time in seconds. Find its velocity and acceleration as a function of time.

$$\text{Velocity} \quad \mathbf{v} = \frac{dx}{dt}$$

$$\text{Acceleration} \quad a = \frac{d^2x}{dt^2}$$

$$x = t^3 - 30t^2 + 5$$

$$a(t) = \frac{d^2x}{dt^2} = 6t - 60$$

Delivery of radio-nuclides to tumors using murine and human anti-CEA antibodies has been studied for many years [70].

Is there another *Browne* hath kild a *Sanders*?
 It is my other selfe hath done the deede,
 I am a thousand, every murtherer is my one selfe,
 I am at one time in a thousand places,
 And I have slaine a thousand *Sanderses*,
 In every shire, each cittie, and each towne,
George Sanders still is murdered by *George Browne*.
 (lines 2397–403)

The use of low molecular weight single chain antibody fragments and pre-targeting has been found to enhance the sensitivity of tumor visualization as well as increasing the delivered therapeutic dose by separating the antibody targeting to the tumor from the subsequent delivery of the therapeutic radionuclide that binds to the tumor-localized antibody.

- The housing supply elasticity determines the level of house prices. Across East Asia, housing prices are high because:
 - 1) the supply price elasticity of housing tends to be low;
 - 2) the share of land in total unit cost is high overall and the highest in large cities; and
 - 3) the supply elasticity of land itself is low.
- Housing prices will be more volatile in response to a demand shock when housing supply elasticity is low. The impact of speculative behavior will be stronger and boom-bust cycles are more likely when supply is inelastic (Malpezzi and Wachter, 2002). We therefore expect East Asian price cycles to be rather volatile.

Box 2.1 Predictors and time frames in propensity modeling

As we have outlined before, in propensity modeling, when we analyze customer behavior before the occurrence of the event of interest, candidate predictors should only be based in the observation period which should not overlap with the event outcome period.

Working with research teams to develop service user involvement

In the deployment phase, there will be no event outcome period, and the observation period will correspond to the current view of the customer at the time of deployment.

- Open cards at the beginning of the observation period (2012-1-1, OPEN_AT_START field)
- Open cards at the end of the observation period (2012-12-31, OPEN_AT_END field)
- Open cards at the end of the latency period (2013-3-1, OPEN_AT_LATENCY)
- Open cards at the end of the event outcome period (2013-7-1,

In our case study, the time frame of the observation period is the whole 2012. Information from the next months will serve only for the definition of the churn target field. When the model will be used for deployment, for instance at July 1, 2013, it will again require 12 months of summarized usage data, July 2012 to June 2013, to score new cases.

- 1) Open cards at the beginning of the observation period (2012-1-1, OPEN_AT_START field)
- 2) Open cards at the end of the observation period (2012-12-31, OPEN_AT_END field)
- 3) Open cards at the end of the latency period (2013-3-1, OPEN_AT_LATENCY)
 - Open cards at the beginning of the period (2012-1-1, OPEN_AT_START field)
 - Open cards at the end of the observation period (2012-12-31, OPEN_AT_END field)

Taking the perspective that it is the human activities that require management rather than the biological systems that we disturb, this chapter will describe an adaptive management approach to environmental management.

Starting out

The competitive nature of research often motivates researchers to incorporate service user involvement into their applications for research funding. Some researchers want to know what benefits service user involvement will bring to their research before they attempt it – but to determine the benefits requires some service user involvement activity to take place in the first place.

- NICE recommends [17] that parents:
 - are reassured that antibiotics are not needed immediately because they are likely to make little difference to symptoms and may have side effects;
 - are given advice about the usual natural history of the infection, including the average total length of the illness (before and after seeing the doctor):
 - acute otitis media (AOM): 4 days (a recent study suggests this should be longer [20]);
 - acute cough/acute bronchitis: 21 days

A patient-centered approach that puts emphasis on building and maintaining a therapeutic relationship between patient, doctor and care team is also referred to as a

relationship-centered approach. According to Beach *et al.* (2006), relationship-centered care is founded upon four principles. Using technological advancements such as remote sensing and geographic information systems, ecologists can determine the most successful ways to harmonize human disturbances with natural ones and identify feasible biological targets for the system of interest. Understanding the scale of the system and its processes is critical, and using large-scale data sets along with remote sensing can help ecologists determine where the system is, where it needs to be, and whether preservation is the right management decision or if more active restoration or rehabilitation is necessary.

- 1) that relationships in health care ought to include the personhood of the participants;
- 2) that affect and emotion are important components of these relationships;
 - a) that all healthcare relationships occur in the context of reciprocal influence and
 - i) that the formation and maintenance of genuine relationships in healthcare is morally valuable.
 - ii) systematic undervaluation of the currency;

Clearly, a central component of such an approach is for doctors to convey that they see their patients as people (i.e. not simply cases with biomedical defects). This is reflected in the excerpt above and part of Fig. 5.4

- a) systematic undervaluation of the currency;
- b) rate of growth of wages kept slower than the rate of growth of labor productivity;
- c) credit allocation directed by the government, and with central regulation of deposit and lending rates significantly below the opportunity cost of capital and its equilibrium level in the economy.

The environmental management of the Florida Everglades is used throughout as an illustrative case study of how ecologists have used an adaptive management approach to restore and preserve an internationally famous ecosystem.

in land use and urban planning approvals;

in government powers to intervene in the markets and to regulate private transactions;

in property taxation and land use transitions; and

in powers to use public lands and public finance to produce new volumes of serviced urban land.

ake radiolabeled nanoparticles an invaluable tool [35].

The adaptive management process is iterative, so that new information on the response of the ecosystem to our management activities is used to improve the next round of decisions. Using technological advancements such as remote sensing and geographic information systems, ecologists can determine the most successful ways to harmonize human disturbances with natural ones and identify feasible biological targets for the system of interest.

CLAUDIO: To make you answer truly to your name.

HERO: Is it not Hero? Who can blot that name With any just reproach?

CLAUDIO: Marry that can Hero!

Understanding the scale of the system and its processes is critical, and using large-scale data sets along with remote sensing can help ecologists determine where the system is,

where it needs to be, and whether preservation is the right management decision or if more active restoration or rehabilitation is necessary.

- i) On a per particle basis, SERS probes are significantly brighter compared to NIR emitting semiconducting quantum dots (QDs), which have been extensively investigated for bioimaging applications. Even simple designs involving individual gold nanoparticles tagged with resonant Raman reporters are nearly 200 times brighter compared to QDs [18].
- ii) The full-width at half-maximum (FWHM) of Raman bands (1-2 nm) are nearly 20-30 times narrower compared to the emission bands of quantum dots (40-60 nm), making spectral multiplexing an order of magnitude higher for SERS probes compared to that attainable with QDs [19].
- iii) The excitation and emission of SERS probes can be easily tuned to the near-infrared (NIR) therapeutic window (650-900 nm), where the endogenous absorption coefficient of tissue is nearly two orders magnitude lower compared to that in the visible parts of electromagnetic spectrum [19]. Furthermore, absence of interference from water and autofluorescence of the tissues in NIR is yet another significant advantage of SERS compared to photoluminescence-based optical imaging techniques.

SERS probes offer remarkable photostability compared to organic fluorophores and QDs, which suffer from either photobleaching or blinking. SERS probes, typically made of gold, are significantly less cytotoxic compared to NIR emitting QDs comprised of CdSe and CdTe.

Typical for such series of survey items is that the formulation is exactly the same for each item and that only one introduction with other possible components is given before the first survey item is mentioned. The items are treated equally because the interview programs use substitution procedures. An example of such an instruction to an interview program could look as follows:

```
#Casibattery 10 1
# item 1
healthcare
#item 2
social services
#item 3
# item 10
social security
#
#Question with 5 answer categories
What is your opinion about our "S"?
```

Examples of concepts-by-intuition include judgments, feelings, evaluations, norms, and behaviors. Most of the time, it is quite obvious that a text presents a feeling (x likes y), a norm (people should behave in a certain way), or behavior (x does y). We will return to the classification of these concepts later.

Title 21 Chapter 1 contains Parts 1 to 1299. The parts that are commonly encountered in the development of the three platforms of therapeutic delivery are listed below:

Part 3 – Product Jurisdiction

Part 4 – Current Good Manufacturing Practice Requirements for Combination Products (effective July 2013)

Part 11 - Electronic Records; Electronic Signatures

Part 58 - Good Laboratory Practice for Nonclinical Laboratory Studies

Part 210 - Current Good Manufacturing Practice in Manufacturing, Processing, Packing, or Holding Of Drugs; General

In the United States, the regulatory requirements of the three platforms of drug delivery are implemented through three separate Centers in the FDA

Stewardship to Natural Capitalism optimization of productive effort aimed at efficient use of the earth's natural capital. The concept of natural capitalism is based on four principles:

- Radical resource efficiency
- Ecological restoration

Efficiency to Eco Efficiency the transition from total quality focused initiatives to also include environmental impact reduction through the implementation of four stages of eco efficient development:

- Increasing process efficiency.
- Reducing material flow by changing consumer preferences for material intensive products.

Business image to environmental champion a commitment to Sustainability Partnerships that is manifested by organizational policies and procedures aimed at implementing environmental best practice.

Taking the perspective that it is the human activities that require management rather than the biological systems that we disturb, this chapter will describe an adaptive management approach to environmental management.

Step 1: Generate random paths through the graph.

Step 2: Keep only those paths that begin with V_{in} and end with V_{out} .

Step 3: If the graph has n vertices, then keep only those paths that enter exactly n vertices.

Step 4: Keep only those paths that enter all of the vertices of the graph at least once.

Step 5: If any paths remain, say "Yes"; otherwise, say "No."

The versatility of polyurethanes is derived in large part from the wide selection of building blocks available to materials designers. Bioinspired research is based on identifying and emulating the principles of biomineralization in natural systems, instead of copying them directly. In fact, most strategies incorporated by natural systems are not directly applicable to engineered materials, so the need for alternative synthetic routes are required for the incorporation of non-natural elements, such as barium, nickel, copper or aluminum, with functional nanoscale properties [1,8]. However, the production of these devices has been achieved at a high price, with the primary challenges currently faced by high-throughput fabrication laboratories including the high cost of laborers and instruments.

In Kupferchlorid und Kupfersulfatpentahydrat (siehe Abb. 4.18) sind giftig und inätzend, Quecksilberchlorid ist sehr giftig und inätzend, Schwefeldioxid ist giftig, Silbernitrat wirkt ätzend. Das Tragen auf einer und Schutzbrille ist erforderlich. Dieser wird auf die

Algorithm 1

Input: transition matrix P , observation matrix $\mathbf{r}(\mathbf{u}_k, z_{k+1})$, costs $\mathbf{g}^\lambda(\mathbf{u}^q)$, $q = 1, \dots, \alpha$, horizon length L

Output: cost $\{\hat{J}_k^\lambda(\mathbf{e}_1), \dots, \hat{J}_{L-1}^\lambda(\mathbf{e}_n)\}_{k=0}^{L-1}$, strategy $\{\hat{\mathbf{u}}_k^{\mathbf{e}_1}, \dots, \hat{\mathbf{u}}_k^{\mathbf{e}_n}\}_{k=0}^{L-1}$

- 1: for $i = 1 : n$ do
- 2: $\hat{J}_{L-1}^\lambda(\mathbf{e}_i) = \min_{\mathbf{u}_{L-1} \in \mathcal{U}} [\mathbf{e}_i^T \mathbf{g}^\lambda(\mathbf{u}_{L-1})]$;
- 3: $\hat{\mathbf{u}}_{L-1}^{\mathbf{e}_i} = \arg \min_{\mathbf{u}_{L-1} \in \mathcal{U}} \hat{J}_{L-1}^\lambda(\mathbf{e}_i)$;
- 4: end for
- 5: **end for**

Porzellanfilternutsche gegeben, zweimal mit Ethanol sowie mit Wasser gewaschen mit denen das $\text{Cr}(\text{H}_2\text{O})_6$ oder Kupfersulfatpentahydrat mit den viel H_2O und Schwefeldioxid-Druckgaszylinder, 2 destilliertes Wasser.

1. In principle there is as much potential for design of isocyanate structures as there is for alcohol and amine co-reactants. In reality, while there are numerous polyisocyanates to choose from, most of the innovation in polyurethane performance comes from the broad range of choices available in the co-reactant alcohols and amines.

2. To a great extent this reflects complications (both industrial and regulatory) associated with making isocyanates, and the comparative ease of making polyol and polyamine structures.

In reality, while there are numerous polyisocyanates to choose from, most of the innovation in polyurethane performance comes from the broad range of choices available in the co-reactant alcohols and amines.

Problems

1.1 The positive sequence impedance data are given in the accompanying table. Use the commonly made assumption that all prefault resistance values are $(1.0 + j0.0)$ pu, and neglect all resistance values.

- C1 (X1, X2): (cs, ss) (cs, al) (al, cu)
 C2 (X1, X3): (cs, ss) (ss, cu) (al, cu)
 C3 (X2, X3): (cs, ss) (cs, al) (cu, cu)

1.2 Using the usual assumptions about the positive and negative sequence impedances of the network elements, what are the currents at breaker B1 for b–c fault for each of the faults in Problem 1.1? What is the voltage between phases b and c for each case?

With the governmental regulatory environment and the general European goal of using industrial solutions employing the least toxic effective components available, there has been increasing industrial and academic emphasis on obtaining urethane properties from systems that do not employ isocyanates.

Table 2.1 Dystonia genetic conditions.

Gene	Locus	Inheritance	Phenotype	Gene product (gene)
<i>DYT 1</i>	9q32-34	AD	Young onset, generalised	Torsin A (<i>TOR1A</i>)
<i>DYT 2</i>	NM	AR	Young onset, generalised	—
<i>DYT 3</i>	Xq13.1	XR	Filipino dystonia–parkinsonism	Gene transcription factor (<i>TAF1</i>)
<i>DYT 4</i>	NM	AD	Laryngeal ± limb dystonia (1 family)	—
<i>DYT 5a</i>	14q22.1-2	AD	Young onset, dopa-responsive	GTP cyclohydrolase 1 (<i>GTPCH1</i>)
<i>DYT 5b</i>	11p16.5	AR	dystonia–parkinsonism	Tyrosine hydroxylase (TH)
<i>DYT 6</i>	8p11.21	AD	Young onset, cranio-cervical or generalised	Thanatos-associated protein 1 (<i>THAP1</i>)
<i>DYT 7</i>	18p	AD	Adult onset, focal dystonia (1 family)	Not identified
<i>DYT 8</i>	2q35	AD	<i>PNKD1</i>	Myofibrillogenesis regulator 1 (<i>MR-1</i>)
<i>DYT 9</i>	1p31	AD	<i>EID1</i> /Episodic chorea or ataxia and spasticity	Glucose transporter 1 (<i>SLC2A1</i>)
<i>DYT 10</i>	16p11-q12	AD	<i>PKD1</i>	<i>PRRT2</i>
<i>DYT 11</i>	7q21.3	AD	Myoclonus dystonia	E-sarcoglycan (<i>SGCE</i>)
<i>DYT 12</i>	19q13.2	AD	Rapid onset dystonia–parkinsonism	Na ⁺ /K ⁺ ATPase α3 subunit (<i>ATPIA3</i>)
<i>DYT 13</i>	1p36	AD	Young onset segmental or generalised dystonia (1 family)	Not identified
<i>DYT 14 = DYT 5a</i>				
<i>DYT 15</i>	18p11	AD	Myoclonus dystonia (1 family)	Not identified
<i>DYT 16</i>	2q31.2	AR	Young onset, generalised dystonia-parkinsonism	Stress-response protein (<i>PRKRA</i>)
<i>DYT 17</i>	20p11-q13	AR	Young onset, mixed phenotype (1 family)	Not identified
<i>DYT 18</i>	1p34.2	AD	<i>EID2</i>	Glucose transporter 1 (<i>SLC2A1</i>)
<i>DYT 19</i>	16q13-22	AD	<i>PKD2</i> (1 family)	Not identified
<i>DYT 20</i>	2q31	AD	<i>PNKD2</i> (1 family)	Not identified
<i>DYT 21</i>	2q14-q21	AD	Adult onset mixed phenotype (1 family)	Not identified

(Continued)

Table 2.1 (Continued)

Gene	Locus	Inheritance	Phenotype	Gene product (gene)
<i>DYT 22</i>	Reserved			
<i>DYT 23</i>	11p14.2	AD	Adult onset cranio-cervical dystonia	Anoctamin 3 (<i>ANO3</i>)
<i>CIZ 1*</i>	9q34.11	AD	Adult onset cervical dystonia	Cip-1-interacting zinc protein
<i>GNAL*</i>	18p11	AD	Mixed phenotype	G protein subunit α_{olf}

AD, autosomal dominant; AR, autosomal recessive; EID, exercise-induced dystonia; NM, not mapped; PKD, paroxysmal kinesigenic dystonia; PNKD, paroxysmal non-kinesigenic dystonia; XR – X-linked recessive.

*Waiting for replication studies and/or not assigned a DYT.

Bioinspired research is based on identifying and emulating the principles of biomineralization in natural systems, instead of copying them directly. In fact, most strategies incorporated by natural systems are not directly applicable to engineered materials, so the need for alternative synthetic routes are required for the incorporation of non-natural elements, such as barium, nickel, copper or aluminum, with functional nanoscale properties [1,8]. However, the production of these devices has been achieved at a high price, with the primary challenges currently faced by high-throughput fabrication laboratories including the high cost of laborers and instruments.

Example 2.1

Problem: The position of a body along the x axis, in metres, is given by the equation $x = t^3 - 30t^2 + 5$, where t is the time in seconds. Find its velocity and acceleration as a function of time.

Governing Equations:

$$\text{Velocity} \quad \mathbf{V} = \frac{dx}{dt}$$

$$\text{Acceleration} \quad a = \frac{d^2x}{dt^2}$$

Solution:

$$x = t^3 - 30t^2 + 5$$

$$a(t) = \frac{d^2x}{dt^2} = 6t - 60$$

Through precisely tuned processes, Nature is able to synthesize a variety of metal oxide nanomaterials under ambient conditions; the magnetic navigation device found in magnetotactic bacteria (MTB) is one such example [17]. Here, magnetite (Fe_3O_4) nanocrystals are aligned with the Earth's geomagnetic field and contained within specific organelles known as magnetosomes [17]. Fresh water salmon, for example, utilizes these magnetic nanoparticles in the nasal cavities of their forehead as a biomagnetic compass during migration [18]. A Q-switch is a device that is similar to a shutter that controls the laser resonator's ability to oscillate.

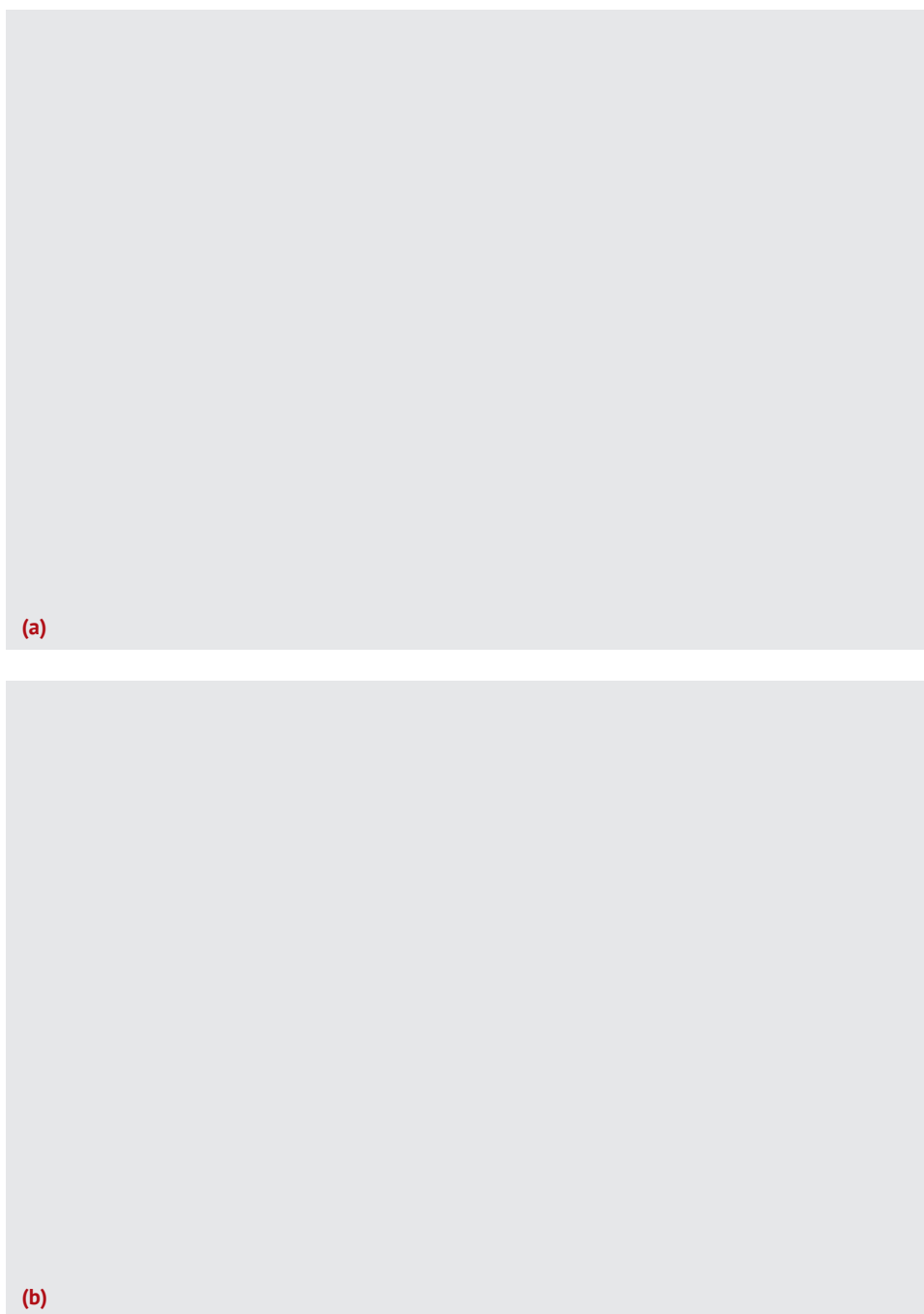


Figure 2.1 (a) Inside the prototype device of the near-field lithography. (b) Illumination of i-line light for exposure from the back side of the near-field photomask.

(Continued)

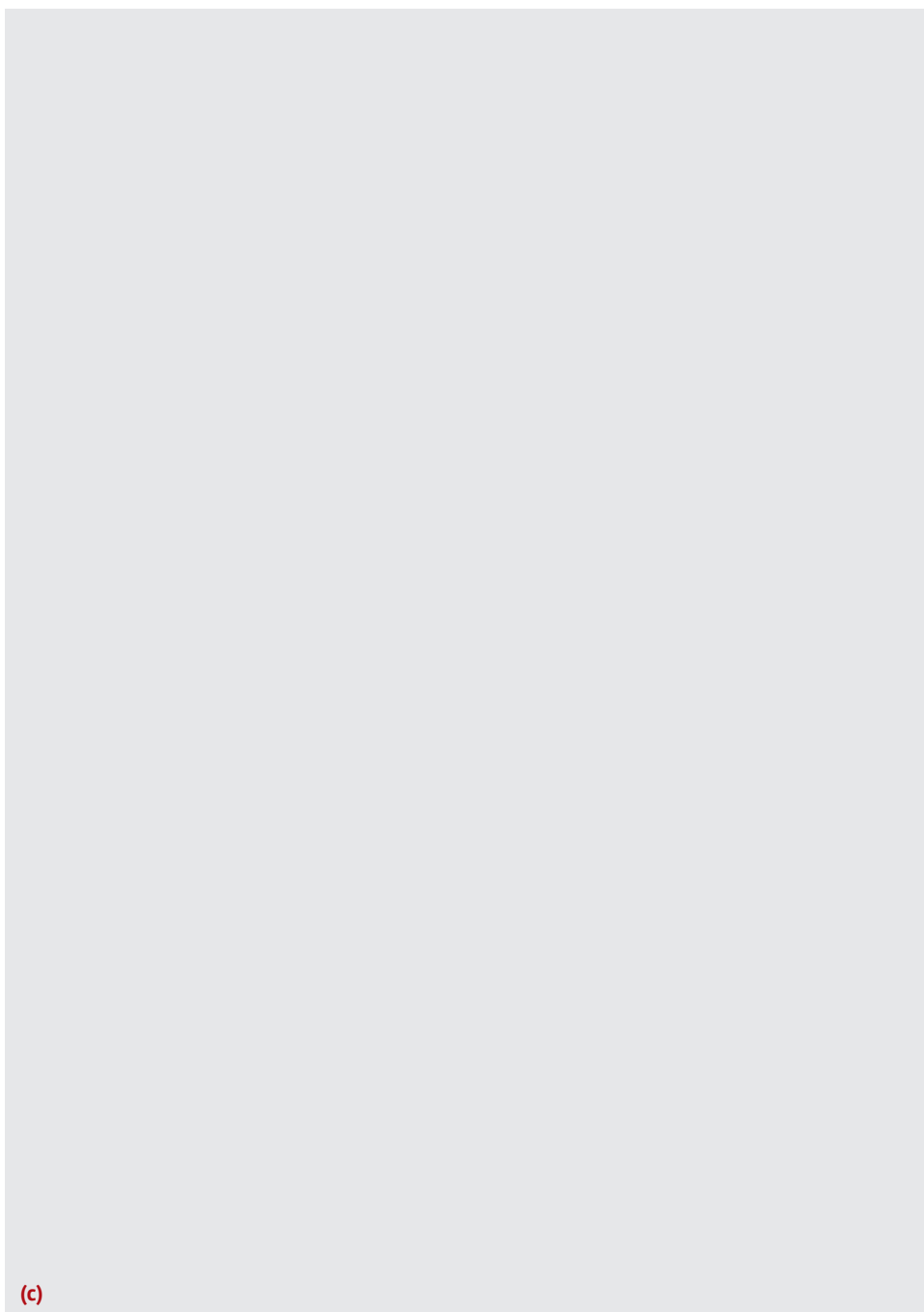


Figure 2.1 (Cont'd) (c) Close-up from the side of the near-field photomask and the photoresist on the wafer. They are brought into contact with each other within the localizing distance of the optical near-field.

Box 2.2 Resources

If you are in crisis or you know someone who is hurting, *please* contact these FREE resources.

Resource	Phone number	Website
National Suicide Prevention Lifeline	1-800-273-8255	http://www.suicidepreventionlifeline.org/
Contact: From breaking point to turning point	(972) 233-2233	http://contactcrisisline.org/
Crisis Call Center	1-800-273-8255 OR Text ANSWER to 839863	http://crisiscallcenter.org/crisisservices.html
The Trevor Project (for LGBTQQ youth)	1-866-488-7386 OR Text the word “Trevor” to 1-202-304-1200	http://www.thetrevorproject.org/
Veterans Crisis Line	1-800-273-8255 and Press 1 OR Text 838255	http://veteranscrisisline.net/

Box 2.3 Predictors and time frames in propensity modeling

As we have outlined before, in propensity modeling, when we analyze customer behavior before the occurrence of the event of interest, candidate predictors should only be based in the observation period which should not overlap with the event outcome period.

Working with research teams to develop service user involvement

In the deployment phase, there will be no event outcome period, and the observation period will correspond to the current view of the customer at the time of deployment. In the deployment phase, there will be no event outcome period, and the observation period will correspond to the current view of the customer at the time of deployment.

$$\rho(z)v_w = \rho_w^{\text{bulk}} v_w \exp(-v_w \beta[\pi(z) - \pi^{\text{bulk}}])$$

$$\rho(z)v_w = \rho_w^{\text{bulk}} v_w \exp(-v_w \beta[\pi(z) - \pi^{\text{bulk}}]) - q_i \beta[\psi(z) - \psi^{\text{bulk}}]$$

In the deployment phase, there will be no event outcome period, and the observation period will correspond to the current view of the customer at the time of deployment.

- Open cards at the beginning of the observation period (2012-1-1, OPEN_AT_START field)
- Open cards at the end of the observation period (2012-12-31, OPEN_AT_END field)
- Open cards at the end of the latency period (2013-3-1, OPEN_AT_LATENCY)
- Open cards at the end of the event outcome period (2013-7-1,

(Continued)

Box 2.3 (Continued)

In our case study, the time frame of the observation period is the whole 2012. Information from the next months will serve only for the definition of the churn target field. When the model will be used for deployment, for instance at July 1, 2013, it will again require 12 months of summarized usage data, July 2012 to June 2013, to score new cases.

- 1) Open cards at the beginning of the observation period (2012-1-1, OPEN_AT_START field)
- 2) Open cards at the end of the observation period (2012-12-31, OPEN_AT_END field)
- 3) Open cards at the end of the latency period (2013-3-1, OPEN_AT_LATENCY)
 - Open cards at the beginning of the period (2012-1-1, OPEN_AT_START field)
 - Open cards at the end of the observation period (2012-12-31, OPEN_AT_END field)

Taking the perspective that it is the human activities that require management rather than the biological systems that we disturb, this chapter will describe an adaptive management approach to environmental management.

Starting out

The competitive nature of research often motivates researchers to incorporate service user involvement into their applications for research funding. Some researchers want to know what benefits service user involvement will bring to their research before they attempt it – but to determine the benefits requires some service user involvement activity to take place in the first place.

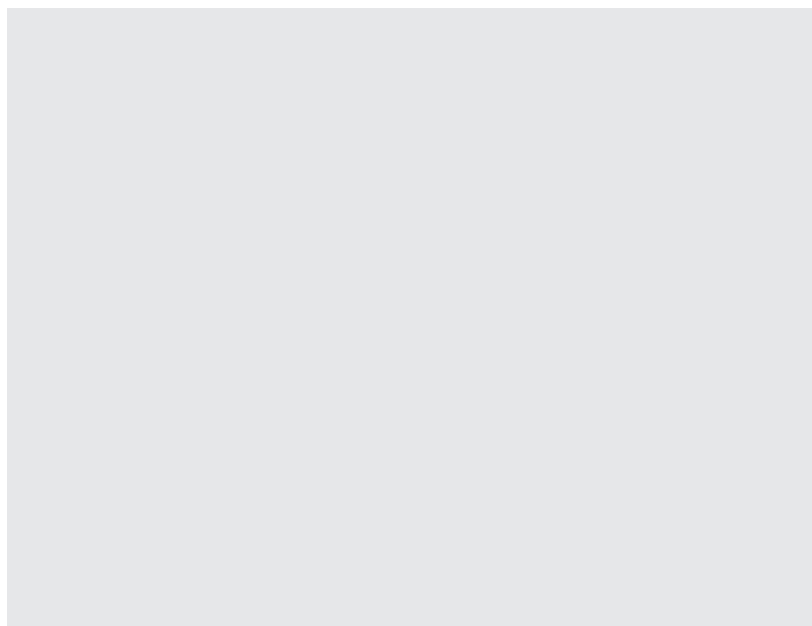
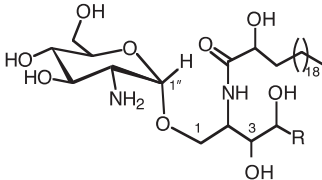
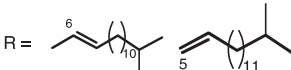
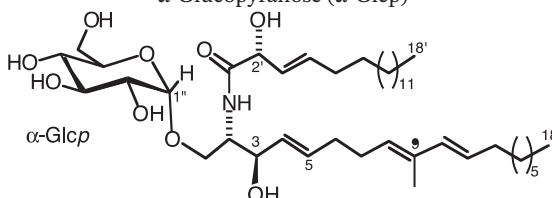
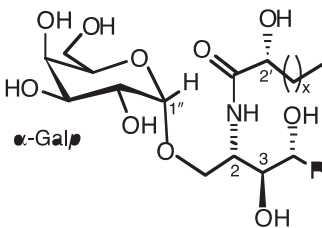


Figure 1.12 Distribution of structures for variable pH samples. *Source:* Reprinted with permission from Ref. [33]; © 2007, American Chemical Society.

Table 2.2 Glycosphingolipids containing an α -glycosyl linkage.

Ceramide / GSL Name	Organism	Biological activity	Reference																														
<div>α-Glucopyranosamine (α-NH₂-Glc_p)</div> <div></div>																																	
<div>R = </div> <div>amphiceramides E and F</div>	<div>Sponge <i>Amphimedon viridis</i></div>	<div>n. r.</div>	<div>Hirsch and Kashman, 1989</div>																														
<div>α-Glucopyranose (α-Glc_p)</div> <div></div>																																	
<div>sarcoehrenoside A</div>	<div>Octocoral <i>Sarcophyton ehrenbergi</i></div>	<div>No antibacterial Reduced iNOS protein expression Anti-inflammatory</div>	<div>Cheng et al., 2009</div>																														
<div></div>																																	
<table><tr><th>Agelasphin</th><th>x</th><th>R</th></tr><tr><td>-7a</td><td>21</td><td>-(CH₂)₁₁-CH₃</td></tr><tr><td>-9a</td><td>21</td><td>-(CH₂)₁₂-CH₃</td></tr><tr><td>-9b</td><td>21</td><td>-(CH₂)₁₁-CH(CH₃)₂</td></tr><tr><td>-11</td><td>21</td><td>-(CH₂)₁₁-CH(CH₃)-C₂H₅</td></tr><tr><td>-13</td><td>21</td><td>-(CH₂)₁₁-CH(CH₃)-C₂H₅</td></tr><tr><td>-7b-1</td><td>20</td><td>-(CH₂)₁₀-CH(CH₃)-C₂H₅</td></tr><tr><td></td><td></td><td>-(CH₂)₁₁-CH(CH₃)₂</td></tr><tr><td>-7b-2</td><td>21</td><td>-(CH₂)₉-CH(CH₃)-C₂H₅</td></tr><tr><td></td><td></td><td>-(CH₂)₁₀-CH(CH₃)₂</td></tr></table>	Agelasphin	x	R	-7a	21	-(CH ₂) ₁₁ -CH ₃	-9a	21	-(CH ₂) ₁₂ -CH ₃	-9b	21	-(CH ₂) ₁₁ -CH(CH ₃) ₂	-11	21	-(CH ₂) ₁₁ -CH(CH ₃)-C ₂ H ₅	-13	21	-(CH ₂) ₁₁ -CH(CH ₃)-C ₂ H ₅	-7b-1	20	-(CH ₂) ₁₀ -CH(CH ₃)-C ₂ H ₅			-(CH ₂) ₁₁ -CH(CH ₃) ₂	-7b-2	21	-(CH ₂) ₉ -CH(CH ₃)-C ₂ H ₅			-(CH ₂) ₁₀ -CH(CH ₃) ₂	<div>Sponge <i>Agelas mauritanus</i></div>	<div>Antitumor Immunostimulatory</div>	<div>Natori et al., 1993, 1994</div>
Agelasphin	x	R																															
-7a	21	-(CH ₂) ₁₁ -CH ₃																															
-9a	21	-(CH ₂) ₁₂ -CH ₃																															
-9b	21	-(CH ₂) ₁₁ -CH(CH ₃) ₂																															
-11	21	-(CH ₂) ₁₁ -CH(CH ₃)-C ₂ H ₅																															
-13	21	-(CH ₂) ₁₁ -CH(CH ₃)-C ₂ H ₅																															
-7b-1	20	-(CH ₂) ₁₀ -CH(CH ₃)-C ₂ H ₅																															
		-(CH ₂) ₁₁ -CH(CH ₃) ₂																															
-7b-2	21	-(CH ₂) ₉ -CH(CH ₃)-C ₂ H ₅																															
		-(CH ₂) ₁₀ -CH(CH ₃) ₂																															

Exercises

- 1 Try to formulate questions that represent concepts-by-intuition and concepts-by-postulation with formative and reflective indicators for the following concepts:
 - A Life satisfaction
 - B Happiness
 - C The importance of the value “honesty”
- 2 In practice, it is seldom clear whether the questions suggested measure what they are supposed to measure.

Notes

- 1 Reproduced from *Journal of Chronic Diseases*, **39**, Brody, J. A. and Schneider, E. L., Diseases and disorders of aging: an hypothesis, pages 871–876, Copyright 1986, with permission from Elsevier.
- 2 Reproduced from *The Journals of Gerontology Series A: Biological Sciences and Medical Sciences*, **58**, Blumenthal, H. T., The aging–disease dichotomy: true or false?, pages M138–M145, Copyright 2003, with permission from Oxford University Press.

References

- Cai, W. and Chen, X. (2007) Nanoplatforms for targeted molecular imaging in living subjects. *Small*, **11**, 1840–54.
- Cheng, M.M., Cuda, G., Bunimovich, Y.L., Gaspari, M., Heath, J.R., Hill, H.D., Mirkin, C.A., Nijdam, A.J., Terracciano, R., Thundat, T. and Ferrari, M. (2006) *Biology*, **10**, 11–19.
- Gupta, A.K. and Gupta, M. (2005) Synthesis and surface engineering of iron oxide nanoparticles for biomedical applications. *Biomaterials*, **26**, 3995–4021.

Multiple Choice Questions

Questions Different types of question i.e. Multiple Choice Questions, Extended Matching Questions. Accordingly, calixarenes containing four phenol groups 39a–e exist as cone conformers. These are quite often put on a website but may still be typeset - Requirements are:

1 Multiple choice questions

For each question below, what is the most likely answer? Select ONE option from the answers supplied.

1.1 Ion Channels and Currents

1.1.1 Potassium



- 1 In a diagram of AP shown below, which one of the following currents is active where answers arrow is pointing?
 - A Ito
 - B IK1
 - C INa
 - D ICa

- 2 In a diagram of AP shown below, which one of the following currents is active where answers arrow is pointing?
 - A Ito
 - B IK1
 - C INa
 - D ICa

- 3 In a diagram of AP shown below, which one of the following currents is active where answers arrow is pointing?
 - A Ito
 - B IK1
 - C INa
 - D ICa

50 | *Multiple Choice Questions*

- 9** In a diagram of AP shown below, which one of the following currents is active where answers arrow is pointing?
- A** Ito
 - B** IK1
 - C** INa
 - D** ICa
- 10** In a diagram of AP shown below, which one of the following currents is active where answers arrow is pointing?
- A** Ito
 - B** IK1
 - C** INa
 - D** ICa
- 11** In a diagram of AP shown below, which one of the following currents is active where answers arrow is pointing?
- A** Ito
 - B** IK1
 - C** INa
 - D** ICa

A

Simulating the Bloch Equations

In a real magnetic resonance (MR) experiment, there are many sources of magnetic fields in addition to \mathbf{B}_0 . The *chemical shift* modulates the effective field strength that a nucleus experiences due to shielding effects of the electron shell. The strength of the effect depends on the bonding state of the hydrogen atom, and is therefore different for spins constituting free water and those that are part of lipids, giving rise to the *fat-water shift*. In addition to \mathbf{B}_1 -fields used to flip the magnetization into the transverse plane, position-dependent magnetic field gradients along the z-axis (see Section 1.6.1) are used to manipulate the magnetization during the experiment. We can therefore express the effective magnetic field in the rotating frame as

$$x = t^3 - 30t^2 + 5 \quad (\text{A.1})$$

Of all these field components, B_0 is the strongest with a typical magnitude of 1.5 or 3 T on clinical magnetic resonance imaging (MRI) scanners. The gradients typically induce field variations in the order of a few tens of millitesla. B_1 usually has a magnitude in the range of tens of 11 T. The chemical shift is very weak, causing a field modulation of 1.3 ppm (parts per million) between water and fat. It is therefore only relevant for B_0 and is negligible for all other field components. B_1 fields are designed to rotate in the (x,y)-plane and therefore do not have a z-component. The precession in such a complex setting can be parameterized by a precession frequency vector

$$a(t) = \frac{d^2x}{dt^2} = 6t - 60 \quad (\text{A.2})$$

and the angle between the magnetization and the magnetic field is given by if \mathbf{M}' was aligned with \mathbf{B} at $t = 0$.

With this vector notation, we can express the precession in the rotating frame 1 as by adding T_2 and T_2 relaxation terms, we can express the Bloch equation (1.26) in the rotating frame as and the longitudinal equilibrium magnetization M_0 as defined in Eq. (1.7) (which is independent of the coordinate system and therefore not marked with a prime). In order to solve the differential equation (AS), we introduce the quantity \mathbf{h}' :

In order to simulate the time evolution of the magnetization, Eq. (All) can be solved for a number of time steps $tk = k \cdot \Delta t$. It is important to note that Eq. (All) was derived under the assumption of a constant matrix \mathbf{W}' , implying a constant \mathbf{B}' -vector in the rotating frame.



Glossary

account classification The way in which suppliers of electricity, natural gas, or fuel oil classify and bill their customers. Commonly used account classifications are “Residential,” “Commercial,” “Industrial,” and “Other.” Suppliers’ definitions of these terms vary from supplier to supplier. In addition, the same customer may be classified differently by each of its energy suppliers.

account of others (natural gas) Natural gas deliveries for the account of others are deliveries to customers by transporters that do not own the natural gas but deliver it for others for a fee. Included are quantities covered by long-term contracts and quantities involved in short-term or spot market sales.

accounting system A method of recording accounting data for a utility or company or a method of supplying accounting information for controlling, evaluating, planning and decision-making.



References

- 1 Perina, J. (1972) Coherence of Light, Van Nostrand, London.
- 2 Louisell, W.H. (1973) Quantum Statistical Properties of Radiation, John Wiley & Sons, Inc., New York.
- 3 Loudon, R. (1973) Quantum Theory of Light, Oxford University Press, Oxford.
- 4 Allen, L. and Eberly, J.H. (1975) Optical Resonance and Two-Level Atoms, John Wiley & Sons, Inc., New York.
- 5 Perina, J. (1984) Quantum Statistics of Linear and Nonlinear Optical Phenomena, D. Reidel Publishing Company, Dordrecht.
- 6 Gardiner, C.W. (1991) Quantum Noise, Springer-Verlag, Berlin, Heidelberg.
- 7 Meystre, P. and Sargent, M. III (1991) Elements of Quantum Optics, Springer-Verlag, Berlin, Heidelberg.
- 8 Walls, D.F. and Milburn, G.J. (1994) Quantum Optics, Springer-Verlag, Berlin, Heidelberg.
- 9 Vogel, W. and Welsch, D.-G. (1994) Lectures on Quantum Optics, Akademie Verlag, Berlin.
- 10 Scully, M.O. and Zubairy, M.S. (1997) Quantum Optics, Cambridge University Press, Cambridge.
- 11 Barnett, S.M. and Radmore, P.M. (1997) Methods in Theoretical Quantum Optics, Clarendon Press, Oxford.
- 12 Puri, R.R. (2001) Mathematical Methods of Quantum Optics, Springer, Berlin.
- 13 Dicke, R.H. (1954) *Physical Review*, 93, 99.
- 14 (a) Perelomov, A. (1986) Generalized Coherent States R. (1990) *Reviews of Modern Physics*, 62, 867.
- 15 Radcliffe, J.M. (1971) *Journal of Physics A: General Physics*, 4, 313.



Index

a

- absorbance spectrum 66, 70
 - diffraction 70
- adhesion 114
- absorption/scattering spectrum, *see* biological windows
- absorption techniques, gas adsorption 243
- air-solvent interface 69
- alkane 88
- alkanethiol-capped gold cluster 246
- alkanethiol molecules, lattice of 88
- alkoxysilanes 77
- alkyl chain ligands 177
- alloy
 - Au/Ag 95
 - nanomaterials, surface segregation 16
- alumina membrane 62
- amorphous silica, calcination 60
- amphiphilic molecules 211, 221
 - lipids 211
- anisotropy 151
- antiferromagnetic materials 180, *see also* iron oxide
 - antiferromagnetism 180
- apolar solvents 175
- atomic force microscope (AFM) 201
- Au-Ni-CNT microrods, scanning electron microscope (SEM) image 219
- b**
- baffling process 203
- band 146
 - conduction 146, 148
 - valence 146
- barcoding 218
- bidentate ligand 176
- binary atomic lattices 187
 - CaF₂ structure 187
 - NaCl structure 187
- binary ordered arrays, formation 88
- binary superlattice 187
- bioconjugation technique 213, 226
- biological tissues, absorption/scattering spectrum 107
- biological windows 105, 107
 - importance 107
- bionano 40, 189
 - interface 37–45
 - cancer cells 37
 - magnetothermal 41
 - photothermal treatment 41
 - schematic presentation 40, 41
- biosensors 75, 77
- block copolymers 208, 210, 211
- blood stream, drugs concentration 75
- body-centered cubic (bcc) phase 209
- Bohr radius 149
- Boltzmann constant 148
- bottom-up techniques 118
- Braggs law 68, 71
 - refractive index 71
 - bionano applications 167
 - bionano aspects 163
 - doping of 160
 - synthesis 151
- bridging group 175



“keywords/abstract

Dear Author,

Keywords and abstracts will normally not be included in the print version of your chapter but only in the online version (unless specifically agreed by Wiley/Wiley VCH)”.

Abstract

The first part of this chapter outlines the requirements for the individual assemblies of a modern UHPLC system. The differences between low-pressure and high-pressure mixing and their advantages and disadvantages are discussed. Furthermore, current UHPLC injection modes are described. The differences between fixed-loop and flow-through autosamplers are explained, and practical hints are given. Regarding the temperature control of the mobile and stationary phases, the influence of temperature on the resulting separation is shown. In addition, the use of column switching valves for routine applications is described. In the context of very narrow peaks in UHPLC, general requirements for UHPLC detectors are discussed. Another focus is the explanation of proper connection technology of the individual UHPLC modules. For this purpose, the influence of plastic- and stainless-steel-based connection technology on the resulting chromatography is shown.

Keywords

high- and low-pressure mixing system; fixed-loop and flow-through injection; column oven; UHPLC detectors; capillaries and fittings

Affiliation for the Authors

Steffen Wiese¹, Michael Heidorn², and Frank Steiner²

¹Chromsystems, Munich and Terence Hetzel, IUTA, Duisburg, Germany

²Thermo Fischer Scientific, Dornierstr. 4, 82110 Germering/Munich, Germany

**Biochemical Principles and
Mechanisms of Biosynthesis
Biodegradation of Polymers**

B. Cornils, W. A. Herrmann (Eds.)

**Applied Homogeneous Catalysis with
Organometallic Compounds**

A Comprehensive Handbook in Two Volumes

1996

ISBN: 978-3-527-29286-1

M. Beller, C. Bolm (Eds.)

Transition Metals for Organic Synthesis

Building Blocks and Fine Chemicals

1998

ISBN: 978-3-527-29501-1

A. Togni, R. L. Halterman (Eds.)

Metallocenes

1998

ISBN: 978-3-527-29539-9

P. J. Stang (Eds.)

Metal-catalyzed Cross-coupling Reactrom

1998

ISBN: 978-3-527-29421-X

B. Cornils, W. A. Herrmann (Eds.)

**Applied Homogeneous
Catalysis with Organometallic
Compounds**

**A Comprehensive Handbook
in Two Volumes**

1996

ISBN: 978-3-527-29286-1

E. Chang, F. Hussain, T. Dillon (Eds.)

**Trust and Reputation for
Service-Oriented
Environments**

**Technologies For Building Business
Intelligence And Consumer Confidence**

2006

ISBN: 978-3-527-01547-9

M. Beller, C. Bolm (Eds.)

**Transition Metals for Organic
Synthesis**

Building Blocks and Fine Chemicals

1998

ISBN: 978-3-527-29501-1

B. Cornils, W. A. Herrmann (Eds.)

The Shanty Chor

**A Comprehensive Handbook in
Two Volumes**

1996

ISBN: 978-3-527-29286-9

A. Togni, R. L. Halterman (Eds.)

Metallocenes

1998

ISBN: 978-3-527-29539-9

H. Misawa, S. Juodkazis (Eds.)

3D Laser Microfabrication

Principles and Applications

2006

ISBN: 978-3-527-31055-5

Wiley Handbooks in

FINANCIAL ENGINEERING AND ECONOMETRICS

Advisory Editor

Ruey S. Tsay

The University of Chicago Booth School of Business USA

The dynamic and interaction between financial markets around the world have changed dramatically under economic globalization. In addition, advances in communication and data collection have changed the way information is processed and used. In this new era, financial instruments have become increasingly sophisticated and their impacts are far-reaching. The recent financial (credit) crisis is a vivid example of the new challenges we face and continue to face in this information age. Analytical skills and ability to extract useful information from mass data, to comprehend the complexity of financial instruments, and to assess the financial risk involved become a necessity for economists, financial managers, and risk management professionals. To master such skills and ability, knowledge from computer science, economics, finance, mathematics and statistics is essential. As such, financial engineering is cross-disciplinary, and its theory and applications advance rapidly.

The goal of this Handbook Series is to provide a one-stop source for students, researchers, and practitioners to learn the knowledge and analytical skills they need to face today's challenges in financial markets. The Series intends to introduce systematically recent developments in different areas of financial engineering and econometrics. The coverage will be broad and thorough with balance in theory and applications. Each volume will be edited by leading researchers and practitioners in the area and covers state-of-the-art methods and theory of the selected topic.

Published Wiley Handbooks in Financial Engineering and Econometrics

Bauwens, Hafner, and Laurent · *Handbook of Volatility Models and Their Applications*

Brandimarte · *Handbook in Monte Carlo Simulation: Applications in Financial Engineering, Risk Management, and Economics*

Chan and Wong · *Handbook of Financial Risk Management: Simulations and Case Studies*

Cruz, Peters, and Shevchenko · *Fundamental Aspects of Operational Risk and Insurance Analytics: A Handbook of Operational Risk*

James, Marsh, and Sarno · *Handbook of Exchange Rates*



Mechanism of Biosynthesis

Nomenklatur der
Organischen Chemie

Edited by Hans-Georg Joost and Gerhard Eisenbrand

*in collaboration with
Gerald Böhm
Uwe Diederichsen*

Second Revised Edition

WILEY Blackwell

Monitoring

An Introduction

Gerald Böhm

WILEY Blackwell

Author

Linda E. Reichl

University of Texas
Center for Complex Quantum Systems
Austin, TX 78712
USA

Cover

Bose–Einstein condensates;
courtesy of Daniel J. Heinzen

All books published by Wiley-VCH are carefully produced. Nevertheless, authors, editors, and publisher do not warrant the information contained in these books, including this book, to be free of errors. Readers are advised to keep in mind that statements, data, illustrations, procedural details or other items may inadvertently be inaccurate.

Library of Congress Card No.: applied for

British Library Cataloguing-in-Publication Data:

A catalogue record for this book is available from the British Library.

Bibliographic information published by the Deutsche Nationalbibliothek

The Deutsche Nationalbibliothek lists this publication in the Deutsche Nationalbibliografie; detailed bibliographic data are available on the Internet at <http://dnb.d-nb.de>.

© 2016 WILEY-VCH Verlag GmbH & Co. KGaA, Boschstr. 12, 69469 Weinheim, Germany

All rights reserved (including those of translation into other languages). No part of this book may be reproduced in any form – by photoprinting, microfilm, or any other means – nor transmitted or translated into a machine language without written permission from the publishers. Registered names, trademarks, etc. used in this book, even when not specifically marked as such, are not to be considered unprotected by law.

Cover Design Formgeber, Mannheim, Germany

Typesetting le-tex publishing services GmbH, Leipzig, Germany

Printing and Binding

Print ISBN 978-3-527-41349-2

ePDF ISBN 978-3-527-69046-6

ePub ISBN 978-3-527-69048-0

Mobi ISBN 978-3-527-69047-3

oBook ISBN 978-3-527-69049-7

Printed on acid-free paper.

This edition first published 2017
© 2017

All rights reserved. No part of this publication may be reproduced, stored in a retrieval system, or transmitted, in any form or by any means, electronic, mechanical, photocopying, recording or otherwise, except as permitted by law. Advice on how to obtain permission to reuse material from this title is available at <http://www.wiley.com/go/permissions>.

The right of Jane Brown and Mark Smith to be identified as the authors of this work has been asserted in accordance with law.

Registered Offices

John Wiley & Sons, Inc., 111 River Street, Hoboken, NJ 07030, USA

John Wiley & Sons Ltd, The Atrium, Southern Gate, Chichester, West Sussex, PO19 8SQ, UK

Editorial Office

The Atrium, Southern Gate, Chichester, West Sussex, PO19 8SQ, UK

For details of our global editorial offices, customer services, and more information about Wiley products visit us at www.wiley.com.

Wiley also publishes its books in a variety of electronic formats and by print-on-demand. Some content that appears in standard print versions of this book may not be available in other formats.

Limit of Liability/Disclaimer of Warranty

While the publisher and authors have used their best efforts in preparing this work, they make no representations or warranties with respect to the accuracy or completeness of the contents of this work and specifically disclaim all warranties, including without limitation any implied warranties of merchantability or fitness for a particular purpose. No warranty may be created or extended by sales representatives, written sales materials or promotional statements for this work. The fact that an organization, website, or product is referred to in this work as a citation and/or potential source of further information does not mean that the publisher and authors endorse the information or services the organization, website, or product may provide or recommendations it may make. This work is sold with the understanding that the publisher is not engaged in rendering professional services. The advice and strategies contained herein may not be suitable for your situation. You should consult with a specialist where appropriate. Further, readers should be aware that websites listed in this work may have changed or disappeared between when this work was written and when it is read. Neither the publisher nor authors shall be liable for any loss of profit or any other commercial damages, including but not limited to special, incidental, consequential, or other damages.

Library of Congress Cataloging-in-Publication Data

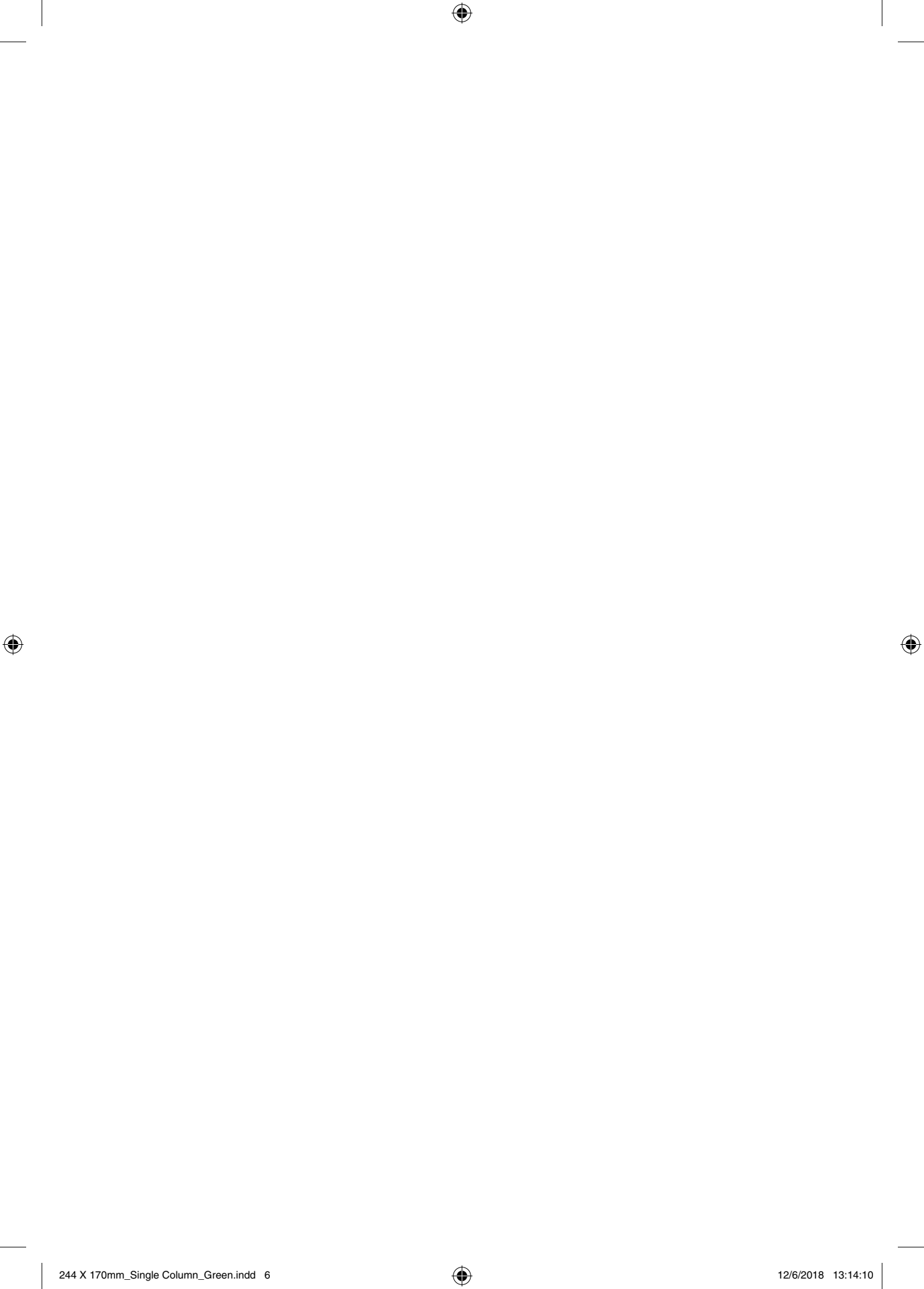
Cover image:

Cover design by

Set in 9.5/12.5pt STIXTwoText by SPi Global, Pondicherry, India

10 9 8 7 6 5 4 3 2 1

to Hans-Martin



Brief Contents

List of Contributors *xi*

Foreword *xiii*

Preface *xv*

Part I Metal Oxide Nanomaterials 1

- 1 The Biomimetic Synthesis of Metal Oxide Nanomaterials 3
- 2 Synthesis of Symmetric and Asymmetric Nanosilica for Materials, Optical and Medical Applications 55
- 3 Sources of Natural Flavors 90
- 4 Mechanism of Color Perception 110
- 5 Preparation of Plant Material for Extraction 150
- 6 Methods of Extraction of Essential Oils 180

Index 000



Contents

List of Contributors *xi*

Foreword *xiii*

Preface *xv*

Part I Metal Oxide Nanomaterials *1*

- 1 The Biomimetic Synthesis of Metal Oxide Nanomaterials** *3*
Leila F. Deravi, Joshua D. Swartz and David W. Wright
 - 1.1 Introduction *3*
 - 1.2 Metal Oxides in Nature *4*
 - 1.2.1 Components of Biomineralization *5*
 - 1.2.2 Biomineralization Optimization *6*
 - 1.3 Biomimetic Synthesis of Metal Oxide Nanomaterials *7*
 - 1.4 Constrained Biomineralization *8*
 - 1.4.1 Bacterial Synthesis of Metal Oxide Nanomaterials *8*
 - 1.4.2 Synthesis of Protein-Functionalized Ferromagnetic Co_3O_4 Nanocrystals *9*
 - 1.4.3 Room-Temperature Synthesis of Barium Titanate *10*
 - 1.4.4.1 Biomimetic Synthesis of Iron Oxide *11*
- 2 Synthesis of Symmetric and Asymmetric Nanosilica for Materials, Optical and Medical Applications** *55*
Yongquan Qu, Jennifer Lien and Ting Guo
 - 2.1 Introduction *55*
 - 2.2 Synthesis of Nanosilica *59*
 - 2.2.1 Symmetric Nanosilica *59*
 - 2.2.1.1 Catalytic Methods *63*
 - 2.2.1.2 Noncatalytic Growth *65*
 - 2.2.2 Asymmetric Silica Nanomaterials *68*
 - 2.2.2.1 Catalytic Growth *68*
 - 2.2.2.2 Noncatalytic Growth *69*
 - 2.3 Characterization *70*
 - 2.4 Applications of Symmetric and Asymmetric Nanosilica *72*

Index *000*



Contents

Foreword *xiii*

Preface *xv*

Part I Metal Oxide Nanomaterials 1

- 1 The Biomimetic Synthesis of Metal Oxide Nanomaterials 3**
 - 1.1 Introduction 3
 - 1.2 Metal Oxides in Nature 4
 - 1.2.1 Components of Biomineralization 5
 - 1.2.2 Biomineralization Optimization 6
 - 1.3 Biomimetic Synthesis of Metal Oxide Nanomaterials 7
 - 1.4 Constrained Biomineralization 8
 - 1.4.1 Bacterial Synthesis of Metal Oxide Nanomaterials 8
 - 1.4.2 Synthesis of Protein-Functionalized Ferromagnetic Co_3O_4 Nanocrystals 9
 - 1.4.3 Room-Temperature Synthesis of Barium Titanate 10
 - 1.4.4 Biomimetic Synthesis of Magnetite 11
 - 1.4.4.1 Biomimetic Synthesis of Iron Oxide 11
- 2 Synthesis of Symmetric and Asymmetric Nanosilica for Materials, Optical and Medical Applications 55**
 - 2.1 Introduction 55
 - 2.2 Synthesis of Nanosilica 59
 - 2.2.1 Symmetric Nanosilica 59
 - 2.2.1.1 Catalytic Methods 63
 - 2.2.1.2 Noncatalytic Growth 65
 - 2.2.2 Asymmetric Silica Nanomaterials 68
 - 2.2.2.1 Catalytic Growth 68
 - 2.2.2.2 Noncatalytic Growth 69
 - 2.3 Characterization 70
 - 2.4 Applications of Symmetric and Asymmetric Nanosilica 72

Index 000



Contents

Foreword *xiii*

Preface *xv*

Part I Metal Oxide Nanomaterials 1

1 The Biomimetic Synthesis of Metal Oxide Nanomaterials 3

Introduction 3

Metal Oxides in Nature 4

 Components of Biomineralization 5

 Biomineralization Optimization 6

Biomimetic Synthesis of Metal Oxide Nanomaterials 7

Constrained Biomineralization 8

 Bacterial Synthesis of Metal Oxide Nanomaterials 8

 Synthesis of Protein-Functionalized Ferromagnetic Co_3O_4 Nanocrystals 9

 Room-Temperature Synthesis of Barium Titanate 10

 Biomimetic Synthesis of Magnetite 11

 Biomimetic Synthesis of Iron Oxide 11

2 Synthesis of Symmetric and Asymmetric Nanosilica for Materials, Optical and Medical Applications 55

Introduction 55

Synthesis of Nanosilica 59

 Symmetric Nanosilica 59

 Catalytic Methods 63

 Noncatalytic Growth 65

 Asymmetric Silica Nanomaterials 68

 Catalytic Growth 68

 Noncatalytic Growth 69

Characterization 70

Applications of Symmetric and Asymmetric Nanosilica 72

Index 000



List of Contributors

Andrew B. Adams

Department of Surgery
Emory Transplant Center
Emory University School of Medicine
Atlanta
USA

Maria-Luisa Alegre, MD, PhD

Associate Professor
Department of Medicine, Section of
Rheumatology
Gwen Knapp Center for Lupus and
Immunology Research
The University of Chicago
Chicago
USA

Agnes M. Azimzadeh, PhD

Assistant Professor of Surgery
Department of Surgery
University of Maryland School of
Medicine
Baltimore
USA

William M. Baldwin III

Department of Immunology
Cleveland Clinic Lerner College of
Medicine
Department of Pathology
Case Western Reserve University
School of Medicine
Cleveland
USA

Jonathan S. Bromberg, MD, PhD

Professor of Surgery and Microbiology
and Immunology
Department of Surgery
University of Maryland School of
Medicine
Baltimore
USA

J. Michael Cecka

UCLA Immunogenetics Center
Department of Pathology and
Laboratory Medicine
David Geffen School of Medicine at
UCLA
Los Angeles
USA

Anil Chandraker, MD, FASN, FRCP

Transplant Research Center
Renal Division
Brigham and Women's Hospital
Harvard Medical School
Boston
USA

Sung Choi, MD

Blood and Marrow Transplantation
Program
Department of Internal Medicine
Division of Hematology/Oncology
University of Michigan
Comprehensive Cancer Center
Ann Arbor
USA

Anita S. Chong, PhD

Department of Surgery, Section of
Transplantation
The University of Chicago
Chicago
USA

Yaozhong Ding, PhD

Assistant Professor
Department of Surgery
University of Maryland School of Medicine
Baltimore
USA

Gunilla Einecke

Department of Nephrology
Hannover Medical School
Hannover
Germany

Robert L. Fairchild

Department of Immunology
Cleveland Clinic Lerner College of
Medicine
Department of Pathology
Case Western Reserve University
School of Medicine
Cleveland
USA

Philip F. Halloran, MD, PhD

Alberta Transplant Applied Genomics
Centre
Department of Medicine
Division of Nephrology and Transplant
Immunology
University of Alberta
Edmonton
Canada

Choli Hartono

Department of Medicine
Weill Cornell Medical College
New York
USA

Timm Heinbokel

Division of Transplant Surgery and
Transplant Surgery Research Laboratory
Brigham and Women's Hospital
Harvard Medical School
Boston
USA

Yiming Huang

Institute for Cellular Therapeutics
University of Louisville
Louisville and Duke University
Raleigh
USA

Suzanne T. Ildstad, MD

Director, Institute for Cellular Therapeutics
Jewish Hospital Distinguished
Professor of Transplantation
Distinguished University Scholar
Professor of Surgery, Physiology,
Immunology
University of Louisville
Louisville and Duke University
Raleigh
USA

Haofeng Ji

Dumont-UCLA Transplantation Center
Division of Liver and Pancreas
Transplantation, Department of Surgery,
David Geffen School of Medicine at UCLA
Los Angeles
USA

Bibo Ke

Dumont-UCLA Transplantation
Center Division of Liver and Pancreas
Transplantation, Department of
Surgery
David Geffen School of Medicine at UCLA
Los Angeles
USA

Foreword

The dilemma of rapidly emerging fields is that reviews are often outdated before they are printed. To make a contribution that would endure, we knew we had to go beyond a snapshot of the current state of fragment-based drug discovery and instead provide a framework for upcoming advances. To achieve this goal, we needed to convince leading scientists to take time from their busy schedules to write chapters. Fortunately, nearly all those we approached agreed; and what you hold in your hands is a virtual, although not comprehensive, “Who’s Who” in fragment-based drug discovery. We are extremely grateful to all of our contributors for the quality of their chapters.

One striking feature of this book is that more than half of the chapters come from industry-based researchers; and even many of the academic contributors have close ties to industry. It has been alleged that the best science is done in academia; this book proves that this is not necessarily the case. Part of the reason may be that many of the techniques involved require expensive equipment and infrastructure as well as large collaborations between scientists from disparate disciplines – collaborations that would be difficult to set up outside industry. The multidisciplinary nature of fragment-based approaches shows in this volume: contributors include computational chemists, NMR spectroscopists, X-ray crystallographers, mass-spectrometrists, as well as organic and medicinal chemists.

Although fragment-based strategies for drug discovery have now pervaded laboratories across the world, the ultimate success of any drug discovery technology is measured in the quantity and quality of drugs that it produces. Fragment-based drug discovery has only been practical for the past decade, too soon to expect it to produce marketed drugs; but we believe these will come in time. Moreover, many of the techniques and concepts described in this book will alter drug discovery endeavors in subtle, tangential ways. Ideally, readers will be inspired to improve the methods described here, or even to develop fundamentally new methods for fragment-based drug discovery. But even if this book only changes the way medicinal chemists approach lead optimization, or persuades them to look more closely at weak but validated hits, it will have served its purpose.

Basely, March 2006

Wolfgang Jahnke
Daniel A. Erlanson



Symbols and Abbreviations

Symbols

α	electron spin quantum number $m_s = 1/2$ angle, alternating parameter anisotropic exchange parameter
α_n	nuclear spin quantum number $m_I = 1/2$
β	spin quantum number $m_s = -1/2$ angle
β_n	nuclear spin quantum number $m_I = -1/2$
δ_{ij}	Kronecker δ
θ	angle Curie-Weiss constant
Δ_H	line-width
$\Delta H_{1/2}$	half height line-width
ΔH_{pp}	peak-to-peak line-width
ΔH_{msl}	maximum-slope line-width
$\Delta H\omega_{1/2}, \Delta H\omega_{pp}$	line-width in frequency
ϵ_0	dielectric constant
ϵ_F	Fermi energy
η	$ J'/J $
Γ	molecular field coefficient
γ	gyromagnetic ratio exchange interaction parameter anisotropic exchange parameter
γ_n	nuclear gyromagnetic ratio
φ	molecular orbital relaxation function
Ψ	molecular orbital
ψ	atomic orbital
ν	frequency
μ	magnetic permeability
μ_0	magnetic permeability of free space



Color Plates

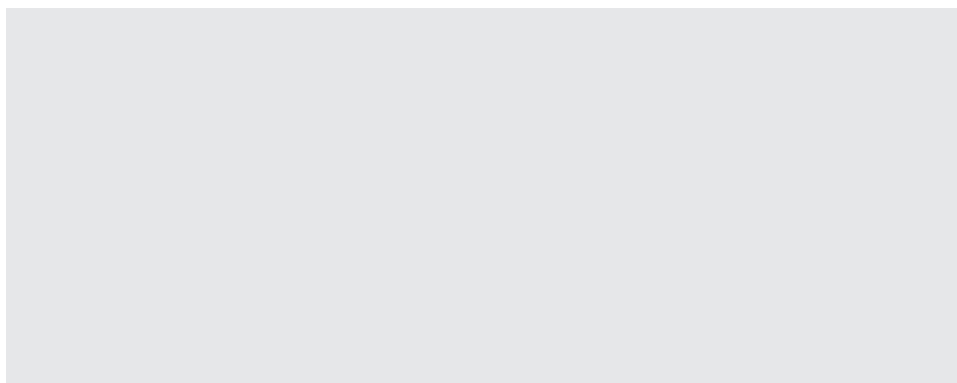


Figure 1.6 See text page 00 for full figure caption.

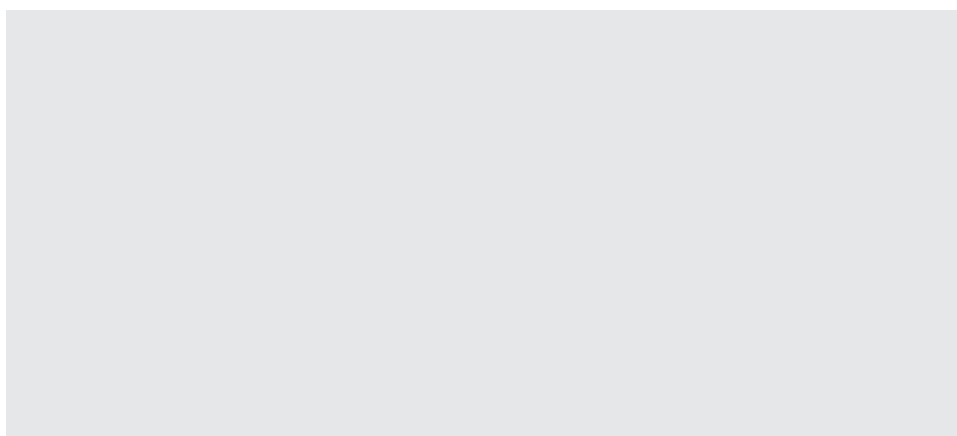


Figure 1.7 See text page 00 for full figure caption.



About the Companion Website

Practical Physiotherapy for Small Animal Practice is accompanied by a companion website:



www.wiley.com/go/

The website includes:

- Client education handouts.



Part IV

Summaries and Visions

Bold Glance into the Future—Where no Man has Gone Before



5

cDNA and Microarray-based Technologies

5.1 Introduction

The molecular characterization of tumor-associated antigens (TAA) recognized by T cells [1] revolutionized the field of tumor immune biology providing conclusive evidence that CD8+ cytotoxic T cells (CTLs) specifically recognize and kill autologous cancer through recognition of molecularly-defined cancer-specific elements.

5.1.1 CEA Gene Family, Genomic Localization, Protein Structure

CEA is encoded by the CEA-related cell-cell adhesion molecule 5 (CEACAM5) gene, which belongs to the CEA gene family and in humans consists of 22 expressed members and 12 pseudogenes [3,4].

5.1.1.1 Animal Models for CEA

Mice are commonly used to analyze the efficacy of tumor therapies and mechanisms of tumor rejection. However, this species cannot be utilized to evaluate CEA-based therapies since no CEACAM5 ortholog exists in rodents.

5.1.1.1.1 Models for CEACAM5 Containing a Bacterial Artificial Chromosome

Either cosmid clones containing the CEACAM5 gene or a bacterial artificial chromosome (BAC) clone, which comprises part of the gene cluster surrounding CEACAM5, served as a genetic source. This cluster includes CEACAM6 and CEACAM3.

Antibody Delivery of Radionuclides, Drugs and Effector Molecules The use of low molecular weight single chain antibody fragments and pre-targeting has been found to enhance the sensitivity of tumor visualization as well as increasing the delivered therapeutic dose by separating the antibody therapeutic radionuclide that binds to the tumor-localized antibody.

SubParagraph Title: Nuclear Angular Momentum and Magnetic Moment The conformational flexibility of calixarenes is usually explained by the presence of intramolecular hydrogen bonds, which is related to the number of free phenol groups. Accordingly, calixarenes containing four phenol groups 39a–e exist as cone conformers.

Book Title: Subtitle, First Edition. Edited by Author/Editor Name.

© 2015 John Wiley & Sons, Ltd. Published 2015 by John Wiley & Sons, Ltd.



5

cDNA and Microarray-based Technologies

Introduction

The molecular characterization of tumor-associated antigens (TAA) recognized by T cells [1] revolutionized the field of tumor immune biology providing conclusive evidence that CD8+ cytotoxic T cells (CTLs) specifically recognize and kill autologous cancer through recognition of molecularly-defined cancer-specific elements.

CEA Gene Family, Genomic Localization, Protein Structure

CEA is encoded by the CEA-related cell-cell adhesion molecule 5 (CEACAM5) gene, which belongs to the CEA gene family and in humans consists of 22 expressed members and 12 pseudogenes [3,4].

Animal Models for CEA

Mice are commonly used to analyze the efficacy of tumor therapies and mechanisms of tumor rejection. However, this species cannot be utilized to evaluate CEA-based therapies since no CEACAM5 ortholog exists in rodents. This problem was circumvented by introducing the human CEACAM5 gene into the germ line of mice [52–54].

Models for CEACAM5 Containing a Bacterial Artificial Chromosome

Either cosmid clones containing the CEACAM5 gene or a bacterial artificial chromosome (BAC) clone, which comprises part of the gene cluster surrounding CEACAM5, served as a genetic source. This cluster includes CEACAM6 and CEACAM3.

Antibody Delivery of Radionuclides, Drugs and Effector Molecules Delivery of radio-nuclides to tumors using murine and human anti-CEA antibodies has been studied for many years [70]. The use of low molecular weight single chain antibody fragments and pre-targeting has been found to enhance the sensitivity of tumor visualization as well as increasing the delivered therapeutic dose by separating the antibody targeting to the tumor from the subsequent delivery of the therapeutic radionuclide that binds to the tumor-localized antibody.

SubParagraph Title: Nuclear Angular Momentum and Magnetic Moment The conformational flexibility of calixarenes is usually explained by the presence of intramolecular hydrogen bonds, which is related to the number of free phenol groups. Accordingly, calixarenes, containing four phenol groups 39a–e exist as cone conformers.

Delivery of radio-nuclides to tumors using murine and human anti-CEA antibodies has been studied for many years [70]. The use of low molecular weight single chain antibody fragments and pre-targeting has been found to enhance the sensitivity of tumor visualization as well as increasing the delivered therapeutic dose by separating the antibody targeting to the tumor from the subsequent delivery of the therapeutic radionuclide that binds to the tumor-localized antibody.

11

Carcinoembryonic Antigen

Decoding the CEA-Related Cell-Cell Adhesion Molecule

The molecular characterization of tumor-associated antigens (TAA) recognized by T cells [1] revolutionized the field of tumor immune biology providing conclusive evidence that CD8+ cytotoxic T cells (CTLs) specifically recognize and kill autologous cancer through recognition of molecularly-defined cancer-specific elements. Since then a myriad of TAA have been identified that has triggered their utilization as anti-cancer vaccines [2–8].

11.1 CEA Biology

11.1.1 CEA Gene Family, Genomic Localization, Protein Structure

CEA is encoded by the CEA-related cell-cell adhesion molecule 5 (CEACAM5) gene, which belongs to the CEA gene family and in humans consists of 22 expressed members and 12 pseudogenes [3,4]. The CEA family has been subdivided into the CEACAM and pregnancy-specific glycoprotein (PSG) subgroups.

11.1.2 CEA as a Tumor Marker for Prognosis and Post-surgery Follow-up

11.1.2.1 Animal Models for CEA

Antibody Delivery of Radionuclides, Drugs and Effector Molecules Using Murine and Human Anti-CEA Antibodies Delivery of radio-nuclides to tumors using murine and human anti-CEA anti-bodies has been studied for many years [70]. The use of low molecular weight single chain antibody fragments and pre-targeting has been found to enhance the sensitivity of tumor visualization as well as increasing the delivered therapeutic dose by separating the antibody targeting to the tumor from the subsequent delivery of the therapeutic radionuclide that binds to the tumor-localized antibody. The use of low molecular weight single chain antibody fragments and pre-targeting has been found to enhance the sensitivity of tumor visualization as well as increasing.

The use of low molecular weight single chain antibody fragments and pre-targeting has been found to enhance the sensitivity of tumor visualization as well as increasing the delivered therapeutic dose by separating the antibody targeting to the tumor from the subsequent delivery of the therapeutic radionuclide that binds to the tumor-localized antibody.



2

Trust and Reputation for Service-Oriented Environments Technologies for Building Business Intelligence and Consumer Confidence

Fillers, Filled Polymers and Polymer Blends and Furthermore Nuclear
Angular Momentum and Magnetism

2.1 Intermolecular Interactions Physical Picture, Computational Methods and Model Potentials Nuclear Angular Momentum and Magnetic Moment

The molecular characterization of tumor-associated antigens (TAA) recognized by T cells [1] revolutionized the field of tumor immune biology providing conclusive evidence that CD8+ cytotoxic T cells (CTLs) specifically recognize and kill autologous cancer through recognition of molecularly-defined cancer-specific elements. Since then a myriad of TAA have been identified that has triggered their utilization as anti-cancer vaccines [2–8].

2.1.1 Networking and Online Games Understanding and Engineering Multiplayer Internet Games Nuclear Angular Momentum and Magnetic Moment

CEA is encoded by the CEA-related cell-cell adhesion molecule 5 (CEACAM5) gene, which belongs to the CEA gene family and in humans consists of 22 expressed members and 12 pseudogenes [3,4]. The CEA family has been subdivided into the CEACAM and pregnancy-specific glycoprotein (PSG) subgroups.

2.1.1.1 Nuclear Angular Momentum and Magnetic Moment Respectively the Digital Photographer's Guide to Color Management

Apically expressed CEA on normal epithelial cells is shed into the lumen possibly by the action of phospholipases and through the exfoliation of turned-over cells. Thus CEA does not have access the bloodstream. Expression on less differentiated unpolarized tumor cells, however, allows released CEA to enter blood and lymphatic vessels through the intercellular spaces, which can lead to elevated CEA concentrations in the sera of tumor patients.

Fillers, Filled Polymers and Polymer Blends and Furthermore Nuclear Angular Momentum and Magnetism CEA is encoded by the CEA-related cell-cell adhesion molecule 5 (CEACAM5) gene, which belongs to the CEA gene family and in humans consists of 22 expressed members and 12 pseudogenes [3,4]. In the past, the CEA family has been subdivided into the CEACAM and pregnancy-specific glycoprotein (PSG) subgroups.

Book Title: Subtitle, First Edition. Edited by Author/Editor Name.

© 2015 John Wiley & Sons, Ltd. Published 2015 by John Wiley & Sons, Ltd.

11

Carcinoembryonic Antigen

Decoding the CEA-Related Cell-Cell Adhesion Molecule

The molecular characterization of tumor-associated antigens (TAA) recognized by T cells [1] revolutionized the field of tumor immune biology providing conclusive evidence that CD8⁺ cytotoxic T cells (CTLs) specifically recognize and kill autologous cancer through recognition of molecularly-defined cancer-specific elements. Since then a myriad of TAA have been identified that has triggered their utilization as anti-cancer vaccines [2–8].

11.1 CEA Biology

11.1.1 CEA Gene Family, Genomic Localization, Protein Structure

CEA is encoded by the CEA-related cell-cell adhesion molecule 5 (CEACAM5) gene, which belongs to the CEA gene family and in humans consists of 22 expressed members and 12 pseudogenes [3,4]. The CEA family has been subdivided into the CEACAM and pregnancy-specific glycoprotein (PSG) subgroups.

11.1.2 CEA as a Tumor Marker for Prognosis and Post-surgery Follow-up

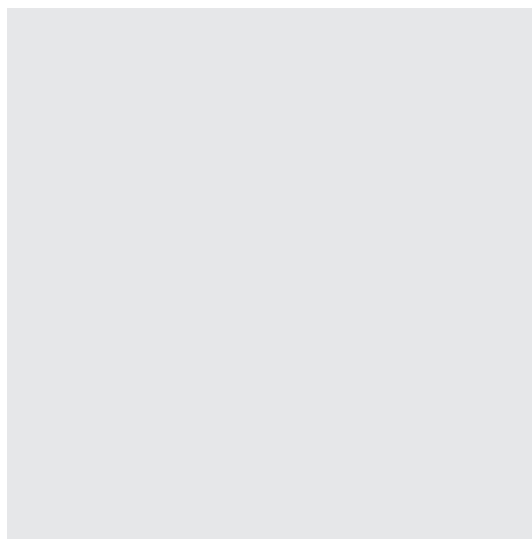
11.1.2.1 Animal Models for CEA

Antibody Delivery of Radionuclides, Drugs and Effector Molecules Using Murine and Human Anti-CEA Antibodies Delivery of radio-nuclides to tumors using murine and human anti-CEA anti-bodies has been studied for many years [70]. The use of low molecular weight single chain antibody fragments and pre-targeting has been found to enhance the sensitivity of tumor visualization as well as increasing the delivered therapeutic dose by separating the antibody targeting to the tumor from the subsequent delivery of the therapeutic radionuclide that binds to the tumor-localized antibody. The use of low molecular weight single chain antibody fragments and pre-targeting has been found to enhance the sensitivity of tumor visualization as well as increasing. The use of low molecular weight single chain antibody fragments and pre-targeting has been found to enhance the sensitivity of tumor visualization as well as increasing the delivered therapeutic dose by separating the antibody targeting to the tumor from the subsequent delivery of the therapeutic radionuclide that binds to the tumor-localized antibody.

11

Carcinoembryonic Antigen

Decoding the CEA-Related Cell-Cell Adhesion Molecule



The molecular characterization of tumor-associated antigens (TAA) recognized by T cells [1] revolutionized the field of tumor immune biology providing conclusive evidence that CD8+ cytotoxic T cells (CTLs) specifically recognize and kill autologous cancer through recognition of molecularly-defined cancer-specific elements. Since then a myriad of TAA have been identified that has triggered their utilization as anti-cancer vaccines [2–8].

11.1 CEA Biology

11.1.1 CEA Gene Family, Genomic Localization, Protein Structure

CEA is encoded by the CEA-related cell-cell adhesion molecule 5 (CEACAM5) gene, which belongs to the CEA gene family and in humans consists of 22 expressed members and 12 pseudogenes [3,4]. The CEA family has been subdivided into the CEACAM and pregnancy-specific glycoprotein (PSG) subgroups.

11.1.2 CEA as a Tumor Marker for Prognosis and Post-surgery Follow-up

11.1.2.1 Animal Models for CEA

Antibody Delivery of Radionuclides, Drugs and Effector Molecules Using Murine and Human Anti-CEA Antibodies Delivery of radio-nuclides to tumors using murine and human anti-CEA anti-bodies has been studied for many years [70]. The use of low molecular weight single chain antibody fragments and pre-targeting has been found to enhance the sensitivity of tumor visualization as well as increasing the delivered therapeutic dose by separating the antibody targeting to the tumor from the subsequent delivery of the therapeutic radionuclide that binds to the tumor-localized antibody. The use of low molecular weight single chain antibody fragments and pre-targeting has been found to enhance the sensitivity of tumor visualization as well as increasing. The use of low molecular weight single chain antibody fragments and pre-targeting has been found to enhance the sensitivity of tumor visualization as well as increasing the delivered therapeutic dose by separating the antibody targeting to the tumor from the subsequent delivery of the therapeutic radionuclide that binds to the tumor-localized antibody.

11

Carcinoembryonic Antigen

Wolfgang Zimmermann^{1,3} and Robert Kammerer²

¹ Helmholtz Centre for Infection Research, Department of Systems Immunology, Inhoffenstr. 7, 38124, Braunschweig, Germany

² Bio Center for Life Science, University of Technology Braunschweig, Spielmannstr. 7, 38106, Braunschweig, Germany

³ Institute for Molecular and Clinical Immunology, Otto-von-Guericke University, Leipziger Str. 44, 39120, Magdeburg, Germany

The very essence of cardiovascular practice is the early detection of heart failure

Sir Thomas Lewis, 1933

11.1 Introduction

The molecular characterization of tumor-associated antigens (TAA) recognized by T cells [1] revolutionized the field of tumor immune biology providing conclusive evidence that CD8+ cytotoxic T cells (CTLs) specifically recognize and kill autologous cancer through recognition of molecularly-defined cancer-specific elements.

11.2 CEA Biology

11.2.1 CEA Gene Family, Genomic Localization, Protein Structure

CEA is encoded by the CEA-related cell-cell adhesion molecule 5 (CEACAM5) gene, which belongs to the CEA gene family and in humans consists of 22 expressed members and 12 pseudogenes [3,4]. The CEA family has been subdivided into the CEACAM and pregnancy-specific glycoprotein (PSG) subgroups. Apically expressed CEA on normal epithelial cells is shed into the lumen possibly by the action of phospholipases and through the exfoliation of turned-over cells. Thus CEA does not have access the bloodstream. Expression on less differentiated unpolarized tumor cells, however, allows released CEA to enter blood and lymphatic vessels through the intercellular spaces, which can lead to elevated CEA concentrations in the sera of tumor patients.

Book Title: Subtitle, First Edition. Edited by Author/Editor Name.

© 2015 John Wiley & Sons, Ltd. Published 2015 by John Wiley & Sons, Ltd.

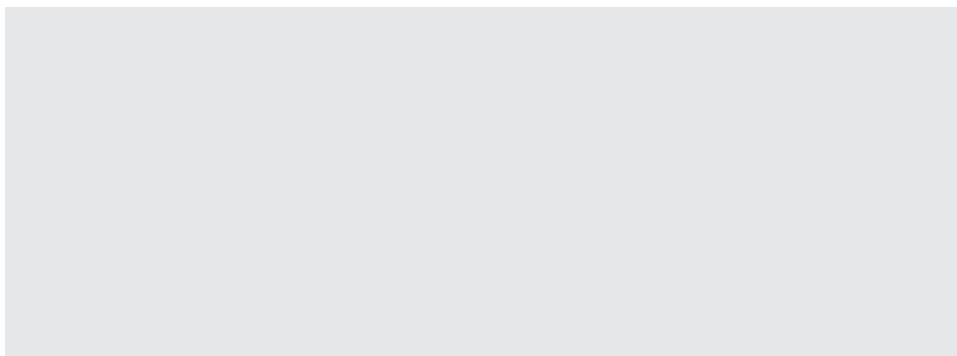


Figure 1.6 Illustration of catalytically grown β -Ga₂O₃ nanoparticles. *Source:* Reprinted with permission from Ref. [38]; © 2007 American Chemical Society.

Traditionally, synthetic approaches for the production of functional metal oxide materials have involved are estimated to reach an outstanding US \$100 billion per Figure 1.6 facility by the year 2020, as the demand for smaller, lighter and faster materials continues to grow [1]. But, more importantly, manufacturers are progressing in this manner at the expense of the environment, as they accumulate hazardous chemical wastes [2]. For decades, research teams in the semiconductor industry have been seeking alternative methods to passivate not only the rate of waste production but also the cost of spending. As mentioned above, the photoresist should be thin according to the distance of localization of the optical near-field around the nanoaperture. On the other hand, the photoresist should have the dry etching resistance so that the latent image can be transferred to the lower layer substrate. To separate the function of the Figure 1.7 thin film and the dry etching resistance, we used a trilayer resist process; the upper layer is an ultrathin photoresist, the middle layer is thin spin on glass (SOG), and the lower layer is a resin.

As mentioned above, the photoresist should be thin according to the distance of localization of the optical near-field around the nanoaperture. On the other hand, the photoresist should have the dry etching resistance so that the latent image can be transferred to the

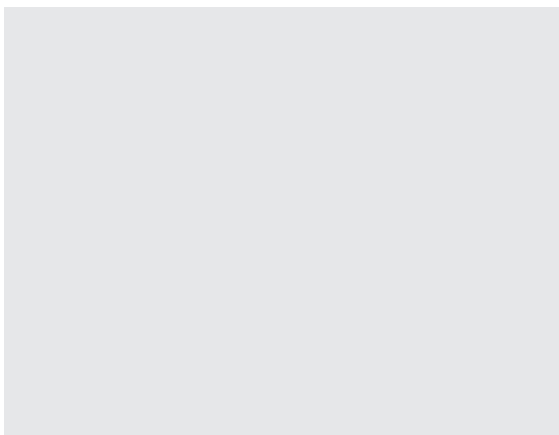


Figure 1.7 Transmission electron microscopy images (scale bar = 20 nm) of magnetosomes from various bacterial strains. (a) Pseudo-hexagonal prism; (b) Cubo-octahedral crystal; (c) Å Tooth-shaped. Transmission electron microscopy images (scale bar = 20 nm) of magnetosomes from various bacterial strains. *Source:* Reproduced with permission from Ref. [17]; © 2007, Wiley-VCH Verlag GmbH & Co. KGaA.

lower layer substrate. To separate the function of the thin film and the dry etching resistance, we used a trilayer resist process; the upper layer is an ultrathin photoresist, the middle layer is thin spin on glass (SOG), and the lower layer is a resin. The patterns of shallow latent images in the upper layer are transferred to the thin SOG layer of excellent dry-etching resistance, and these are transferred in the lower layer further.

Traditionally, synthetic approaches for the production of functional metal oxide materials have involved high-temperature reaction environments with energy intensive techniques such as laser ablation, ion implantation, chemical vapor deposition (CVD), photolithography or thermal decomposition [1]. The incorporation of these techniques has provided a rapid prototyping technique, essential for the commercial development of current minimum feature-sized semiconducting integrated circuits. However, the production of these devices has been achieved at a high price, with the primary challenges currently faced by high-throughput fabrication laboratories including the high cost of laborers and instruments, high temperature reaction conditions, and a surplus in generated waste [1]. In fact, the cost of fabrication facilities are estimated to reach an outstanding US \$100 billion per facility by the year 2020, as the demand for smaller, lighter and faster materials continues to grow [1]. But, more importantly, manufacturers are progressing in this manner at the expense of the environment, as they accumulate hazardous chemical wastes [2]. For decades, research teams in the semiconductor industry have been seeking alternative methods to passivate not only the rate of waste production but also the cost of spending.

As mentioned above, the photoresist should be thin according to the distance of localization of the optical near-field around the nanoaperture. On the other hand, the photoresist should have the dry etching resistance so that the latent image can be transferred to the lower layer substrate. To separate the function of the thin film and the dry etching resistance, we used a trilayer resist process; the upper layer is an ultrathin photoresist, the middle layer is thin spin on glass (SOG), and the lower layer is a resin. The patterns of shallow latent images in the upper layer are transferred to the thin SOG layer of excellent dry-etching resistance, and these are transferred in the lower layer further.

Figure 1.8 shows the appearance of a prototype device of optical near-field lithography [7]. The features of the prototype device are as follows. This device is compact, with a footprint of about 2m [1]. It has symmetric structure to compensate thermal expansion and temperature drift, and the hanging controlling structure is introduced to avoid floor vibrations. In addition, it has a double clean structure, and the near-field photomask and the wafer are kept in a local clean environment by controlling a flow of clean air of the device inside.

Bioinspired research is based on identifying and emulating the principles of biomineralization in natural systems, instead of copying them directly. In fact, most strategies incorporated by natural systems are not directly applicable to engineered materials, so the need for alternative synthetic routes are required for the incorporation of non-natural elements, such as barium, nickel, copper or aluminum, with functional nanoscale properties [1,8]. From a materials perspective, highly intact biological structures such as diatoms, bacteria, proteins or butterfly wings provide an excellent source of inspiration for their synthesis. In this chapter we have included the details of a wide variety of mediated nanomaterial syntheses, their response to variable parameters, and their ability to retain a functionalized, controlled stability over time.

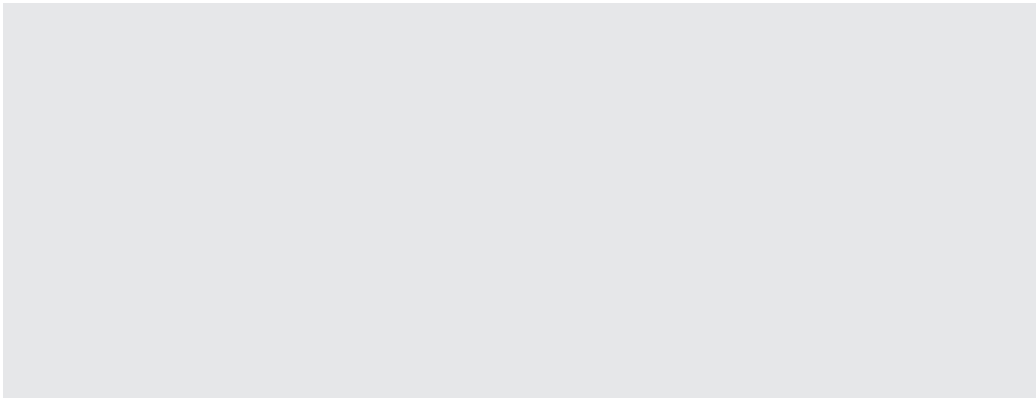


Figure 1.8 Appearance of a prototype device of optical near-field lithography.

As mentioned above, the photoresist should be thin according to the distance of localization of the optical near-field around the nanoaperture. On the other hand, the photoresist should have the dry etching resistance so that the latent image can be transferred to the lower layer substrate. To separate the function of the thin film and the dry etching resistance, we used a trilayer resist process; the upper layer is an ultrathin photoresist, the middle layer is thin spin on glass (SOG), and the lower layer is a resin. The patterns of shallow latent images in the upper layer are transferred to the thin SOG layer of excellent dry-etching resistance, and these are transferred in the lower layer further.

Figure 1.8 shows the appearance of a prototype device of optical near-field lithography [7]. The features of the prototype device are as follows. This device is compact, with a footprint of about 2m [2]. It has symmetric structure to compensate thermal expansion and temperature

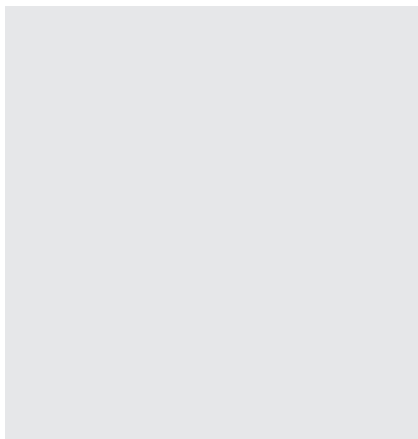


Figure 1.9 Distribution of structures for variable pH samples. *Source:* Reprinted with permission from Ref. [33]; © 2007, American Chemical Society.

Figure 1.10 (a) Inside the prototype device of the near-field lithography. (b) Illumination of i-line light for exposure from the back side of the near-field photomask. (c) Close-up from the side of the near-field photomask and the photoresist on the wafer. They are brought into contact with each other within the localizing distance of the optical near-field.

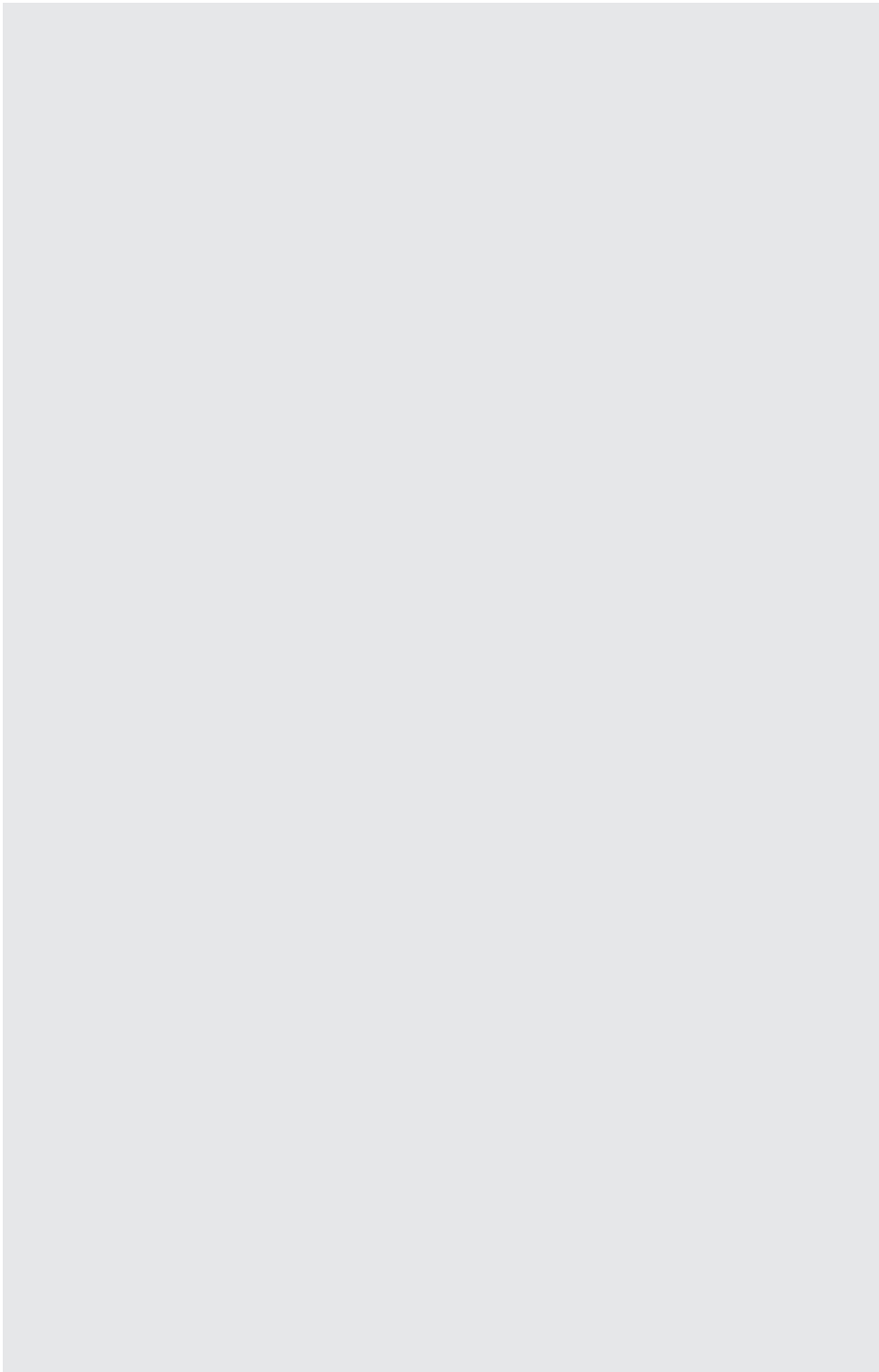


Table 1.1 Results for the comparison of processes.

Performance metric	NH ₃	CH ₄	C ₃ H ₈ ref.	C ₃ H ₈ POX
Energy efficiency	27%	30%	23%	16%
Volumetric fuel energy density (Wh l ⁻¹)	1570	170	1740	1920
Gravimetric fuel energy density (Wh kg ⁻¹)	2580	1610	2540	3900
Volumetric system energy density (Wh l ⁻¹)	1510	130	1650	1800
Gravimetric system energy density (Wh kg ⁻¹)	2370	320	2320	3340

drift, and the hanging controlling structure is introduced to avoid floor vibrations. In addition, it has a double clean structure, and the near-field photomask and the wafer are kept in a local clean environment by controlling a flow of clean air of the device inside.

Bioinspired research is based on identifying and emulating the principles of biomineralization in natural systems, Figure 1.9 instead of copying them directly. In fact, most strategies incorporated by natural systems are not directly applicable to engineered materials, so the need for alternative synthetic routes are required for the incorporation of non-natural elements, such as barium, nickel, copper or aluminum, with functional nanoscale properties [1,8]. Table 1.1 from a materials perspective, highly intact biological structures such as diatoms, bacteria, proteins or butterfly wings provide an excellent source of inspiration for their synthesis. In this chapter we have included the details of a wide variety of mediated nanomaterial syntheses, their response to variable parameters, and their ability to retain a functionalized, controlled stability over time.

The lowest system energy densities. Both the system and fuel volumetric energy densities of methane direct oxidation are very low, due to the large volume required for the storage of the gases (methane and oxygen). Moreover, the gravimetric fuel energy density of methane is

Table 1.2 Propagation rate constants (k_p) and the selectivity parameters ($\beta = k_p/k_{tr1}$) for the polymerization of ϵ -caprolactone [95].^{a)}

Active species	$\frac{k_p}{L \text{ mol}^{-1} \text{ s}^{-1}}$	$b = \frac{k_p}{k_{tr1}} / \frac{L \text{ mol}^{-1}}{L \text{ mol}^{-1}}$
...-(CH ₂) ₅ O ⁻ Na ⁺	□1.70	1.6×10^3
...-(CH ₂) ₅ O-Sm[O(CH ₂) ₅ -...] ₂	2.00	2.0×10^3
...-(CH ₂) ₅ O-Al(C ₂ H ₅) ₂	0.03	4.6×10^4
...-(CH ₂) ₅ O-Al[CH ₂ CH(CH ₃) ₂] ₂	0.03	7.7×10^4
...-(CH ₂) ₅ O-Al[O(CH ₂) ₅ -...] ₂	0.50	3.0×10^5
...-(CH ₂) ₅ O-AlO ₂ SB ^{b)}	0.35	□10 ⁶

a) Polymerization conditions: 20°C, THF solvent.

b) Polymerization conditions: 80°C, THF solvent, SBO2: (S)-(+)-2,2'-[1,1'-binaphthyl-2,2'-diylbis-(nitrylomethylidyne)]-diphenolate ligand (A. Duda and A. Kowalski, unpublished results). SB=Schiff's base.

Table 1.3 Results for the comparison of processes.

Performance metric	NH ₃	CH ₄	C ₃ H ₈ ref.	C ₃ H ₃ POX
Energy efficiency	27%	30%	23%	16%
Volumetric fuel energy density (Wh l ⁻¹)	1570	170	1740	1920
Gravimetric fuel energy density (Wh kg ⁻¹)	2580	1610	2540	3900
Volumetric system energy density (Wh l ⁻¹)	1510	130	1650	1800
Gravimetric system energy density (Wh kg ⁻¹)	2370	320	2320	3340

Data from Higinbotham et al. 1967. The membrane potential was measured as – 110 mV Table from Taiz & Zeiger Thrid Ed Table 6.1

Table 1.4 Results for the comparison of processes.

R of functional molecule ^a	Cycle	Catalyst ^b	Conversion (%)	M _n (kg mol ⁻¹)	M _w /M _n	Reference
CH ₃ , CH=CH ₂ , (CH ₂) ₃ COOH	D ₄	SR	~90	10–43	—	[87]
CH=CH ₂ , (CH ₂) ₃ NHSi(CH ₃) ₃ , (CH ₂) ₃ -acrylate, (CH ₂) ₃ COOH	D ₄	SR	80–90	0.8–1.2	1.4–1.9	[57]
H	D ₄	AC	80	8	1.9	[88]
H, CH ₃ , CH=CH ₂ , (CH ₂) ₃ COOH	D ₄	SR	—	—	—	[89]

a) The chain-terminating agent has the following structure: R–Si(CH₃)₂–O–Si(CH₃)₂–R, unless stated in the table.

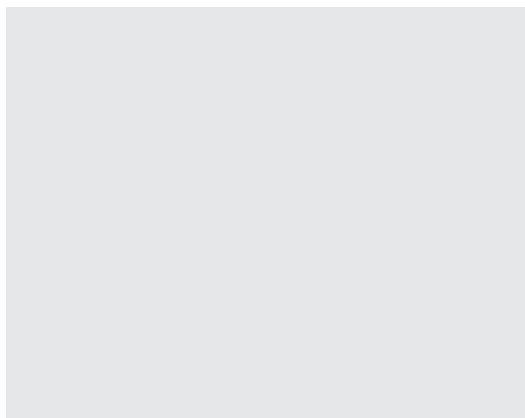
b) SR: sulfonic resin; AC: activated clay.

low, due to the mass of oxygen which is accounted for [2]. The large difference in gravimetric energy density of methane direct oxidation is due to the mass of the gas Table 1.2 cartridges. Despite lower energy conversion efficiency, the propane-based processes lead to higher energy densities than the ammonia-based process, because of the intrinsic difference in energy density between the two fuels. From a materials perspective, highly intact biological structures such as diatoms, bacteria. In this chapter we have included the details of a wide variety of mediated nanomaterial syntheses, their response to variable parameters, and their ability to retain a functionalized, controlled stability over time. With the exception of the

Table 1.5 Results for the comparison of processes.

Characteristic	Issues	Needs
Laminar flows	Mixing relies on molecular diffusion only and is slow	Efficient micromixers of low pressure drop
Small size	Difficult to load enough catalyst and ensure complete conversion	Develop deposition schemes and structures to load enough catalyst; high integration of reactor(s) and separation units for compact systems; fast chemistry/process; very active (and selective) catalyst.
Reactors shake in portable devices	Moveable parts break; bypass from pellet settling can occur	Monolithic structures with no moveable parts
High pressure drop	Pressure drop increases with decreasing pellet size	Open (extruded monolith-like) geometries
Transient operation very common	Most designs rely on steady state operation and control; catalysts, which are stable under steady state conditions, may deactivate during start up and shut down; start-up can be slow.	Get heat in and out of the system quickly; develop appropriate designs and strategies; models for dynamics.

Figure 1.11 Distribution of structures for variable pH samples. *Source:* Reprinted with permission from Ref. [33]; © 2007, American Chemical Society.



process requiring gas storage, the fuel energy density and system energy density give the same qualitative comparison among processes.

Thus, replicates on the same array and replicates in different experiments should not be mixed since they have different characteristics and cannot be treated as independent replicates. Important issues are:

- are the distributional assumptions valid is the number of replicates sufficient to detect the fold change that you are interested in?
- are the replicates independent of each other?
 - is the number of replicates sufficient to detect the fold change because it does not conversion efficiency that you are interested in?
 - are outliers removed from the samples?

Most commonly, modifications of four different tests are applied in microarray data analysis. These tests are implemented in statistical software packages such as R/Bioconductor or SAS:

- 1) Student's t-test is the number of replicates sufficient to detect the fold change that you are interested
- 2) Welch's test is the number of replicates sufficient to detect the fold because it does not conversion efficiency change that you are interested
- 3) Permutation tests.

While the first two tests assume Gaussian distributed data and the P -values are calculated by a probability distribution, the latter two are nonparametric and the P -values are calculated based on combinatorial arguments.

- | | |
|-----------------------------------|--------------------|
| • Distilled water | 23.3 μl |
| • 10 \times PCR buffer | 4.0 μl |
| • dNTP Mix (FDD) | 0.3 μl |
| • H-AP primer (2 μM)* | 4.0 μl |
| • H-T11M (2 μM) | 4.0 μl |
| • cDNA template | 4.0 μl |
| • Taq DNA polymerase | 0.4 μl |
| • Total volume | 40.0 μl |

Table 1.6 Species of marine invertebrates containing glycolipids.

Phylum	Subphylum	Class	Trivial name	Species
Chordata	Tunicata	Ascidacea	Tunicate	<i>Microcosmus sulcatus</i> (now accepted <i>M. vulgaris</i> ⁽¹⁾) <i>Phallusia fumigata</i>
Cnidaria	—	Anthozoa	Soft coral	1) <i>Lobophytum crassum</i> 2) <i>Lobophytum</i> sp. 3) <i>Sarcophyton ehrenbergi</i> 4) <i>Metridium senile</i>
Echinodermata	Asterozoa	Asteroidea	Sea anemone Starfish	• <i>Acanthaster planci</i> • <i>Allostichaster inaequalis</i> • <i>Anasterias minuta</i> • <i>Aphelasterias japonica</i> • <i>Asterias amurensis</i> • <i>Asterias amurensis versicolor</i> • <i>Asterias rubens</i> • <i>Stellaster equestris</i>
		Ophiuroidea	Brittle star	<i>Ophiocoma scolopendrina</i>
	Crinozoa	Crinoidea	Feather star	<i>Comanthus japonica</i> (now accepted <i>Oxycomanthus japonicus</i> ⁽¹⁾) <i>Comanthina schlegeli</i> (now accepted <i>Comaster schlegelii</i>)

Source: Queen Square Brain Bank.

Both the system and fuel volumetric energy densities of methane direct oxidation are very low, due to the large volume required for the storage of the gases (methane and oxygen). Moreover, the gravimetric fuel energy density of methane is low, due to the mass of oxygen which is accounted for [2]. The large difference in gravimetric energy density of methane direct oxidation is due to the mass of the gas cartridges.

Yields, and reaction specificities. The first detailed study of the mechanism of these “on water” reactions has now been reported by Jung and Marcus [10]. Synthetic aqueous organic synthesis was born, also because efficient work-up procedures are possible for these “on water” reactions. For a general review, the reader is referred to Chapter 7.

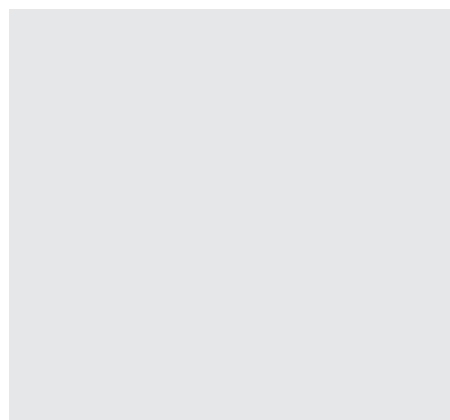


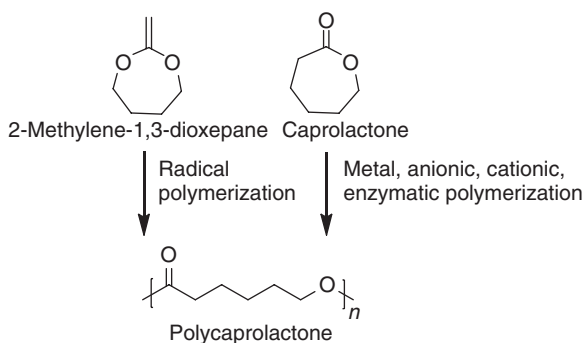
Figure 1.12 Distribution of structures for variable pH samples. *Source:* Reprinted with permission from Ref. [33]; © 2007, American Chemical Society.

11.3 Water, the Ultimate Green Solvent

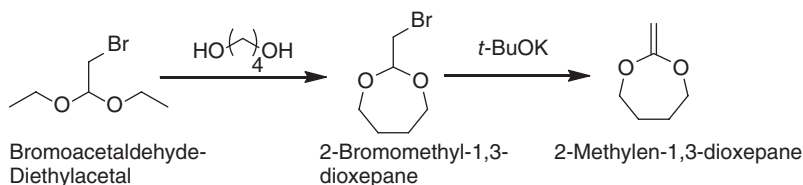
Fredrik Nilsson

In the second half of the 1990s, it was recognized that “benign by design” was too strongly restricted to environmental care, and Anastas and Williamson [13] even concluded, “one obvious but important point: nothing is benign.” The holistic concept of green chemistry became accepted world-wide. Although attempts have been made to quantify the degree of greenness, particularly by Sheldon [15], it has not been found possible to include the many complex factors that determine “greenness” in generally applicable parameters.

Aspirin as a Household Remedy Against Fever, Inflammation, and Pain Soon after the introduction of ASA into medical use under the brandname “aspirin,” Anastas in his many influential publications.



Scheme 1.31



Scheme 1.32

... As soon as you feel yourself ill, you should go to bed and have a hot-water bottle at your feet. You should drink hot chamomilae tea or grog in order to sweat and should take 3 tablets of aspirin a day. If you follow these instructions you will recover with in a few days, in most cases...

Kölner Stadtanzeiger, March 6, 1924

This extract is remarkable for several reasons: during the past 25 years of practical use, aspirin had become a drug whose name was not only well known to health professionals but also to the general public.

Certainly, the flu pandemia with millions of victims alone in Europe at the beginning of the last century as well as the limited availability of antipyretic analgesics other than aspirin contributed to this. However, the compound was generally recommended—and accepted—by the lay man and doctors—as a household remedy for treating pain, fever, inflammation, and many other kinds of feeling bad, although essentially nothing was known about the mechanisms of Anastas in his many influential publications. The holistic concept of green chemistry became accepted world-wide. Although attempts have been made to quantify the degree of greenness, particularly by action behind these multiple activities of the drug.

Thus, replicates on the same array and replicates in different experiments should not be mixed since they have different characteristics and cannot be treated as independent replicates. Important issues are:

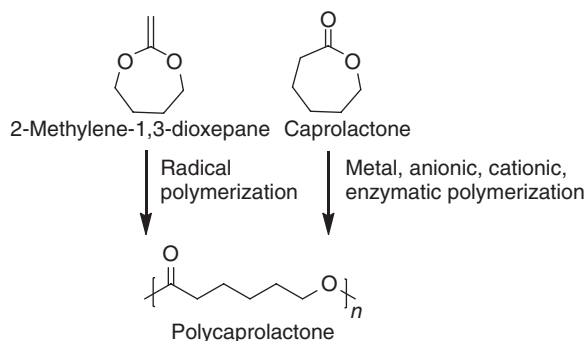
Most commonly, modifications of four different tests are applied in microarray data analysis. These tests are implemented in statistical software packages such as R/Bioconductor or SAS.

The conformational flexibility of calixarenes is usually explained by the presence of intramolecular hydrogen bonds, which is related to the number of free phenol groups. Accordingly, calixarenes containing four phenol groups 39a–e exist as cone conformers.

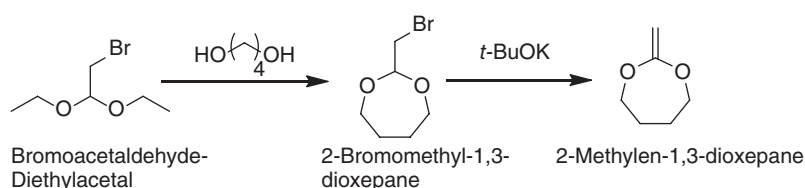
$$\rho(z)v_w = \rho_w^{\text{bulk}} v_w \exp(-v_w \beta [\pi(z) - \pi^{\text{bulk}}]) \quad (2.17)$$

$$\rho(z)v_w = \rho_w^{\text{bulk}} v_w \exp(-v_w \beta [\pi(z) - \pi^{\text{bulk}}]) - q_i \beta [\psi(z) - \psi^{\text{bulk}}] \quad (2.18)$$

Both the system and fuel volumetric energy densities of methane direct oxidation are very low, due to the large volume required for the storage of the gases (methane and oxygen). Moreover, the gravimetric fuel energy density of methane is low, due to the mass of oxygen which is accounted for [2]. The comparison of the two idealized possibilities for propane fuel processing reactions shows that energy conversion efficiency is not a suitable metric for man-portable applications, because it does not account for the water weight and volume;



Scheme 1.31



Scheme 1.32

the higher energy efficiency of steam reforming is due to the generation of additional hydrogen in the reactor.

The lowest system energy densities. Both the system and fuel volumetric energy densities of methane direct oxidation are very low, due to the large volume required for the storage of the gases (methane and oxygen). Moreover, the gravimetric fuel energy density of methane is low, due to the mass of oxygen which is accounted for [2]. The large difference in gravimetric energy density of methane direct oxidation is due to the mass of the gas Table 1.2 cartridges. Despite lower energy conversion efficiency, the propane-based processes lead to higher energy densities than the ammonia-based process, because of the intrinsic difference in energy density between the two fuels. From a materials perspective, highly intact biological structures such as diatoms, bacteria. In this chapter we have included the details of a wide variety of mediated nanomaterial syntheses, their response to variable parameters, and their ability to retain a functionalized, controlled stability over time. With the exception of the process requiring gas storage, the fuel energy density and system energy density give the same qualitative comparison among processes.

The conformational flexibility of calixarenes is usually explained by the presence of intramolecular hydrogen bonds, which is related to the number of free phenol groups. Accordingly, calixarenes containing four phenol groups 39a–e exist as cone conformers.

$$V_i = [A_i r + (B_i / r^2)] \cos(\theta) \quad (2.19)$$

While the first two tests assume Gaussian distributed data and the *P*-values are calculated by a probability distribution, the latter two are nonparametric and the *P*-values are

Instrumental Box 4**Numerical Data Analysis**

The incorporation of these techniques has provided a rapid prototyping technique, essential for the commercial development of current minimum feature-sized semiconducting integrated circuits. However, the production of these devices has been achieved at a high price, with the primary challenges currently faced by high-throughput fabrication laboratories including the high cost of laborers and instruments, high-temperature reaction conditions, and a surplus in generated waste [1].

The versatility of biology's incredible portfolio encourages researchers to develop modified syntheses derived from Nature. Hence, their findings have been successfully organized into the field of biomimetics, or bioinspired research technological applications [8].

Source: The versatility of biology's incredible portfolio encourages researchers to develop modified syntheses derived from Nature

Instrumental Box 5

The incorporation of these techniques has provided a rapid prototyping technique, essential for the commercial development of current minimum feature-sized semiconducting integrated circuits. However, the production of these devices has been achieved at a high price, with the primary challenges currently faced by high-throughput fabrication laboratories including the high cost of laborers and instruments, high-temperature reaction conditions, and a surplus in generated waste [1].

In fact, the cost of fabrication facilities are estimated to reach an outstanding US \$100 billion per facility by the year 2020, as the demand for smaller, lighter and faster materials continues to grow [1].

calculated based on combinatorial arguments. Thus, replicates on the same array and replicates in different possibilities for propane experiments should not be mixed since they have different characteristics and cannot be treated as independent replicates. Important issues are:

$$E_1 = \frac{9\varepsilon_2\varepsilon_3}{\varepsilon_2\varepsilon_a + 2\varepsilon_3\varepsilon_b} E_0 (\cos\theta\hat{r} - \sin\theta\hat{\theta}) \quad (2.20)$$

Traditionally, synthetic approaches for the production of functional metal oxide materials have involved high-temperature reaction environments with energy-intensive techniques such as laser ablation, ion implantation, chemical vapor deposition (CVD), photolithography or thermal decomposition [1].

The ligation products are used immediately for transformation or stored at -20°C. For transformation, add 10 ml of each ligation mix to freshly thawed GH-competent cells and mix

Instrumental Box 6

The incorporation of these techniques has provided a rapid prototyping technique, essential for the commercial development of current minimum feature-sized semiconducting integrated circuits. However, the production of these devices has been achieved at a high price, with the primary challenges currently faced by high-throughput fabrication laboratories including the high cost of laborers and instruments, high-temperature reaction conditions, and a surplus in generated waste [1].

In fact, the cost of fabrication facilities are estimated to reach an outstanding US \$100 billion per facility by the year 2020, as the demand for smaller, lighter and faster materials continues to grow [1].

Biomimetics infers the manipulating and mimicking of natural architectures and processes of biologically produced minerals (biominerals) to direct the synthesis of non-natural materials.

well by finger-tipping and incubate on ice for 45 min. The large difference in gravimetric energy density of methane direct oxidation is due to the mass of the gas cartridges.

Both the system and fuel volumetric energy densities of methane direct oxidation are very low, due to the large volume required for the storage of the gases (methane and oxygen). Moreover, the gravimetric fuel energy density of methane is low, due to the mass of oxygen which is accounted for [2]. Despite lower energy conversion efficiency, the propane-based processes lead to higher energy densities than the ammonia-based process, because of the intrinsic difference in energy density between the two fuels. The comparison of the two idealized possibilities for propane fuel processing reactions shows that energy conversion efficiency is not a suitable metric for man-portable applications, because it does not account for the water weight and volume; the higher energy efficiency of steam reforming is due to the generation of additional hydrogen in the reactor.

The lowest system energy densities. Both the system and fuel volumetric energy densities of methane direct oxidation are very low, due to the large volume required for the storage of the gases (methane and oxygen). Moreover, the gravimetric fuel energy density of methane is low, due to the mass of oxygen which is accounted for [2]. The large difference in gravi-

One striking feature of this book is that more than half of the chapters come from industry-based researchers; and even many of the academic contributors have close ties to industry. It has been alleged that the best science is done in academia; this book proves that this is not necessarily the case.

Part of the reason may be that many of the techniques involved require expensive equipment and infrastructure as well as large collaborations between scientists from disparate disciplines—collaborations that would be difficult to set up outside industry. The multidisciplinary nature of fragment-based approaches shows in this volume: contributors include computational chemists, NMR spectroscopists, X-ray crystallographers, mass-spectrometrists, as well as organic and medicinal chemists.

One striking feature of this book is that more than half of the chapters come from industry-based researchers; and even many of the academic contributors have close ties to industry. It has been alleged that the best science is done in academia; this book proves that this is not necessarily the case.

Part of the reason may be that many of the techniques involved require expensive equipment and infrastructure as well as large collaborations between scientists from disparate disciplines—collaborations that would be difficult to set up outside industry. The multidisciplinary nature of fragment-based approaches shows in this volume: contributors include computational chemists, NMR spectroscopists, X-ray crystallographers, mass-spectrometrists, as well as organic and medicinal chemists.

metric energy density of methane direct oxidation is due to the mass of the gas Table 1.2 cartridges. Despite lower energy conversion efficiency, the propane-based processes lead to higher energy densities than the ammonia-based process, because of the intrinsic difference in energy density between the two fuels. From a materials perspective, highly intact biological structures such as diatoms, bacteria. In this chapter we have included the details of a wide variety of mediated nanomaterial syntheses, their response to variable parameters, and their ability to retain a functionalized, controlled stability over time. With the exception of the process requiring gas storage, the fuel energy density and system energy density give the same qualitative comparison among processes.

The ligation products are used immediately for transformation or stored at -20°C . For transformation, add 10 ml of each ligation mix to freshly thawed GH-competent cells and mix well by finger-tipping and incubate on ice for 45 min. Traditionally, synthetic approaches for the production of functional metal oxide materials have involved high-temperature reaction environments with energy-intensive techniques such as laser ablation, ion implantation, chemical vapor deposition (CVD), photolithography or thermal decomposition [1].

The dilemma of rapidly emerging fields is that reviews are often outdated before they are printed. To make a contribution that would endure, we knew we had to go beyond a snapshot of the current state of fragment-based drug discovery and instead provide a framework for upcoming advances. To achieve this goal, we needed to convince leading scientists to take time from their busy schedules to write chapters. Fortunately, nearly all those we approached agreed; and what you hold in your hands is a virtual, although not comprehensive, “Who’s Who” in fragment-based drug discovery. We are extremely grateful to all of our contributors for the quality of their chapters.

Fragment-based drug discovery has only been practical for the past decade, too soon to expect it to produce marketed drugs; but we believe these will come in time.

Techniques described in this book Moreover, many of the techniques and concepts described in this book will alter drug discovery endeavors in subtle, tangential ways. Ideally, readers will be inspired to improve the methods described here, or even to develop fundamentally new methods for fragment-based drug discovery. But even if this book only changes the way medicinal chemists approach lead optimization, or persuades them to look more closely at weak but validated hits, it will have served its purpose.

For instance, the architecture of one of the most abundant biological species on the planet – the virus – has recently been manipulated to serve as containers for the synthesis of a variety of functional molecular cargoes.

In fact, the cost of fabrication facilities are estimated to reach an outstanding US \$100 billion per facility by the year 2020, as the demand for smaller, lighter and faster materials continues to grow¹. But, more importantly, manufacturers are progressing in this manner at the expense of the environment, as they accumulate semiconductor hazardous chemical wastes [2].

For decades, research teams in the semiconductor industry have been seeking alternative methods to passivate not only the rate of waste production but also the cost of spending. The most accessible resource for the synthesis of functional materials under ambient conditions is found in biology.

Traditionally, synthetic approaches for the production of functional metal oxide materials have involved high-temperature reaction environments with energy intensive techniques such as laser ablation, ion implantation, chemical vapor deposition (CVD), photolithography or thermal decomposition [1]. The incorporation of these techniques has provided a rapid prototyping technique, essential for the commercial development of current minimum fragment-based drug discovery and instead provide a framework for upcoming advances.

The versatility of biology's incredible portfolio encourages researchers to develop modified syntheses derived from Nature. Hence, their findings have been successfully organized into the field of biomimetics, or bioinspired research, which encompasses alternative approaches towards developing nanomaterials with technological applications [8]. Based primarily on the designs, mechanisms and processes found in Nature, biomimetics.

As mentioned above, the photoresist should be thin according to the distance of localization of the optical near-field around the nanoaperture. On the other hand, the photoresist should have the dry etching resistance so that the latent image can be transferred to the lower layer substrate. To separate the function of the thin film and the dry etching resistance, we used a trilayer resist process; the upper layer is an ultrathin photoresist, the middle layer is thin spin on glass (SOG), and the lower layer is a resin.

The patterns of shallow latent images in the upper layer are transferred to the thin SOG layer of excellent dry-etching resistance, and these are transferred in the lower layer further. Figure 6.8 shows the appearance of a prototype device of optical near-field lithography [7]. The features of the prototype device are as follows. This device is compact, with a footprint of about 2×2 . It has symmetric structure to compensate thermal expansion and temperature drift, and the hanging structure is introduced to avoid floor vibrations.

Bioinspired research is based on identifying and emulating the principles of biomineralization in natural systems, instead of copying them directly. In fact, most strategies incorpo-

¹ A Q-switch is a device that is similar to a shutter that controls the laser resonator's ability to oscillate. In fact, the cost of fabrication facilities are estimated to reach an outstanding US \$100 billion per facility by the year 2020, as the demand for smaller.

rated by natural systems are not directly applicable to engineered materials, so the need for alternative synthetic routes are required for the incorporation of non-natural elements, such as barium, nickel, copper or aluminum, with functional nanoscale properties [1,8]. To achieve this goal, we needed to convince leading scientists to take time from their busy schedules to write chapters. feature-sized semiconducting integrated circuits. However, the production of these devices has been achieved at a high price, with the primary challenges currently faced by high-throughput fabrication laboratories including the high cost of laborers and instruments, at a high price, with the primary challenges currently faced by high-throughput fabrication laboratories including the high cost of laborers and instruments, high temperature reaction conditions, and a surplus in generated waste [1].

- 120 For decades, research teams in the semiconductor industry have been seeking alternative methods to passivate not only the rate of waste production but also the cost of spending. The most accessible resource for the synthesis of functional materials under ambient conditions is found in biology.

Bioinspired research is based on identifying and emulating the principles of biomineralization in natural systems, instead of copying them directly. In fact, most strategies incorporated by natural systems are not directly applicable to engineered materials, so the need for alternative synthetic routes are required for the incorporation of non-natural elements, such as barium, nickel, copper or aluminum, with functional nanoscale properties [1,8]. However, the production of these devices has been achieved at a high price, with the primary challenges currently faced by high-throughput fabrication laboratories including the high cost of laborers and instruments.

In Kupferchlorid und Kupfersulfatpentahydrat (siehe Abb. 4.18) sind giftig und inätzend, Quecksilberchlorid ist sehr giftig und inätzend, Schwefeldioxid ist giftig, Silbernitrat wirkt ätzend. Das Tragen einer Schutzbrille ist erforderlich. Dieser wird auf die Porzellanfilternutsche gegeben, zweimal mit Ethanol sowie mit Wasser gewaschen mit denen das $\text{Cr}(\text{H}_2\text{O})_6$ oder Kupfersulfatpentahydrat mit den viel H_2O und Schwefeldioxid-Druckgaszylinder,² destilliertes Wasser.

Surprisingly, the properties associated with metal oxides in technology are not so far removed from what is observed in natural systems. Through precisely tuned processes, Nature is able to synthesize a variety of metal oxide nanomaterials under ambient conditions; the magnetic navigation device found in magnetotactic bacteria (MTB) is one such example [17]. Here, magnetite (Fe_3O_4) nanocrystals are aligned with the Earth's geomagnetic field and contained within specific organelles known as magnetosomes [17]. Fresh water salmon, for example, utilizes these magnetic nanoparticles in the nasal cavities of their forehead as a biomagnetic compass during migration [18].

² A Q-switch is a device that is similar to a shutter that controls the laser resonator's ability to oscillate. This shutter effect allows one to spoil the resonator's 'Q-factor', keeping it low to prevent lasing action. Under these conditions, the laser highly intact biological structures such as diatoms, bacteria, proteins or butterfly wings gain material is able to store higher levels of energy. The extra stored energy is subsequently extracted as laser light emission in the form of extremely short pulse width, high-peak-power pulses.

1

cDNA and Microarray-based Technologies

CHAPTER MENU

Introduction, 1
 CEA Gene Family, Genomic Localization, Protein Structure, 1
 Animal Models for CEA, 1
 Models for CEACAM5 Containing a Bacterial Artificial Chromosome, 2

1.1 Introduction

The molecular characterization of tumor-associated antigens (TAA) recognized by T cells [1] revolutionized the field of tumor immune biology providing conclusive evidence that CD8+ cytotoxic T cells (CTLs) specifically recognize and kill autologous cancer through recognition of molecularly-defined cancer-specific elements.

1.2 CEA Gene Family, Genomic Localization, Protein Structure

CEA is encoded by the CEA-related cell-cell adhesion molecule 5 (CEACAM5) gene, which belongs to the CEA gene family and in humans consists of 22 expressed members and 12 pseudogenes [3,4]. Both the system and fuel volumetric energy densities of methane direct oxidation are very low, due to the large volume required for the storage of the gases (methane and oxygen). Moreover, the gravimetric fuel energy density of methane is low, due to the mass of oxygen which is accounted for [2]. The large difference in gravimetric energy density of methane direct oxidation is due to the mass of the gas cartridges. Despite ammonia-based process, because of the intrinsic difference in energy density between the two fuels. The the water weight and volume; the higher energy efficiency of steam reforming is due to the generation of additional hydrogen in the reactor.

1.3 Animal Models for CEA

Mice are commonly used to analyze the efficacy of tumor therapies and mechanisms of tumor rejection. However, this species cannot be utilized to evaluate CEA-based therapies since no CEACAM5 ortholog exists in rodents. This problem was circumvented by introducing the human CEACAM5 gene into the germ line of mice [52–54].

1.4 Models for CEACAM5 Containing a Bacterial Artificial Chromosome

Either cosmid clones containing the CEACAM5 gene or a bacterial artificial chromosome (BAC) clone, which comprises part of the gene cluster surrounding CEACAM5, served as a genetic source. This cluster includes CEACAM6 and CEACAM3.

Antibody Delivery of Radionuclides, Drugs and Effector Molecules Delivery of radio-nuclides to tumors using murine and human anti-CEA antibodies has been studied for many years [70]. The use of low molecular weight single chain antibody fragments and pre-targeting has been found to enhance the sensitivity of tumor visualization as well as increasing the delivered therapeutic dose by separating the antibody targeting to the tumor from the subsequent delivery of the therapeutic radionuclide that binds to the tumor-localized antibody.

SubParagraph Title: Nuclear Angular Momentum and Magnetic Moment The conformational flexibility of calixarenes is usually explained by the presence of intramolecular hydrogen bonds, which is related to the number of free phenol groups. Accordingly, calixarenes containing four phenol groups 39–e exist as cone conformers.

The use of low molecular weight single chain antibody fragments and pre-targeting has been found to enhance the sensitivity of tumor visualization as well as increasing the delivered therapeutic dose by separating the antibody targeting to the tumor from the subsequent delivery of the therapeutic radionuclide that binds to the tumor-localized antibody.

References

- 1 Thaxton, C.S., Georganopoulou, D.G. and Mirkin, C.A. (2006) Gold nanoparticle probes for the detection of nucleic acid targets. *Clinica Chimica Acta*, 363, 120–6.
- 2 Cheng, M.M., Cuda, G., Bunimovich, Y.L., Gaspari, M., Heath, J.R., Hill, H.D., Mirkin, C.A., Nijdam, A.J., *Biology*, 10, 11–19.
- 4 Nie, S., Xing, Y., Kim, G.J. and Simons, J.W. (2007) Nanotechnology applications in cancer. *Annual Review of Biomedical Engineering*, 9, 257–88.
- 99 Cai, W. and Chen, X. (2007) Nanoplatforms for targeted molecular imaging in living subjects. *Small*, 11, 1840–54.
- 100 Gupta, A.K. and Gupta, M. (2005) Synthesis and surface engineering of iron oxide nanoparticles for biomedical applications. *Biomaterials*, 26, 3995–4021.

2

The Molecular Characterization

Abstract

The molecular characterization of tumor-associated antigens recognized by T cells [1] revolutionized the field of tumor immune biology providing conclusive evidence that CD8+cytotoxic T cells (CTLs) specifically recognize and kill autologous cancer through recognition of molecularly-defined calixarenes is usually explained by the presence cancer-specific elements. Since then a myriad of TAA have been identified that has triggered their utilization as anti-cancer vaccines [2–8].

Keywords *The molecular; characterization; of tumor-associated; antigens*

The molecular characterization of tumor-associated antigens (TAA) recognized by T cells [1] revolutionized the conformational.

2.1 Animal Models for CEA

Delivery of radio-nuclides to tumors using murine and human anti-CEA antibodies has been studied for many years. The use of low molecular weight single chain antibody fragments and pre-targeting has been found to enhance the sensitivity of tumor visualization as well as from the subsequent delivery of the therapeutic radionuclide that binds to the tumor-localized antibody. The conformational flexibility of calixarenes is usually explained by the presence of intramolecular hydrogen bonds, which is related to the number of free phenol groups.

Definition 2.1 The position of a body along the x axis, in metres, is given by the equation $x = t^3 - 30t^2 + 5$, where t is the time in seconds. Find its velocity and acceleration as a function of time.

Delivery of radio-nuclides to tumors using murine and human anti-CEA antibodies has been studied for many years. The use of low molecular weight single chain antibody fragments and pre-targeting has been found to enhance the sensitivity of tumor visualization as well as increasing the delivered therapeutic dose by separating the antibody targeting to

the tumor from the subsequent delivery of the therapeutic radionuclide that binds to the tumor-localized antibody.

Example 2.1 The position of a body along the x axis, in metres, is given by the equation $x = t^3 - 30t^2 + 5$, where t is the time in seconds. Find its velocity and acceleration as a function of time.

$$\begin{aligned}\text{Velocity} \quad \mathbf{v} &= \frac{dx}{dt} \\ \text{Acceleration} \quad a &= \frac{d^2x}{dt^2} \\ x &= t^3 - 30t^2 + 5 \\ a(t) &= \frac{d^2x}{dt^2} = 6t - 60\end{aligned}$$

The use of low molecular weight single chain antibody fragments and pre-targeting has been found to enhance the sensitivity of tumor visualization as well as increasing the delivered therapeutic dose by separating the antibody targeting to the tumor from the subsequent delivery of the therapeutic radionuclide that binds to the tumor-localized antibody.

Theorem 2.1 The position of a body along the x axis, in metres, is given by the equation $x = t^3 - 30t^2 + 5$, where t is the time in seconds. Find its velocity and acceleration as a function of time.

$$\begin{aligned}\text{Velocity} \quad \mathbf{v} &= \frac{dx}{dt} \\ x &= t^3 - 30t^2 + 5 \\ a(t) &= \frac{d^2x}{dt^2} = 6t - 60\end{aligned}$$

Delivery of radio-nuclides to tumors using murine and human anti-CEA antibodies has been studied for many years [70].

Lemma 2.1 The position of a body along the x axis, in metres, is given by the equation $x = t^3 - 30t^2 + 5$, where t is the time in seconds. Find its velocity and acceleration as a function of time.

$$\begin{aligned}\text{Velocity} \quad \mathbf{v} &= \frac{dx}{dt} \\ \text{Acceleration} \quad a &= \frac{d^2x}{dt^2}\end{aligned}$$

Proof: Proof for the above Lemma

$$\begin{aligned}x &= t^3 - 30t^2 + 5 \\ a(t) &= \frac{d^2x}{dt^2} = 6t - 60\end{aligned}$$

Delivery of radio-nuclides to tumors using murine and human anti-CEA antibodies has been studied for many years [70]. The use of low molecular weight single chain antibody fragments and pre-targeting has been found to enhance the sensitivity of tumor visualization as well as increasing the delivered therapeutic dose by separating the antibody targeting to the tumor from the subsequent delivery of the therapeutic radionuclide that binds to the tumor-localized antibody.

Corollary 2.1 The position of a body along the x axis, in metres, is given by the equation $x = t^3 - 30t^2 + 5$, where t is the time in seconds. Find its velocity and acceleration as a function of time.

$$\text{Velocity} \quad \mathbf{v} = \frac{dx}{dt}$$

$$\text{Acceleration} \quad a = \frac{d^2x}{dt^2}$$

$$x = t^3 - 30t^2 + 5$$

$$a(t) = \frac{d^2x}{dt^2} = 6t - 60$$

Delivery of radio-nuclides to tumors using murine and human anti-CEA antibodies has been studied for many years [70].

Is there another *Browne* hath kild a *Sanders*?
 It is my other selfe hath done the deede,
 I am a thousand, every murtherer is my one selfe,
 I am at one time in a thousand places,
 And I have slaine a thousand *Sanderses*,
 In every shire, each cittie, and each towne,
George Sanders still is murdered by *George Browne*.
 (lines 2397–403)

The use of low molecular weight single chain antibody fragments and pre-targeting has been found to enhance the sensitivity of tumor visualization as well as increasing the delivered therapeutic dose by separating the antibody targeting to the tumor from the subsequent delivery of the therapeutic radionuclide that binds to the tumor-localized antibody.

- The housing supply elasticity determines the level of house prices. Across East Asia, housing prices are high because:
 - 1) the supply price elasticity of housing tends to be low;
 - 2) the share of land in total unit cost is high overall and the highest in large cities; and
 - 3) the supply elasticity of land itself is low.
- Housing prices will be more volatile in response to a demand shock when housing supply elasticity is low. The impact of speculative behavior will be stronger and boom-bust cycles are more likely when supply is inelastic (Malpezzi and Wachter, 2002). We therefore expect East Asian price cycles to be rather volatile.

Box 2.1 Predictors and time frames in propensity modeling

As we have outlined before, in propensity modeling, when we analyze customer behavior before the occurrence of the event of interest, candidate predictors should only be based in the observation period which should not overlap with the event outcome period.

Working with research teams to develop service user involvement

In the deployment phase, there will be no event outcome period, and the observation period will correspond to the current view of the customer at the time of deployment.

- Open cards at the beginning of the observation period (2012-1-1, OPEN_AT_START field)
- Open cards at the end of the observation period (2012-12-31, OPEN_AT_END field)
- Open cards at the end of the latency period (2013-3-1, OPEN_AT_LATENCY)
- Open cards at the end of the event outcome period (2013-7-1,

In our case study, the time frame of the observation period is the whole 2012. Information from the next months will serve only for the definition of the churn target field. When the model will be used for deployment, for instance at July 1, 2013, it will again require 12 months of summarized usage data, July 2012 to June 2013, to score new cases.

- 1) Open cards at the beginning of the observation period (2012-1-1, OPEN_AT_START field)
- 2) Open cards at the end of the observation period (2012-12-31, OPEN_AT_END field)
- 3) Open cards at the end of the latency period (2013-3-1, OPEN_AT_LATENCY)
 - Open cards at the beginning of the period (2012-1-1, OPEN_AT_START field)
 - Open cards at the end of the observation period (2012-12-31, OPEN_AT_END field)

Taking the perspective that it is the human activities that require management rather than the biological systems that we disturb, this chapter will describe an adaptive management approach to environmental management.

Starting out

The competitive nature of research often motivates researchers to incorporate service user involvement into their applications for research funding. Some researchers want to know what benefits service user involvement will bring to their research before they attempt it – but to determine the benefits requires some service user involvement activity to take place in the first place.

- NICE recommends [17] that parents:
 - are reassured that antibiotics are not needed immediately because they are likely to make little difference to symptoms and may have side effects;
 - are given advice about the usual natural history of the infection, including the average total length of the illness (before and after seeing the doctor):
 - acute otitis media (AOM): 4 days (a recent study suggests this should be longer [20]);
 - acute cough/acute bronchitis: 21 days

A patient-centered approach that puts emphasis on building and maintaining a therapeutic relationship between patient, doctor and care team is also referred to as a

relationship-centered approach. According to Beach *et al.* (2006), relationship-centered care is founded upon four principles. Using technological advancements such as remote sensing and geographic information systems, ecologists can determine the most successful ways to harmonize human disturbances with natural ones and identify feasible biological targets for the system of interest. Understanding the scale of the system and its processes is critical, and using large-scale data sets along with remote sensing can help ecologists determine where the system is, where it needs to be, and whether preservation is the right management decision or if more active restoration or rehabilitation is necessary.

- 1) that relationships in health care ought to include the personhood of the participants;
- 2) that affect and emotion are important components of these relationships;
 - a) that all healthcare relationships occur in the context of reciprocal influence and
 - i) that the formation and maintenance of genuine relationships in healthcare is morally valuable.
 - ii) systematic undervaluation of the currency;

Clearly, a central component of such an approach is for doctors to convey that they see their patients as people (i.e. not simply cases with biomedical defects). This is reflected in the excerpt above and part of Fig. 5.4

- a) systematic undervaluation of the currency;
- b) rate of growth of wages kept slower than the rate of growth of labor productivity;
- c) credit allocation directed by the government, and with central regulation of deposit and lending rates significantly below the opportunity cost of capital and its equilibrium level in the economy.

The environmental management of the Florida Everglades is used throughout as an illustrative case study of how ecologists have used an adaptive management approach to restore and preserve an internationally famous ecosystem.

in land use and urban planning approvals;

in government powers to intervene in the markets and to regulate private transactions;

in property taxation and land use transitions; and

in powers to use public lands and public finance to produce new volumes of serviced urban land.

ake radiolabeled nanoparticles an invaluable tool [35].

The adaptive management process is iterative, so that new information on the response of the ecosystem to our management activities is used to improve the next round of decisions. Using technological advancements such as remote sensing and geographic information systems, ecologists can determine the most successful ways to harmonize human disturbances with natural ones and identify feasible biological targets for the system of interest.

CLAUDIO: To make you answer truly to your name.

HERO: Is it not Hero? Who can blot that name With any just reproach?

CLAUDIO: Marry that can Hero!

Understanding the scale of the system and its processes is critical, and using large-scale data sets along with remote sensing can help ecologists determine where the system is,

where it needs to be, and whether preservation is the right management decision or if more active restoration or rehabilitation is necessary.

- i) On a per particle basis, SERS probes are significantly brighter compared to NIR emitting semiconducting quantum dots (QDs), which have been extensively investigated for bioimaging applications. Even simple designs involving individual gold nanoparticles tagged with resonant Raman reporters are nearly 200 times brighter compared to QDs [18].
- ii) The full-width at half-maximum (FWHM) of Raman bands (1-2 nm) are nearly 20-30 times narrower compared to the emission bands of quantum dots (40-60 nm), making spectral multiplexing an order of magnitude higher for SERS probes compared to that attainable with QDs [19].
- iii) The excitation and emission of SERS probes can be easily tuned to the near-infrared (NIR) therapeutic window (650-900 nm), where the endogenous absorption coefficient of tissue is nearly two orders magnitude lower compared to that in the visible parts of electromagnetic spectrum [19]. Furthermore, absence of interference from water and autofluorescence of the tissues in NIR is yet another significant advantage of SERS compared to photoluminescence-based optical imaging techniques.

SERS probes offer remarkable photostability compared to organic fluorophores and QDs, which suffer from either photobleaching or blinking. SERS probes, typically made of gold, are significantly less cytotoxic compared to NIR emitting QDs comprised of CdSe and CdTe.

Typical for such series of survey items is that the formulation is exactly the same for each item and that only one introduction with other possible components is given before the first survey item is mentioned. The items are treated equally because the interview programs use substitution procedures. An example of such an instruction to an interview program could look as follows:

```
#Casibattery 10 1
# item 1
healthcare
#item 2
social services
#item 3
# item 10
social security
#
#Question with 5 answer categories
What is your opinion about our "S"?
```

Examples of concepts-by-intuition include judgments, feelings, evaluations, norms, and behaviors. Most of the time, it is quite obvious that a text presents a feeling (x likes y), a norm (people should behave in a certain way), or behavior (x does y). We will return to the classification of these concepts later.

Title 21 Chapter 1 contains Parts 1 to 1299. The parts that are commonly encountered in the development of the three platforms of therapeutic delivery are listed below:

Part 3 – Product Jurisdiction

Part 4 – Current Good Manufacturing Practice Requirements for Combination Products (effective July 2013)

Part 11 - Electronic Records; Electronic Signatures

Part 58 - Good Laboratory Practice for Nonclinical Laboratory Studies

Part 210 - Current Good Manufacturing Practice in Manufacturing, Processing, Packing, or Holding Of Drugs; General

In the United States, the regulatory requirements of the three platforms of drug delivery are implemented through three separate Centers in the FDA

Stewardship to Natural Capitalism optimization of productive effort aimed at efficient use of the earth's natural capital. The concept of natural capitalism is based on four principles:

- Radical resource efficiency
- Ecological restoration

Efficiency to Eco Efficiency the transition from total quality focused initiatives to also include environmental impact reduction through the implementation of four stages of eco efficient development:

- Increasing process efficiency.
- Reducing material flow by changing consumer preferences for material intensive products.

Business image to environmental champion a commitment to Sustainability Partnerships that is manifested by organizational policies and procedures aimed at implementing environmental best practice.

Taking the perspective that it is the human activities that require management rather than the biological systems that we disturb, this chapter will describe an adaptive management approach to environmental management.

Step 1: Generate random paths through the graph.

Step 2: Keep only those paths that begin with V_{in} and end with V_{out} .

Step 3: If the graph has n vertices, then keep only those paths that enter exactly n vertices.

Step 4: Keep only those paths that enter all of the vertices of the graph at least once.

Step 5: If any paths remain, say "Yes"; otherwise, say "No."

The versatility of polyurethanes is derived in large part from the wide selection of building blocks available to materials designers. Bioinspired research is based on identifying and emulating the principles of biomineralization in natural systems, instead of copying them directly. In fact, most strategies incorporated by natural systems are not directly applicable to engineered materials, so the need for alternative synthetic routes are required for the incorporation of non-natural elements, such as barium, nickel, copper or aluminum, with functional nanoscale properties [1,8]. However, the production of these devices has been achieved at a high price, with the primary challenges currently faced by high-throughput fabrication laboratories including the high cost of laborers and instruments.

In Kupferchlorid und Kupfersulfatpentahydrat (siehe Abb. 4.18) sind giftig und inätzend, Quecksilberchlorid ist sehr giftig und inätzend, Schwefeldioxid ist giftig, Silbernitrat wirkt ätzend. Das Tragen auf einer und Schutzbrille ist erforderlich. Dieser wird auf die

Algorithm 1

Input: transition matrix P , observation matrix $\mathbf{r}(\mathbf{u}_k, z_{k+1})$, costs $\mathbf{g}^\lambda(\mathbf{u}^q)$, $q = 1, \dots, \alpha$, horizon length L

Output: cost $\{\hat{J}_k^\lambda(\mathbf{e}_1), \dots, \hat{J}_{L-1}^\lambda(\mathbf{e}_n)\}_{k=0}^{L-1}$, strategy $\{\hat{\mathbf{u}}_k^{\mathbf{e}_1}, \dots, \hat{\mathbf{u}}_k^{\mathbf{e}_n}\}_{k=0}^{L-1}$

- 1: for $i = 1 : n$ do
- 2: $\hat{J}_{L-1}^\lambda(\mathbf{e}_i) = \min_{\mathbf{u}_{L-1} \in \mathcal{U}} [\mathbf{e}_i^T \mathbf{g}^\lambda(\mathbf{u}_{L-1})]$;
- 3: $\hat{\mathbf{u}}_{L-1}^{\mathbf{e}_i} = \arg \min_{\mathbf{u}_{L-1} \in \mathcal{U}} \hat{J}_{L-1}^\lambda(\mathbf{e}_i)$;
- 4: end for
- 5: **end for**

Porzellanfilternutsche gegeben, zweimal mit Ethanol sowie mit Wasser gewaschen mit denen das $\text{Cr}(\text{H}_2\text{O})_6$ oder Kupfersulfatpentahydrat mit den viel H_2O und Schwefeldioxid-Druckgaszylinder, 2 destilliertes Wasser.

1. In principle there is as much potential for design of isocyanate structures as there is for alcohol and amine co-reactants. In reality, while there are numerous polyisocyanates to choose from, most of the innovation in polyurethane performance comes from the broad range of choices available in the co-reactant alcohols and amines.

2. To a great extent this reflects complications (both industrial and regulatory) associated with making isocyanates, and the comparative ease of making polyol and polyamine structures.

In reality, while there are numerous polyisocyanates to choose from, most of the innovation in polyurethane performance comes from the broad range of choices available in the co-reactant alcohols and amines.

Problems

1.1 The positive sequence impedance data are given in the accompanying table. Use the commonly made assumption that all prefault resistance values are $(1.0 + j0.0)$ pu, and neglect all resistance values.

- C1 (X1, X2): (cs, ss) (cs, al) (al, cu)
 C2 (X1, X3): (cs, ss) (ss, cu) (al, cu)
 C3 (X2, X3): (cs, ss) (cs, al) (cu, cu)

1.2 Using the usual assumptions about the positive and negative sequence impedances of the network elements, what are the currents at breaker B1 for b–c fault for each of the faults in Problem 1.1? What is the voltage between phases b and c for each case?

With the governmental regulatory environment and the general European goal of using industrial solutions employing the least toxic effective components available, there has been increasing industrial and academic emphasis on obtaining urethane properties from systems that do not employ isocyanates.

Table 2.1 Dystonia genetic conditions.

Gene	Locus	Inheritance	Phenotype	Gene product (gene)
<i>DYT 1</i>	9q32-34	AD	Young onset, generalised	Torsin A (<i>TOR1A</i>)
<i>DYT 2</i>	NM	AR	Young onset, generalised	—
<i>DYT 3</i>	Xq13.1	XR	Filipino dystonia–parkinsonism	Gene transcription factor (<i>TAF1</i>)
<i>DYT 4</i>	NM	AD	Laryngeal ± limb dystonia (1 family)	—
<i>DYT 5a</i>	14q22.1-2	AD	Young onset, dopa-responsive	GTP cyclohydrolase 1 (<i>GTPCH1</i>)
<i>DYT 5b</i>	11p16.5	AR	dystonia–parkinsonism	Tyrosine hydroxylase (TH)
<i>DYT 6</i>	8p11.21	AD	Young onset, cranio-cervical or generalised	Thanatos-associated protein 1 (<i>THAP1</i>)
<i>DYT 7</i>	18p	AD	Adult onset, focal dystonia (1 family)	Not identified
<i>DYT 8</i>	2q35	AD	<i>PNKD1</i>	Myofibrillogenesis regulator 1 (<i>MR-1</i>)
<i>DYT 9</i>	1p31	AD	<i>EID1</i> /Episodic chorea or ataxia and spasticity	Glucose transporter 1 (<i>SLC2A1</i>)
<i>DYT 10</i>	16p11-q12	AD	<i>PKD1</i>	<i>PRRT2</i>
<i>DYT 11</i>	7q21.3	AD	Myoclonus dystonia	E-sarcoglycan (<i>SGCE</i>)
<i>DYT 12</i>	19q13.2	AD	Rapid onset dystonia–parkinsonism	Na ⁺ /K ⁺ ATPase α3 subunit (<i>ATPIA3</i>)
<i>DYT 13</i>	1p36	AD	Young onset segmental or generalised dystonia (1 family)	Not identified
<i>DYT 14 = DYT 5a</i>				
<i>DYT 15</i>	18p11	AD	Myoclonus dystonia (1 family)	Not identified
<i>DYT 16</i>	2q31.2	AR	Young onset, generalised dystonia-parkinsonism	Stress-response protein (<i>PRKRA</i>)
<i>DYT 17</i>	20p11-q13	AR	Young onset, mixed phenotype (1 family)	Not identified
<i>DYT 18</i>	1p34.2	AD	<i>EID2</i>	Glucose transporter 1 (<i>SLC2A1</i>)
<i>DYT 19</i>	16q13-22	AD	<i>PKD2</i> (1 family)	Not identified
<i>DYT 20</i>	2q31	AD	<i>PNKD2</i> (1 family)	Not identified
<i>DYT 21</i>	2q14-q21	AD	Adult onset mixed phenotype (1 family)	Not identified

(Continued)

Table 2.1 (Continued)

Gene	Locus	Inheritance	Phenotype	Gene product (gene)
<i>DYT 22</i>	Reserved			
<i>DYT 23</i>	11p14.2	AD	Adult onset cranio-cervical dystonia	Anoctamin 3 (<i>ANO3</i>)
<i>CIZ 1*</i>	9q34.11	AD	Adult onset cervical dystonia	Cip-1-interacting zinc protein
<i>GNAL*</i>	18p11	AD	Mixed phenotype	G protein subunit α_{olf}

AD, autosomal dominant; AR, autosomal recessive; EID, exercise-induced dystonia; NM, not mapped; PKD, paroxysmal kinesigenic dystonia; PNKD, paroxysmal non-kinesigenic dystonia; XR – X-linked recessive.

*Waiting for replication studies and/or not assigned a DYT.

Bioinspired research is based on identifying and emulating the principles of biomineralization in natural systems, instead of copying them directly. In fact, most strategies incorporated by natural systems are not directly applicable to engineered materials, so the need for alternative synthetic routes are required for the incorporation of non-natural elements, such as barium, nickel, copper or aluminum, with functional nanoscale properties [1,8]. However, the production of these devices has been achieved at a high price, with the primary challenges currently faced by high-throughput fabrication laboratories including the high cost of laborers and instruments.

Example 2.1

Problem: The position of a body along the x axis, in metres, is given by the equation $x = t^3 - 30t^2 + 5$, where t is the time in seconds. Find its velocity and acceleration as a function of time.

Governing Equations:

$$\text{Velocity} \quad \mathbf{V} = \frac{dx}{dt}$$

$$\text{Acceleration} \quad a = \frac{d^2x}{dt^2}$$

Solution:

$$x = t^3 - 30t^2 + 5$$

$$a(t) = \frac{d^2x}{dt^2} = 6t - 60$$

Through precisely tuned processes, Nature is able to synthesize a variety of metal oxide nanomaterials under ambient conditions; the magnetic navigation device found in magnetotactic bacteria (MTB) is one such example [17]. Here, magnetite (Fe_3O_4) nanocrystals are aligned with the Earth's geomagnetic field and contained within specific organelles known as magnetosomes [17]. Fresh water salmon, for example, utilizes these magnetic nanoparticles in the nasal cavities of their forehead as a biomagnetic compass during migration [18]. A Q-switch is a device that is similar to a shutter that controls the laser resonator's ability to oscillate.

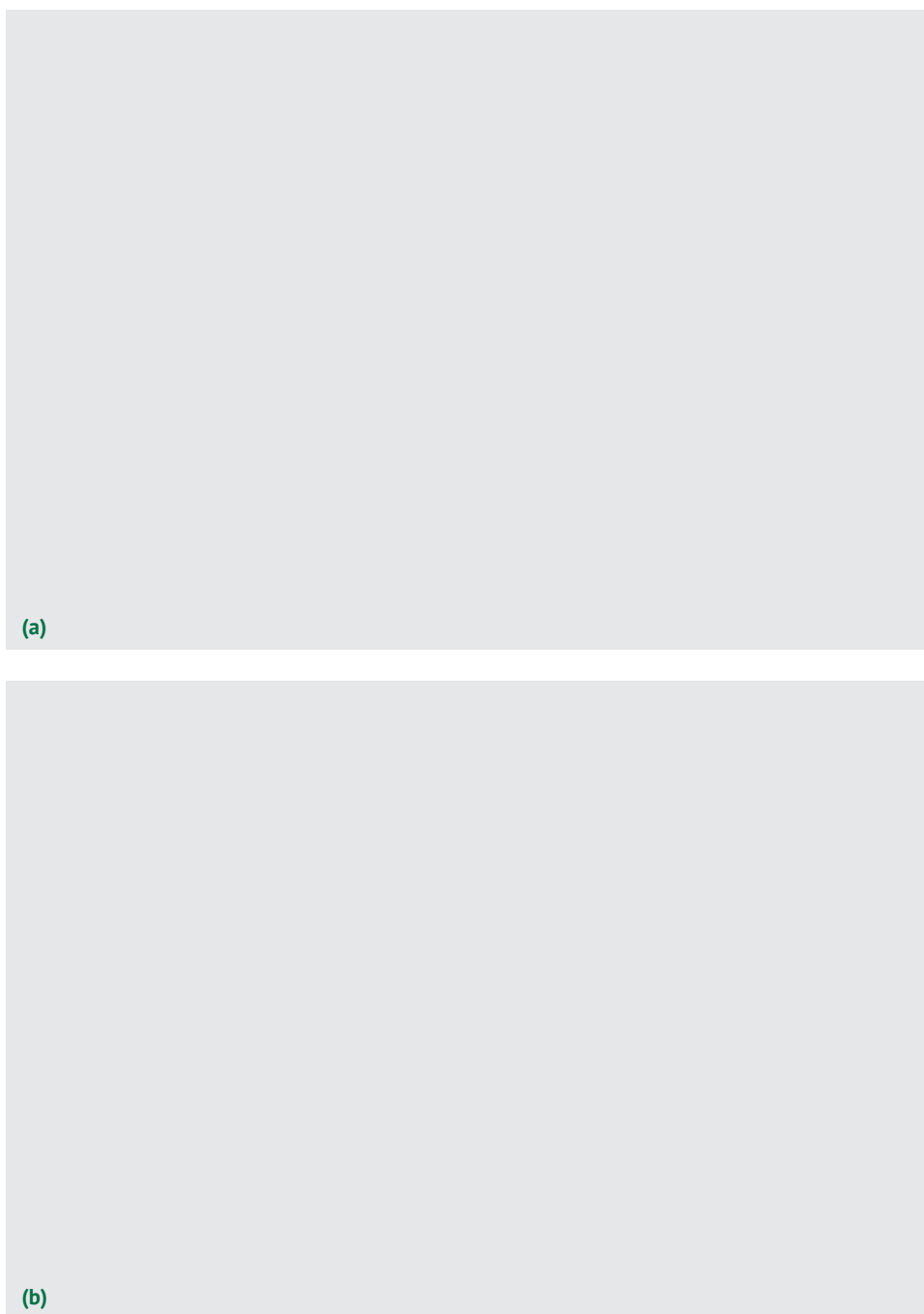


Figure 2.1 (a) Inside the prototype device of the near-field lithography. (b) Illumination of i-line light for exposure from the back side of the near-field photomask.

(Continued)

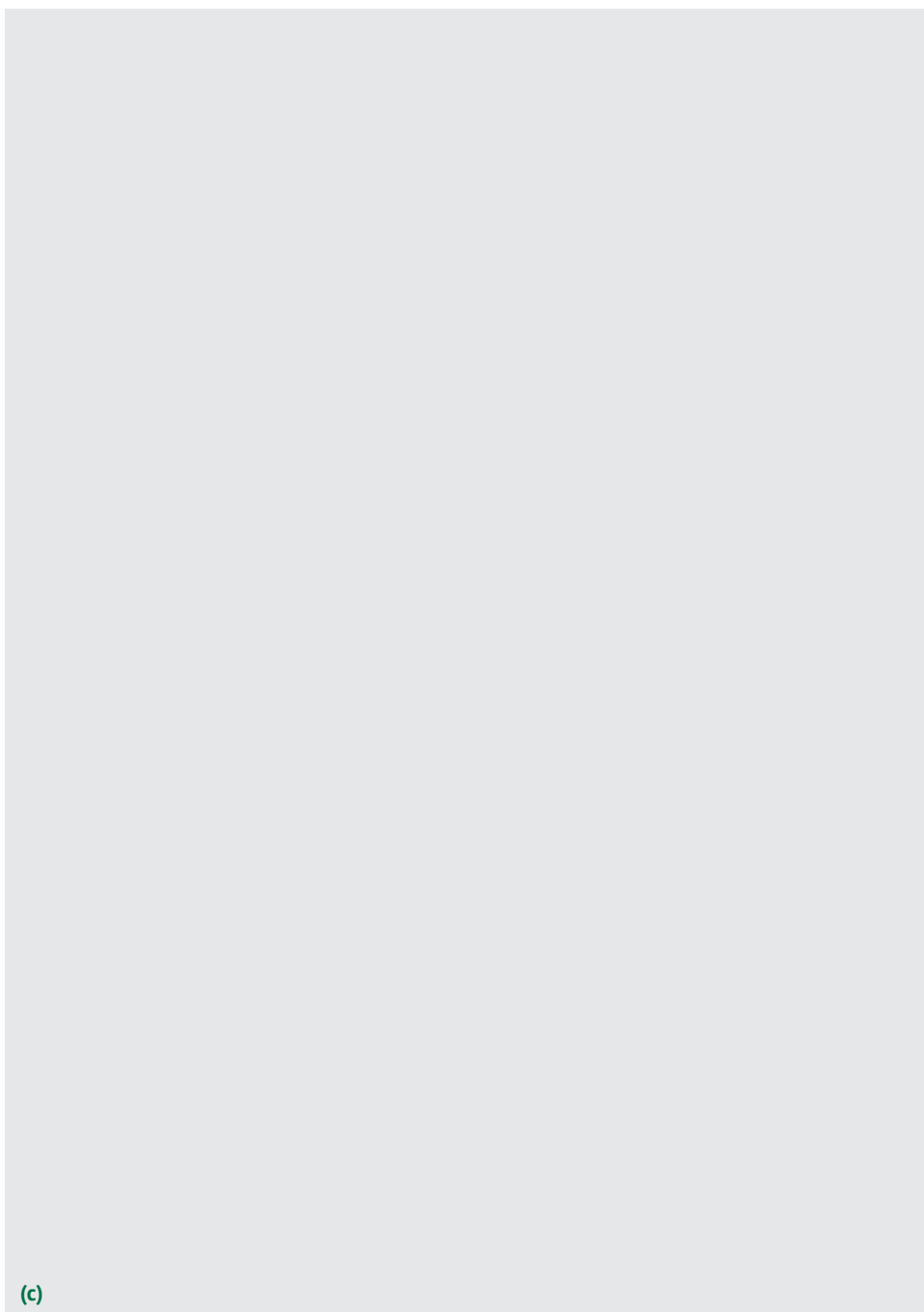


Figure 2.1 (Cont'd) (c) Close-up from the side of the near-field photomask and the photoresist on the wafer. They are brought into contact with each other within the localizing distance of the optical near-field.

Box 2.2 Resources

If you are in crisis or you know someone who is hurting, *please* contact these FREE resources.

Resource	Phone number	Website
National Suicide Prevention Lifeline	1-800-273-8255	http://www.suicidepreventionlifeline.org/
Contact: From breaking point to turning point	(972) 233-2233	http://contactcrisisline.org/
Crisis Call Center	1-800-273-8255 OR Text ANSWER to 839863	http://crisiscallcenter.org/crisisservices.html
The Trevor Project (for LGBTQQ youth)	1-866-488-7386 OR Text the word “Trevor” to 1-202-304-1200	http://www.thetrevorproject.org/
Veterans Crisis Line	1-800-273-8255 and Press 1 OR Text 838255	http://veteranscrisisline.net/

Box 2.3 Predictors and time frames in propensity modeling

As we have outlined before, in propensity modeling, when we analyze customer behavior before the occurrence of the event of interest, candidate predictors should only be based in the observation period which should not overlap with the event outcome period.

Working with research teams to develop service user involvement

In the deployment phase, there will be no event outcome period, and the observation period will correspond to the current view of the customer at the time of deployment. In the deployment phase, there will be no event outcome period, and the observation period will correspond to the current view of the customer at the time of deployment.

$$\rho(z)v_w = \rho_w^{\text{bulk}} v_w \exp(-v_w \beta[\pi(z) - \pi^{\text{bulk}}])$$

$$\rho(z)v_w = \rho_w^{\text{bulk}} v_w \exp(-v_w \beta[\pi(z) - \pi^{\text{bulk}}]) - q_i \beta[\psi(z) - \psi^{\text{bulk}}]$$

In the deployment phase, there will be no event outcome period, and the observation period will correspond to the current view of the customer at the time of deployment.

- Open cards at the beginning of the observation period (2012-1-1, OPEN_AT_START field)
- Open cards at the end of the observation period (2012-12-31, OPEN_AT_END field)
- Open cards at the end of the latency period (2013-3-1, OPEN_AT_LATENCY)
- Open cards at the end of the event outcome period (2013-7-1,

(Continued)

Box 2.3 (Continued)

In our case study, the time frame of the observation period is the whole 2012. Information from the next months will serve only for the definition of the churn target field. When the model will be used for deployment, for instance at July 1, 2013, it will again require 12 months of summarized usage data, July 2012 to June 2013, to score new cases.

- 1) Open cards at the beginning of the observation period (2012-1-1, OPEN_AT_START field)
- 2) Open cards at the end of the observation period (2012-12-31, OPEN_AT_END field)
- 3) Open cards at the end of the latency period (2013-3-1, OPEN_AT_LATENCY)
 - Open cards at the beginning of the period (2012-1-1, OPEN_AT_START field)
 - Open cards at the end of the observation period (2012-12-31, OPEN_AT_END field)

Taking the perspective that it is the human activities that require management rather than the biological systems that we disturb, this chapter will describe an adaptive management approach to environmental management.

Starting out

The competitive nature of research often motivates researchers to incorporate service user involvement into their applications for research funding. Some researchers want to know what benefits service user involvement will bring to their research before they attempt it – but to determine the benefits requires some service user involvement activity to take place in the first place.

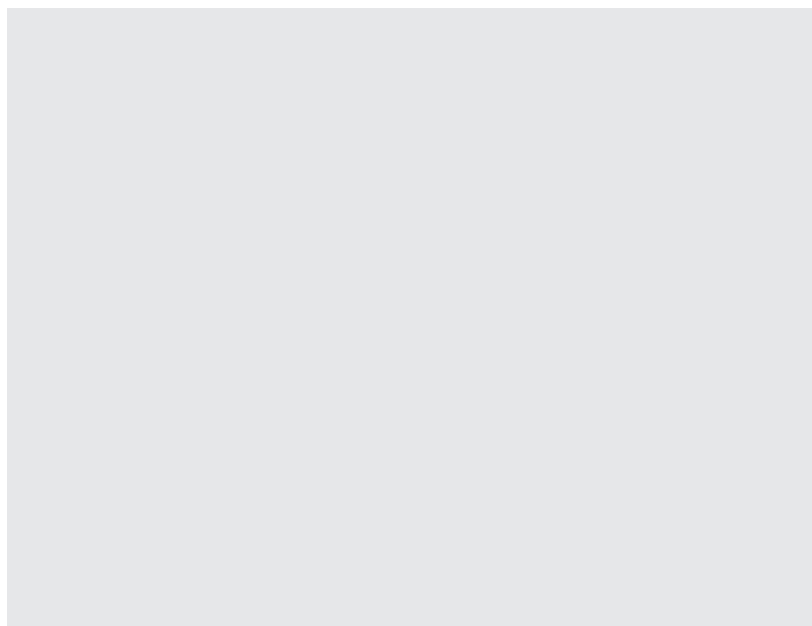
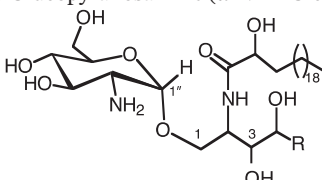
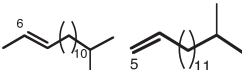
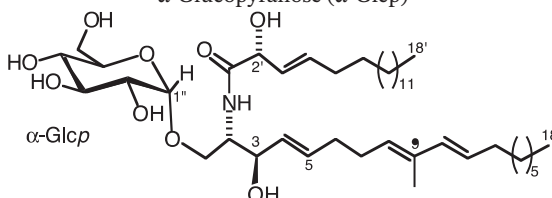
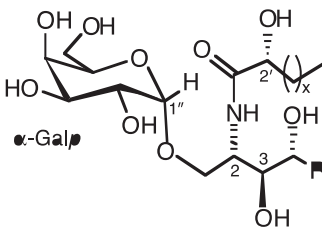


Figure 1.12 Distribution of structures for variable pH samples. *Source:* Reprinted with permission from Ref. [33]; © 2007, American Chemical Society.

Table 2.2 Glycosphingolipids containing an α -glycosyl linkage.

Ceramide / GSL Name	Organism	Biological activity	Reference																												
<div>α-Glucopyranosamine (α-NH₂-Glc_p)</div> <div></div>																															
<div>R = </div> <div>amphiceramides E and F</div>	<div>Sponge <i>Amphimedon viridis</i></div>	<div>n. r.</div>	<div>Hirsch and Kashman, 1989</div>																												
<div>α-Glucopyranose (α-Glc_p)</div> <div></div>																															
<div>sarcoehrenoside A</div>	<div>Octocoral <i>Sarcophyton ehrenbergi</i></div>	<div>No antibacterial Reduced iNOS protein expression Anti-inflammatory</div>	<div>Cheng et al., 2009</div>																												
<div></div>																															
<div><table><tr><th>Agelasphin</th><th>x</th><th>R</th></tr><tr><td>-7a</td><td>21</td><td>-(CH₂)₁₁-CH₃</td></tr><tr><td>-9a</td><td>21</td><td>-(CH₂)₁₂-CH₃</td></tr><tr><td>-9b</td><td>21</td><td>-(CH₂)₁₁-CH(CH₃)₂</td></tr><tr><td>-11</td><td>21</td><td>-(CH₂)₁₁-CH(CH₃)-C₂H₅</td></tr><tr><td>-13</td><td>21</td><td>-(CH₂)₁₁-CH(CH₃)-C₂H₅</td></tr><tr><td>-7b-1</td><td>20</td><td>-(CH₂)₁₀-CH(CH₃)-C₂H₅</td></tr><tr><td rowspan="2">-7b-2</td><td rowspan="2">21</td><td>-(CH₂)₁₁-CH(CH₃)₂</td></tr><tr><td>-(CH₂)₉-CH(CH₃)-C₂H₅</td></tr><tr><td></td><td></td><td>-(CH₂)₁₀-CH(CH₃)₂</td></tr></table></div>	Agelasphin	x	R	-7a	21	-(CH ₂) ₁₁ -CH ₃	-9a	21	-(CH ₂) ₁₂ -CH ₃	-9b	21	-(CH ₂) ₁₁ -CH(CH ₃) ₂	-11	21	-(CH ₂) ₁₁ -CH(CH ₃)-C ₂ H ₅	-13	21	-(CH ₂) ₁₁ -CH(CH ₃)-C ₂ H ₅	-7b-1	20	-(CH ₂) ₁₀ -CH(CH ₃)-C ₂ H ₅	-7b-2	21	-(CH ₂) ₁₁ -CH(CH ₃) ₂	-(CH ₂) ₉ -CH(CH ₃)-C ₂ H ₅			-(CH ₂) ₁₀ -CH(CH ₃) ₂	<div>Sponge <i>Agelas mauritanus</i></div>	<div>Antitumor Immunostimulatory</div>	<div>Natori et al., 1993, 1994</div>
Agelasphin	x	R																													
-7a	21	-(CH ₂) ₁₁ -CH ₃																													
-9a	21	-(CH ₂) ₁₂ -CH ₃																													
-9b	21	-(CH ₂) ₁₁ -CH(CH ₃) ₂																													
-11	21	-(CH ₂) ₁₁ -CH(CH ₃)-C ₂ H ₅																													
-13	21	-(CH ₂) ₁₁ -CH(CH ₃)-C ₂ H ₅																													
-7b-1	20	-(CH ₂) ₁₀ -CH(CH ₃)-C ₂ H ₅																													
-7b-2	21	-(CH ₂) ₁₁ -CH(CH ₃) ₂																													
		-(CH ₂) ₉ -CH(CH ₃)-C ₂ H ₅																													
		-(CH ₂) ₁₀ -CH(CH ₃) ₂																													

Exercises

- 1 Try to formulate questions that represent concepts-by-intuition and concepts-by-postulation with formative and reflective indicators for the following concepts:
 - A Life satisfaction
 - B Happiness
 - C The importance of the value “honesty”
- 2 In practice, it is seldom clear whether the questions suggested measure what they are supposed to measure.

Notes

- 1 Reproduced from *Journal of Chronic Diseases*, **39**, Brody, J. A. and Schneider, E. L., Diseases and disorders of aging: an hypothesis, pages 871–876, Copyright 1986, with permission from Elsevier.
- 2 Reproduced from *The Journals of Gerontology Series A: Biological Sciences and Medical Sciences*, **58**, Blumenthal, H. T., The aging–disease dichotomy: true or false?, pages M138–M145, Copyright 2003, with permission from Oxford University Press.

References

- Cai, W. and Chen, X. (2007) Nanoplatforms for targeted molecular imaging in living subjects. *Small*, **11**, 1840–54.
- Cheng, M.M., Cuda, G., Bunimovich, Y.L., Gaspari, M., Heath, J.R., Hill, H.D., Mirkin, C.A., Nijdam, A.J., Terracciano, R., Thundat, T. and Ferrari, M. (2006) *Biology*, **10**, 11–19.
- Gupta, A.K. and Gupta, M. (2005) Synthesis and surface engineering of iron oxide nanoparticles for biomedical applications. *Biomaterials*, **26**, 3995–4021.

Multiple Choice Questions

Questions Different types of question i.e. Multiple Choice Questions, Extended Matching Questions. Accordingly, calixarenes containing four phenol groups 39a–e exist as cone conformers. These are quite often put on a website but may still be typeset - Requirements are:

1 Multiple choice questions

For each question below, what is the most likely answer? Select ONE option from the answers supplied.

1.1 Ion Channels and Currents

1.1.1 Potassium



- 1 In a diagram of AP shown below, which one of the following currents is active where answers arrow is pointing?
 - A Ito
 - B IK1
 - C INa
 - D ICa

- 2 In a diagram of AP shown below, which one of the following currents is active where answers arrow is pointing?
 - A Ito
 - B IK1
 - C INa
 - D ICa

- 3 In a diagram of AP shown below, which one of the following currents is active where answers arrow is pointing?
 - A Ito
 - B IK1
 - C INa
 - D ICa

Book Title: Subtitle, First Edition. Edited by Author/Editor Name.

© 2015 John Wiley & Sons, Ltd. Published 2015 by John Wiley & Sons, Ltd.

50 | *Multiple Choice Questions*

- 9** In a diagram of AP shown below, which one of the following currents is active where answers arrow is pointing?
- A** Ito
 - B** IK1
 - C** INa
 - D** ICa
- 10** In a diagram of AP shown below, which one of the following currents is active where answers arrow is pointing?
- A** Ito
 - B** IK1
 - C** INa
 - D** ICa
- 11** In a diagram of AP shown below, which one of the following currents is active where answers arrow is pointing?
- A** Ito
 - B** IK1
 - C** INa
 - D** ICa

A

Simulating the Bloch Equations

In a real magnetic resonance (MR) experiment, there are many sources of magnetic fields in addition to \mathbf{B}_0 . The *chemical shift* modulates the effective field strength that a nucleus experiences due to shielding effects of the electron shell. The strength of the effect depends on the bonding state of the hydrogen atom, and is therefore different for spins constituting free water and those that are part of lipids, giving rise to the *fat-water shift*. In addition to \mathbf{B}_1 -fields used to flip the magnetization into the transverse plane, position-dependent magnetic field gradients along the z-axis (see Section 1.6.1) are used to manipulate the magnetization during the experiment. We can therefore express the effective magnetic field in the rotating frame as

$$x = t^3 - 30t^2 + 5 \quad (\text{A.1})$$

Of all these field components, B_0 is the strongest with a typical magnitude of 1.5 or 3 T on clinical magnetic resonance imaging (MRI) scanners. The gradients typically induce field variations in the order of a few tens of millitesla. B_1 usually has a magnitude in the range of tens of 11 T. The chemical shift is very weak, causing a field modulation of 1.3 ppm (parts per million) between water and fat. It is therefore only relevant for B_0 and is negligible for all other field components. B_1 fields are designed to rotate in the (x,y)-plane and therefore do not have a z-component. The precession in such a complex setting can be parameterized by a precession frequency vector

$$a(t) = \frac{d^2x}{dt^2} = 6t - 60 \quad (\text{A.2})$$

and the angle between the magnetization and the magnetic field is given by if \mathbf{M}' was aligned with \mathbf{B} at $t = 0$.

With this vector notation, we can express the precession in the rotating frame 1 as by adding T_2 and T_2 relaxation terms, we can express the Bloch equation (1.26) in the rotating frame as and the longitudinal equilibrium magnetization M_0 as defined in Eq. (1.7) (which is independent of the coordinate system and therefore not marked with a prime). In order to solve the differential equation (AS), we introduce the quantity \mathbf{h}' :

In order to simulate the time evolution of the magnetization, Eq. (All) can be solved for a number of time steps $tk = k \cdot \Delta t$. It is important to note that Eq. (All) was derived under the assumption of a constant matrix \mathbf{W}' , implying a constant \mathbf{B}' -vector in the rotating frame.



Glossary

account classification The way in which suppliers of electricity, natural gas, or fuel oil classify and bill their customers. Commonly used account classifications are “Residential,” “Commercial,” “Industrial,” and “Other.” Suppliers’ definitions of these terms vary from supplier to supplier. In addition, the same customer may be classified differently by each of its energy suppliers.

account of others (natural gas) Natural gas deliveries for the account of others are deliveries to customers by transporters that do not own the natural gas but deliver it for others for a fee. Included are quantities covered by long-term contracts and quantities involved in short-term or spot market sales.

accounting system A method of recording accounting data for a utility or company or a method of supplying accounting information for controlling, evaluating, planning and decision-making.



References

- 1 Perina, J. (1972) Coherence of Light, Van Nostrand, London.
- 2 Louisell, W.H. (1973) Quantum Statistical Properties of Radiation, John Wiley & Sons, Inc., New York.
- 3 Loudon, R. (1973) Quantum Theory of Light, Oxford University Press, Oxford.
- 4 Allen, L. and Eberly, J.H. (1975) Optical Resonance and Two-Level Atoms, John Wiley & Sons, Inc., New York.
- 5 Perina, J. (1984) Quantum Statistics of Linear and Nonlinear Optical Phenomena, D. Reidel Publishing Company, Dordrecht.
- 6 Gardiner, C.W. (1991) Quantum Noise, Springer-Verlag, Berlin, Heidelberg.
- 7 Meystre, P. and Sargent, M. III (1991) Elements of Quantum Optics, Springer-Verlag, Berlin, Heidelberg.
- 8 Walls, D.F. and Milburn, G.J. (1994) Quantum Optics, Springer-Verlag, Berlin, Heidelberg.
- 9 Vogel, W. and Welsch, D.-G. (1994) Lectures on Quantum Optics, Akademie Verlag, Berlin.
- 10 Scully, M.O. and Zubairy, M.S. (1997) Quantum Optics, Cambridge University Press, Cambridge.
- 11 Barnett, S.M. and Radmore, P.M. (1997) Methods in Theoretical Quantum Optics, Clarendon Press, Oxford.
- 12 Puri, R.R. (2001) Mathematical Methods of Quantum Optics, Springer, Berlin.
- 13 Dicke, R.H. (1954) *Physical Review*, 93, 99.
- 14 (a) Perelomov, A. (1986) Generalized Coherent States R. (1990) *Reviews of Modern Physics*, 62, 867.
- 15 Radcliffe, J.M. (1971) *Journal of Physics A: General Physics*, 4, 313.



Index

a

absorbance spectrum 66, 70
 diffraction 70
 adhesion 114
 absorption/scattering spectrum, *see* biological windows
 absorption techniques, gas adsorption 243
 air-solvent interface 69
 alkane 88
 alkanethiol-capped gold cluster 246
 alkanethiol molecules, lattice of 88
 alkoxysilanes 77
 alkyl chain ligands 177
 alloy
 Au/Ag 95
 nanomaterials, surface segregation 16
 alumina membrane 62
 amorphous silica, calcination 60
 amphiphilic molecules 211, 221
 lipids 211
 anisotropy 151
 antiferromagnetic materials 180, *see also*
 iron oxide
 antiferromagnetism 180
 apolar solvents 175
 atomic force microscope (AFM) 201
 Au-Ni-CNT microrods, scanning electron
 microscope (SEM) image 219

b

baffling process 203
 band 146
 conduction 146, 148

 valence 146
 barcoding 218
 bidentate ligand 176
 binary atomic lattices 187
 CaF₂ structure 187
 NaCl structure 187
 binary ordered arrays, formation 88
 binary superlattice 187
 bioconjugation technique 213, 226
 biological tissues, absorption/scattering
 spectrum 107
 biological windows 105, 107
 importance 107
 bionano 40, 189
 interface 37–45
 cancer cells 37
 magnetothermal 41
 photothermal treatment 41
 schematic presentation 40, 41
 biosensors 75, 77
 block copolymers 208, 210, 211
 blood stream, drugs concentration 75
 body-centered cubic (bcc) phase 209
 Bohr radius 149
 Boltzmann constant 148
 bottom-up techniques 118
 Braggs law 68, 71
 refractive index 71
 bionano applications 167
 bionano aspects 163
 doping of 160
 synthesis 151
 bridging group 175



“keywords/abstract

Dear Author,

Keywords and abstracts will normally not be included in the print version of your chapter but only in the online version (unless specifically agreed by Wiley/Wiley VCH)”.

Abstract

The first part of this chapter outlines the requirements for the individual assemblies of a modern UHPLC system. The differences between low-pressure and high-pressure mixing and their advantages and disadvantages are discussed. Furthermore, current UHPLC injection modes are described. The differences between fixed-loop and flow-through autosamplers are explained, and practical hints are given. Regarding the temperature control of the mobile and stationary phases, the influence of temperature on the resulting separation is shown. In addition, the use of column switching valves for routine applications is described. In the context of very narrow peaks in UHPLC, general requirements for UHPLC detectors are discussed. Another focus is the explanation of proper connection technology of the individual UHPLC modules. For this purpose, the influence of plastic- and stainless-steel-based connection technology on the resulting chromatography is shown.

Keywords

high- and low-pressure mixing system; fixed-loop and flow-through injection; column oven; UHPLC detectors; capillaries and fittings

Affiliation for the Authors

Steffen Wiese¹, Michael Heidorn², and Frank Steiner²

¹Chromsystems, Munich and Terence Hetzel, IUTA, Duisburg, Germany

²Thermo Fischer Scientific, Dornierstr. 4, 82110 Germering/Munich, Germany